Ab Initio Molecular Dynamics: Theory and Implementation

Dominik Marx and Jürg Hutter

AB INITIO MOLECULAR DYNAMICS:
THEORY AND IMPLEMENTATION

DOMINIK MARX

Lehrstuhl für Theoretische Chemie, Ruhr–Universität Bochum
Universitätsstrasse 150, 44780 Bochum
Germany
E-mail: dominik.marx@theochem.ruhr-uni-bochum.de

JÜRG HUTTER

Organisch–chemisches Institut, Universität Zürich
Winterthurerstrasse 190, 8057 Zürich
Switzerland
E-mail: hutter@oci.unizh.ch

The rapidly growing field of *ab initio* molecular dynamics is reviewed in the spirit of a series of lectures given at the Winterschool 2000 at the *John von Neumann Institute for Computing, Jülich.* Several such molecular dynamics schemes are compared which arise from following various approximations to the fully coupled Schrödinger equation for electrons and nuclei. Special focus is given to the Car–Parrinello method with discussion of both strengths and weaknesses in addition to its range of applicability. To shed light upon why the Car–Parrinello approach works several alternate perspectives of the underlying ideas are presented. The implementation of *ab initio* molecular dynamics within the framework of plane wave–pseudopotential density functional theory is given in detail, including diagonalization and minimization techniques as required for the Born–Oppenheimer variant. Efficient algorithms for the most important computational kernel routines are presented. The adaptation of these routines to distributed memory parallel computers is discussed using the implementation within the computer code `CPMD` as an example. Several advanced techniques from the field of molecular dynamics, (constant temperature dynamics, constant pressure dynamics) and electronic structure theory (free energy functional, excited states) are introduced. The combination of the path integral method with *ab initio* molecular dynamics is presented in detail, showing its limitations and possible extensions. Finally, a wide range of applications from materials science to biochemistry is listed, which shows the enormous potential of *ab initio* molecular dynamics for both explaining and predicting properties of molecules and materials on an atomic scale.

1 Setting the Stage: Why *Ab Initio* Molecular Dynamics ?

Classical molecular dynamics using "predefined potentials", either based on empirical data or on independent electronic structure calculations, is well established as a powerful tool to investigate many–body condensed matter systems. The broadness, diversity, and level of sophistication of this technique is documented in several monographs as well as proceedings of conferences and scientific schools [12,135,270,217,69,59,177]. At the very heart of any molecular dynamics scheme is the question of how to describe – that is in practice how to approximate – the interatomic interactions. The traditional route followed in molecular dynamics is to determine these potentials in advance. Typically, the full interaction is broken up into two–body, three–body and many–body contributions, long–range and short–range terms etc., which have to be represented by suitable functional forms, see

Sect. 2 of Ref. [253] for a detailed account. After decades of intense research, very elaborate interaction models including the non–trivial aspect to represent them analytically were devised [253,539,584].

Despite overwhelming success – which will however not be praised in this review – the need to devise a "fixed model potential" implies serious drawbacks, see the introduction sections of several earlier reviews [513,472] for a more complete digression on these aspects. Among the most delicate ones are systems where (i) many different atom or molecule types give rise to a myriad of different interatomic interactions that have to be parameterized and / or (ii) the electronic structure and thus the bonding pattern changes qualitatively in the course of the simulation. These systems can be called "chemically complex".

The reign of traditional molecular dynamics *and* electronic structure methods was greatly extended by the family of techniques that is called here "*ab initio* molecular dynamics". Other names that are currently in use are for instance Car–Parrinello, Hellmann–Feynman, first principles, quantum chemical, on–the–fly, direct, potential–free, quantum, etc. molecular dynamics. The basic idea underlying every *ab initio* molecular dynamics method is to compute the forces acting on the nuclei from electronic structure calculations that are performed "on–the–fly" as the molecular dynamics trajectory is generated. In this way, the electronic variables are not integrated out beforehand, but are considered as active degrees of freedom. This implies that, given a suitable approximate solution of the many–electron problem, also "chemically complex" systems can be handled by molecular dynamics. But this also implies that the approximation is shifted from the level of selecting the model potential to the level of selecting a particular approximation for solving the Schrödinger equation.

Applications of *ab initio* molecular dynamics are particularly widespread in materials science and chemistry, where the aforementioned difficulties (i) and (ii) are particularly severe. A collection of problems that were already tackled by *ab initio* molecular dynamics including the pertinent references can be found in Sect. 5. The power of this novel technique lead to an explosion of the activity in this field in terms of the number of published papers. The locus can be located in the late–eighties, see the squares in Fig. 1 that can be interpreted as a measure of the activity in the area of *ab initio* molecular dynamics. As a matter of fact the time evolution of the number of citations of a particular paper, the one by Car and Parrinello from 1985 entitled "Unified Approach for Molecular Dynamics and Density–Functional Theory" [108], parallels the trend in the entire field, see the circles in Fig. 1. Thus, the resonance that the Car and Parrinello paper evoked and the popularity of the entire field go hand in hand in the last decade. Incidentally, the 1985 paper by Car and Parrinello is the last one included in the section "Trends and Prospects" in the reprint collection of "key papers" from the field of atomistic computer simulations [135]. That the entire field of *ab initio* molecular dynamics has grown mature is also evidenced by a separate PACS classification number (71.15.Pd "Electronic Structure: Molecular dynamics calculations (Car–Parrinello) and other numerical simulations") that was introduced in 1996 into the *Physics and Astronomy Classification Scheme* [486].

Despite its obvious advantages, it is evident that a price has to be payed for
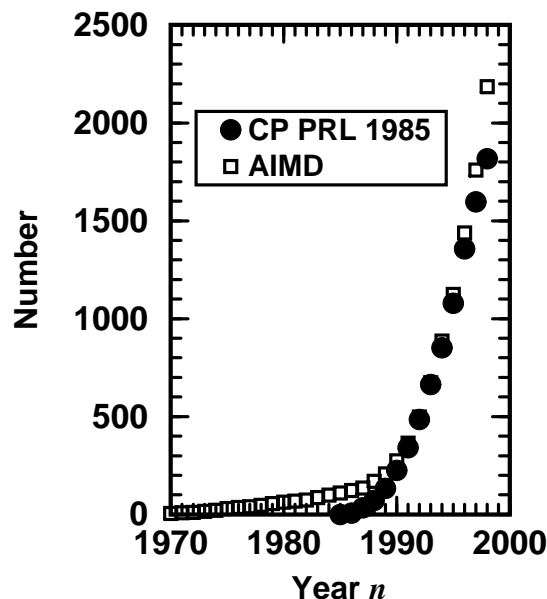
Figure 1. Publication and citation analysis. Squares: number of publications which appeared up to the year n that contain the keyword "*ab initio* molecular dynamics" (or synonyma such as "first principles MD", "Car–Parrinello simulations" etc.) in title, abstract or keyword list. Circles: number of publications which appeared up to the year n that cite the 1985 paper by Car and Parrinello [108] (including misspellings of the bibliographic reference). Self–citations and self–papers are excluded, i.e. citations of Ref. [108] in their own papers and papers coauthored by R. Car and / or M. Parrinello are *not* considered in the respective statistics. The analysis is based on the CAPLUS ("Chemical Abstracts Plus"), INSPEC ("Physics Abstracts"), and SCI ("Science Citation Index") data bases at STN International. Updated statistics from Ref. [405].

putting molecular dynamics on *ab initio* grounds: the correlation lengths and relaxation times that are accessible are much smaller than what is affordable via standard molecular dynamics. Another appealing feature of standard molecular dynamics is less evident, namely the "experimental aspect of playing with the potential". Thus, tracing back the properties of a given system to a simple physical picture or mechanism is much harder in *ab initio* molecular dynamics. The bright side is that new phenomena, which were not forseen before starting the simulation, can simply happen if necessary. This gives *ab initio* molecular dynamics a truly predictive power.

Ab initio molecular dynamics can also be viewed from another corner, namely from the field of classical trajectory calculations [649,541]. In this approach, which has its origin in gas phase molecular dynamics, a *global* potential energy surface is constructed in a first step either empirically or based on electronic structure calculations. In a second step, the dynamical evolution of the nuclei is generated by using classical mechanics, quantum mechanics or semi / quasiclassical approx-

imations of various sorts. In the case of using classical mechanics to describe the dynamics – the focus of the present overview – the limiting step for large systems is the first one, why so? There are $3N - 6$ internal degrees of freedom that span the global potential energy surface of an unconstrained N–body system. Using for simplicity 10 discretization points per coordinate implies that of the order of 10^{3N-6} electronic structure calculations are needed in order to map such a global potential energy surface. Thus, the computational workload for the first step grows roughly like $\sim 10^N$ with increasing system size. This is what might be called the "dimensionality bottleneck" of calculations that rely on *global* potential energy surfaces, see for instance the discussion on p. 420 in Ref. [254].

What is needed in *ab initio* molecular dynamics instead? Suppose that a useful trajectory consists of about 10^M molecular dynamics steps, i.e. 10^M electronic structure calculations are needed to generate one trajectory. Furthermore, it is assumed that 10^n independent trajectories are necessary in order to average over different initial conditions so that 10^{M+n} *ab initio* molecular dynamics steps are required in total. Finally, it is assumed that each single–point electronic structure calculation needed to devise the global potential energy surface and one *ab initio* molecular dynamics time step requires roughly the same amount of CPU time. Based on this truly simplistic order of magnitude estimate, the advantage of *ab initio* molecular dynamics vs. calculations relying on the computation of a global potential energy surface amounts to about $10^{3N-6-M-n}$. The crucial point is that for a given statistical accuracy (that is for M and n fixed and independent on N) and for a given electronic structure method, the computational advantage of "on–the–fly" approaches grows like $\sim 10^N$ with system size.

Of course, considerable progress has been achieved in trajectory calculations by carefully selecting the discretization points and reducing their number, choosing sophisticated representations and internal coordinates, exploiting symmetry etc. but basically the scaling $\sim 10^N$ with the number of nuclei remains a problem. Other strategies consist for instance in reducing the number of active degrees of freedom by constraining certain internal coordinates, representing less important ones by a (harmonic) bath or friction, or building up the global potential energy surface in terms of few–body fragments. All these approaches, however, invoke approximations beyond the ones of the electronic structure method itself. Finally, it is evident that the computational advantage of the "on–the–fly" approaches diminish as more and more trajectories are needed for a given (small) system. For instance extensive averaging over many different initial conditions is required in order to calculate quantitatively scattering or reactive cross sections. Summarizing this discussion, it can be concluded that *ab initio* molecular dynamics is the method of choice to investigate large and "chemically complex" systems.

Quite a few review articles dealing with *ab initio* molecular dynamics appeared in the nineties [513,223,472,457,224,158,643,234,463,538,405] and the interested reader is referred to them for various complementary viewpoints. In the present overview article, emphasis is put on both broadness of the approaches and depth of the presentation. Concerning the broadness, the discussion starts from the Schrödinger equation. Classical, Ehrenfest, Born–Oppenheimer, and Car–Parrinello molecular dynamics are "derived" from the time–dependent mean–field approach that is ob-

tained after separating the nuclear and electronic degrees of freedom. The most extensive discussion is related to the features of the basic Car–Parrinello approach but all three *ab initio* approaches to molecular dynamics are contrasted and partly compared. The important issue of how to obtain the correct forces in these schemes is discussed in some depth. The most popular electronic structure theories implemented within *ab initio* molecular dynamics, density functional theory in the first place but also the Hartree–Fock approach, are sketched. Some attention is also given to another important ingredient in *ab initio* molecular dynamics, the choice of the basis set.

Concerning the depth, the focus of the present discussion is clearly the implementation of both the basic Car–Parrinello and Born–Oppenheimer molecular dynamics schemes in the CPMD package [142]. The electronic structure approach in CPMD is Hohenberg–Kohn–Sham density functional theory within a plane wave / pseudopotential implementation and the Generalized Gradient Approximation. The formulae for energies, forces, stress, pseudopotentials, boundary conditions, optimization procedures, parallelization etc. are given for this particular choice to solve the electronic structure problem. One should, however, keep in mind that a variety of other powerful *ab initio* molecular dynamics codes are available (for instance CASTEP [116], CP-PAW [143], fhi98md [189], NWChem [446], VASP [663]) which are partly based on very similar techniques. The classic Car–Parrinello approach [108] is then extended to other ensembles than the microcanonical one, other electronic states than the ground state, and to a fully quantum–mechanical representation of the nuclei. Finally, the wealth of problems that can be addressed using *ab initio* molecular dynamics is briefly sketched at the end, which also serves implicitly as the "Summary and Conclusions" section.

2 Basic Techniques: Theory

2.1 Deriving Classical Molecular Dynamics

The starting point of the following discussion is non–relativistic quantum mechanics as formalized via the time–dependent Schrödinger equation

$$i\hbar\frac{\partial}{\partial t}\Phi(\{\mathbf{r}_i\}, \{\mathbf{R}_I\}; t) = \mathcal{H}\Phi(\{\mathbf{r}_i\}, \{\mathbf{R}_I\}; t) \tag{1}$$

in its position representation in conjunction with the standard Hamiltonian

$$\mathcal{H} = -\sum_I \frac{\hbar^2}{2M_I}\nabla_I^2 - \sum_i \frac{\hbar^2}{2m_e}\nabla_i^2 + \sum_{i\langle j} \frac{e^2}{|\mathbf{r}_i - \mathbf{r}_j|} - \sum_{I,i} \frac{e^2 Z_I}{|\mathbf{R}_I - \mathbf{r}_i|} + \sum_{I\langle J} \frac{e^2 Z_I Z_J}{|\mathbf{R}_I - \mathbf{R}_J|}$$

$$= -\sum_I \frac{\hbar^2}{2M_I}\nabla_I^2 - \sum_i \frac{\hbar^2}{2m_e}\nabla_i^2 + V_{\mathrm{n-e}}(\{\mathbf{r}_i\}, \{\mathbf{R}_I\})$$

$$= -\sum_I \frac{\hbar^2}{2M_I}\nabla_I^2 + \mathcal{H}_e(\{\mathbf{r}_i\}, \{\mathbf{R}_I\}) \tag{2}$$

for the electronic $\{\mathbf{r}_i\}$ and nuclear $\{\mathbf{R}_I\}$ degrees of freedom. The more convenient atomic units (a.u.) will be introduced at a later stage for reasons that will soon

become clear. Thus, only the bare electron–electron, electron–nuclear, and nuclear–nuclear Coulomb interactions are taken into account.

The goal of this section is to derive classical molecular dynamics [12,270,217] starting from Schrödinger's wave equation and following the elegant route of Tully [650,651]. To this end, the nuclear and electronic contributions to the total wavefunction $\Phi(\{\mathbf{r}_i\}, \{\mathbf{R}_I\}; t)$, which depends on *both* the nuclear and electronic coordinates, *have* to be separated. The simplest possible form is a product ansatz

$$\Phi(\{\mathbf{r}_i\}, \{\mathbf{R}_I\}; t) \approx \Psi(\{\mathbf{r}_i\}; t) \, \chi(\{\mathbf{R}_I\}; t) \, \exp\left[\frac{i}{\hbar} \int_{t_0}^{t} dt' \tilde{E}_{\mathrm{e}}(t')\right] \quad , \tag{3}$$

where the nuclear and electronic wavefunctions are separately normalized to unity at every instant of time, i.e. $\langle \chi; t | \chi; t \rangle = 1$ and $\langle \Psi; t | \Psi; t \rangle = 1$, respectively. In addition, a convenient phase factor

$$\tilde{E}_{\mathrm{e}} = \int d\mathbf{r} d\mathbf{R} \; \Psi^{\star}(\{\mathbf{r}_i\}; t) \chi^{\star}(\{\mathbf{R}_I\}; t) \, \mathcal{H}_{\mathrm{e}} \, \Psi(\{\mathbf{r}_i\}; t) \, \chi(\{\mathbf{R}_I\}; t) \tag{4}$$

was introduced at this stage such that the final equations will look nice; $\int d\mathbf{r} d\mathbf{R}$ refers to the integration over all $i = 1, \ldots$ and $I = 1, \ldots$ variables $\{\mathbf{r}_i\}$ and $\{\mathbf{R}_I\}$, respectively. It is mentioned in passing that this approximation is called a one–determinant or single–configuration ansatz for the *total* wavefunction, which at the end must lead to a mean–field description of the coupled dynamics. Note also that this product ansatz (excluding the phase factor) differs from the Born–Oppenheimer ansatz [340,350] for separating the fast and slow variables

$$\Phi_{\mathrm{BO}}(\{\mathbf{r}_i\}, \{\mathbf{R}_I\}; t) = \sum_{k=0}^{\infty} \tilde{\Psi}_k(\{\mathbf{r}_i\}, \{\mathbf{R}_I\}) \tilde{\chi}_k(\{\mathbf{R}_I\}; t) \tag{5}$$

even in its one–determinant limit, where only a single electronic state k (evaluated for the nuclear configuration $\{\mathbf{R}_I\}$) is included in the expansion.

Inserting the separation ansatz Eq. (3) into Eqs. (1)–(2) yields (after multiplying from the left by $\langle \Psi |$ and $\langle \chi |$ and imposing energy conservation $d \langle \mathcal{H} \rangle / dt \equiv 0$) the following relations

$$i\hbar \frac{\partial \Psi}{\partial t} = -\sum_i \frac{\hbar^2}{2m_{\mathrm{e}}} \nabla_i^2 \Psi + \left\{ \int d\mathbf{R} \, \chi^{\star}(\{\mathbf{R}_I\}; t) V_{\mathrm{n-e}}(\{\mathbf{r}_i\}, \{\mathbf{R}_I\}) \chi(\{\mathbf{R}_I\}; t) \right\} \Psi \tag{6}$$

$$i\hbar \frac{\partial \chi}{\partial t} = -\sum_I \frac{\hbar^2}{2M_I} \nabla_I^2 \chi + \left\{ \int d\mathbf{r} \, \Psi^{\star}(\{\mathbf{r}_i\}; t) \mathcal{H}_{\mathrm{e}}(\{\mathbf{r}_i\}, \{\mathbf{R}_I\}) \Psi(\{\mathbf{r}_i\}; t) \right\} \chi \quad . \tag{7}$$

This set of coupled equations defines the basis of the time–dependent self–consistent field (TDSCF) method introduced as early as 1930 by Dirac [162], see also Ref. [158]. Both electrons and nuclei move quantum–mechanically in time–dependent effective potentials (or self–consistently obtained average fields) obtained from appropriate averages (quantum mechanical expectation values $\langle \ldots \rangle$) over the other class of degrees of freedom (by using the nuclear and electronic wavefunctions, respectively). Thus, the single–determinant ansatz Eq. (3) produces, as already anticipated, a mean–field description of the coupled nuclear–electronic quantum dynamics. This is the price to pay for the simplest possible separation of electronic and nuclear variables.

The next step in the derivation of classical molecular dynamics is the task to approximate the nuclei as classical point particles. How can this be achieved in the framework of the TDSCF approach, given one quantum–mechanical wave equation describing all nuclei? A well–known route to extract classical mechanics from quantum mechanics in general starts with rewriting the corresponding wavefunction

$$\chi(\{\mathbf{R}_I\}; t) = A(\{\mathbf{R}_I\}; t) \, \exp\left[iS(\{\mathbf{R}_I\}; t)/\hbar\right] \tag{8}$$

in terms of an amplitude factor A and a phase S which are both considered to be real and $A \rangle 0$ in this polar representation, see for instance Refs. [163,425,535]. After transforming the nuclear wavefunction in Eq. (7) accordingly and after separating the real and imaginary parts, the TDSCF equation for the nuclei

$$\frac{\partial S}{\partial t} + \sum_I \frac{1}{2M_I} \left(\nabla_I S\right)^2 + \int d\mathbf{r} \, \Psi^\star \mathcal{H}_e \Psi = \hbar^2 \sum_I \frac{1}{2M_I} \frac{\nabla_I^2 A}{A} \tag{9}$$

$$\frac{\partial A}{\partial t} + \sum_I \frac{1}{M_I} \left(\nabla_I A\right) \left(\nabla_I S\right) + \sum_I \frac{1}{2M_I} A \left(\nabla_I^2 S\right) = 0 \tag{10}$$

is (exactly) re–expressed in terms of the new variables A and S. This so–called "quantum fluid dynamical representation" Eqs. (9)–(10) can actually be used to solve the time–dependent Schrödinger equation [160]. The relation for A, Eq. (10), can be rewritten as a continuity equation [163,425,535] with the help of the identification of the nuclear density $|\chi|^2 \equiv A^2$ as directly obtained from the definition Eq. (8). This continuity equation is independent of $\hbar$ and ensures locally the conservation of the particle probability $|\chi|^2$ associated to the nuclei in the presence of a flux.

More important for the present purpose is a more detailed discussion of the relation for S, Eq. (9). This equation contains one term that depends on $\hbar$, a contribution that vanishes if the classical limit

$$\frac{\partial S}{\partial t} + \sum_I \frac{1}{2M_I} \left(\nabla_I S\right)^2 + \int d\mathbf{r} \, \Psi^\star \mathcal{H}_e \Psi = 0 \tag{11}$$

is taken as $\hbar \to 0$; an expansion in terms of $\hbar$ would lead to a hierarchy of semiclassical methods [425,259]. The resulting equation is now isomorphic to equations of motion in the Hamilton–Jacobi formulation [244,540]

$$\frac{\partial S}{\partial t} + \mathcal{H}\left(\{\mathbf{R}_I\}, \{\nabla_I S\}\right) = 0 \tag{12}$$

of classical mechanics with the classical Hamilton function

$$\mathcal{H}(\{\mathbf{R}_I\}, \{\mathbf{P}_I\}) = T(\{\mathbf{P}_I\}) + V(\{\mathbf{R}_I\}) \tag{13}$$

defined in terms of (generalized) coordinates $\{\mathbf{R}_I\}$ and their conjugate momenta $\{\mathbf{P}_I\}$. With the help of the connecting transformation

$$\mathbf{P}_I \equiv \nabla_I S \tag{14}$$

the Newtonian equation of motion $\dot{\mathbf{P}}_I = -\nabla_I V(\{\mathbf{R}_I\})$ corresponding to Eq. (11)

$$\frac{d\mathbf{P}_I}{dt} = -\nabla_I \int d\mathbf{r}\ \Psi^\star \mathcal{H}_e \Psi \qquad \text{or}$$

$$M_I \ddot{\mathbf{R}}_I(t) = -\nabla_I \int d\mathbf{r}\ \Psi^\star \mathcal{H}_e \Psi \tag{15}$$

$$= -\nabla_I V_e^E(\{\mathbf{R}_I(t)\}) \tag{16}$$

can be read off. Thus, the nuclei move according to classical mechanics in an effective potential V_e^E due to the electrons. This potential is a function of only the nuclear positions at time t as a result of averaging $\mathcal{H}_e$ over the electronic degrees of freedom, i.e. computing its quantum expectation value $\langle \Psi | \mathcal{H}_e | \Psi \rangle$, while keeping the nuclear positions fixed at their instantaneous values $\{\mathbf{R}_I(t)\}$.

However, the nuclear wavefunction still occurs in the TDSCF equation for the electronic degrees of freedom and has to be replaced by the positions of the nuclei for consistency. In this case the classical reduction can be achieved simply by replacing the nuclear density $|\chi(\{\mathbf{R}_I\}; t)|^2$ in Eq. (6) in the limit $\hbar \to 0$ by a product of delta functions $\prod_I \delta(\mathbf{R}_I - \mathbf{R}_I(t))$ centered at the instantaneous positions $\{\mathbf{R}_I(t)\}$ of the classical nuclei as given by Eq. (15). This yields e.g. for the position operator

$$\int d\mathbf{R}\ \chi^\star(\{\mathbf{R}_I\}; t)\ \mathbf{R}_I\ \chi(\{\mathbf{R}_I\}; t) \ \overset{\hbar \to 0}{\longrightarrow}\ \mathbf{R}_I(t) \tag{17}$$

the required expectation value. This classical limit leads to a time–dependent wave equation for the electrons

$$i\hbar \frac{\partial \Psi}{\partial t} = -\sum_i \frac{\hbar^2}{2m_e} \nabla_i^2 \Psi + V_{n-e}(\{\mathbf{r}_i\}, \{\mathbf{R}_I(t)\}) \Psi$$

$$= \mathcal{H}_e(\{\mathbf{r}_i\}, \{\mathbf{R}_I(t)\})\ \Psi(\{\mathbf{r}_i\}, \{\mathbf{R}_I\}; t) \tag{18}$$

which evolve self–consistently as the classical nuclei are propagated via Eq. (15). Note that now $\mathcal{H}_e$ and thus Ψ depend *parametrically* on the classical nuclear *positions* $\{\mathbf{R}_I(t)\}$ at time t through $V_{n-e}(\{\mathbf{r}_i\}, \{\mathbf{R}_I(t)\})$. This means that feedback between the classical and quantum degrees of freedom is incorporated in both directions (at variance with the "classical path" or Mott non–SCF approach to dynamics [650,651]).

The approach relying on solving Eq. (15) together with Eq. (18) is sometimes called "Ehrenfest molecular dynamics" in honor of Ehrenfest who was the first to address the question [a] of how Newtonian classical dynamics can be derived from Schrödinger's wave equation [174]. In the present case this leads to a hybrid or mixed approach because only the nuclei are forced to behave like classical particles, whereas the electrons are still treated as quantum objects.

Although the TDSCF approach underlying Ehrenfest molecular dynamics clearly is a mean–field theory, transitions between electronic states are included

---

[a] The opening statement of Ehrenfest's famous 1927 paper [174] reads:
"Es ist wünschenswert, die folgende Frage möglichst elementar beantworten zu können: *Welcher Rückblick ergibt sich vom Standpunkt der Quantenmechanik auf die Newtonschen Grundgleichungen der klassischen Mechanik?*"

in this scheme. This can be made evident by expanding the *electronic* wavefunction Ψ (as opposed to the *total* wavefunction Φ according to Eq. (5)) in terms of many electronic states or determinants Ψ_k

$$\Psi(\{\mathbf{r}_i\}, \{\mathbf{R}_I\}; t) = \sum_{k=0}^{\infty} c_k(t) \Psi_k(\{\mathbf{r}_i\}; \{\mathbf{R}_I\}) \tag{19}$$

with complex coefficients $\{c_k(t)\}$. In this case, the coefficients $\{|c_k(t)|^2\}$ (with $\sum_k |c_k(t)|^2 \equiv 1$) describe explicitly the time evolution of the populations (occupations) of the different states $\{k\}$ whereas interferences are included via the $\{c_k^\star c_{l \neq k}\}$ contributions. One possible choice for the basis functions $\{\Psi_k\}$ is the adiabatic basis obtained from solving the time–independent electronic Schrödinger equation

$$\mathcal{H}_e(\{\mathbf{r}_i\}; \{\mathbf{R}_I\}) \Psi_k = E_k(\{\mathbf{R}_I\}) \Psi_k(\{\mathbf{r}_i\}; \{\mathbf{R}_I\}) \ , \tag{20}$$

where $\{\mathbf{R}_I\}$ are the instantaneous nuclear positions at time t according to Eq. (15). The actual equations of motion in terms of the expansion coefficients $\{c_k\}$ are presented in Sect. 2.2.

At this stage a further simplification can be invoked by restricting the total electronic wave function Ψ to be the ground state wave function Ψ_0 of $\mathcal{H}_e$ at each instant of time according to Eq. (20) and $|c_0(t)|^2 \equiv 1$ in Eq. (19). This should be a good approximation if the energy difference between Ψ_0 and the first excited state Ψ_1 is everywhere large compared to the thermal energy $k_B T$, roughly speaking. In this limit the nuclei move according to Eq. (15) on a single potential energy surface

$$V_e^E = \int d\mathbf{r} \ \Psi_0^\star \mathcal{H}_e \Psi_0 \equiv E_0(\{\mathbf{R}_I\}) \tag{21}$$

that can be computed by solving the *time–independent* electronic Schrödinger equation Eq. (20)

$$\mathcal{H}_e \Psi_0 = E_0 \Psi_0 \ , \tag{22}$$

for the ground state only. This leads to the identification $V_e^E \equiv E_0$ via Eq. (21), i.e. in this limit the Ehrenfest potential is identical to the ground–state Born–Oppenheimer potential.

As a consequence of this observation, it is conceivable to decouple the task of generating the nuclear dynamics from the task of computing the potential energy surface. In a first step E_0 is computed for many nuclear configurations by solving Eq. (22). In a second step, these data points are fitted to an analytical functional form to yield a global potential energy surface [539], from which the gradients can be obtained analytically. In a third step, the Newtonian equation of motion Eq. (16) is solved on this surface for many different initial conditions, producing a "swarm" of classical trajectories. This is, in a nutshell, the basis of *classical trajectory calculations* on global potential energy surfaces [649,541].

As already alluded to in the general introduction, such approaches suffer severely from the "dimensionality bottleneck" as the number of active nuclear degrees of freedom increases. One traditional way out of this dilemma is to approximate the

global potential energy surface

$$V_e^E \approx V_e^{approx}(\{\mathbf{R}_I\}) = \sum_{I=1}^{N} v_1(\mathbf{R}_I) + \sum_{I\langle J}^{N} v_2(\mathbf{R}_I, \mathbf{R}_J)$$
$$+ \sum_{I\langle J\langle K}^{N} v_3(\mathbf{R}_I, \mathbf{R}_J, \mathbf{R}_K) + \cdots \qquad (23)$$

in terms of a truncated expansion of many–body contributions [253,12,270]. At this stage, the electronic degrees of freedom are replaced by interaction potentials $\{v_n\}$ and are not featured as explicit degrees of freedom in the equations of motion. Thus, the mixed quantum / classical problem is reduced to purely classical mechanics, once the $\{v_n\}$ are determined. *Classical molecular dynamics*

$$M_I\ddot{\mathbf{R}}_I(t) = -\nabla_I V_e^{approx}(\{\mathbf{R}_I(t)\}) \qquad (24)$$

relies crucially on this idea, where typically only two–body v_2 or three–body v_3 interactions are taken into account [12,270], although more sophisticated models to include non–additive interactions such as polarization exist. This amounts to a dramatic simplification and removes the dimensionality bottleneck as the global potential surface is constructed from a manageable sum of additive few–body contributions — at the price of introducing a drastic approximation and of basically excluding chemical transformations from the realm of simulations.

As a result of this derivation, the essential assumptions underlying classical molecular dynamics become transparent: the electrons follow adiabatically the classical nuclear motion and can be integrated out so that the nuclei evolve on a single Born–Oppenheimer potential energy surface (typically but not necessarily given by the electronic ground state), which is in general approximated in terms of few–body interactions.

Actually, classical molecular dynamics for *many*–body systems is only made possible by somehow decomposing the global potential energy. In order to illustrate this point consider the simulation of $N = 500$ Argon atoms in the liquid phase [175] where the interactions can faithfully be described by additive two–body terms, i.e. $V_e^{approx}(\{\mathbf{R}_I\}) \approx \sum_{I\langle J}^{N} v_2(|\mathbf{R}_I - \mathbf{R}_J|)$. Thus, the determination of the pair potential v_2 from *ab initio* electronic structure calculations amounts to computing and fitting a one–dimensional function. The corresponding task to determine a global potential energy surface amounts to doing that in about 10^{1500} dimensions, which is simply impossible (and on top of that not necessary for Nobel gases!).

2.2 Ehrenfest Molecular Dynamics

A way out of the dimensionality bottleneck other than to approximate the global potential energy surface Eq. (23) or to reduce the number of active degrees of freedom is to take seriously the classical nuclei approximation to the TDSCF equations, Eq. (15) and (18). This amounts to computing the Ehrenfest force by actually solv-

ing numerically

$$M_I \ddot{\mathbf{R}}_I(t) = -\nabla_I \int d\mathbf{r} \, \Psi^\star \mathcal{H}_e \Psi$$
$$= -\nabla_I \langle \Psi \left| \mathcal{H}_e \right| \Psi \rangle \qquad (25)$$
$$= -\nabla_I \langle \mathcal{H}_e \rangle$$
$$= -\nabla_I V_e^E$$

$$i\hbar \frac{\partial \Psi}{\partial t} = \left[-\sum_i \frac{\hbar^2}{2m_e} \nabla_i^2 + V_{n-e}(\{\mathbf{r}_i\}, \{\mathbf{R}_I(t)\}) \right] \Psi$$
$$= \mathcal{H}_e \Psi \qquad (26)$$

the coupled set of equations simultaneously. Thereby, the *a priori* construction of any type of potential energy surface is avoided from the outset by solving the time–dependent electronic Schrödinger equation "on–the–fly". This allows one to compute the force from $\nabla_I \langle \mathcal{H}_e \rangle$ for each configuration $\{\mathbf{R}_I(t)\}$ generated by molecular dynamics; see Sect. 2.5 for the issue of using the so–called "Hellmann–Feynman forces" instead.

The corresponding equations of motion in terms of the adiabatic basis Eq. (20) and the time–dependent expansion coefficients Eq. (19) read [650,651]

$$M_I \ddot{\mathbf{R}}_I(t) = -\sum_k |c_k(t)|^2 \nabla_I E_k - \sum_{k,l} c_k^\star c_l \left(E_k - E_l \right) \mathbf{d}_I^{kl} \qquad (27)$$

$$i\hbar \dot{c}_k(t) = c_k(t) E_k - i\hbar \sum_{I,l} c_l(t) \dot{\mathbf{R}}_I \mathbf{d}_I^{kl} \quad , \qquad (28)$$

where the coupling terms are given by

$$\mathbf{d}_I^{kl}(\{\mathbf{R}_I(t)\}) = \int d\mathbf{r} \, \Psi_k^\star \nabla_I \Psi_l \qquad (29)$$

with the property $\mathbf{d}_I^{kk} \equiv \mathbf{0}$. The Ehrenfest approach is thus seen to include rigorously non–adiabatic transitions between different electronic states Ψ_k and Ψ_l within the framework of classical nuclear motion and the *mean–field* (TDSCF) approximation to the electronic structure, see e.g. Refs. [650,651] for reviews and for instance Ref. [532] for an implementation in terms of time–dependent density functional theory.

The restriction to one electronic state in the expansion Eq. (19), which is in most cases the ground state Ψ_0, leads to

$$M_I \ddot{\mathbf{R}}_I(t) = -\nabla_I \langle \Psi_0 \left| \mathcal{H}_e \right| \Psi_0 \rangle \qquad (30)$$

$$i\hbar \frac{\partial \Psi_0}{\partial t} = \mathcal{H}_e \Psi_0 \qquad (31)$$

as a special case of Eqs. (25)–(26); note that $\mathcal{H}_e$ is time–dependent via the nuclear coordinates $\{\mathbf{R}_I(t)\}$. A point worth mentioning here is that the propagation of the wavefunction is unitary, i.e. the wavefunction preserves its norm and the set of orbitals used to build up the wavefunction will stay orthonormal, see Sect. 2.6.

Ehrenfest molecular dynamics is certainly the oldest approach to "on–the–fly" molecular dynamics and is typically used for collision– and scattering–type problems [154,649,426,532]. However, it was never in widespread use for systems with many active degrees of freedom typical for condensed matter problems for reasons that will be outlined in Sec. 2.6 (although a few exceptions exist [553,34,203,617] but here the number of explicitly treated electrons is fairly limited with the exception of Ref. [617]).

2.3 Born–Oppenheimer Molecular Dynamics

An alternative approach to include the electronic structure in molecular dynamics simulations consists in straightforwardly solving the *static* electronic structure problem in each molecular dynamics step given the set of *fixed* nuclear positions at that instance of time. Thus, the electronic structure part is reduced to solving a *time–independent* quantum problem, e.g. by solving the time–independent Schrödinger equation, concurrently to propagating the nuclei via classical molecular dynamics. Thus, the time–dependence of the electronic structure is a consequence of nuclear motion, and not intrinsic as in Ehrenfest molecular dynamics. The resulting Born–Oppenheimer molecular dynamics method is defined by

$$M_I \ddot{\mathbf{R}}_I(t) = -\nabla_I \min_{\Psi_0} \{ \langle \Psi_0 | \mathcal{H}_e | \Psi_0 \rangle \} \tag{32}$$

$$E_0 \Psi_0 = \mathcal{H}_e \Psi_0 \tag{33}$$

for the electronic ground state. A deep difference with respect to Ehrenfest dynamics concerning the nuclear equation of motion is that the minimum of $\langle \mathcal{H}_e \rangle$ has to be reached in each Born–Oppenheimer molecular dynamics step according to Eq. (32). In Ehrenfest dynamics, on the other hand, a wavefunction that minimized $\langle \mathcal{H}_e \rangle$ initially will also stay in its respective minimum as the nuclei move according to Eq. (30)!

A natural and straightforward extension [281] of ground–state Born–Oppenheimer dynamics is to apply the same scheme to any excited electronic state Ψ_k without considering any interferences. In particular, this means that also the "diagonal correction terms" [340]

$$D_I^{kk}(\{\mathbf{R}_I(t)\}) = -\int d\mathbf{r} \, \Psi_k^\star \nabla_I^2 \Psi_k \tag{34}$$

are *always* neglected; the inclusion of such terms is discussed for instance in Refs. [650,651]. These terms renormalize the Born–Oppenheimer or "clamped nuclei" potential energy surface E_k of a given state Ψ_k (which might also be the ground state Ψ_0) and lead to the so–called "adiabatic potential energy surface" of that state [340]. Whence, Born–Oppenheimer molecular dynamics should not be called "adiabatic molecular dynamics", as is sometime done.

It is useful for the sake of later reference to formulate the Born–Oppenheimer equations of motion for the special case of effective one–particle Hamiltonians. This might be the Hartree–Fock approximation defined to be the variational minimum of the energy expectation value $\langle \Psi_0 | \mathcal{H}_e | \Psi_0 \rangle$ given a single Slater determinant $\Psi_0 = \det\{\psi_i\}$ subject to the constraint that the one–particle orbitals ψ_i are orthonormal

$\langle \psi_i | \psi_j \rangle = \delta_{ij}$. The corresponding constraint minimization of the total energy with respect to the orbitals

$$\min_{\{\psi_i\}} \left\{ \langle \Psi_0 | \mathcal{H}_e | \Psi_0 \rangle \right\} \Bigg|_{\{\langle \psi_i | \psi_j \rangle = \delta_{ij}\}} \qquad (35)$$

can be cast into Lagrange's formalism

$$\mathcal{L} = - \langle \Psi_0 | \mathcal{H}_e | \Psi_0 \rangle + \sum_{i,j} \Lambda_{ij} \left(\langle \psi_i | \psi_j \rangle - \delta_{ij} \right) \qquad (36)$$

where Λ_{ij} are the associated Lagrangian multipliers. Unconstrained variation of this Lagrangian with respect to the orbitals

$$\frac{\delta \mathcal{L}}{\delta \psi_i^\star} \overset{!}{=} 0 \qquad (37)$$

leads to the well–known Hartree–Fock equations

$$\mathcal{H}_e^{\mathrm{HF}} \psi_i = \sum_j \Lambda_{ij} \psi_j \qquad (38)$$

as derived in standard text books [604,418]; the diagonal canonical form $\mathcal{H}_e^{\mathrm{HF}} \psi_i = \epsilon_i \psi_i$ is obtained after a unitary transformation and $\mathcal{H}_e^{\mathrm{HF}}$ denotes the effective one–particle Hamiltonian, see Sect. 2.7 for more details. The equations of motion corresponding to Eqs. (32)–(33) read

$$M_I \ddot{\mathbf{R}}_I(t) = -\nabla_I \min_{\{\psi_i\}} \left\{ \langle \Psi_0 | \mathcal{H}_e^{\mathrm{HF}} | \Psi_0 \rangle \right\} \qquad (39)$$

$$0 = -\mathcal{H}_e^{\mathrm{HF}} \psi_i + \sum_j \Lambda_{ij} \psi_j \qquad (40)$$

for the Hartree–Fock case. A similar set of equations is obtained if Hohenberg–Kohn–Sham density functional theory [458,168] is used, where $\mathcal{H}_e^{\mathrm{HF}}$ has to be replaced by the Kohn–Sham effective one–particle Hamiltonian H_e^{KS}, see Sect. 2.7 for more details. Instead of diagonalizing the one–particle Hamiltonian an alternative but equivalent approach consists in directly performing the constraint minimization according to Eq. (35) via nonlinear optimization techniques.

Early applications of Born–Oppenheimer molecular dynamics were performed in the framework of a semiempirical approximation to the electronic structure problem [669,671]. But only a few years later an *ab initio* approach was implemented within the Hartree–Fock approximation [365]. Born–Oppenheimer dynamics started to become popular in the early nineties with the availability of more efficient electronic structure codes in conjunction with sufficient computer power to solve "interesting problems", see for instance the compilation of such studies in Table 1 in a recent overview article [82].

Undoubtedly, the breakthrough of Hohenberg–Kohn–Sham density functional theory in the realm of chemistry – which took place around the same time – also helped a lot by greatly improving the "price / performance ratio" of the electronic structure part, see e.g. Refs. [694,590]. A third and possibly the crucial reason that boosted the field of *ab initio* molecular dynamics was the pioneering introduction of

the Car–Parrinello approach [108], see also Fig. 1. This technique opened novel avenues to treat large–scale problems via *ab initio* molecular dynamics and catalyzed the entire field by making "interesting calculations" possible, see also the closing section on applications.

2.4 Car–Parrinello Molecular Dynamics

2.4.1 Motivation

A non–obvious approach to cut down the computational expenses of molecular dynamics which includes the electrons in a single state was proposed by Car and Parrinello in 1985 [108]. In retrospect it can be considered to combine the advantages of both Ehrenfest and Born–Oppenheimer molecular dynamics. In Ehrenfest dynamics the time scale and thus the time step to integrate Eqs. (30) and (31) simultaneously is dictated by the intrinsic dynamics of the electrons. Since electronic motion is much faster than nuclear motion, the largest possible time step is that which allows to integrate the electronic equations of motion. Contrary to that, there is no electron dynamics whatsoever involved in solving the Born–Oppenheimer Eqs. (32)–(33), i.e. they can be integrated on the time scale given by nuclear motion. However, this means that the electronic structure problem has to be solved self–consistently at each molecular dynamics step, whereas this is avoided in Ehrenfest dynamics due to the possibility to propagate the wavefunction by applying the Hamiltonian to an initial wavefunction (obtained e.g. by one self–consistent diagonalization).

From an algorithmic point of view the main task achieved in ground–state Ehrenfest dynamics is simply to keep the wavefunction automatically minimized as the nuclei are propagated. This, however, might be achieved – in principle – by another sort of deterministic dynamics than first–order Schrödinger dynamics. In summary, the "Best of all Worlds Method" should (i) integrate the equations of motion on the (long) time scale set by the nuclear motion but nevertheless (ii) take intrinsically advantage of the smooth time–evolution of the dynamically evolving electronic subsystem as much as possible. The second point allows to circumvent explicit diagonalization or minimization to solve the electronic structure problem for the next molecular dynamics step. Car–Parrinello molecular dynamics is an efficient method to satisfy requirement (ii) in a numerically stable fashion and makes an acceptable compromise concerning the length of the time step (i).

2.4.2 Car–Parrinello Lagrangian and Equations of Motion

The basic idea of the Car–Parrinello approach can be viewed to exploit the quantum–mechanical adiabatic time–scale separation of fast electronic and slow nuclear motion by transforming that into classical–mechanical adiabatic energy–scale separation in the framework of dynamical systems theory. In order to achieve this goal the two–component quantum / classical problem is mapped onto a two–component purely classical problem with two separate energy scales at the expense of loosing the explicit time–dependence of the quantum subsystem dynamics. Furthermore, the central quantity, the energy of the electronic subsystem $\langle \Psi_0 | \mathcal{H}_e | \Psi_0 \rangle$

evaluated with some wavefunction Ψ_0, is certainly a function of the nuclear positions $\{\mathbf{R}_I\}$. But at the same time it *can* be considered to be a functional of the wavefunction Ψ_0 and thus of a set of one–particle orbitals $\{\psi_i\}$ (or in general of other functions such as two–particle geminals) used to build up this wavefunction (being for instance a Slater determinant $\Psi_0 = \det\{\psi_i\}$ or a combination thereof). Now, in classical mechanics the force on the nuclei is obtained from the derivative of a Lagrangian with respect to the nuclear positions. This suggests that a functional derivative with respect to the orbitals, which are interpreted as classical fields, might yield the force on the orbitals, given a suitable Lagrangian. In addition, possible constraints within the set of orbitals have to be imposed, such as e.g. orthonormality (or generalized orthonormality conditions that include an overlap matrix).

Car and Parrinello postulated the following class of Lagrangians [108]

$$\mathcal{L}_{\mathrm{CP}} = \underbrace{\sum_I \frac{1}{2} M_I \dot{\mathbf{R}}_I^2 + \sum_i \frac{1}{2} \mu_i \left\langle \dot{\psi}_i \middle| \dot{\psi}_i \right\rangle}_{\text{kinetic energy}} - \underbrace{\langle \Psi_0 | \mathcal{H}_e | \Psi_0 \rangle}_{\text{potential energy}} + \underbrace{constraints}_{\text{orthonormality}} \quad (41)$$

to serve this purpose. The corresponding Newtonian equations of motion are obtained from the associated Euler–Lagrange equations

$$\frac{d}{dt} \frac{\partial \mathcal{L}}{\partial \dot{\mathbf{R}}_I} = \frac{\partial \mathcal{L}}{\partial \mathbf{R}_I} \quad (42)$$

$$\frac{d}{dt} \frac{\delta \mathcal{L}}{\delta \dot{\psi}_i^\star} = \frac{\delta \mathcal{L}}{\delta \psi_i^\star} \quad (43)$$

like in classical mechanics, but here for both the nuclear positions and the orbitals; note $\psi_i^\star = \langle \psi_i |$ and that the constraints are holonomic [244]. Following this route of ideas, generic Car–Parrinello equations of motion are found to be of the form

$$M_I \ddot{\mathbf{R}}_I(t) = -\frac{\partial}{\partial \mathbf{R}_I} \langle \Psi_0 | \mathcal{H}_e | \Psi_0 \rangle + \frac{\partial}{\partial \mathbf{R}_I} \{constraints\} \quad (44)$$

$$\mu_i \ddot{\psi}_i(t) = -\frac{\delta}{\delta \psi_i^\star} \langle \Psi_0 | \mathcal{H}_e | \Psi_0 \rangle + \frac{\delta}{\delta \psi_i^\star} \{constraints\} \quad (45)$$

where μ_i $(= \mu)$ are the "fictitious masses" or inertia parameters assigned to the orbital degrees of freedom; the units of the mass parameter μ are energy times a squared time for reasons of dimensionality. Note that the constraints within the total wavefunction lead to "constraint forces" in the equations of motion. Note also that these constraints

$$constraints = constraints \ (\{\psi_i\}, \{\mathbf{R}_I\}) \quad (46)$$

might be a function of both the set of orbitals $\{\psi_i\}$ and the nuclear positions $\{\mathbf{R}_I\}$. These dependencies have to be taken into account properly in deriving the Car–Parrinello equations following from Eq. (41) using Eqs. (42)–(43), see Sect. 2.5 for a general discussion and see e.g. Ref. [351] for a case with an additional dependence of the wavefunction constraint on nuclear positions.

According to the Car–Parrinello equations of motion, the nuclei evolve in time at a certain (instantaneous) physical temperature $\propto \sum_I M_I \dot{\mathbf{R}}_I^2$, whereas a "fictitious temperature" $\propto \sum_i \mu_i \langle \dot{\psi}_i | \dot{\psi}_i \rangle$ is associated to the electronic degrees of freedom. In this terminology, "low electronic temperature" or "cold electrons" means that the electronic subsystem is close to its instantaneous minimum energy $\min_{\{\psi_i\}} \langle \Psi_0 | \mathcal{H}_e | \Psi_0 \rangle$, i.e. close to the exact Born–Oppenheimer surface. Thus, a ground–state wavefunction optimized for the initial configuration of the nuclei will stay close to its ground state also during time evolution if it is kept at a sufficiently low temperature.

The remaining task is to separate in practice nuclear and electronic motion such that the fast electronic subsystem stays cold also for long times but still follows the slow nuclear motion adiabatically (or instantaneously). Simultaneously, the nuclei are nevertheless kept at a much higher temperature. This can be achieved in nonlinear classical dynamics via decoupling of the two subsystems and (quasi–) adiabatic time evolution. This is possible if the power spectra stemming from both dynamics do not have substantial overlap in the frequency domain so that energy transfer from the "hot nuclei" to the "cold electrons" becomes practically impossible on the relevant time scales. This amounts in other words to imposing and maintaining a metastability condition in a complex dynamical system for sufficiently long times. How and to which extend this is possible in practice was investigated in detail in an important investigation based on well–controlled model systems [467,468] (see also Sects. 3.2 and 3.3 in Ref. [513]), with more mathematical rigor in Ref. [86], and in terms of a generalization to a second level of adiabaticity in Ref. [411].

2.4.3   Why Does the Car–Parrinello Method Work ?

In order to shed light on the title question, the dynamics generated by the Car–Parrinello Lagrangian Eq. (41) is analyzed [467] in more detail invoking a "classical dynamics perspective" of a simple model system (eight silicon atoms forming a periodic diamond lattice, local density approximation to density functional theory, normconserving pseudopotentials for core electrons, plane wave basis for valence orbitals, 0.3 fs time step with $\mu = 300$ a.u., in total 20 000 time steps or 6.3 ps, for full details see Ref. [467]); a concise presentation of similar ideas can be found in Ref. [110]. For this system the vibrational density of states or power spectrum of the electronic degrees of freedom, i.e. the Fourier transform of the statistically averaged velocity autocorrelation function of the classical fields

$$f(\omega) = \int_0^\infty dt \cos(\omega t) \sum_i \left\langle \dot{\psi}_i; t \, \middle| \, \dot{\psi}_i; 0 \right\rangle \tag{47}$$

is compared to the highest–frequency phonon mode $\omega_n^{\max}$ of the nuclear subsystem in Fig. 2. From this figure it is evident that for the chosen parameters the nuclear and electronic subsystems are dynamically separated: their power spectra do not overlap so that energy transfer from the hot to the cold subsystem is expected to be prohibitively slow, see Sect. 3.3 in Ref. [513] for a similar argument.

This is indeed the case as can be verified in Fig. 3 where the conserved energy E_{cons}, physical total energy E_{phys}, electronic energy V_e, and fictitious kinetic energy
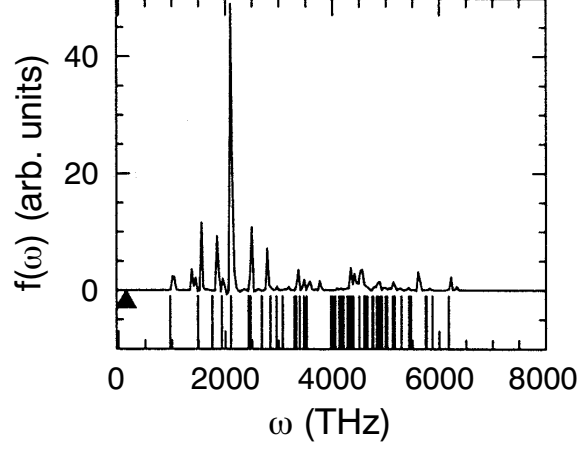
Figure 2. Vibrational density of states Eq. (47) (continuous spectrum in upper part) and harmonic approximation thereof Eq. (52) (stick spectrum in lower part) of the electronic degrees of freedom compared to the highest–frequency phonon mode $\omega_{\mathrm{n}}^{\mathrm{max}}$ (triangle) for a model system; for further details see text. Adapted from Ref. [467].

of the electrons T_{e}

$$E_{\mathrm{cons}} = \sum_i \frac{1}{2}\mu_i \left\langle \dot{\psi}_i \Big| \dot{\psi}_i \right\rangle + \sum_I \frac{1}{2}M_I \dot{\mathbf{R}}_I^2 + \langle \Psi_0 | \mathcal{H}_{\mathrm{e}} | \Psi_0 \rangle \tag{48}$$

$$E_{\mathrm{phys}} = \sum_I \frac{1}{2}M_I \dot{\mathbf{R}}_I^2 + \langle \Psi_0 | \mathcal{H}_{\mathrm{e}} | \Psi_0 \rangle = E_{\mathrm{cons}} - T_{\mathrm{e}} \tag{49}$$

$$V_{\mathrm{e}} = \langle \Psi_0 | \mathcal{H}_{\mathrm{e}} | \Psi_0 \rangle \tag{50}$$

$$T_{\mathrm{e}} = \sum_i \frac{1}{2}\mu_i \left\langle \dot{\psi}_i \Big| \dot{\psi}_i \right\rangle \tag{51}$$

are shown for the same system as a function of time. First of all, there should be a conserved energy quantity according to classical dynamics since the constraints are holonomic [244]. Indeed "the Hamiltonian" or conserved energy E_{cons} is a constant of motion (with relative variations smaller than 10^{-6} and with no drift), which serves as an extremely sensitive check of the molecular dynamics algorithm. Contrary to that the electronic energy V_{e} displays a simple oscillation pattern due to the simplicity of the phonon modes.

Most importantly, the fictitious kinetic energy of the electrons T_{e} is found to perform *bound* oscillations around a *constant*, i.e. the electrons "do not heat up" systematically in the presence of the hot nuclei; note that T_{e} is a measure for deviations from the exact Born–Oppenheimer surface. Closer inspection shows actually two time scales of oscillations: the one visible in Fig. 3 stems from the drag exerted by the moving nuclei on the electrons and is the mirror image of the V_{e} fluctuations. Superimposed on top of that (not shown, but see Fig. 4(b)) are small–amplitude high frequency oscillations intrinsic to the fictitious electron dynamics with a period of only a fraction of the visible mode. These oscillations are actually instrumental
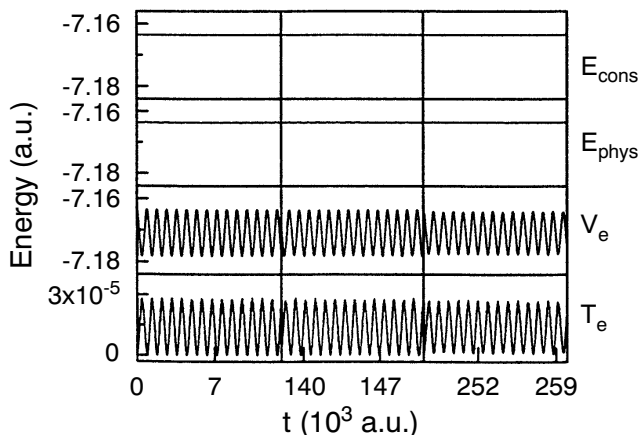
17

Figure 3. Various energies Eqs. (48)–(51) for a model system propagated via Car–Parrinello molecular dynamics for at short (up to 300 fs), intermediate, and long times (up to 6.3 ps); for further details see text. Adapted from Ref. [467].

for the stability of the Car–Parrinello dynamics, vide infra. But already the visible variations are three orders of magnitude smaller than the physically meaningful oscillations of V_e. As a result, E_{phys} defined as $E_{cons} - T_e$ or equivalently as the sum of the nuclear kinetic energy and the electronic total energy (which serves as the potential energy for the nuclei) is essentially constant on the relevant energy and time scales. Thus, it behaves approximately like the strictly conserved total energy in classical molecular dynamics (with only nuclei as dynamical degrees of freedom) or in Born–Oppenheimer molecular dynamics (with fully optimized electronic degrees of freedom) and is therefore often denoted as the "physical total energy". This implies that the resulting physically significant dynamics of the nuclei yields an excellent approximation to microcanonical dynamics (and assuming ergodicity to the microcanonical ensemble). Note that a different explanation was advocated in Ref. [470] (see also Ref. [472], in particular Sect. VIII.B and C), which was however revised in Ref. [110]. A discussion similar in spirit to the one outlined here [467] is provided in Ref. [513], see in particular Sect. 3.2 and 3.3.

Given the adiabatic separation and the stability of the propagation, the central question remains if the forces acting on the nuclei are actually the "correct" ones in Car–Parrinello molecular dynamics. As a reference serve the forces obtained from full self–consistent minimizations of the electronic energy $\min_{\{\psi_i\}} \langle \Psi_0 | \mathcal{H}_e | \Psi_0 \rangle$ at each time step, i.e. Born–Oppenheimer molecular dynamics with extremely well converged wavefunctions. This is indeed the case as demonstrated in Fig. 4(a): the physically meaningful dynamics of the x–component of the force acting on one silicon atom in the model system obtained from stable Car–Parrinello fictitious dynamics propagation of the electrons and from iterative minimizations of the electronic energy are extremely close.

Better resolution of one oscillation period in (b) reveals that the gross deviations are also oscillatory but that they are four orders of magnitudes smaller than
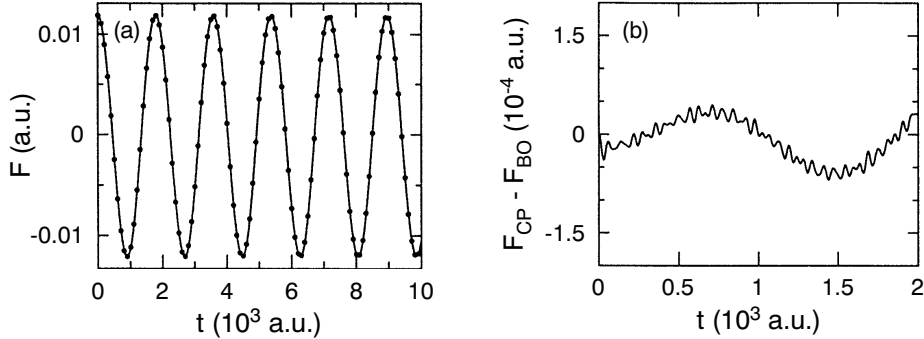
18

Figure 4. (a) Comparison of the x–component of the force acting on one atom of a model system obtained from Car–Parrinello (solid line) and well–converged Born–Oppenheimer (dots) molecular dynamics. (b) Enlarged view of the difference between Car–Parrinello and Born–Oppenheimer forces; for further details see text. Adapted from Ref. [467].

the physical variations of the force resolved in Fig. 4(a). These correspond to the "large–amplitude" oscillations of T_e visible in Fig. 3 due to the drag of the nuclei exerted on the quasi–adiabatically following electrons having a *finite* dynamical mass μ. Note that the inertia of the electrons also dampens artificially the nuclear motion (typically on a few–percent scale, see Sect. V.C.2 in Ref. [75] for an analysis and a renormalization correction of M_I) but decreases as the fictitious mass approaches the adiabatic limit $\mu \to 0$. Superimposed on the gross variation in (b) are again high–frequency *bound oscillatory small–amplitude* fluctuations like for T_e. They lead *on physically relevant time scales* (i.e. those visible in Fig. 4(a)) to "averaged forces" that are very close to the exact ground–state Born–Oppenheimer forces. This feature is an important ingredient in the derivation of adiabatic dynamics [467,411].

In conclusion, the Car–Parrinello force can be said to deviate at most instants of time from the exact Born–Oppenheimer force. However, this does not disturb the physical time evolution due to (i) the smallness and boundedness of this difference *and* (ii) the intrinsic averaging effect of small–amplitude high–frequency oscillations within a few molecular dynamics time steps, i.e. on the sub–femtosecond time scale which is irrelevant for *nuclear* dynamics.

2.4.4 How to Control Adiabaticity ?

An important question is under which circumstances the adiabatic separation can be achieved, and how it can be controlled. A simple harmonic analysis of the frequency spectrum of the orbital classical fields close to the minimum defining the ground state yields [467]

$$\omega_{ij} = \left(\frac{2(\epsilon_i - \epsilon_j)}{\mu} \right)^{1/2} \quad , \tag{52}$$

19

where ϵ_j and ϵ_i are the eigenvalues of occupied and unoccupied orbitals, respectively; see Eq. (26) in Ref. [467] for the case where both orbitals are occupied ones. It can be seen from Fig. 2 that the harmonic approximation works faithfully as compared to the exact spectrum; see Ref. [471] and Sect. IV.A in Ref. [472] for a more general analysis of the associated equations of motion. Since this is in particular true for the lowest frequency $\omega_e^{\min}$, the handy analytic estimate for the lowest possible electronic frequency

$$\omega_e^{\min} \propto \left(\frac{E_{\mathrm{gap}}}{\mu}\right)^{1/2} \quad , \tag{53}$$

shows that this frequency increases like the square root of the electronic energy difference E_{gap} between the lowest unoccupied and the highest occupied orbital. On the other hand it increases similarly for a decreasing fictitious mass parameter μ.

In order to guarantee the adiabatic separation, the frequency difference $\omega_e^{\min} - \omega_n^{\max}$ should be large, see Sect. 3.3 in Ref. [513] for a similar argument. But both the highest phonon frequency $\omega_n^{\max}$ and the energy gap E_{gap} are quantities that a dictated by the physics of the system. Whence, the only parameter in our hands to control adiabatic separation is the fictitious mass, which is therefore also called "adiabaticity parameter". However, decreasing μ not only shifts the electronic spectrum upwards on the frequency scale, but also stretches the entire frequency spectrum according to Eq. (52). This leads to an increase of the maximum frequency according to

$$\omega_e^{\max} \propto \left(\frac{E_{\mathrm{cut}}}{\mu}\right)^{1/2} \quad , \tag{54}$$

where E_{cut} is the largest kinetic energy in an expansion of the wavefunction in terms of a plane wave basis set, see Sect. 3.1.3.

At this place a limitation to decrease μ arbitrarily kicks in due to the maximum length of the molecular dynamics time step $\Delta t^{\max}$ that can be used. The time step is inversely proportional to the highest frequency in the system, which is $\omega_e^{\max}$ and thus the relation

$$\Delta t^{\max} \propto \left(\frac{\mu}{E_{\mathrm{cut}}}\right)^{1/2} \tag{55}$$

governs the largest time step that is possible. As a consequence, Car–Parrinello simulators have to find their way between Scylla and Charybdis and have to make a compromise on the control parameter μ; typical values for large–gap systems are $\mu = 500$–1500 a.u. together with a time step of about 5–10 a.u. (0.12–0.24 fs). Recently, an algorithm was devised that optimizes μ during a particular simulation given a fixed accuracy criterion [87]. Note that a poor man's way to keep the time step large and still increase μ in order to satisfy adiabaticity is to choose heavier nuclear masses. That depresses the largest phonon or vibrational frequency $\omega_n^{\max}$ of the nuclei (at the cost of renormalizing all *dynamical* quantities in the sense of classical isotope effects).

Up to this point the entire discussion of the stability and adiabaticity issues was based on model systems, approximate and mostly qualitative in nature. But recently it was actually proven [86] that the deviation or the absolute error Δ_μ of the Car–Parrinello trajectory relative to the trajectory obtained on the exact Born–Oppenheimer potential energy surface is controlled by μ:

Theorem 1 iv.): There are constants $C \rangle 0$ and $\mu^\star \rangle 0$ such that

$$\Delta_\mu = \left| \mathbf{R}^\mu(t) - \mathbf{R}^0(t) \right| + \left| |\psi^\mu; t\rangle - |\psi^0; t\rangle \right| \leq C\mu^{1/2} \quad , \quad 0 \leq t \leq T \qquad (56)$$

and the fictitious kinetic energy satisfies

$$T_{\mathrm{e}} = \frac{1}{2}\mu \left\langle \dot\psi^\mu; t \, \middle| \, \dot\psi^\mu; t \right\rangle \leq C\mu \quad , \quad 0 \leq t \leq T \qquad (57)$$

for all values of the parameter μ satisfying $0 \langle \mu \leq \mu^\star$, where up to time $T \rangle 0$ there exists a unique nuclear trajectory on the exact Born–Oppenheimer surface with $\omega_{\mathrm{e}}^{\mathrm{min}} \rangle 0$ for $0 \leq t \leq T$, i.e. there is "always" a finite electronic excitation gap. Here, the superscript μ or 0 indicates that the trajectory was obtained via Car–Parrinello molecular dynamics using a finite mass μ or via dynamics on the exact Born–Oppenheimer surface, respectively. Note that not only the nuclear trajectory is shown to be close to the correct one, but also the wavefunction is proven to stay close to the fully converged one up to time T. Furthermore, it was also investigated what happens if the initial wavefunction at $t = 0$ is not the minimum of the electronic energy $\langle \mathcal{H}_{\mathrm{e}} \rangle$ but trapped in an excited state. In this case it is found that the propagated wavefunction will keep on oscillating at $t \rangle 0$ also for $\mu \to 0$ and not even time averages converge to any of the eigenstates. Note that this does not preclude Car–Parrinello molecular dynamics in excited states, which is possible given a properly "minimizable" expression for the electronic energy, see e.g. Refs. [281,214]. However, this finding might have crucial implications for electronic level–crossing situations.

What happens if the electronic gap is very small or even vanishes $E_{\mathrm{gap}} \to 0$ as is the case for metallic systems? In this limit, all the above–given arguments break down due to the occurrence of zero–frequency electronic modes in the power spectrum according to Eq. (53), which necessarily overlap with the phonon spectrum. Following an idea of Sprik [583] applied in a classical context it was shown that the coupling of separate Nosé–Hoover thermostats [12,270,217] to the nuclear and electronic subsystem can maintain adiabaticity by counterbalancing the energy flow from ions to electrons so that the electrons stay "cool" [74]; see Ref. [204] for a similar idea to restore adiabaticity. Although this method is demonstrated to work in practice [464], this *ad hoc* cure is not entirely satisfactory from both a theoretical and practical point of view so that the well–controlled Born–Oppenheimer approach is recommended for strongly metallic systems. An additional advantage for metallic systems is that the latter is also better suited to sample many $\mathbf{k}$–points (see Sect. 3.1.3), allows easily for fractional occupation numbers [458,168], and can handle efficiently the so–called charge sloshing problem [472].

2.4.5 The Quantum Chemistry Viewpoint

In order to understand Car–Parrinello molecular dynamics also from the "quantum chemistry perspective", it is useful to formulate it for the special case of the Hartree–Fock approximation using

$$\mathcal{L}_{\mathrm{CP}} = \sum_I \frac{1}{2} M_I \dot{\mathbf{R}}_I^2 + \sum_i \frac{1}{2} \mu_i \left\langle \dot{\psi}_i \mid \dot{\psi}_i \right\rangle$$
$$- \left\langle \Psi_0 | \mathcal{H}_{\mathrm{e}}^{\mathrm{HF}} | \Psi_0 \right\rangle + \sum_{i,j} \Lambda_{ij} \left(\left\langle \psi_i \mid \psi_j \right\rangle - \delta_{ij} \right) \quad . \tag{58}$$

The resulting equations of motion

$$M_I \ddot{\mathbf{R}}_I(t) = -\nabla_I \left\langle \Psi_0 \left| \mathcal{H}_{\mathrm{e}}^{\mathrm{HF}} \right| \Psi_0 \right\rangle \tag{59}$$

$$\mu_i \ddot{\psi}_i(t) = -\mathcal{H}_{\mathrm{e}}^{\mathrm{HF}} \psi_i + \sum_j \Lambda_{ij} \psi_j \tag{60}$$

are very close to those obtained for Born–Oppenheimer molecular dynamics Eqs. (39)–(40) except for (i) no need to minimize the electronic total energy expression and (ii) featuring the additional fictitious kinetic energy term associated to the orbital degrees of freedom. It is suggestive to argue that both sets of equations become identical if the term $|\mu_i \ddot{\psi}_i(t)|$ is small at any time t compared to the physically relevant forces on the right–hand–side of both Eq. (59) and Eq. (60). This term being zero (or small) means that one is at (or close to) the minimum of the electronic energy $\langle \Psi_0 | \mathcal{H}_{\mathrm{e}}^{\mathrm{HF}} | \Psi_0 \rangle$ since time derivatives of the orbitals $\{\psi_i\}$ can be considered as variations of Ψ_0 and thus of the expectation value $\langle \mathcal{H}_{\mathrm{e}}^{\mathrm{HF}} \rangle$ itself. In other words, no forces act on the wavefunction if $\mu_i \ddot{\psi}_i \equiv 0$. In conclusion, the Car–Parrinello equations are expected to produce the correct dynamics and thus physical trajectories in the microcanonical ensemble in this idealized limit. But if $|\mu_i \ddot{\psi}_i(t)|$ is small for all i, this also implies that the associated kinetic energy $T_{\mathrm{e}} = \sum_i \mu_i \langle \dot{\psi}_i | \dot{\psi}_i \rangle / 2$ is small, which connects these more qualitative arguments with the previous discussion [467].

At this stage, it is also interesting to compare the structure of the Lagrangian Eq. (58) and the Euler–Lagrange equation Eq. (43) for Car–Parrinello dynamics to the analogues equations (36) and (37), respectively, used to derive "Hartree–Fock statics". The former reduce to the latter if the dynamical aspect and the associated time evolution is neglected, that is in the limit that the nuclear and electronic momenta are absent or constant. Thus, the Car–Parrinello ansatz, namely Eq. (41) together with Eqs. (42)–(43), can also be viewed as a prescription to derive a new class of "dynamical *ab initio* methods" in very general terms.

2.4.6 The Simulated Annealing and Optimization Viewpoints

In the discussion given above, Car–Parrinello molecular dynamics was motivated by "combining" the positive features of both Ehrenfest and Born–Oppenheimer molecular dynamics as much as possible. Looked at from another side, the Car–Parrinello method can also be considered as an ingenious way to perform *global* optimizations (minimizations) of nonlinear functions, here $\langle \Psi_0 | \mathcal{H}_{\mathrm{e}} | \Psi_0 \rangle$, in a high–dimensional parameter space including complicated constraints. The optimization

parameters are those used to represent the total wavefunction Ψ_0 in terms of simpler functions, for instance expansion coefficients of the orbitals in terms of Gaussians or plane waves, see e.g. Refs. [583,375,693,608] for applications of the same idea in other fields.

Keeping the nuclei frozen for a moment, one could start this optimization procedure from a "random wavefunction" which certainly does not minimize the electronic energy. Thus, its fictitious kinetic energy is high, the electronic degrees of freedom are "hot". This energy, however, can be extracted from the system by systematically cooling it to lower and lower temperatures. This can be achieved in an elegant way by adding a non–conservative damping term to the electronic Car–Parrinello equation of motion Eq. (45)

$$\mu_i \ddot{\psi}_i(t) = -\frac{\delta}{\delta \psi_i^\star} \langle \Psi_0 | \mathcal{H}_e | \Psi_0 \rangle + \frac{\delta}{\delta \psi_i^\star} \{constraints\} - \gamma_e \mu_i \psi_i \ , \qquad (61)$$

where $\gamma_e \geq 0$ is a friction constant that governs the rate of energy dissipation [610]; alternatively, dissipation can be enforced in a discrete fashion by reducing the velocities by multiplying them with a constant factor $\langle 1$. Note that this deterministic and dynamical method is very similar in spirit to simulated annealing [332] invented in the framework of the stochastic Monte Carlo approach in the canonical ensemble. If the energy dissipation is done slowly, the wavefunction will find its way down to the minimum of the energy. At the end, an intricate global optimization has been performed!

If the nuclei are allowed to move according to Eq. (44) in the presence of another damping term a combined or simultaneous optimization of both electrons and nuclei can be achieved, which amounts to a "global geometry optimization". This perspective is stressed in more detail in the review Ref. [223] and an implementation of such ideas within the CADPAC quantum chemistry code is described in Ref. [692]. This operational mode of Car–Parrinello molecular dynamics is related to other optimization techniques where it is aimed to optimize simultaneously both the structure of the nuclear skeleton and the electronic structure. This is achieved by considering the nuclear coordinates and the expansion coefficients of the orbitals as variation parameters on the same footing [49,290,608]. But Car–Parrinello molecular dynamics is more than that because even if the nuclei continuously move according to Newtonian dynamics at finite temperature an initially optimized wavefunction will stay optimal along the nuclear trajectory.

2.4.7 The Extended Lagrangian Viewpoint

There is still another way to look at the Car–Parrinello method, namely in the light of so–called "extended Lagrangians" or "extended system dynamics" [14], see e.g. Refs. [136,12,270,585,217] for introductions. The basic idea is to couple additional degrees of freedom to the Lagrangian of interest, thereby "extending" it by increasing the dimensionality of phase space. These degrees of freedom are treated like classical particle coordinates, i.e. they are in general characterized by "positions", "momenta", "masses", "interactions" and a "coupling term" to the particle's positions and momenta. In order to distinguish them from the physical degrees of freedom, they are often called "fictitious degrees of freedom".

The corresponding equations of motion follow from the Euler–Lagrange equations and yield a microcanonical ensemble in the extended phase space where the Hamiltonian of the extended system is strictly conserved. In other words, the Hamiltonian of the physical (sub–) system is no more (strictly) conserved, and the produced ensemble is no more the microcanonical one. Any extended system dynamics is constructed such that time–averages taken in that part of phase space that is associated to the physical degrees of freedom (obtained from a partial trace over the fictitious degrees of freedom) are physically meaningful. Of course, dynamics and thermodynamics of the system are affected by adding fictitious degrees of freedom, the classic examples being temperature and pressure control by thermostats and barostats, see Sect. 4.2.

In the case of Car–Parrinello molecular dynamics, the basic Lagrangian for Newtonian dynamics of the nuclei is actually extended by classical *fields* $\{\psi_i(\mathbf{r})\}$, i.e. functions instead of coordinates, which represent the quantum wavefunction. Thus, vector products or absolute values have to be generalized to scalar products and norms of the fields. In addition, the "positions" of these fields $\{\psi_i\}$ actually have a physical meaning, contrary to their momenta $\{\dot{\psi}_i\}$.

2.5 What about Hellmann–Feynman Forces ?

An important ingredient in all dynamics methods is the efficient calculation of the forces acting on the nuclei, see Eqs. (30), (32), and (44). The straightforward numerical evaluation of the derivative

$$\mathbf{F}_I = -\nabla_I \langle \Psi_0 | \mathcal{H}_e | \Psi_0 \rangle \tag{62}$$

in terms of a finite–difference approximation of the total electronic energy is both too costly and too inaccurate for dynamical simulations. What happens if the gradients are evaluated analytically? In addition to the derivative of the Hamiltonian itself

$$\begin{aligned} \nabla_I \langle \Psi_0 | \mathcal{H}_e | \Psi_0 \rangle = {} & \langle \Psi_0 | \nabla_I \mathcal{H}_e | \Psi_0 \rangle \\ & + \langle \nabla_I \Psi_0 | \mathcal{H}_e | \Psi_0 \rangle + \langle \Psi_0 | \mathcal{H}_e | \nabla_I \Psi_0 \rangle \end{aligned} \tag{63}$$

there are in general also contributions from variations of the wavefunction $\sim \nabla_I \Psi_0$. In general means here that these contributions vanish exactly

$$\mathbf{F}_I^{\mathrm{HFT}} = - \langle \Psi_0 | \nabla_I \mathcal{H}_e | \Psi_0 \rangle \tag{64}$$

if the wavefunction is an exact eigenfunction (or stationary state wavefunction) of the particular Hamiltonian under consideration. This is the content of the often–cited Hellmann–Feynman Theorem [295,186,368], which is also valid for many variational wavefunctions (e.g. the Hartree–Fock wavefunction) provided that *complete basis sets* are used. If this is not the case, which has to be assumed for numerical calculations, the additional terms have to be evaluated explicitly.

In order to proceed a Slater determinant $\Psi_0 = \det\{\psi_i\}$ of one–particle orbitals ψ_i, which themselves are expanded

$$\psi_i = \sum_\nu c_{i\nu} \, f_\nu(\mathbf{r}; \{\mathbf{R}_I\}) \tag{65}$$

in terms of a linear combination of basis functions $\{f_\nu\}$, is used in conjunction with an effective one–particle Hamiltonian (such as e.g. in Hartree–Fock or Kohn–Sham theories). The basis functions might depend explicitly on the nuclear positions (in the case of basis functions with origin such as atom–centered orbitals), whereas the expansion coefficients always carry an implicit dependence. This means that from the outset two sorts of forces are expected

$$\nabla_I \psi_i = \sum_\nu \left(\nabla_I c_{i\nu}\right) \, f_\nu(\mathbf{r}; \{\mathbf{R}_I\}) + \sum_\nu c_{i\nu} \, \left(\nabla_I f_\nu(\mathbf{r}; \{\mathbf{R}_I\})\right) \tag{66}$$

in addition to the Hellmann–Feynman force Eq. (64).

Using such a linear expansion Eq. (65), the force contributions stemming from the nuclear gradients of the wavefunction in Eq. (63) can be disentangled into two terms. The first one is called "incomplete–basis–set correction" (IBS) in solid state theory [49,591,180] and corresponds to the "wavefunction force" [494] or "Pulay force" in quantum chemistry [494,496]. It contains the nuclear gradients of the basis functions

$$\mathbf{F}_I^{\text{IBS}} = -\sum_{i\nu\mu} \left(\left\langle \nabla_I f_\nu \left| \mathcal{H}_{\text{e}}^{\text{NSC}} - \epsilon_i \right| f_\mu \right\rangle + \left\langle f_\nu \left| \mathcal{H}_{\text{e}}^{\text{NSC}} - \epsilon_i \right| \nabla f_\mu \right\rangle \right) \tag{67}$$

and the (in practice non–self–consistent) effective one–particle Hamiltonian [49,591]. The second term leads to the so–called "non–self–consistency correction" (NSC) of the force [49,591]

$$\mathbf{F}_I^{\text{NSC}} = -\int d\mathbf{r} \, \left(\nabla_I n\right) \left(V^{\text{SCF}} - V^{\text{NSC}} \right) \tag{68}$$

and is governed by the difference between the self–consistent ("exact") potential or field V^{SCF} and its non–self–consistent (or approximate) counterpart V^{NSC} associated to $\mathcal{H}_{\text{e}}^{\text{NSC}}$; $n(\mathbf{r})$ is the charge density. In summary, the total force needed in *ab initio* molecular dynamics simulations

$$\mathbf{F}_I = \mathbf{F}_I^{\text{HFT}} + \mathbf{F}_I^{\text{IBS}} + \mathbf{F}_I^{\text{NSC}} \tag{69}$$

comprises in general three qualitatively different terms; see the tutorial article Ref. [180] for a further discussion of core vs. valence states and the effect of pseudopotentials. Assuming that self–consistency is exactly satisfied (which is *never* going to be the case in numerical calculations), the force $\mathbf{F}_I^{\text{NSC}}$ vanishes and $\mathcal{H}_{\text{e}}^{\text{SCF}}$ has to be used to evaluate $\mathbf{F}_I^{\text{IBS}}$. The Pulay contribution vanishes in the limit of using a complete basis set (which is also not possible to achieve in actual calculations).

The most obvious simplification arises if the wavefunction is expanded in terms of originless basis functions such as plane waves, see Eq. (100). In this case the Pulay force vanishes exactly, which applies of course to all *ab initio* molecular dynamics schemes (i.e. Ehrenfest, Born–Oppenheimer, and Car–Parrinello) using that particular basis set. This statement is true for calculations where the number of plane waves is fixed. If the number of plane waves changes, such as in (constant pressure) calculations with varying cell volume / shape where the energy cutoff is strictly fixed instead, Pulay stress contributions crop up [219,245,660,211,202], see Sect. 4.2. If basis sets with origin are used instead of plane waves Pulay forces arise always and have to be included explicitly in force calculations, see e.g. Refs. [75,370,371] for such methods. Another interesting simplification of the same origin is noted in passing:

there is no basis set superposition error (BSSE) [88] in plane wave–based electronic structure calculations.

A non–obvious and more delicate term in the context of *ab initio* molecular dynamics is the one stemming from non–self–consistency Eq. (68). This term vanishes only if the wavefunction Ψ_0 is an eigenfunction of the Hamiltonian *within the subspace spanned by the finite basis set used*. This demands less than the Hellmann–Feynman theorem where Ψ_0 has to be an exact eigenfunction of the Hamiltonian and a complete basis set has to be used in turn. In terms of electronic structure calculations complete self–consistency (within a given incomplete basis set) has to be reached in order that $\mathbf{F}_I^{\mathrm{NSC}}$ vanishes. Thus, in numerical calculations the NSC term can be made arbitrarily small by optimizing the effective Hamiltonian and by determining its eigenfunctions to very high accuracy, but it can never be suppressed completely.

The crucial point is, however, that in Car–Parrinello as well as in Ehrenfest molecular dynamics it is not the minimized expectation value of the electronic Hamiltonian, i.e. $\min_{\Psi_0}\{\langle\Psi_0|\mathcal{H}_{\mathrm{e}}|\Psi_0\rangle\}$, that yields the consistent forces. What is merely needed is to evaluate the expression $\langle\Psi_0|\mathcal{H}_{\mathrm{e}}|\Psi_0\rangle$ with the Hamiltonian and the associated wavefunction available at a certain time step, compare Eq. (32) to Eq. (44) or (30). In other words, it is not required (concerning the present discussion of the contributions to the force!) that the expectation value of the electronic Hamiltonian is actually completely minimized for the nuclear configuration at that time step. Whence, full self–consistency is not required for this purpose in the case of Car–Parrinello (and Ehrenfest) molecular dynamics. As a consequence, the non–self–consistency correction to the force $\mathbf{F}_I^{\mathrm{NSC}}$ Eq. (68) is irrelevant in Car–Parrinello (and Ehrenfest) simulations.

In Born–Oppenheimer molecular dynamics, on the other hand, the expectation value of the Hamiltonian has to be minimized for each nuclear configuration before taking the gradient to obtain the consistent force! In this scheme there is (independently from the issue of Pulay forces) *always* the non–vanishing contribution of the non–self–consistency force, which is unknown by its very definition (if it were know, the problem was solved, see Eq. (68)). It is noted in passing that there are estimation schemes available that correct *approximately* for this systematic error in Born–Oppenheimer dynamics and lead to significant time–savings, see e.g. Ref. [344].

Heuristically one could also argue that within Car–Parrinello dynamics the non–vanishing non–self–consistency force is kept under control or counterbalanced by the non–vanishing "mass times acceleration term" $\mu_i\ddot{\psi}_i(t)\approx 0$, which is small but not identical to zero and oscillatory. This is sufficient to keep the propagation stable, whereas $\mu_i\ddot{\psi}_i(t)\equiv 0$, i.e. an extremely tight minimization $\min_{\Psi_0}\{\langle\Psi_0|\mathcal{H}_{\mathrm{e}}|\Psi_0\rangle\}$, is required by its very definition in order to make the Born–Oppenheimer approach stable, compare again Eq. (60) to Eq. (40). Thus, also from this perspective it becomes clear that the fictitious kinetic energy of the electrons and thus their fictitious temperature is a measure for the departure from the exact Born–Oppenheimer surface during Car–Parrinello dynamics.

Finally, the present discussion shows that nowhere in these force derivations was *made use of* the Hellmann–Feynman theorem as is sometimes stated. Actually, it is known for a long time that this theorem is quite useless for numerical electronic

structure calculations, see e.g. Refs. [494,49,496] and references therein. Rather *it turns out* that in the case of Car–Parrinello calculations using a plane wave basis the resulting relation for the force, namely Eq. (64), looks like the one obtained by simply invoking the Hellmann–Feynman theorem at the outset.

It is interesting to recall that the Hellmann–Feynman theorem as applied to a non–eigenfunction of a Hamiltonian yields only a first–order perturbative estimate of the exact force [295,368]. The same argument applies to *ab initio* molecular dynamics calculations where possible force corrections according to Eqs. (67) and (68) are neglected without justification. Furthermore, such simulations can of course not strictly conserve the total Hamiltonian E_{cons} Eq. (48). Finally, it should be stressed that possible contributions to the force in the nuclear equation of motion Eq. (44) due to *position–dependent* wavefunction *constraints* have to be evaluated following the same procedure. This leads to similar "correction terms" to the force, see e.g. Ref. [351] for such a case.

2.6 Which Method to Choose ?

Presumably the most important question for practical applications is which *ab initio* molecular dynamics method is the most efficient in terms of computer time given a specific problem. An *a priori* advantage of both the Ehrenfest and Car–Parrinello schemes over Born–Oppenheimer molecular dynamics is that no diagonalization of the Hamiltonian (or the equivalent minimization of an energy functional) is necessary, except at the very first step in order to obtain the initial wavefunction. The difference is, however, that the Ehrenfest time–evolution according to the time–dependent Schrödinger equation Eq. (26) conforms to a unitary propagation [341,366,342]

$$\Psi(t_0 + \Delta t) = \exp\left[-i\mathcal{H}_\text{e}(t_0)\Delta t/\hbar\right]\Psi(t_0) \tag{70}$$

$$\begin{aligned}
\Psi(t_0 + m\,\Delta t) = {} & \exp\left[-i\mathcal{H}_\text{e}(t_0 + (m-1)\Delta t)\,\Delta t/\hbar\right] \\
& \times \cdots \\
& \times \exp\left[-i\mathcal{H}_\text{e}(t_0 + 2\Delta t)\,\Delta t/\hbar\right] \\
& \times \exp\left[-i\mathcal{H}_\text{e}(t_0 + \Delta t)\,\Delta t/\hbar\right] \\
& \times \exp\left[-i\mathcal{H}_\text{e}(t_0)\,\Delta t/\hbar\right]\Psi(t_0)
\end{aligned} \tag{71}$$

$$\Psi(t_0 + t^{\text{max}}) \overset{\Delta t \rightarrow 0}{=} \mathsf{T}\exp\left[-\frac{i}{\hbar}\int_{t_0}^{t_0 + t^{\text{max}}} dt\,\mathcal{H}_\text{e}(t)\right]\Psi(t_0) \tag{72}$$

for infinitesimally short times given by the time step $\Delta t = t^{\text{max}}/m$; here T is the time–ordering operator and $\mathcal{H}_\text{e}(t)$ is the Hamiltonian (which is *implicitly* time–dependent via the positions $\{\mathbf{R}_I(t)\}$) evaluated at time t using e.g. split operator techniques [183]. Thus, the wavefunction Ψ will conserve its norm and in particular orbitals used to expand it will stay orthonormal, see e.g. Ref. [617]. In Car–Parrinello molecular dynamics, on the contrary, the orthonormality has to be imposed brute force by Lagrange multipliers, which amounts to an additional orthogonalization at each molecular dynamics step. If this is not properly done, the orbitals will become non–orthogonal and the wavefunction unnormalized, see e.g. Sect. III.C.1 in Ref. [472].

But this theoretical disadvantage of Car–Parrinello vs. Ehrenfest dynamics is in reality more than compensated by the possibility to use a much larger time step in order to propagate the electronic (and thus nuclear) degrees of freedom in the former scheme. In both approaches, there is the time scale inherent to the nuclear motion τ_n and the one stemming from the electronic dynamics τ_e. The first one can be estimated by considering the highest phonon or vibrational frequency and amounts to the order of $\tau_n \sim 10^{-14}$ s (or 0.01 ps or 10 fs, assuming a maximum frequency of about 4000 cm^{-1}). This time scale depends only on the physics of the problem under consideration and yields an upper limit for the timestep $\Delta t^{\max}$ that can be used in order to integrate the equations of motion, e.g. $\Delta t^{\max} \approx \tau_n/10$.

The fasted electronic motion in Ehrenfest dynamics can be estimated within a plane wave expansion by $\omega_e^E \sim E_{\text{cut}}$, where E_{cut} is the maximum kinetic energy included in the expansion. A realistic estimate for reasonable basis sets is $\tau_e^E \sim 10^{-16}$ s, which leads to $\tau_e^E \approx \tau_n/100$. The analogues relation for Car–Parrinello dynamics reads however $\omega_e^{CP} \sim (E_{\text{cut}}/\mu)^{1/2}$ according to the analysis in Sect. 2.4, see Eq. (54). Thus, in addition to reducing ω_e^{CP} by introducing a finite electron mass μ, the maximum electronic frequency increases much more slowly in Car–Parrinello than in Ehrenfest molecular dynamics with increasing basis set size. An estimate for the same basis set and a typical fictitious mass yields about $\tau_e^{CP} \sim 10^{-15}$ s or $\tau_e^{CP} \approx \tau_n/10$. According to this simple estimate, the time step can be about one order of magnitude larger if Car–Parrinello second–order fictitious–time electron dynamics is used instead of Ehrenfest first–order real–time electron dynamics.

The time scale and thus time step problem inherent to Ehrenfest dynamics prompted some attempts to releave it. In Ref. [203] the equations of motion of electrons and nuclei were integrated using two different time steps, the one of the nuclei being 20–times as large as the electronic one. The powerful technology of multiple–time step integration theory [636,639] could also be applied in order to ameliorate the time scale disparity [585]. A different approach borrowed from plasma simulations consists in decreasing the nuclear masses so that their time evolution is artificially speeded up [617]. As a result, the *nuclear* dynamics is fictitious (in the presence of real–time electron dynamics!) and has to be rescaled to the proper mass ratio after the simulation.

In both Ehrenfest and Car–Parrinello schemes the explicitly treated electron dynamics limits the largest time step that can be used in order to integrate simultaneously the coupled equations of motion for nuclei and electrons. This limitation does of course not exist in Born–Oppenheimer dynamics since there is no explicit electron dynamics so that the maximum time step is simply given by the one intrinsic to nuclear motion, i.e. $\tau_e^{BO} \approx \tau_n$. This is formally an order of magnitude advantage with respect to Car–Parrinello dynamics.

Do these back–of–the–envelope estimates have anything to do with reality? Fortunately, several state–of–the–art studies are reported in the literature for physically similar systems where all three molecular dynamics schemes have been employed. Ehrenfest simulations [553,203] of a dilute $K_x \cdot (KCl)_{1-x}$ melt were performed using a time step of 0.012–0.024 fs. In comparison, a time step as large as 0.4 fs could be used to produce a stable Car–Parrinello simulation of electrons in liquid ammonia [155,156]. Since the physics of these systems has a similar nature —

"unbound electrons" dissolved in liquid condensed matter (localizing as F–centers, polarons, bipolarons, etc.) — the time step difference of about a factor of ten confirms the crude estimate given above. In a Born–Oppenheimer simulation [569] of again $K_x \cdot (KCl)_{1-x}$ but up to a higher concentration of unbound electrons the time step used was 0.5 fs.

The time–scale advantage of Born–Oppenheimer vs. Car–Parrinello dynamics becomes more evident if the nuclear dynamics becomes fairly slow, such as in liquid sodium [343] or selenium [331] where a time step of 3 fs was used. This establishes the above–mentioned order of magnitude advantage of Born–Oppenheimer vs. Car–Parrinello dynamics in advantageous cases. However, it has to be taken into account that in simulations [331] with such a large time step dynamical information is limited to about 10 THz, which corresponds to frequencies below roughly 500 cm^{-1}. In order to resolve vibrations in molecular systems with stiff covalent bonds the time step has to be decreased to less than a femtosecond (see the estimate given above) also in Born–Oppenheimer dynamics.

The comparison of the overall performance of Car–Parrinello and Born–Oppenheimer molecular dynamics in terms of computer time is a delicate issue. For instance it depends crucially on the choice made concerning the accuracy of the conservation of the energy E_{cons} as defined in Eq. (48). Thus, this issue is to some extend subject of "personal taste" as to what is considered to be a "sufficiently accurate" energy conservation. In addition, this comparison might to different conclusions as a function of system size. In order to nevertheless shed light on this point, microcanonical simulations of 8 silicon atoms were performed with various parameters using Car–Parrinello and Born–Oppenheimer molecular dynamics as implemented in the CPMD package [142]. This large–gap system was initially extremely well equilibrated and the runs were extended to 8 ps (and a few to 12 ps with no noticeable difference) at a temperature of about 360–370 K (with ±80 K root–mean–square fluctuations). The wavefunction was expanded up to $E_{cut} = 10$ Ry at the Γ–point of a simple cubic supercell and LDA was used to describe the interactions. In both cases the velocity Verlet scheme was used to integrate the equations of motion, see Eqs. (231). It is noted in passing that also the velocity Verlet algorithm [638] allows for stable integration of the equations of motion contrary to the statements in Ref. [513] (see Sect. 3.4 and Figs. 4–5).

In Car–Parrinello molecular dynamics two different time steps were used, 5 a.u. and 10 a.u. (corresponding to about 0.24 fs), in conjunction with a fictitious electron mass of $\mu = 400$ a.u.; this mass parameter is certainly not optimized and thus the time step could be increased furthermore. Also the largest time step lead to perfect adiabaticity (similar to the one documented in Fig. 3), i.e. E_{phys} Eq. (49) and T_e Eq. (51) did not show a systematic drift relative to the energy scale set by the variations of V_e Eq. (50). Within Born–Oppenheimer molecular dynamics the minimization of the energy functional was done using the highly efficient DIIS (direct inversion in the iterative subspace) scheme using 10 "history vectors", see Sect. 3.6. In this case, the time step was either 10 a.u. or 100 a.u. and three convergence criteria were used; note that the large time step corresponding to 2.4 fs is already at the limit to be used to investigate typical *molecular* systems (with frequencies up to 3–4000 cm^{-1}). The convergence criterion is based on the
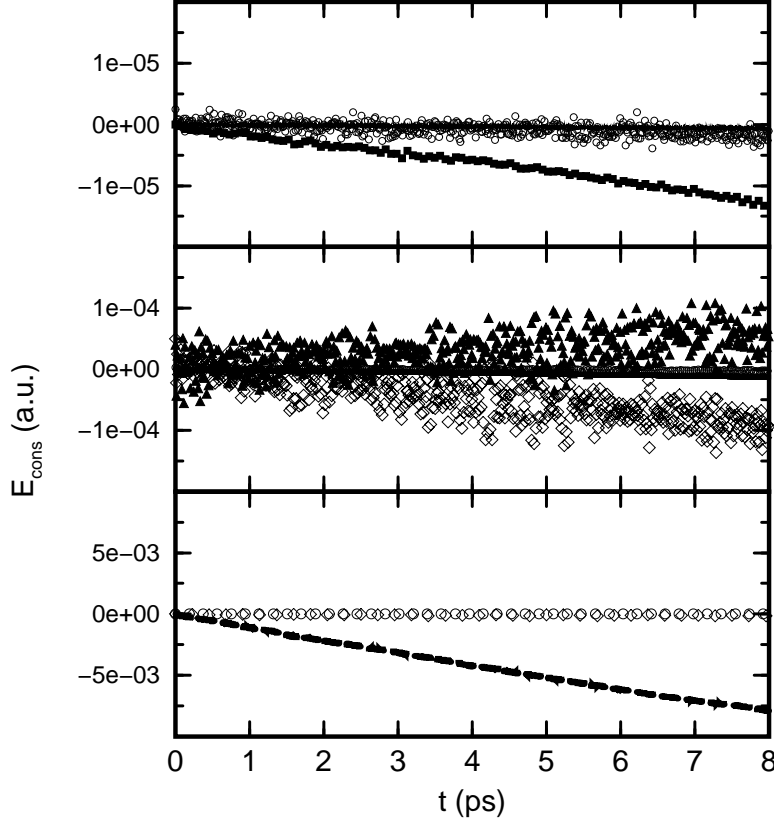
Figure 5. Conserved energy E_{cons} defined in Eq. (48) from Car–Parrinello (CP) and Born–Oppenheimer (BO) molecular dynamics simulations of a model system for various time steps and convergence criteria using the CPMD package [142]; see text for further details and Table 1 for the corresponding timings. Top: solid line: CP, 5 a.u.; open circles: CP, 10 a.u.; filled squares: BO, 10 a.u., 10^{-6}. Middle: open circles: CP, 10 a.u.; filled squares: BO, 10 a.u., 10^{-6}; filled triangles: BO, 100 a.u., 10^{-6}; open diamonds: BO, 100 a.u., 10^{-5}. Bottom: open circles: CP, 10 a.u.; open diamonds: BO, 100 a.u., 10^{-5}; dashed line: BO, 100 a.u., 10^{-4}.

largest element of the wavefunction gradient which was required to be smaller than 10^{-6}, 10^{-5} or 10^{-4} a.u.; note that the resulting energy convergence shows roughly a quadratic dependence on this criterion.

The outcome of this comparison is shown in Fig. 5 in terms of the time evolution of the conserved energy E_{cons} Eq. (48) on energy scales that cover more than three orders of magnitude in absolute accuracy. Within the present comparison ultimate energy stability was obtained using Car–Parrinello molecular dynamics with the shortest time step of 5 a.u., which conserves the energy of the total system to about 6×10^{-8} a.u. per picosecond, see solid line in Fig. 5(top). Increasing the

Table 1. Timings in CPU seconds and energy conservation in a.u. / ps for Car–Parrinello (CP) and Born–Oppenheimer (BO) molecular dynamics simulations of a model system for 1 ps of trajectory on an IBM RS6000 / model 390 (Power2) workstation using the CPMD package [142]; see Fig. 5 for corresponding energy plots.

Method	Time step (a.u.)	Convergence (a.u.)	Conservation (a.u./ps)	Time (s)
CP	5	—	6×10^{-8}	3230
CP	7	—	1×10^{-7}	2310
CP	10	—	3×10^{-7}	1610
BO	10	10^{-6}	1×10^{-6}	16590
BO	50	10^{-6}	1×10^{-6}	4130
BO	100	10^{-6}	6×10^{-6}	2250
BO	100	10^{-5}	1×10^{-5}	1660
BO	100	10^{-4}	1×10^{-3}	1060

time step to 10 a.u. leads to an energy conservation of about 3×10^{-7} a.u./ps and much larger energy fluctuations, see open circles in Fig. 5(top). The computer time needed in order to generate one picosecond of Car–Parrinello trajectory increases – to a good approximation – linearly with the increasing time step, see Table 1. The most stable Born–Oppenheimer run was performed with a time step of 10 a.u. and a convergence of 10^{-6}. This leads to an energy conservation of about 1×10^{-6} a.u./ps, see filled squares in Fig. 5(top).

As the maximum time step in Born–Oppenheimer dynamics is only related to the time scale associated to nuclear motion it could be increased from 10 to 100 a.u. while keeping the convergence at the same tight limit of 10^{-6}. This worsens the energy conservation slightly (to about 6×10^{-6} a.u./ps), whereas the energy *fluctuations* increase dramatically, see filled triangles in Fig. 5(middle) and note the change of scale compared to Fig. 5(top). The overall gain is an acceleration of the Born–Oppenheimer simulation by a factor of about seven to eight, see Table 1. In the Born–Oppenheimer scheme, the computer time needed for a fixed amount of simulated physical time decreases only sublinearly with increasing time step since the initial guess for the iterative minimization degrades in quality as the time step is made larger. Further savings of computer time can be easily achieved by decreasing the quality of the wavefunction convergence from 10^{-6} to 10^{-5} and finally to 10^{-4}, see Table 1. This is unfortunately tied to a significant decrease of the energy conservation from 6×10^{-6} a.u./ps at 10^{-6} (filled triangles) to about 1×10^{-3} a.u./ps at 10^{-4} (dashed line) using the same 100 a.u. time step, see Fig. 5(bottom) but note the change of scale compared to Fig. 5(middle).

In conclusion, Born–Oppenheimer molecular dynamics can be made as fast as (or even faster than) Car–Parrinello molecular dynamics (as measured by the amount of CPU time spent per picosecond) at the expense of sacrificing accuracy in terms of energy conservation. In the "classical molecular dynamics community" there is a general consensus that this conservation law should be taken seriously being a measure of the numerical quality of the simulation. In the "quantum chemistry and total energy communities" this issue is typically of less concern. There, it is rather the quality of the convergence of the wavefunction or energy (as achieved in every individual molecular dynamics step) that is believed to be crucial in order to gauge the quality of a particular simulation.

Finally, it is worth commenting in this particular section on a paper entitled "A comparison of Car–Parrinello and Born–Oppenheimer generalized valence bond molecular dynamics" [229]. In this paper one (computationally expensive) term in the nuclear equations of motion is neglected [648,405]. It is well known that using a basis set with origin, such as Gaussians $f_\nu^G(\mathbf{r}; \{\mathbf{R}_I\})$ centered at the nuclei, see Eq. (99), produces various Pulay forces, see Sect. 2.5. In particular a linear expansion Eq. (65) or (97) based on such orbitals introduces a position dependence into the orthogonality constraint

$$\langle \psi_i | \psi_j \rangle = \sum_{\nu\mu} c_{i\nu}^\star c_{j\mu} \underbrace{\langle f_\nu^G | f_\mu^G \rangle}_{S_{\nu\mu}} = \delta_{ij} \tag{73}$$

that is hidden in the overlap matrix $S_{\nu\mu}(\{\mathbf{R}_I\})$ which involves the basis functions. According to Eq. (44) this term produces a constraint force of the type

$$\sum_{ij} \Lambda_{ij} \sum_{\nu\mu} c_{i\nu}^\star c_{j\mu} \frac{\partial}{\partial \mathbf{R}_I} S_{\nu\mu}(\{\mathbf{R}_I\}) \tag{74}$$

in the correct Car–Parrinello equation of motion *for the nuclei* similar to the one contained in the electronic equation of motion Eq. (45). This term has to be included in order to yield exact Car–Parrinello trajectories and thus energy conservation, see e.g. Eq. (37) in Ref. [351] for a similar situation. In the case of Born–Oppenheimer molecular dynamics, on the contrary, this term is always absent in the nuclear equation of motion, see Eq. (32). Thus, the particular implementation [229] underlying the comparison between Car–Parrinello and Born–Oppenheimer molecular dynamics is an approximate one from the outset concerning the Car–Parrinello part; it can be argued that this was justified in the early papers [281,282] where the basic feasibility of both the Hartree Fock– and generalized valence bond–based Car–Parrinello molecular dynamics techniques was demonstrated [285]. Most importantly, this approximation implies that the energy E_{cons} Eq. (48) *cannot be rigorously conserved* in this particular version of Car–Parrinello molecular dynamics. However, energy conservation of E_{cons} was used in Ref. [229] to compare the efficiency and accuracy of these two approaches to GVB *ab initio* molecular dynamics (using DIIS for the Born–Oppenheimer simulations as done in the above–given comparison). Thus, the final conclusion that for "... approaches that utilize non–space–fixed bases to describe the electronic wave function, Born–Oppenheimer AIMD is the method of choice, both in terms of accuracy and speed" [229] cannot be drawn from this specific comparison for the reasons outlined above (independently of the particular basis set or electronic structure method used).

The toy system investigated here (see Fig. 5 and Table 1), i.e. 8 silicon atoms in a periodic supercell, is for the purpose of comparing different approaches to *ab initio* molecular dynamics quite similar to the system used in Ref. [229], i.e. clusters of 4 or 6 sodium atoms (in addition, qualitatively identical results where reported in Sect. 4 for silicon clusters). Thus, it is admissible to compare the energy conservations reported in Figs. 1 and 2 of Ref. [229] to the ones depicted here in Fig. 5 noting that the longest simulations reported in Ref. [229] reached only 1 ps. It should be

stressed that the energy conservation seen in Fig. 5(top) is routinely achieved in Car–Parrinello molecular dynamics simulations.

2.7 Electronic Structure Methods

2.7.1 Introduction

Up to this point, the electronic structure method to calculate the *ab initio* forces $\nabla_I \langle \Psi | \mathcal{H}_e | \Psi \rangle$ was not specified in detail. It is immediately clear that *ab initio* molecular dynamics is not tied to any particular approach, although very accurate techniques are of course prohibitively expensive. It is also evident that the strength or weakness of a particular *ab initio* molecular dynamics scheme is intimately connected to the strength or weakness of the chosen electronic structure method. Over the years a variety of different approaches such as density functional [108,679,35,472,343,36], Hartree–Fock [365,254,191,379,281,284,316,293], generalized valence bond (GVB) [282,283,228,229,230], complete active space SCF (CASSCF) [566,567], full configuration interaction (FCI) [372], semiempirical [669,671,91,190,114,666,280] or other approximate [473,454,551,455,170,171,26] methods were combined with molecular dynamics, and this list is certainly incomplete.

The focus of the present review clearly is Car–Parrinello molecular dynamics in conjunction with Hohenberg–Kohn–Sham density functional theory [301,338]. In the following, only those parts of density functional theory are presented that impact directly on *ab initio* molecular dynamics. For a deeper presentation and in particular for a discussion of the assumptions and limitations of this approach (both conceptually and in practice) the reader is referred to the existing excellent literature [591,320,458,168]. For simplicity, the formulae are presented for the spin–unpolarized or restricted special case.

Following the exposition of density functional theory, the fundamentals of Hartree–Fock theory, which is often considered to be the basis of quantum chemistry, are introduced for the same special case. Finally, a glimpse is given at post Hartree–Fock methods. Again, an extensive text–book literature exists for these wavefunction–based approaches to electronic structure calculations [604,418]. The very useful connection between the density–based and wavefunction–based methods goes back to Löwdin's work in the mid fifties and is e.g. worked out in Chapt. 2.5 of Ref. [458], where Hartree–Fock theory is formulated in density–matrix language.

2.7.2 Density Functional Theory

The total ground–state energy of the interacting system of electrons with classical nuclei fixed at positions $\{\mathbf{R}_I\}$ can be obtained

$$\min_{\Psi_0} \left\{ \langle \Psi_0 | \mathcal{H}_e | \Psi_0 \rangle \right\} = \min_{\{\phi_i\}} E^{KS}[\{\phi_i\}]$$

as the minimum of the Kohn–Sham energy [301,338]

$$E^{KS}[\{\phi_i\}] = T_s[\{\phi_i\}] + \int d\mathbf{r} \ V_{ext}(\mathbf{r}) \ n(\mathbf{r}) + \frac{1}{2} \int d\mathbf{r} \ V_H(\mathbf{r}) \ n(\mathbf{r}) + E_{xc}[n] \ , \quad (75)$$

which is an explicit functional of the set of auxiliary functions $\{\phi_i(\mathbf{r})\}$ that satisfy the orthonormality relation $\langle \phi_i \mid \phi_j \rangle = \delta_{ij}$. This is a dramatic simplification since the minimization with respect to all possible *many–body* wavefunctions $\{\Psi\}$ is replaced by a minimization with respect to a set of orthonormal one–particle functions, the Kohn–Sham orbitals $\{\phi_i\}$. The associated electronic one–body density or charge density

$$n(\mathbf{r}) = \sum_i^{\text{occ}} f_i \mid \phi_i(\mathbf{r}) \mid^2 \tag{76}$$

is obtained from a single Slater determinant built from the occupied orbitals, where $\{f_i\}$ are integer occupation numbers.

The first term in the Kohn–Sham functional Eq. (75) is the kinetic energy of a non–interacting reference system

$$T_{\text{s}}[\{\phi_i\}] = \sum_i^{\text{occ}} f_i \left\langle \phi_i \left| -\frac{1}{2}\nabla^2 \right| \phi_i \right\rangle \tag{77}$$

consisting of the same number of electrons exposed to the same external potential as in the fully interacting system. The second term comes from the fixed external potential

$$V_{\text{ext}}(\mathbf{r}) = -\sum_I \frac{Z_I}{|\mathbf{R}_I - \mathbf{r}|} + \sum_{I\langle J} \frac{Z_I Z_J}{|\mathbf{R}_I - \mathbf{R}_J|} \tag{78}$$

in which the electrons move, which comprises the Coulomb interactions between electrons and nuclei and in the definition used here also the internuclear Coulomb interactions; this term changes in the first place if core electrons are replaced by pseudopotentials, see Sect. 3.1.5 for further details. The third term is the Hartree energy, i.e. the classical electrostatic energy of two charge clouds which stem from the electronic density and is obtained from the Hartree potential

$$V_{\text{H}}(\mathbf{r}) = \int d\mathbf{r}' \ \frac{n(\mathbf{r}')}{\mid \mathbf{r} - \mathbf{r}' \mid} \ , \tag{79}$$

which in turn is related to the density via

$$\nabla^2 V_{\text{H}}(\mathbf{r}) = -4\pi n(\mathbf{r}) \tag{80}$$

Poisson's equation. The last contribution in the Kohn–Sham functional, the exchange–correlation functional $E_{\text{xc}}[n]$, is the most intricate contribution to the total electronic energy. The electronic exchange and correlation effects are lumped together and basically define this functional as the remainder between the exact energy and its Kohn–Sham decomposition in terms of the three previous contributions.

The minimum of the Kohn–Sham functional is obtained by varying the energy functional Eq. (75) for a fixed number of electrons with respect to the density Eq. (76) or with respect to the orbitals subject to the orthonormality constraint,

see e.g. the discussion following Eq. (35) for a similar variational procedure. This leads to the Kohn–Sham equations

$$\left\{ -\frac{1}{2}\nabla^2 + V_{\text{ext}}(\mathbf{r}) + V_{\text{H}}(\mathbf{r}) + \frac{\delta E_{\text{xc}}[n]}{\delta n(\mathbf{r})} \right\} \phi_i(\mathbf{r}) = \sum_j \Lambda_{ij}\phi_j(\mathbf{r}) \qquad (81)$$

$$\left\{ -\frac{1}{2}\nabla^2 + V^{\text{KS}}(\mathbf{r}) \right\} \phi_i(\mathbf{r}) = \sum_j \Lambda_{ij}\phi_j(\mathbf{r}) \qquad (82)$$

$$H_{\text{e}}^{\text{KS}}\phi_i(\mathbf{r}) = \sum_j \Lambda_{ij}\phi_j(\mathbf{r}) \ , \qquad (83)$$

which are one–electron equations involving an effective *one–particle* Hamiltonian H_{e}^{KS} with the local potential V^{KS}. Note that H_{e}^{KS} nevertheless embodies the electronic *many–body* effects by virtue of the exchange–correlation potential

$$\frac{\delta E_{\text{xc}}[n]}{\delta n(\mathbf{r})} = V_{\text{xc}}(\mathbf{r}) \ . \qquad (84)$$

A unitary transformation within the space of the occupied orbitals leads to the canonical form

$$H_{\text{e}}^{\text{KS}}\phi_i = \epsilon_i\phi_i \qquad (85)$$

of the Kohn–Sham equations, where $\{\epsilon_i\}$ are the eigenvalues. In conventional static density functional or "band structure" calculations this set of equations has to be solved self–consistently in order to yield the density, the orbitals and the Kohn–Sham potential for the electronic ground state [487]. The corresponding total energy Eq. (75) can be written as

$$E^{\text{KS}} = \sum_i \epsilon_i - \frac{1}{2}\int d\mathbf{r} \ V_{\text{H}}(\mathbf{r}) \ n(\mathbf{r}) + E_{\text{xc}}[n] - \int d\mathbf{r} \ \frac{\delta E_{\text{xc}}[n]}{\delta n(\mathbf{r})} \ n(\mathbf{r}) \ , \qquad (86)$$

where the sum over Kohn–Sham eigenvalues is the so–called "band–structure energy".

Thus, Eqs. (81)–(83) together with Eqs. (39)–(40) define Born–Oppenheimer molecular dynamics within Kohn–Sham density functional theory, see e.g. Refs. [232,616,594,35,679,472,36,343,344] for such implementations. The functional derivative of the Kohn–Sham functional with respect to the orbitals, the Kohn–Sham force acting on the orbitals, can be expressed as

$$\frac{\delta E^{\text{KS}}}{\delta \phi_i^\star} = f_i H_{\text{e}}^{\text{KS}}\phi_i \ , \qquad (87)$$

which makes clear the connection to Car–Parrinello molecular dynamics, see Eq. (45). Thus, Eqs. (59)–(60) have to be solved with the effective one–particle Hamiltonian in the Kohn–Sham formulation Eqs. (81)–(83). In the case of Ehrenfest dynamics presented in Sect. 2.2, which will not be discussed in further detail at this stage, the Runge–Gross time–dependent generalization of density functional theory [258] has to be invoked instead, see e.g. Refs. [203,617,532].

Crucial to any application of density functional theory is the approximation of the unknown exchange and correlation functional. A discussion focussed on the

utilization of such functionals in the framework of *ab initio* molecular dynamics is for instance given in Ref. [588]. Those exchange–correlation functionals that will be considered in the implementation part, Sect. 3.3, belong to the class of the "Generalized Gradient Approximation"

$$E_{xc}^{GGA}[n] = \int d\mathbf{r} \ n(\mathbf{r}) \ \varepsilon_{xc}^{GGA}(n(\mathbf{r}); \nabla n(\mathbf{r})) \ , \tag{88}$$

where the unknown functional is approximated by an integral over a function that depends only on the density and its gradient at a given point in space, see Ref. [477] and references therein. The combined exchange–correlation function is typically split up into two additive terms ε_x and ε_c for exchange and correlation, respectively. In the simplest case it is the exchange and correlation energy density $\varepsilon_{xc}^{LDA}(n)$ of an interacting but homogeneous electron gas at the density given by the "local" density $n(\mathbf{r})$ at space–point $\mathbf{r}$ in the inhomogeneous system. This simple but astonishingly powerful approximation [320] is the famous local density approximation LDA [338] (or local spin density LSD in the spin–polarized case [40]), and a host of different parameterizations exist in the literature [458,168]. The self–interaction correction [475] SIC as applied to LDA was critically assessed for molecules in Ref. [240] with a disappointing outcome.

A significant improvement of the accuracy was achieved by introducing the gradient of the density as indicated in Eq. (88) beyond the well–known straightforward gradient expansions. These so–called GGAs (also denoted as "gradient corrected" or "semilocal" functionals) extended the applicability of density functional calculation to the realm of chemistry, see e.g. Refs. [476,42,362,477,478,479] for a few "popular functionals" and Refs. [318,176,577,322] for extensive tests on molecules, complexes, and solids, respectively.

Another considerable advance was the successful introduction of "hybrid functionals" [43,44] that include to some extent "exact exchange" [249] in addition to a standard GGA. Although such functionals can certainly be implemented within a plane wave approach [262,128], they are prohibitively time–consuming as outlined at the end of Sect. 3.3. A more promising route in this respect are those functionals that include higher–order powers of the gradient (or the local kinetic energy density) in the sense of a generalized gradient expansion beyond the first term. Promising results could be achieved by including Laplacian or local kinetic energy terms [493,192,194,662], but at this stage a sound judgment concerning their "prize / performance ratio" has to await further scrutinizing tests. The "optimized potential method" (OPM) or "optimized effective potentials" (OEP) are another route to include "exact exchange" within density functional theory, see e.g. Sect. 13.6 in Ref. [588] or Ref. [251] for overviews. Here, the exchange–correlation functional $E_{xc}^{OPM} = E_{xc}[\{\phi_i\}]$ depends on the individual orbitals instead of only on the density or its derivatives.

2.7.3 Hartree–Fock Theory

Hartree–Fock theory is derived by invoking the variational principle in a restricted space of wavefunctions. The antisymmetric ground–state electronic wavefunction is approximated by a single Slater determinant $\Psi_0 = \det\{\psi_i\}$ which is constructed

from a set of one–particle spin orbitals $\{\psi_i\}$ required to be mutually orthonormal $\langle\psi_i|\psi_j\rangle = \delta_{ij}$. The corresponding variational minimum of the total electronic energy $\mathcal{H}_e$ defined in Eq. (2)

$$E^{\mathrm{HF}}[\{\psi_i\}] = \sum_i \int d\mathbf{r}\,\psi_i^\star(\mathbf{r})\left[-\frac{1}{2}\nabla^2 + V_{\mathrm{ext}}(\mathbf{r})\right]\psi_i(\mathbf{r})$$
$$+\frac{1}{2}\sum_{ij}\int\int d\mathbf{r}\,d\mathbf{r}'\,\psi_i^\star(\mathbf{r})\psi_j^\star(\mathbf{r}')\,\frac{1}{|\mathbf{r}-\mathbf{r}'|}\,\psi_i(\mathbf{r})\psi_j(\mathbf{r}')$$
$$+\frac{1}{2}\sum_{ij}\int\int d\mathbf{r}\,d\mathbf{r}'\,\psi_i^\star(\mathbf{r})\psi_j^\star(\mathbf{r}')\,\frac{1}{|\mathbf{r}-\mathbf{r}'|}\,\psi_j(\mathbf{r})\psi_i(\mathbf{r}') \qquad (89)$$

yields the lowest energy and the "best" wavefunction within a one–determinant ansatz; the external Coulomb potential V_{ext} was already defined in Eq. (78). Carrying out the constraint minimization within this ansatz (see Eq. (36) in Sect. 2.3 for a sketch) leads to

$$\left\{-\frac{1}{2}\nabla^2 + V_{\mathrm{ext}}(\mathbf{r}) + \sum_j \mathcal{J}_j(\mathbf{r}) - \sum_j \mathcal{K}_j(\mathbf{r})\right\}\psi_i(\mathbf{r}) = \sum_j \Lambda_{ij}\psi_j(\mathbf{r}) \qquad (90)$$

$$\left\{-\frac{1}{2}\nabla^2 + V^{\mathrm{HF}}(\mathbf{r})\right\}\psi_i(\mathbf{r}) = \sum_j \Lambda_{ij}\psi_j(\mathbf{r}) \qquad (91)$$

$$H_e^{\mathrm{HF}}\psi_i(\mathbf{r}) = \sum_j \Lambda_{ij}\psi_j(\mathbf{r}) \qquad (92)$$

the Hartree–Fock integro–differential equations. In analogy to the Kohn–Sham equations Eqs. (81)–(83) these are effective one–particle equations that involve an effective one–particle Hamiltonian H_e^{HF}, the (Hartree–) Fock operator. The set of canonical orbitals

$$H_e^{\mathrm{HF}}\psi_i = \epsilon_i\psi_i \qquad (93)$$

is obtained similarly to Eq. (85). The Coulomb operator

$$\mathcal{J}_j(\mathbf{r})\,\psi_i(\mathbf{r}) = \left[\int d\mathbf{r}'\,\psi_j^\star(\mathbf{r}')\frac{1}{|\mathbf{r}-\mathbf{r}'|}\psi_j(\mathbf{r}')\right]\,\psi_i(\mathbf{r}) \qquad (94)$$

and the exchange operator

$$\mathcal{K}_j(\mathbf{r})\,\psi_i(\mathbf{r}) = \left[\int d\mathbf{r}'\,\psi_j^\star(\mathbf{r}')\frac{1}{|\mathbf{r}-\mathbf{r}'|}\psi_i(\mathbf{r}')\right]\,\psi_j(\mathbf{r}) \qquad (95)$$

are most easily defined via their action on a particular orbital ψ_i. It is found that upon acting on orbital $\psi_i(\mathbf{r})$ the exchange operator for the j–th state "exchanges" $\psi_j(\mathbf{r}') \to \psi_i(\mathbf{r}')$ in the kernel as well as replaces $\psi_i(\mathbf{r}) \to \psi_j(\mathbf{r})$ in its argument, compare to the Coulomb operator. Thus, $\mathcal{K}$ is a non–local operator as its action on a function ψ_i at point $\mathbf{r}$ in space requires the evaluation and thus the knowledge of that function throughout all space by virtue of $\int d\mathbf{r}'\,\psi_i(\mathbf{r}')\ldots$ the required integration. In this sense the exchange operator does not possess a simple classical interpretation like the Coulomb operator $\mathcal{C}$, which is the counterpart of

the Hartree potential V_H in Kohn–Sham theory. The exchange operator vanishes exactly if the antisymmetrization requirement of the wavefunction is relaxed, i.e. only the Coulomb contribution survives if a Hartree product is used to represent the wavefunction.

The force acting on the orbitals is defined

$$\frac{\delta E^{HF}}{\delta \psi_i^\star} = H_e^{HF} \psi_i \tag{96}$$

similarly to Eq. (87). At this stage, the various *ab initio* molecular dynamics schemes based on Hartree–Fock theory are defined, see Eqs. (39)–(40) for Born–Oppenheimer molecular dynamics and Eqs. (59)–(60) for Car–Parrinello molecular dynamics. In the case of Ehrenfest molecular dynamics the time–dependent Hartree–Fock formalism [162] has to be invoked instead.

2.7.4 Post Hartree–Fock Theories

Although post Hartree–Fock methods have a very unfavorable scaling of the computational cost as the number of electrons increases, a few case studies were performed with such correlated quantum chemistry techniques. For instance *ab initio* molecular dynamics was combined with GVB [282,283,228,229,230], CASSCF [566,567], as well as FCI [372] approaches, see also references therein. It is noted in passing that Car–Parrinello molecular dynamics can only be implemented straightforwardly if energy and wavefunction are "consistent". This is not the case in perturbation theories such as e.g. the widely used Møller–Plesset approach [292]: within standard MP2 the energy is correct to second order, whereas the wavefunction is the one given by the uncorrelated HF reference. As a result, the derivative of the MP2 energy with respect to the wavefunction Eq. (96) does not yield the correct force on the HF wavefunction in the sense of fictitious dynamics. Such problems are of course absent from the Born–Oppenheimer approach to sample configuration space, see e.g. Ref. [328,317,33] for MP2, density functional, and multireference CI *ab initio* Monte Carlo schemes.

It should be kept in mind that the rapidly growing workload of post HF calculations, although extremely powerful in principle, limits the number of explicitly treated electrons to only a few. The rapid development of correlated electronic structure methods that scale linearly with the number of electrons will certainly broaden the range of applicability of this class of techniques in the near future.

2.8 Basis Sets

2.8.1 Gaussians and Slater Functions

Having selected a specific electronic structure method the next choice is related to which basis set to use in order to represent the orbitals ψ_i in terms of simple analytic functions f_ν with well–known properties. In general a *linear* combination of such basis functions

$$\psi_i(\mathbf{r}) = \sum_\nu c_{i\nu} f_\nu(\mathbf{r}; \{\mathbf{R}_I\}) \tag{97}$$

is used, which represents exactly any reasonable function in the limit of using a complete set of basis functions. In quantum chemistry, Slater–type basis functions (STOs)

$$f_{\mathbf{m}}^{\mathrm{S}}(\mathbf{r}) = N_{\mathbf{m}}^{\mathrm{S}}\, r_x^{m_x} r_y^{m_y} r_z^{m_z}\ \exp\left[-\zeta_{\mathbf{m}}|\mathbf{r}|\right] \tag{98}$$

with an exponentially decaying radial part and Gaussian–type basis functions (GTOs)

$$f_{\mathbf{m}}^{\mathrm{G}}(\mathbf{r}) = N_{\mathbf{m}}^{\mathrm{G}}\, r_x^{m_x} r_y^{m_y} r_z^{m_z}\ \exp\left[-\alpha_{\mathbf{m}} r^2\right] \tag{99}$$

have received widespread use, see e.g. Ref. [292] for a concise overview–type presentation. Here, $N_{\mathbf{m}}$, $\zeta_{\mathbf{m}}$ and $\alpha_{\mathbf{m}}$ are constants that are typically kept fixed during a molecular electronic structure calculation so that only the orbital expansion coefficients $c_{i\nu}$ need to be optimized. In addition, fixed linear combinations of the above–given "primitive" basis functions can be used for a given angular momentum channel $\mathbf{m}$, which defines the "contracted" basis sets.

The Slater or Gaussian basis functions are in general centered at the positions of the nuclei, i.e. $\mathbf{r} \to \mathbf{r} - \mathbf{R}_I$ in Eq. (98)–(99), which leads to the linear combination of *atomic orbitals* (LCAO) ansatz to solve differential equations algebraically. Furthermore, their derivatives as well as the resulting matrix elements are efficiently obtained by differentiation and integration in real–space. However, Pulay forces (see Sect. 2.5) will result for such basis functions that are fixed at atoms (or bonds) if the atoms are allowed to move, either in geometry optimization or molecular dynamics schemes. This disadvantage can be circumvented by using *freely* floating Gaussians that are distributed in space [582], which form an originless basis set since it is localized but not atom–fixed.

2.8.2 Plane Waves

A vastly different approach has its roots in solid–state theory. Here, the ubiquitous periodicity of the underlying lattice produces a periodic potential and thus imposes the same periodicity on the density (implying Bloch's Theorem, Born–von Karman periodic boundary conditions etc., see e.g. Chapt. 8 in Ref. [27]). This heavily suggests to use plane waves as the generic basis set in order to expand the periodic part of the orbitals, see Sect. 3.1.2. Plane waves are defined as

$$f_{\mathbf{G}}^{\mathrm{PW}}(\mathbf{r}) = N \exp\left[i\mathbf{G}\mathbf{r}\right]\ , \tag{100}$$

where the normalization is simply given by $N = 1/\sqrt{\Omega}$; Ω is the volume of the periodic (super–) cell. Since plane waves form a complete and orthonormal set of functions they can be used to expand orbitals according to Eq. (97), where the labeling ν is simply given by the vector $\mathbf{G}$ in reciprocal space / G–space (including only those $\mathbf{G}$–vectors that satisfy the particular periodic boundary conditions). The total electronic energy is found to have a particularly simple form when expressed in plane waves [312].

It is important to observe that plane waves are originless functions, i.e. they do *not* depend on the positions of the nuclei $\{\mathbf{R}_I\}$. This implies that the Pulay forces Eq. (67) vanish exactly even within a *finite* basis (and using a fixed number of plane waves, see the discussion related to "Pulay stress" in Sect. 2.5), which

tremendously facilitates force calculations. This also implies that plane waves are a very unbiased basis set in that they are "delocalized" in space and do not "favor" certain atoms or regions over others, i.e. they can be considered as an ultimately "balanced basis set" in the language of quantum chemistry. Thus, the only way to improve the quality of the basis is to increase the "energy cutoff" E_{cut}, i.e. to increase the largest $|\mathbf{G}|$–vector that is included in the finite expansion Eq. (97). This blind approach is vastly different from the traditional procedures in quantum chemistry that are needed in order to produce reliable basis sets [292]. Another appealing feature is that derivatives in real–space are simply multiplications in G–space, and both spaces can be efficiently connected via Fast Fourier Transforms (FFTs). Thus, one can easily evaluate operators in that space in which they are diagonal, see for instance the flow charts in Fig. 6 or Fig. 7.

According to the well–known "No Free Lunch Theorem" there cannot be only advantages connected to using plane waves. The first point is that the pseudopotential approximation is intimately connected to using plane waves, why so? A plane wave basis is basically a lattice–symmetry–adapted three–dimensional Fourier decomposition of the orbitals. This means that increasingly large Fourier components are needed in order to resolve structures in real space on decreasingly small distance scales. But already orbitals of first row atoms feature quite strong and rapid oscillations close to the nuclei due to the Pauli principle, which enforces a nodal structure onto the wavefunction by imposing orthogonality of the orbitals. However, most of chemistry is ruled by the valence electrons, whereas the core electrons are essentially inert. In practice, this means that the innermost electrons can be taken out of explicit calculations. Instead they are represented by a smooth and nodeless effective potential, the so–called pseudopotential [296,297,484,485,139], see for instance Refs. [487,578,221] for reviews in the context of "solid state theory" and Refs. [145,166] for pseudopotentials as used in "quantum chemistry". The resulting pseudo wavefunction is made as smooth as possible close to the nuclear core region. This also means that properties that depend crucially on the wavefunction close to the core cannot be obtained straightforwardly from such calculations. In the field of plane wave calculations the introduction of "soft" norm–conserving *ab initio* pseudopotentials was a breakthrough both conceptually [274] and in practice [28]. Another important contribution, especially for transition metals, was the introduction of the so–called ultrasoft pseudopotentials by Vanderbilt [661]. This approaches lead to the powerful technique of plane wave–pseudopotential electronic structure calculations in the framework of density functional theory [312,487]. Within this particular framework the issue of pseudopotentials is elaborated in more detail in Sect. 3.1.5.

Another severe shortcoming of plane waves is the backside of the medal of being an unbiased basis set: there is no way to shuffle more basis functions into regions in space where they are more needed than in other regions. This is particularly bad for systems with strong inhomogeneities. Such examples are all–electron calculations or the inclusion of semi–core states, a few heavy atoms in a sea of light atoms, and (semi–) finite systems such as surfaces or molecules with a large vacuum region in order to allow the long–range Coulomb interactions to decay. This is often referred to as the multiple length scale deficiency of plane wave calculations.

2.8.3 Generalized Plane Waves

An extremely appealing and elegant generalization of the plane wave concept [263,264] consists in defining them in curved ξ–space

$$f_{\mathbf{G}}^{\mathrm{GPW}}(\xi) = N \det{}^{1/2} J \exp\left[i\mathbf{G}\,\mathbf{r}(\xi)\right] \tag{101}$$

$$\det J = \left|\frac{\partial r^i}{\partial \xi^j}\right| \ ,$$

where $\det J$ is the Jacobian of the transformation from Cartesian to curvilinear coordinates $\mathbf{r} \to \xi(\mathbf{r})$ with $\xi = (\xi^1, \xi^2, \xi^3)$ and $N = 1/\sqrt{\Omega}$ as for regular plane waves. These functions are orthonormal, form a complete basis set, can be used for $\mathbf{k}$–point sampling after replacing $\mathbf{G}$ by $\mathbf{G} + \mathbf{k}$ in Eq. (101), are originless (but nevertheless localized) so that Pulay forces are absent, can be manipulated via efficient FFT techniques, and reduce to standard plane waves in the special case of an Euclidean space $\xi(\mathbf{r}) = \mathbf{r}$. Thus, they can be used equally well like plane waves in linear expansions of the sort Eq. (65) underlying most of electronic structure calculations. The Jacobian of the transformation is related to the Riemannian metric tensor

$$g_{ij} = \sum_{k=1}^{3} \frac{\partial \xi^k}{\partial r^i} \frac{\partial \xi^k}{\partial r^j}$$

$$\det J = \det{}^{-1/2}\{g_{ij}\} \tag{102}$$

which defines the metric of the ξ–space. The metric and thus the curvilinear co-ordinate system itself is considered as a variational parameter in the original fully adaptive–coordinate approach [263,264], see also Refs. [159,275,276,277,278]. Thus, a uniform grid in curved Riemannian space is non–uniform or distorted when viewed in flat Euclidean space (where $g_{ij} = \delta_{ij}$) such that the density of grid points (or the "local" cutoff energy of the expansion in terms of G–vectors) is highest in regions close to the nuclei and lowest in vacuum regions, see Fig. 2 in Ref. [275].

Concerning actual calculations, this means that a lower number of generalized plane waves than standard plane waves are needed in order to achieve a given accuracy [263], see Fig. 1 in Ref. [275]. This allows even for all–electron approaches to electronic structure calculations where plane waves fail [431,497]. More recently, the distortion of the metric was frozen spherically around atoms by introducing deformation functions [265,266], which leads to a concept closely connected to non–uniform atom–centered meshes in real–space methods [431], see below. In such non–fully–adaptive approaches using *predefined* coordinate transformations attention has to be given to Pulay force contributions which have to be evaluated explicitly [265,431].

2.8.4 Wavelets

Similar to using generalized plane waves is the idea to exploit the powerful multiscale–properties of wavelets. Since this approach requires an extensive introductory discussion (see e.g. Ref. [242] for a gentle introduction) and since it seems still quite far from being used in large–scale electronic structure calculations the interested reader is referred to original papers [134,674,699,652,241,25] and the general

wavelet literature cited therein. Wavelet–based methods allow intrinsically to exploit multiple length scales without introducing Pulay forces and can be efficiently handled by fast wavelet transforms. In addition, they are also a powerful route to linear scaling or "order–N" methods [453,243] as first demonstrated in Ref. [241] with the calculation of the Hartree potential for an all–electron uranium dimer.

2.8.5 Mixed and Augmented Basis Sets

Localized Gaussian basis functions on the one hand and plane waves on the other hand are certainly two extreme cases. There has been a tremendous effort to combine such localized and originless basis functions in order to exploit their mutual strengths. This resulted in a rich collection of mixed and augmented basis sets with very specific implementation requirements. This topic will not be covered here and the interested reader is referred to Refs. [75,654,498,370,371] and references given therein for some recent implementations used in conjunction with *ab initio* molecular dynamics.

2.8.6 Wannier Functions

An alternative to the plane wave basis set in the framework of periodic calculations in solid–state theory are Wannier functions, see for instance Sect. 10 in Ref. [27]. These functions are formally obtained from a unitary transformation of the Bloch orbitals Eq. (114) and have the advantage that they can be exponentially localized under certain circumstances. The so–called maximally localized generalized Wannier functions [413] are the periodic analogues of Boys' localized orbitals defined for isolated systems. Recently the usefulness of Wannier functions for numerical purposes was advocated by several groups, see Refs. [339,184,413,10] and references given therein.

2.8.7 Real Space Grids

A quite different approach is to leave conventional basis set approaches altogether and to resort to real–space methods where continuous space is replaced by a discrete space $\mathbf{r} \to r_{\mathbf{p}}$. This entails that the derivative operator or the entire energy expression has to be discretized in some way. The high–order central–finite difference approach leads to the expression

$$-\frac{1}{2}\nabla^2\psi_i(\mathbf{r}) \overset{h\to 0}{=} -\frac{1}{2}\Bigg[\sum_{n_x=-N}^{N} C_{n_x}\ \psi_i(r_{p_x} + n_x h, r_{p_y}, r_{p_z})$$
$$+ \sum_{n_y=-N}^{N} C_{n_y}\ \psi_i(r_{p_x}, r_{p_y} + n_y h, r_{p_z})$$
$$+ \sum_{n_z=-N}^{N} C_{n_z}\ \psi_i(r_{p_x}, r_{p_y}, r_{p_z} + n_z h)\Bigg] + \mathcal{O}\left(h^{2N+2}\right) \ (103)$$

for the Laplacian which is correct up to the order h^{2N+2}. Here, h is the uniform grid spacing and $\{C_{\mathbf{n}}\}$ are known expansion coefficients that depend on the selected order [130]. Within this scheme, not only the grid spacing h but also the order are

disposable parameters that can be optimized for a particular calculation. Note that the discretization points in continuous space can also be considered to constitute a sort of "finite basis set" – despite different statements in the literature – and that the "infinite basis set limit" is reached as $h \to 0$ for N fixed. A variation on the theme are Mehrstellen schemes where the discretization of the entire differential equation and not only of the derivative operator is optimized [89].

The first real–space approach devised for *ab initio* molecular dynamics was based on the lowest–order finite–difference approximation in conjunction with a equally–spaced cubic mesh in real space [109]. A variety of other implementations of more sophisticated real–space methods followed and include e.g. non–uniform meshes, multigrid acceleration, different discretization techniques, and finite–element methods [686,61,39,130,131,632,633,431,634]. Among the chief advantages of the real–space methods is that linear scaling approaches [453,243] can be implemented in a natural way and that the multiple–length scale problem can be coped with by adapting the grid. However, the extension to such non–uniform meshes induces the (in)famous Pulay forces (see Sect. 2.5) if the mesh moves as the nuclei move.

3 Basic Techniques: Implementation within the CPMD Code

3.1 Introduction and Basic Definitions

This section discusses the implementation of the plane wave–pseudopotential molecular dynamics method within the CPMD computer code [142]. It concentrates on the basics leaving advanced methods to later chapters. In addition all formulas are for the non-spin polarized case. This allows to show the essential features of a plane wave code as well as the reasons for its high performance in detail. The implementation of other versions of the presented algorithms and of the more advanced techniques in Sect. 4 is in most cases very similar.

There are many reviews on the pseudopotential plane wave method alone or in connection with the Car–Parrinello algorithm. Older articles [312,157,487,591] as well as the book by Singh [578] concentrate on the electronic structure part. Other reviews [513,472,223,224] present the plane wave method in connection with the molecular dynamics technique.

3.1.1 Unit Cell and Plane Wave Basis

The unit cell of a periodically repeated system is defined by the Bravais lattice vectors $\mathbf{a}_1$, $\mathbf{a}_2$, and $\mathbf{a}_3$. The Bravais vectors can be combined into a three by three matrix $\mathbf{h} = [\mathbf{a}_1, \mathbf{a}_2, \mathbf{a}_3]$ [459]. The volume Ω of the cell is calculated as the determinant of $\mathbf{h}$

$$\Omega = \det \mathbf{h} \ . \tag{104}$$

Further, scaled coordinates $\mathbf{s}$ are introduced that are related to $\mathbf{r}$ via $\mathbf{h}$

$$\mathbf{r} = \mathbf{h}\mathbf{s} \ . \tag{105}$$

Distances in scaled coordinates are related to distances in real coordinates by the metric tensor $\mathcal{G} = \mathbf{h}^{\mathrm{t}}\mathbf{h}$

$$(\mathbf{r}_i - \mathbf{r}_j)^2 = (\mathbf{s}_i - \mathbf{s}_j)^{\mathrm{t}}\mathcal{G}(\mathbf{s}_i - \mathbf{s}_j) \ . \tag{106}$$

Periodic boundary conditions can be enforced by using

$$\mathbf{r}_{\mathrm{pbc}} = \mathbf{r} - \mathbf{h}\big[\mathbf{h}^{-1}\mathbf{r}\big]_{\mathrm{NINT}} \ , \tag{107}$$

where $[\cdots]_{\mathrm{NINT}}$ denotes the nearest integer value. The coordinates $\mathbf{r}_{\mathrm{pbc}}$ will be always within the box centered around the origin of the coordinate system. Reciprocal lattice vectors $\mathbf{b}_i$ are defined as

$$\mathbf{b}_i \cdot \mathbf{a}_j = 2\pi\,\delta_{ij} \tag{108}$$

and can also be arranged to a three by three matrix

$$[\mathbf{b}_1, \mathbf{b}_2, \mathbf{b}_3] = 2\pi(\mathbf{h}^{\mathrm{t}})^{-1} \ . \tag{109}$$

Plane waves build a complete and orthonormal basis with the above periodicity (see also the section on plane waves in Sect. 2.8)

$$f_{\mathbf{G}}^{\mathrm{PW}}(\mathbf{r}) = \frac{1}{\sqrt{\Omega}}\exp[i\mathbf{G}\cdot\mathbf{r}] = \frac{1}{\sqrt{\Omega}}\exp[2\pi\,i\,\mathbf{g}\cdot\mathbf{s}] \ , \tag{110}$$

with the reciprocal space vectors

$$\mathbf{G} = 2\pi(\mathbf{h}^{\mathrm{t}})^{-1}\mathbf{g} \ , \tag{111}$$

where $\mathbf{g} = [i, j, k]$ is a triple of integer values. A periodic function can be expanded in this basis

$$\psi(\mathbf{r}) = \psi(\mathbf{r} + \mathbf{L}) = \frac{1}{\sqrt{\Omega}}\sum_{\mathbf{G}}\psi(\mathbf{G})\exp[i\,\mathbf{G}\cdot\mathbf{r}] \ , \tag{112}$$

where $\psi(\mathbf{r})$ and $\psi(\mathbf{G})$ are related by a three-dimensional Fourier transform. The direct lattice vectors $\mathbf{L}$ connect equivalent points in different cells.

3.1.2 Plane Wave Expansions

The Kohn–Sham potential (see Eq. (82)) of a periodic system exhibits the same periodicity as the direct lattice

$$V^{\mathrm{KS}}(\mathbf{r}) = V^{\mathrm{KS}}(\mathbf{r} + \mathbf{L}) \ , \tag{113}$$

and the Kohn–Sham orbitals can be written in Bloch form (see e.g. Ref. [27])

$$\Psi(\mathbf{r}) = \Psi_i(\mathbf{r}, \mathbf{k}) = \exp[i\,\mathbf{k}\cdot\mathbf{r}]\ u_i(\mathbf{r}, \mathbf{k}) \ , \tag{114}$$

where $\mathbf{k}$ is a vector in the first Brillouin zone. The functions $u_i(\mathbf{r}, \mathbf{k})$ have the periodicity of the direct lattice

$$u_i(\mathbf{r}, \mathbf{k}) = u_i(\mathbf{r} + \mathbf{L}, \mathbf{k}) \ . \tag{115}$$

The index i runs over all states and the states have an occupation $f_i(\mathbf{k})$ associated with them. The periodic functions $u_i(\mathbf{r}, \mathbf{k})$ are now expanded in the plane wave basis

$$u_i(\mathbf{r}, \mathbf{k}) = \frac{1}{\sqrt{\Omega}} \sum_{\mathbf{G}} c_i(\mathbf{G}, \mathbf{k}) \exp[i\mathbf{G} \cdot \mathbf{r}] \quad, \tag{116}$$

and the Kohn–Sham orbitals are

$$\phi_i(\mathbf{r}, \mathbf{k}) = \frac{1}{\sqrt{\Omega}} \sum_{\mathbf{G}} c_i(\mathbf{G}, \mathbf{k}) \exp[i(\mathbf{G} + \mathbf{k}) \cdot \mathbf{r}] \quad, \tag{117}$$

where $c_i(\mathbf{G}, \mathbf{k})$ are complex numbers. With this expansion the density can also be expanded into a plane wave basis

$$n(\mathbf{r}) = \frac{1}{\Omega} \sum_i \int d\mathbf{k} \, f_i(\mathbf{k}) \sum_{\mathbf{G}, \mathbf{G}'} c_i^{\star}(\mathbf{G}', \mathbf{k}) c_i(\mathbf{G}, \mathbf{k}) \exp[i(\mathbf{G} + \mathbf{k}) \cdot \mathbf{r}] \tag{118}$$

$$= \sum_{\mathbf{G}} n(\mathbf{G}) \exp[i\, \mathbf{G} \cdot \mathbf{r}] \quad, \tag{119}$$

where the sum over $\mathbf{G}$ vectors in Eq. (119) expands over double the range given by the wavefunction expansion. This is one of the main advantages of the plane wave basis. Whereas for atomic orbital basis sets the number of functions needed to describe the density grows quadratically with the size of the system, there is only a linear dependence for plane waves.

3.1.3 **K**–*Points and Cutoffs*

In actual calculations the infinite sums over $\mathbf{G}$ vectors and cells has to be truncated. Furthermore, we have to approximate the integral over the Brillouin zone by a finite sum over special $\mathbf{k}$–points

$$\int d\mathbf{k} \rightarrow \sum_{\mathbf{k}} w_{\mathbf{k}} \quad, \tag{120}$$

where w_k are the weights of the integration points. Schemes on how to choose the integration points efficiently are available in the literature [30,123,435] where also an overview [179] on the use of $\mathbf{k}$–points in the calculation of the electronic structure of solids can be found.

The truncation of the plane wave basis rests on the fact that the Kohn–Sham potential $V^{\mathrm{KS}}(\mathbf{G})$ converges rapidly with increasing modulus of $\mathbf{G}$. For this reason, at each $\mathbf{k}$–point, only $\mathbf{G}$ vectors with a kinetic energy lower than a given maximum cutoff

$$\frac{1}{2} \, |\mathbf{k} + \mathbf{G}|^2 \leq E_{\mathrm{cut}} \tag{121}$$

are included in the basis. With this choice of the basis the precision of the calculation within the approximations of density functional theory is controlled by one parameter E_{cut} only.

The number of plane waves for a given cutoff depends on the unit cell and the $\mathbf{k}$–point. An estimate for the size of the basis at the center of the Brillouin zone is

$$N_{\mathrm{PW}} = \frac{1}{2\pi^2} \, \Omega \, E_{\mathrm{cut}}^{3/2} \quad , \tag{122}$$

where E_{cut} is in Hartree units. The basis set needed to describe the density calculated from the Kohn-Sham orbitals has a corresponding cutoff that is four times the cutoff of the orbitals. The number of plane waves needed at a given density cutoff is therefore eight times the number of plane waves needed for the orbitals.

It is a common approximation in density functional theory calculations [536,169] to use approximate electronic densities. Instead of using the full description, the density is expanded in an auxiliary basis. An incomplete plane wave basis can be considered as an auxiliary basis with special properties [371]. Because of the filter property of plane waves the new density is an optimal approximation to the true density. No additional difficulties in calculations of the energy or forces appear. The only point to control is, if the accuracy of the calculation is still sufficient.

Finally, sums over all unit cells in real space have to be truncated. The only term in the final energy expression with such a sum is the real space part of the Ewald sum (see Sect. 3.2). This term is not a major contribution to the workload in a density functional calculation, that is the cutoff can be set rather generously.

3.1.4 Real Space Grid

A function given as a finite linear combination of plane waves can also be defined as a set of functional values on a equally spaced grid in real space. The sampling theorem (see e.g. Ref. [492]) gives the maximal grid spacing that still allows to hold the same information as the expansion coefficients of the plane waves. The real space sampling points $\mathbf{R}$ are defined

$$\mathbf{R} = \mathbf{h} \, \mathbf{N} \mathbf{q} \quad , \tag{123}$$

where $\mathbf{N}$ is a diagonal matrix with the entries $1/N_s$ and $\mathbf{q}$ is a vector of integers ranging from 0 to $N_s - 1$ (s = x, y, z). To fulfill the sampling theorem N_s has to be bigger than $2 \max(\mathbf{g}_s) + 1$. To be able to use fast Fourier techniques, N_s must be decomposable into small prime numbers (typically 2, 3, and 5). In applications the smallest number N_s that fulfills the above requirements is chosen.

A periodic function can be calculated at the real space grid points

$$f(\mathbf{R}) = \sum_{\mathbf{G}} f(\mathbf{G}) \exp[i \, \mathbf{G} \cdot \mathbf{R}] \tag{124}$$

$$= \sum_{\mathbf{g}} f(\mathbf{G}) \exp\left[2\pi \, i \, \left((\mathbf{h}^{\mathrm{t}})^{-1} \mathbf{g}\right) \cdot (\mathbf{h} \mathbf{N} \mathbf{q})\right] \tag{125}$$

$$= \sum_{\mathbf{g}} f(\mathbf{G}) \exp\left[\frac{2\pi}{N_{\mathrm{x}}} i g_{\mathrm{x}} q_{\mathrm{x}}\right] \exp\left[\frac{2\pi}{N_{\mathrm{y}}} i g_{\mathrm{y}} q_{\mathrm{y}}\right] \exp\left[\frac{2\pi}{N_{\mathrm{z}}} i g_{\mathrm{z}} q_{\mathrm{z}}\right] \quad . \tag{126}$$

The function $f(\mathbf{G})$ is zero outside the cutoff region and the sum over $\mathbf{g}$ can be extended over all indices in the cube $-\mathbf{g}_{\mathrm{s}}^{\mathrm{max}} \ldots \mathbf{g}_{\mathrm{s}}^{\mathrm{max}}$. The functions $f(\mathbf{R})$ and

$f(\mathbf{G})$ are related by three–dimensional Fourier transforms

$$f(\mathbf{R}) = \text{inv\_FT} [f(\mathbf{G})] \tag{127}$$

$$f(\mathbf{G}) = \text{fw\_FT} [f(\mathbf{R})] \ . \tag{128}$$

The Fourier transforms are defined by

$$[\text{inv\_FT} [f(\mathbf{G})]]_{uvw} = \sum_{j=0}^{N_x-1} \sum_{k=0}^{N_y-1} \sum_{l=0}^{N_z-1} f_{jkl}^{\mathbf{G}}$$
$$\exp\left[i\frac{2\pi}{N_x} j\,u\right] \exp\left[i\frac{2\pi}{N_y} k\,v\right] \exp\left[i\frac{2\pi}{N_z} l\,w\right] \tag{129}$$

$$[\text{fw\_FT} [f(\mathbf{R})]]_{jkl} = \sum_{u=0}^{N_x-1} \sum_{v=0}^{N_y-1} \sum_{w=0}^{N_z-1} f_{uvw}^{\mathbf{R}}$$
$$\exp\left[-i\frac{2\pi}{N_x} j\,u\right] \exp\left[-i\frac{2\pi}{N_y} k\,v\right] \exp\left[-i\frac{2\pi}{N_z} l\,w\right] \ , \tag{130}$$

where the appropriate mappings of $\mathbf{q}$ and $\mathbf{g}$ to the indices

$$[u, v, w] = \mathbf{q} \tag{131}$$

$$\{j, k, l\} = \mathbf{g}_s \quad \text{if} \ \ \mathbf{g}_s \geq 0 \tag{132}$$

$$\{j, k, l\} = N_s + \mathbf{g}_s \quad \text{if} \ \ \mathbf{g}_s \langle 0 \tag{133}$$

have to be used. From Eqs. (129) and (130) it can be seen, that the calculation of the three–dimensional Fourier transforms can be performed by a series of one dimensional Fourier transforms. The number of transforms in each direction is $N_x N_y$, $N_x N_z$, and $N_y N_z$ respectively. Assuming that the one-dimensional transforms are performed within the fast Fourier transform framework, the number of operations per transform of length n is approximately $5n \log n$. This leads to an estimate for the number of operations for the full three-dimensional transform of $5N \log N$, where $N = N_x N_y N_z$.

3.1.5 Pseudopotentials

In order to minimize the size of the plane wave basis necessary for the calculation, core electrons are replaced by pseudopotentials. The pseudopotential approximation in the realm of solid–state theory goes back to the work on orthogonalized plane waves [298] and core state projector methods [485]. Empirical pseudopotentials were used in plane wave calculations [294,703] but new developments have considerably increased efficiency and reliability of the method. Pseudopotential are required to correctly represent the long range interactions of the core and to produce pseudo–wavefunction solutions that approach the full wavefunction outside a core radius r_c. Inside this radius the pseudopotential and the wavefunction should be as smooth as possible, in order to allow for a small plane wave cutoff. For the pseudo–wavefunction this requires that the nodal structure of the valence wavefunctions is replaced by a smooth function. In addition it is desired that a pseudopotential is transferable [238,197], this means that one and the same pseudopotential can be

used in calculations of different chemical environment resulting in calculations with comparable accuracy.

A first major step to achieve all this conflicting goals was the introduction of "norm–conservation" [622,593]. Norm–conserving pseudopotentials have to be angular momentum dependent. In their most general form they are semi–local

$$V^{\mathrm{PP}}(\mathbf{r}, \mathbf{r}') = \sum_{lm} Y_{lm}(\mathbf{r}) V_l(\mathbf{r}) \delta_{\mathbf{r},\mathbf{r}'} Y_{lm}(\mathbf{r}') \ , \tag{134}$$

where Y_{lm} are spherical harmonics. A minimal set of requirements and a construction scheme for soft, semi–local pseudopotentials were developed [274,28]. Since then many variations of the original method have been proposed, concentrating either on an improvement in softness or in transferability. Analytic representations of the core part of the potential [326,626,627,509] were used. Extended norm-conservation [564] was introduced to enhance transferability and new concepts to increase the softness were presented [659,509,369]. More information on pseudopotentials and their construction can be found in recent review articles [487,578,221].

Originally generated in a semi-local form, most applications use the fully separable form. Pseudopotentials can be transformed to the separable form using atomic wavefunctions [335,73,659]. Recently [239,288] a new type of separable, norm-conserving pseudopotentials was introduced. Local and non-local parts of these pseudopotentials have a simple analytic form and only a few parameters are needed to characterize the potential. These parameters are globally optimized in order to reproduce many properties of atoms and ensure a good transferability.

A separable non-local pseudopotential can be put into general form (this includes all the above mentioned types)

$$V^{\mathrm{PP}}(\mathbf{r}, \mathbf{r}') = (V_{\mathrm{core}}(\mathbf{r}) + \Delta V_{\mathrm{local}}(\mathbf{r})) \, \delta_{\mathbf{r},\mathbf{r}'} + \sum_{k,l} P_k^\star(\mathbf{r}) h_{kl} P_l(\mathbf{r}') \ . \tag{135}$$

The local part has been split into a core ($\sim 1/r$ for $r \to \infty$) and a short-ranged local part in order to facilitate the derivation of the final energy formula. The actual form of the core potential will be defined later. The local potential $\Delta V_{\mathrm{local}}$ and the projectors P_k are atom-centered functions of the form

$$\varphi(\mathbf{r}) = \varphi(|\mathbf{r} - \mathbf{R}_I|) \, Y_{lm}(\theta, \phi) \ , \tag{136}$$

that can be expanded in plane waves

$$\varphi(\mathbf{r}) = \sum_{\mathbf{G}} \varphi(G) \exp[i\mathbf{G} \cdot \mathbf{r}] \, S_I(\mathbf{G}) \, Y_{lm}(\tilde{\theta}, \tilde{\phi}) \ , \tag{137}$$

$\mathbf{R}_I$ denote atomic positions and the so–called structure factors S_I are defined as

$$S_I(\mathbf{G}) = \exp[-i\mathbf{G} \cdot \mathbf{R}_I] \ . \tag{138}$$

The functions $\varphi(G)$ are calculated from $\varphi(r)$ by a Bessel transform

$$\varphi(G) = 4\pi \, (-i)^l \int_0^\infty dr \, r^2 \, \varphi(r) \, j_l(Gr) \ , \tag{139}$$

where j_l are spherical Bessel functions of the first kind. The local pseudopotential and the projectors of the nonlocal part in Fourier space are given by

$$\Delta V_{\text{local}}(\mathbf{G}) = \frac{4\pi}{\Omega} \int_0^\infty dr \, r^2 \, \Delta V_{\text{local}}(r) j_0(Gr) \tag{140}$$

$$P_k(\mathbf{G}) = \frac{4\pi}{\sqrt{\Omega}} (-i)^l \int_0^\infty dr \, r^2 \, P_k(r) \, j_l(Gr) \, Y_{lm}(\tilde{\theta}, \tilde{\phi}) \; , \tag{141}$$

where lm are angular momentum quantum numbers associated with projector α.

3.2 Electrostatic Energy

3.2.1 General Concepts

The electrostatic energy of a system of nuclear charges Z_I at positions $\mathbf{R}_I$ and an electronic charge distribution $n(\mathbf{r})$ consists of three parts: the Hartree energy of the electrons, the interaction energy of the electrons with the nuclei and the internuclear interactions

$$\begin{aligned}
E_{\text{ES}} = \; & \frac{1}{2} \iint d\mathbf{r} \, d\mathbf{r}' \, \frac{n(\mathbf{r})n(\mathbf{r}')}{|\mathbf{r} - \mathbf{r}'|} \\
& + \sum_I \int d\mathbf{r} \, V_{\text{core}}^I(\mathbf{r}) n(\mathbf{r}) + \frac{1}{2} \sum_{I \neq J} \frac{Z_I Z_J}{|\mathbf{R}_I - \mathbf{R}_J|} \; .
\end{aligned} \tag{142}$$

The Ewald method (see e.g. Ref. [12]) can be used to avoid singularities in the individual terms when the system size is infinite. In order to achieve this a Gaussian core charge distribution associated with each nuclei is defined

$$n_{\text{c}}^I(\mathbf{r}) = -\frac{Z_I}{(\mathrm{R}_I^{\text{c}})^3} \pi^{-3/2} \exp\left[-\left(\frac{\mathbf{r} - \mathbf{R}_I}{\mathrm{R}_I^{\text{c}}} \right)^2 \right] \; . \tag{143}$$

It is convenient at this point to make use of the arbitrariness in the definition of the core potential and define it to be the potential of the Gaussian charge distribution of Eq. (143)

$$V_{\text{core}}^I(\mathbf{r}) = \int d\mathbf{r}' \, \frac{n_{\text{c}}^I(\mathbf{r}')}{|\mathbf{r} - \mathbf{r}'|} = -\frac{Z_I}{|\mathbf{r} - \mathbf{R}_I|} \text{erf}\left[\frac{|\mathbf{r} - \mathbf{R}_I|}{\mathrm{R}_I^{\text{c}}} \right] \; , \tag{144}$$

where erf is the error function. The interaction energy of this Gaussian charge

distributions is now added and subtracted from the total electrostatic energy

$$
\begin{aligned}
E_{\mathrm{ES}} = {} & \frac{1}{2} \iint d\mathbf{r}\, d\mathbf{r}'\, \frac{n(\mathbf{r})n(\mathbf{r}')}{|\mathbf{r}-\mathbf{r}'|} \\
& + \frac{1}{2} \iint d\mathbf{r}\, d\mathbf{r}'\, \frac{n_{\mathrm{c}}(\mathbf{r})n_{\mathrm{c}}(\mathbf{r}')}{|\mathbf{r}-\mathbf{r}'|} \\
& + \iint d\mathbf{r}\, d\mathbf{r}'\, \frac{n_{\mathrm{c}}(\mathbf{r})n(\mathbf{r}')}{|\mathbf{r}-\mathbf{r}'|} \\
& + \frac{1}{2} \sum_{I \neq J} \frac{Z_I Z_J}{|\mathbf{R}_I - \mathbf{R}_J|} \\
& - \frac{1}{2} \iint d\mathbf{r}\, d\mathbf{r}'\, \frac{n_{\mathrm{c}}(\mathbf{r})n_{\mathrm{c}}(\mathbf{r}')}{|\mathbf{r}-\mathbf{r}'|} \quad ,
\end{aligned}
\tag{145}
$$

where $n_{\mathrm{c}}(\mathbf{r}) = \sum_I n_{\mathrm{c}}^I(\mathbf{r})$. The first three terms can be combined to the electrostatic energy of a total charge distribution $n_{\mathrm{tot}}(\mathbf{r}) = n(\mathbf{r}) + n_{\mathrm{c}}(\mathbf{r})$. The remaining terms are rewritten as a double sum over nuclei and a sum over self–energy terms of the Gaussian charge distributions

$$
\begin{aligned}
E_{\mathrm{ES}} = {} & \frac{1}{2} \iint d\mathbf{r}\, d\mathbf{r}'\, \frac{n_{\mathrm{tot}}(\mathbf{r})n_{\mathrm{tot}}(\mathbf{r}')}{|\mathbf{r}-\mathbf{r}'|} \\
& + \frac{1}{2} \sum_{I \neq J} \frac{Z_I Z_J}{|\mathbf{R}_I - \mathbf{R}_J|} \mathrm{erfc}\left[\frac{|\mathbf{R}_I - \mathbf{R}_J|}{\sqrt{\mathrm{R}_I^{\mathrm{c}\,2} + \mathrm{R}_J^{\mathrm{c}\,2}}} \right] - \sum_I \frac{1}{\sqrt{2\pi}} \frac{Z_I^2}{R_I^{\mathrm{c}}} \quad ,
\end{aligned}
\tag{146}
$$

where erfc denotes the complementary error function.

3.2.2 Periodic Systems

For a periodically repeated system the total energy per unit cell is derived from the above expression by using the solution to Poisson's equation in Fourier space for the first term and make use of the quick convergence of the second term in real space. The total charge is expanded in plane waves with expansion coefficients

$$
n_{\mathrm{tot}}(\mathbf{G}) = n(\mathbf{G}) + \sum_I n_{\mathrm{c}}^I(\mathbf{G}) S_I(\mathbf{G})
\tag{147}
$$

$$
= n(\mathbf{G}) - \frac{1}{\Omega} \sum_I \frac{Z_I}{\sqrt{4\pi}} \exp\left[-\frac{1}{2} G^2 R_I^{\mathrm{c}\,2} \right] S_I(\mathbf{G}) \ .
\tag{148}
$$

This leads to the electrostatic energy for a periodic system

$$
E_{\mathrm{ES}} = 2\pi\, \Omega \sum_{\mathbf{G} \neq 0} \frac{|n_{\mathrm{tot}}(\mathbf{G})|^2}{G^2} + E_{\mathrm{ovrl}} - E_{\mathrm{self}} \quad ,
\tag{149}
$$

where

$$
E_{\mathrm{ovrl}} = \sum_{I,J}{}' \sum_{\mathbf{L}} \frac{Z_I Z_J}{|\mathbf{R}_I - \mathbf{R}_J - \mathbf{L}|} \mathrm{erfc}\left[\frac{|\mathbf{R}_I - \mathbf{R}_J - \mathbf{L}|}{\sqrt{\mathrm{R}_I^{\mathrm{c}\,2} + \mathrm{R}_J^{\mathrm{c}\,2}}} \right]
\tag{150}
$$

and

$$E_{\mathrm{self}} = \sum_I \frac{1}{\sqrt{2\pi}} \frac{Z_I^2}{R_I^{\mathrm{c}}} \ . \tag{151}$$

Here, the sums expand over all atoms in the simulation cell, all direct lattice vectors $\mathbf{L}$, and the prime in the first sum indicates that $I \langle J$ is imposed for $\mathbf{L} = \mathbf{0}$.

3.2.3   Cluster Boundary Conditions

The possibility to use fast Fourier transforms to calculate the electrostatic energy is one of the reasons for the high performance of plane wave calculations. However, plane wave based calculations imply periodic boundary conditions. This is appropriate for crystal calculations but very unnatural for molecule or slab calculations. For neutral systems this problem is circumvented by use of the supercell method. Namely, the molecule is periodically repeated but the distance between each molecule and its periodic images is so large that their interaction is negligible. This procedure is somewhat wasteful but can lead to satisfactory results.

Handling charged molecular systems is, however, considerably more difficult, due to the long range Coulomb forces. A charged periodic system has infinite energy and the interaction between images cannot really be completely eliminated. In order to circumvent this problem several solutions have been proposed. The simplest fix-up is to add to the system a neutralizing background charge. This is achieved trivially as the $\mathbf{G} = \mathbf{0}$ term in Eq. (149) is already eliminated. This leads to finite energies but does not eliminate the interaction between the images and makes the calculation of absolute energies difficult. Other solutions involve performing a set of different calculations on the system such that extrapolation to the limit of infinitely separated images is possible. This procedure is lengthy and one cannot use it easily in molecular dynamics applications. It has been shown, that it is possible to estimate the correction to the total energy for the removal of the image charges [378]. Still it seems not easy to incorporate this scheme into the frameworks of molecular dynamics. Another method [60,702,361] works with the separation of the long and short range parts of the Coulomb forces. In this method the low–order multipole moments of the charge distribution are separated out and handled analytically. This method was used in the context of coupling *ab initio* and classical molecular dynamics [76].

The long-range forces in Eq. (146) are contained in the first term. This term can be written

$$\frac{1}{2} \int\!\!\int d\mathbf{r}\, d\mathbf{r}' \frac{n_{\mathrm{tot}}(\mathbf{r}) n_{\mathrm{tot}}(\mathbf{r}')}{|\mathbf{r} - \mathbf{r}'|} = \frac{1}{2} \int d\mathbf{r}\, V_{\mathrm{H}}(\mathbf{r}) n_{\mathrm{tot}}(\mathbf{r}) \ , \tag{152}$$

where the electrostatic potential $V_{\mathrm{H}}(\mathbf{r})$ is the solution of Poisson's equation (see Eq. (80)). There are two approaches to solve Poisson's equation subject to the boundary conditions $V_{\mathrm{H}}(\mathbf{r}) \to 0$ for $\mathbf{r} \to \infty$ implemented in CPMD. Both of them rely on fast Fourier transforms, thus keeping the same framework as for the periodic case.

The first method is due to Hockney [300] and was first applied to density functional plane wave calculations in Ref. [36]. In the following outline, for the sake of simplicity,

a one-dimensional case is presented. The charge density is assumed to be non-zero only within an interval L and sampled on N equidistant points. These points are denoted by x_p. The potential can then be written

$$V_{\mathrm{H}}(x_p) = \frac{L}{N} \sum_{p'=-\infty}^{\infty} G(x_p - x_{p'})n(x_{p'}) \tag{153}$$

$$= \frac{L}{N} \sum_{p'=0}^{N} G(x_p - x_{p'})n(x_{p'}) \tag{154}$$

for $p = 0, 1, 2, \ldots N$, where $G(x_p - x_{p'})$ is the corresponding Green's function. In Hockney's algorithm this equation is replaced by the cyclic convolution

$$\tilde{V}_{\mathrm{H}}(x_p) = \frac{L}{N} \sum_{p'=0}^{2N+1} \tilde{G}(x_p - x_{p'})\tilde{n}(x_{p'}) \tag{155}$$

where $p = 0, 1, 2, \ldots 2N + 1$, and

$$\tilde{n}(x_p) = \begin{cases} n(x_p) & 0 \ \leq p \leq N \\ 0 & N \leq p \leq 2N+1 \end{cases} \tag{156}$$

$$\tilde{G}(x_p) = G(x_p) \qquad -(N+1) \leq p \leq N \tag{157}$$

$$\tilde{n}(x_p) = \tilde{n}(x_p + L) \tag{158}$$

$$\tilde{G}(x_p) = \tilde{G}(x_p + L) \tag{159}$$

The solution $\tilde{V}_{\mathrm{H}}(x_p)$ can be obtained by a series of fast Fourier transforms and has the desired property

$$\tilde{V}_{\mathrm{H}}(x_p) = V_{\mathrm{H}}(x_p) \quad \text{for } 0 \leq p \leq N \ . \tag{160}$$

To remove the singularity of the Green's function at $x = 0$, $G(x)$ is modified for small x and the error is corrected by using the identity

$$G(x) = \frac{1}{x}\mathrm{erf}\left[\frac{x}{r_{\mathrm{c}}}\right] + \frac{1}{x}\mathrm{erfc}\left[\frac{x}{r_{\mathrm{c}}}\right] \ , \tag{161}$$

where r_{c} is chosen such, that the short-ranged part can be accurately described by a plane wave expansion with the density cutoff. In an optimized implementation Hockney's method requires the double amount of memory and two additional fast Fourier transforms on the box of double size (see Fig. 6 for a flow chart). Hockney's method can be generalized to systems with periodicity in one (wires) and two (slabs) dimensions. It was pointed out [173] that Hockney's method gives the exact solution to Poisson's equation for isolated systems if the boundary condition (zero density at the edges of the box) are fulfilled.

A different, fully reciprocal space based method, that can be seen as an approximation to Hockney's method, was recently proposed [393]. The final expression for the Hartree energy is also based on the splitting of the Green's function in Eq. (161)

$$E_{\mathrm{ES}} = 2\pi \Omega \sum_{\mathbf{G}} V_{\mathrm{H}}^{\mathrm{MT}}(\mathbf{G})n_{\mathrm{tot}}^{\star}(\mathbf{G}) + E_{\mathrm{ovrl}} - E_{\mathrm{self}} \ . \tag{162}$$
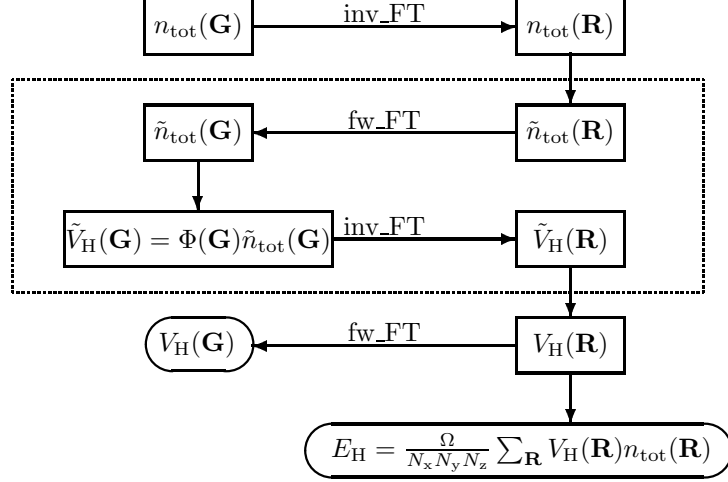
Figure 6. Flow chart for the calculation of long-ranged part of the electrostatic energy using the method by Hockney [300]. The part inside the dashed box is calculated most efficiently with the procedure outlined by Eastwood and Brownrigg [173].

The potential function is calculated from two parts,

$$V_H^{MT}(\mathbf{G}) = \bar{V}_H(\mathbf{G}) + \tilde{V}_H(\mathbf{G}) \ , \tag{163}$$

where $\tilde{V}_H(\mathbf{G})$ is the analytic part, calculated from a Fourier transform of erfc

$$\tilde{V}_H(\mathbf{G}) = \frac{4\pi}{G^2} \left(1 - \exp\left[-\frac{G^2 r_c^2}{4} \right] \right) n(\mathbf{G}) \tag{164}$$

and $\bar{V}_H(\mathbf{G})$ is calculated from a discrete Fourier transform of the Green's function on an appropriate grid. The calculation of the Green's function can be done at the beginning of the calculation and has not to be repeated again. It is reported [393] that a cutoff of ten to twenty percent higher than the one employed for the charge density gives converged results. The same technique can also be applied for systems that are periodic in one and two dimensions [394].

If the boundary conditions are appropriately chosen, the discrete Fourier transforms for the calculation of $\bar{V}_H(\mathbf{G})$ can be performed analytically [437]. This is possible for the limiting case where $r_c = 0$ and the boundary conditions are on a sphere of radius R for the cluster. For a one-dimensional system we choose a torus of radius R and for the two-dimensional system a slab of thickness Z. The electrostatic potential for these systems are listed in Table 2, where $G_{xy} = \left[g_x^2 + g_y^2 \right]^{1/2}$ and J_n and K_n are the Bessel functions of the first and second kind of integer order n.

Hockney's method requires a computational box such that the charge density is negligible at the edges. This is equivalent to the supercell approach [510]. Practical experience tells that a minimum distance of about 3 Å of all atoms to the edges of

Table 2. Fourier space formulas for the Hartree energy, see text for definitions.

Dim.	periodic	$(G^2/4\pi)V_{\mathrm{H}}(\mathbf{G})$	$V_{\mathrm{H}}(\mathbf{0})$
0	–	$(1 - \cos[RG])\,n(\mathbf{G})$	$2\pi R^2 n(0)$
1	z	$(1 + R\,(G_{\mathrm{xy}}J_1(RG_{\mathrm{xy}})\,K_0(Rg_{\mathrm{z}})$	
		$-g_{\mathrm{z}}J_0(RG_{\mathrm{xy}})\,K_1(Rg_{\mathrm{z}})))\,n(\mathbf{G})$	0
2	x, y	$(1 - (-1)^{g_{\mathrm{z}}}\exp[-GZ/2])\,n(\mathbf{G})$	0
3	x, y, z	$n(\mathbf{G})$	0

the box is sufficient for most systems. The Green's function is then applied to the charge density in a box double this size. The Green's function has to be calculated only once at the beginning of the calculation. The other methods presented in this chapter require a computational box of double the size of the Hockney method as they are applying the artificially periodic Green's function within the computational box. This can only be equivalent to the exact Hockney method if the box is enlarged to double the size. In plane wave calculations computational costs grow linearly with the volume of the box. Therefore Hockney's method will prevail over the others in accuracy, speed, and memory requirements in the limit of large systems. The direct Fourier space methods have advantages through their easy implementation and for small systems, if not full accuracy is required, i.e. if they are used with smaller computational boxes. In addition, they can be of great use in calculations with classical potentials.

3.3 Exchange and Correlation Energy

Exchange and correlation functionals implemented in the CPMD code are of the local type with gradient corrections. These type of functionals can be written as (see also Eqs. (88) and (84))

$$E_{\mathrm{xc}} = \int d\mathbf{r}\,\varepsilon_{\mathrm{xc}}(n, \nabla n)\,n(\mathbf{r}) = \Omega \sum_{\mathbf{G}} \varepsilon_{\mathrm{xc}}(\mathbf{G})n^{\star}(\mathbf{G}) \tag{165}$$

with the corresponding potential

$$V_{\mathrm{xc}}(\mathbf{r}) = \frac{\partial F_{\mathrm{xc}}}{\partial n} - \sum_s \frac{\partial}{\partial \mathbf{r}_s}\left[\frac{\partial F_{\mathrm{xc}}}{\partial(\partial_s n)}\right]\ , \tag{166}$$

where $F_{\mathrm{xc}} = \varepsilon_{\mathrm{xc}}(n, \nabla n)n$ and $\partial_s n$ is the s-component of the density gradient.

Exchange and correlation functionals have complicated analytical forms that give rise to high frequency components in $\varepsilon_{\mathrm{xc}}(\mathbf{G})$. Although these high frequency components do not enter the sum in Eq. (165) due to the filter effect of the density, they affect the calculation of $\varepsilon_{\mathrm{xc}}$. As the functionals are only local in real space, not in Fourier space, they have to be evaluated on a real space grid. The function $\varepsilon_{\mathrm{xc}}(\mathbf{G})$ can then be calculated by a Fourier transform. Therefore the exact calculation of E_{xc} would require a grid with infinite resolution. However, the high frequency components are usually very small and even a moderate grid gives accurate results. The use of a finite grid results in an effective redefinition of the exchange and

correlation energy

$$E_{\mathrm{xc}} = \frac{\Omega}{N_{\mathrm{x}}N_{\mathrm{y}}N_{\mathrm{z}}} \sum_{\mathbf{R}} \varepsilon_{\mathrm{xc}}(n, \nabla n)(\mathbf{R})n(\mathbf{R}) = \Omega \sum_{\mathbf{G}} \tilde{\varepsilon}_{\mathrm{xc}}(\mathbf{G})n(\mathbf{G}) \ , \qquad (167)$$

where $\tilde{\varepsilon}_{\mathrm{xc}}(\mathbf{G})$ is the finite Fourier transform of $\varepsilon_{\mathrm{xc}}(\mathbf{R})$. This definition of E_{xc} allows the calculation of all gradients analytically. In most applications the real space grid used in the calculation of the density and the potentials is also used for the exchange and correlation energy. Grids with higher resolution can be used easily. The density is calculated on the new grid by use of Fourier transforms and the resulting potential is transfered back to the original grid. With this procedure the different grids do not have to be commensurate.

The above redefinition has an undesired side effect. The new exchange and correlation energy is no longer translationally invariant. Only translations by a multiple of the grid spacing do not change the total energy. This introduces a small modulation of the energy hyper surface [685], known as "ripples". Highly accurate optimizations of structures and the calculation of harmonic frequencies can be affected by the ripples. Using a denser grid for the calculation of E_{xc} is the only solution to avoid these problems.

The calculation of a gradient corrected functional within the plane wave framework can be conducted using Fourier transforms [685]. The flowchart of the calculation is presented in Fig. 7. With the use of Fourier transforms the calculation of second derivatives of the charge density is avoided, leading to a numerically stable algorithm. To this end the identity

$$\frac{\partial F_{\mathrm{xc}}}{\partial(\partial_s n)} = \frac{\partial F_{\mathrm{xc}}}{\partial|\nabla n|} \frac{\partial_s n}{|\nabla n|} \qquad (168)$$

is used.

This is the place to say some words on functionals that include exact exchange. As mentioned in Sect. 2.7 this type of functional has been very popular recently and improvements of results over GGA–type density functionals for many systems and properties have been reported. However, the calculation of the Hartree–Fock exchange causes a considerable performance problem in plane wave calculations. The Hartree–Fock exchange energy is defined as [604]

$$E_{\mathrm{HFX}} = \sum_{ij} \int\int d\mathbf{r}d\mathbf{r}' \frac{\rho_{ij}(\mathbf{r})\rho_{ij}(\mathbf{r}')}{|\mathbf{r} - \mathbf{r}'|} \ , \qquad (169)$$

where

$$\rho_{ij}(\mathbf{r}) = \phi_i(\mathbf{r})\phi_j(\mathbf{r}). \qquad (170)$$

From this expression the wavefunction force is easily derived and can be calculated in Fourier space

$$\frac{1}{f_i}\frac{\partial E_{\mathrm{HFX}}}{\partial c_i^{\star}(\mathbf{G})} = \sum_j \sum_{\mathbf{G}'} V_{\mathrm{HFX}}^{ij}(\mathbf{G} - \mathbf{G}')c_j(\mathbf{G}') \ . \qquad (171)$$

The force calculation is best performed in real space, whereas the potential is calculated in Fourier space. For a system with N_{b} electronic states and N real space
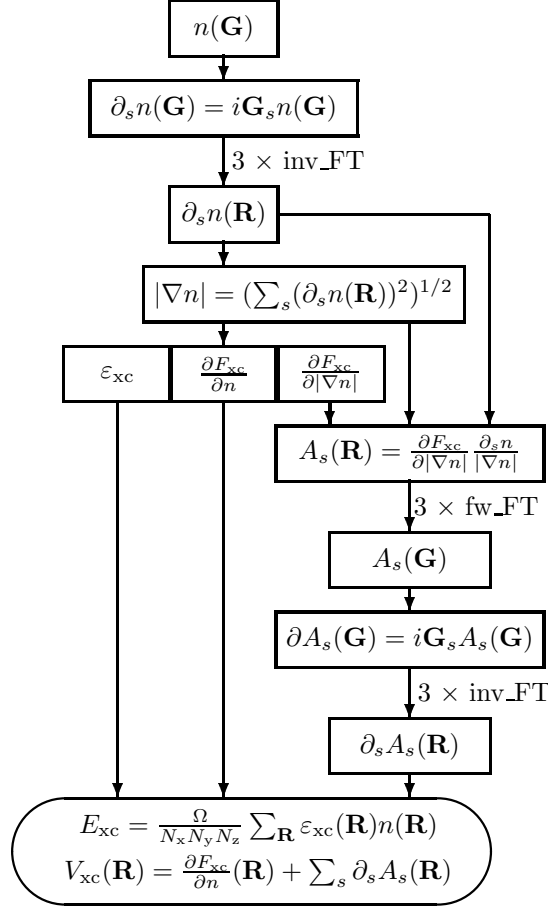
Figure 7. Flow chart for the calculation of the energy and potential of a gradient corrected exchange and correlation functional.

grid points, a total of $5N_{\mathrm{b}}^2$ three–dimensional transforms are needed, resulting in approximately $25N_{\mathrm{b}}^2 N \log N$ operations needed to perform the calculation. This has to be compared to the $15N_{\mathrm{b}}N \log N$ operations needed for the other Fourier transforms of the charge density and the application of the local potential and the $4N_{\mathrm{b}}^2 N$ operations for the orthogonalization step. In calculations dominated by the Fourier transforms an additional factor of at least N_{b} is needed. If on the other hand orthogonalization dominates an increase in computer time by a factor of $5 \log N$ is expected. Therefore, at least an order of magnitude more computer time is needed for calculations including exact exchange compared to ordinary density functional calculations. Consequently, hybrid functionals will only be used in exceptional cases together with plane waves [262,128].

3.4 Total Energy, Gradients, and Stress Tensor

3.4.1 Total Energy

Molecular dynamics calculations with interaction potentials derived from density functional theory require the evaluation of the total energy and derivatives with respect to the parameters of the Lagrangian. In this section formulas are given in Fourier space for a periodic system. The total energy can be calculated as a sum of kinetic, external (local and non-local pseudopotential), exchange and correlation, and electrostatic energy (to be compared with Eq. (75))

$$E_{\text{total}} = E_{\text{kin}} + E_{\text{local}}^{\text{PP}} + E_{\text{nonlocal}}^{\text{PP}} + E_{\text{xc}} + E_{\text{ES}} \ . \tag{172}$$

The individual terms are defined by

$$E_{\text{kin}} = \sum_{\mathbf{k}} w_{\mathbf{k}} \sum_{i} \sum_{\mathbf{G}} \frac{1}{2} f_i(\mathbf{k}) \, |\mathbf{G} + \mathbf{k}|^2 \, |c_i(\mathbf{G}, \mathbf{k})|^2 \tag{173}$$

$$E_{\text{local}}^{\text{PP}} = \sum_{I} \sum_{\mathbf{G}} \Delta V_{\text{local}}^I(\mathbf{G}) \, S_I(\mathbf{G}) n^\star(\mathbf{G}) \tag{174}$$

$$E_{\text{nonlocal}}^{\text{PP}} = \sum_{\mathbf{k}} w_{\mathbf{k}} \sum_{i} f_i(\mathbf{k}) \sum_{I} \sum_{\alpha,\beta \in I} \left(F_{I,i}^\alpha(\mathbf{k}) \right)^\star h_{\alpha\beta}^I F_{I,i}^\beta(\mathbf{k}) \tag{175}$$

$$E_{\text{xc}} = \Omega \sum_{\mathbf{G}} \epsilon_{\text{xc}}(\mathbf{G}) n^\star(\mathbf{G}) \tag{176}$$

$$E_{\text{ES}} = 2\pi \, \Omega \sum_{\mathbf{G} \neq 0} \frac{|n_{\text{tot}}(\mathbf{G})|^2}{G^2} + E_{\text{ovrl}} - E_{\text{self}}. \tag{177}$$

The overlap between the projectors of the non-local pseudopotential and the Kohn–Sham orbitals has been introduced in the equation above

$$F_{I,i}^\alpha(\mathbf{k}) = \frac{1}{\sqrt{\Omega}} \sum_{\mathbf{G}} P_\alpha^I(\mathbf{G}) \, S_I(\mathbf{G} + \mathbf{k}) \, c_i^\star(\mathbf{G}, \mathbf{k}) \ . \tag{178}$$

An alternative expression, using the Kohn–Sham eigenvalues $\epsilon_i(\mathbf{k})$ can also be used

$$\begin{aligned}
E_{\text{total}} = & \sum_{\mathbf{k}} w_{\mathbf{k}} \sum_{i} f_i(\mathbf{k}) \epsilon_i(\mathbf{k}) \\
& - \Omega \sum_{\mathbf{G}} \left(V_{\text{xc}}(\mathbf{G}) - \varepsilon_{\text{xc}}(\mathbf{G}) \right) n^\star(\mathbf{G}) \\
& - 2\pi \, \Omega \sum_{\mathbf{G} \neq 0} \frac{|n(\mathbf{G})|^2 - |n_{\text{c}}(\mathbf{G})|^2}{G^2} + E_{\text{ovrl}} - E_{\text{self}} \\
& + \Delta E_{\text{tot}} \ ,
\end{aligned} \tag{179}$$

to be compared to Eq. (86). The additional term ΔE_{tot} in Eq. (179) is needed to have an expression for the energy that is quadratic in the variations of the charge density, as it is true for Eq. (172). Without the correction term, which is zero for the exact charge density, small differences between the computed and the exact

density could give rise to large errors in the total energy [129]. The correction energy can be calculated from

$$\Delta E_{\text{tot}} = -2\pi\,\Omega\,\sum_{\mathbf{G}\neq 0}\left(\frac{n^{\text{in}}(\mathbf{G})}{G^2}-\frac{n^{\text{out}}(\mathbf{G})}{G^2}\right)(n^{\text{out}}(\mathbf{G}))^\star$$
$$-\Omega\sum_{\mathbf{G}}\left(V_{\text{xc}}^{\text{in}}(\mathbf{G})-V_{\text{xc}}^{\text{out}}(\mathbf{G})\right)(n^{\text{out}}(\mathbf{G}))^\star, \tag{180}$$

where n^{in} and n^{out} are the input and output charge densities and $V_{\text{xc}}^{\text{in}}$ and $V_{\text{xc}}^{\text{out}}$ the corresponding exchange and correlation potentials. This term leads to the so–called "non–self–consistency correction" of the force, introduced in Eq. (68).

The use of an appropriate $\mathbf{k}$–point mesh is the most efficient method to calculate the total energy of a periodic system. Equivalent, although not as efficient, the calculation can be performed using a supercell consisting of replications of the unit cell and a single integration point for the Brillouin zone. In systems where the translational symmetry is broken, e.g. disorder systems, liquids, or thermally excited crystals, periodic boundary conditions can still be used if combined with a supercell approach. Many systems investigated with the here described method fall into these categories, and therfore most calculations using the Car-Parrinello molecular dynamics approach are using supercells and a single $\mathbf{k}$–point "integration scheme". The only point calculated is the center of the Brillouin zone (Γ–point; $\mathbf{k}=\mathbf{0}$). For the remainder of this chapter, all formulas are given for the Γ–point approximation.

3.4.2 Wavefunction Gradient

Analytic derivatives of the total energy with respect to the parameters of the calculation are needed for stable molecular dynamics calculations. All derivatives needed are easily accessible in the plane wave pseudopotential approach. In the following Fourier space formulas are presented

$$\frac{1}{f_i}\frac{\partial E_{\text{total}}}{\partial c_i^\star(\mathbf{G})} = \frac{1}{2}\,G^2\,c_i(\mathbf{G})$$
$$+\sum_{\mathbf{G}'}V_{\text{loc}}^\star(\mathbf{G}-\mathbf{G}')c_i(\mathbf{G}')$$
$$+\sum_{I}\sum_{\alpha,\beta}\left(F_{I,i}^\alpha\right)^\star h_{\alpha\beta}^I P_\beta^I(\mathbf{G})S_I(\mathbf{G})\ , \tag{181}$$

where V_{loc} is the local potential

$$V_{\text{loc}}(\mathbf{G}) = \sum_I \Delta V_{\text{local}}^I(\mathbf{G})S_I(\mathbf{G}) + V_{\text{xc}}(\mathbf{G}) + 4\pi\,\frac{n_{\text{tot}}(\mathbf{G})}{G^2}\ . \tag{182}$$

Wavefunction gradients are needed in optimization calculations and in the Car-Parrinello molecular dynamics approach.

3.4.3 Gradient for Nuclear Positions

The derivative of the total energy with respect to nuclear positions is needed for structure optimization and in molecular dynamics, that is

$$\frac{\partial E_{\text{total}}}{\partial \mathbf{R}_{I,s}} = \frac{\partial E_{\text{local}}^{\text{PP}}}{\partial \mathbf{R}_{I,s}} + \frac{\partial E_{\text{nonlocal}}^{\text{PP}}}{\partial \mathbf{R}_{I,s}} + \frac{\partial E_{\text{ES}}}{\partial \mathbf{R}_{I,s}} \ , \tag{183}$$

as the kinetic energy E_{kin} and the exchange and correlation energy E_{xc} do not depend directly on the atomic positions, the relevant parts are

$$\frac{\partial E_{\text{local}}^{\text{PP}}}{\partial \mathbf{R}_{I,s}} = -\Omega \sum_{\mathbf{G}} i\mathbf{G}_s \, \Delta V_{\text{local}}^I(\mathbf{G}) \, S_I(\mathbf{G}) \, n^\star(\mathbf{G}) \tag{184}$$

$$\frac{\partial E_{\text{nonlocal}}^{\text{PP}}}{\partial \mathbf{R}_{I,s}} = \sum_i f_i \sum_{\alpha,\beta \in I} \left\{ \left(F_{I,i}^\alpha\right)^\star h_{\alpha\beta}^I \left(\frac{\partial F_{I,i}^\beta}{\partial \mathbf{R}_{I,s}}\right) + \left(\frac{\partial F_{I,i}^\alpha}{\partial \mathbf{R}_{I,s}}\right)^\star h_{\alpha,\beta}^I F_{I,i}^\beta \right\} \tag{185}$$

$$\frac{\partial E_{\text{ES}}}{\partial \mathbf{R}_{I,s}} = -\Omega \sum_{\mathbf{G} \neq 0} i\mathbf{G}_s \, \frac{n_{\text{tot}}^\star(\mathbf{G})}{G^2} \, n_{\text{c}}^I(\mathbf{G}) \, S_I(\mathbf{G}) + \frac{\partial E_{\text{ovrl}}}{\partial \mathbf{R}_{I,s}} \ . \tag{186}$$

The contribution of the projectors of the non-local pseudopotentials is calculated from

$$\frac{\partial F_{I,i}^\alpha}{\partial \mathbf{R}_{I,s}} = -\frac{1}{\sqrt{\Omega}} \sum_{\mathbf{G}} i\mathbf{G}_s \, P_\alpha^I(\mathbf{G}) \, S_I(\mathbf{G}) \, c_i^\star(\mathbf{G}, \mathbf{k}) \ . \tag{187}$$

Finally, the real space part contribution of the Ewald sum is

$$\frac{\partial E_{\text{ovrl}}}{\partial \mathbf{R}_{I,s}} = \sum_J{}' \sum_{\mathbf{L}} \left\{ \frac{Z_I Z_J}{|\mathbf{R}_I - \mathbf{R}_J - \mathbf{L}|^3} \text{erfc}\left[\frac{|\mathbf{R}_I - \mathbf{R}_J - \mathbf{L}|}{\sqrt{R_I^{\text{c}\,2} + R_J^{\text{c}\,2}}}\right] \right.$$
$$\left. + \frac{2}{\sqrt{\pi}} \frac{1}{\sqrt{R_I^{\text{c}\,2} + R_J^{\text{c}\,2}}} \frac{Z_I Z_J}{|\mathbf{R}_I - \mathbf{R}_J - \mathbf{L}|^2} \exp\left[-\frac{|\mathbf{R}_I - \mathbf{R}_J - \mathbf{L}|^2}{\sqrt{R_I^{\text{c}\,2} + R_J^{\text{c}\,2}}}\right] \right\}$$
$$\times (\mathbf{R}_{I,s} - \mathbf{R}_{J,s} - \mathbf{L}_s) \ . \tag{188}$$

The self energy E_{self} is independent of the atomic positions and does not contribute to the forces.

3.4.4 Internal Stress Tensor

For calculations where the supercell is changed (e.g. the combination of the Car–Parrinello method with the Parrinello–Rahman approach [201,55]) the electronic internal stress tensor is required. The electronic part of the internal stress tensor is defined as [440,441] (see also Sect. 4.2.3)

$$\Pi_{uv} = -\frac{1}{\Omega} \sum_s \frac{\partial E_{\text{total}}}{\partial \mathbf{h}_{us}} \mathbf{h}_{sv}^{\text{t}} \ . \tag{189}$$

An important identity for the derivation of the stress tensor is

$$\frac{\partial \Omega}{\partial \mathbf{h}_{uv}} = \Omega (\mathbf{h}^{\text{t}})_{uv}^{-1} \ . \tag{190}$$

The derivatives of the total energy with respect to the components of the cell matrix $\mathbf{h}$ can be performed on every part of the total energy individually,

$$\frac{\partial E_{\text{total}}}{\partial \mathbf{h}_{uv}} = \frac{\partial E_{\text{kin}}}{\partial \mathbf{h}_{uv}} + \frac{\partial E_{\text{local}}^{\text{PP}}}{\partial \mathbf{h}_{uv}} + \frac{\partial E_{\text{nonlocal}}^{\text{PP}}}{\partial \mathbf{h}_{uv}} + \frac{\partial E_{\text{xc}}}{\partial \mathbf{h}_{uv}} + \frac{\partial E_{\text{ES}}}{\partial \mathbf{h}_{uv}} \ . \tag{191}$$

Using Eq. (190) extensively, the derivatives can be calculated for the case of a plane wave basis in Fourier space [202],

$$\frac{\partial E_{\text{kin}}}{\partial \mathbf{h}_{uv}} = -\sum_i f_i \sum_{\mathbf{G}} \sum_s \mathbf{G}_u \mathbf{G}_s (\mathbf{h}^{\text{t}})_{sv}^{-1} |c_i(\mathbf{G})|^2 \tag{192}$$

$$\frac{\partial E_{\text{local}}^{\text{PP}}}{\partial \mathbf{h}_{uv}} = \Omega \sum_I \sum_{\mathbf{G}} \left(\frac{\partial \Delta V_{\text{local}}^I(\mathbf{G})}{\partial h_{uv}} \right) S_I(\mathbf{G}) n^\star(\mathbf{G}) \tag{193}$$

$$\frac{\partial E_{\text{nonlocal}}^{\text{PP}}}{\partial \mathbf{h}_{uv}} = \sum_i f_i \sum_I \sum_{\alpha,\beta \in I} \left\{ (F_{I,i}^\alpha)^\star h_{\alpha\beta}^I \left(\frac{\partial F_{I,i}^\beta}{\partial \mathbf{h}_{uv}} \right) + \left(\frac{\partial F_{I,i}^\alpha}{\partial \mathbf{h}_{uv}} \right)^\star h_{\alpha,\beta}^I F_{I,i}^\beta \right\} \tag{194}$$

$$\frac{\partial E_{\text{xc}}}{\partial \mathbf{h}_{uv}} = -\sum_{\mathbf{G}} n^\star(\mathbf{G}) \left[V_{\text{xc}}(\mathbf{G}) - \varepsilon_{\text{xc}}(\mathbf{G}) \right] (\mathbf{h}^{\text{t}})_{uv}^{-1}$$
$$+ \sum_s \sum_{\mathbf{G}} i \mathbf{G}_u n^\star(\mathbf{G}) \left(\frac{\partial F_{\text{xc}}(\mathbf{G})}{\partial (\partial_s n)} \right) (\mathbf{h}^{\text{t}})_{sv}^{-1} \tag{195}$$

$$\frac{\partial E_{\text{ES}}}{\partial \mathbf{h}_{uv}} = 2\pi \Omega \sum_{\mathbf{G} \neq 0} \sum_s \left\{ -\frac{|n_{\text{tot}}(\mathbf{G})|^2}{G^2} \delta_{us} \right.$$
$$+ \frac{n_{\text{tot}}^\star(\mathbf{G})}{G^2} \left(\frac{n_{\text{tot}}(\mathbf{G})}{G^2} \right.$$
$$\left. + \frac{1}{2} \sum_I n_{\text{c}}^I(\mathbf{G})(R_{\text{c}}^I)^2 \right) \mathbf{G}_u \mathbf{G}_s \right\} \mathbf{G}_u \mathbf{G}_s (\mathbf{h}^{\text{t}})_{sv}^{-1}$$
$$+ \frac{\partial E_{\text{ovrl}}}{\partial \mathbf{h}_{uv}} \ . \tag{196}$$

Finally, the derivative of the overlap contribution to the electrostatic energy is

$$\frac{\partial E_{\text{ovrl}}}{\partial \mathbf{h}_{uv}} = -\sum_{I,J}' \sum_{\mathbf{L}} \left\{ \frac{Z_I Z_J}{|\mathbf{R}_I - \mathbf{R}_J - \mathbf{L}|^3} \text{erfc} \left[\frac{|\mathbf{R}_I - \mathbf{R}_J - \mathbf{L}|}{\sqrt{R_I^{\text{c}\,2} + R_J^{\text{c}\,2}}} \right] \right.$$
$$\left. + \frac{2}{\sqrt{\pi}\sqrt{R_I^{\text{c}\,2} + R_J^{\text{c}\,2}}} \frac{Z_I Z_J}{|\mathbf{R}_I - \mathbf{R}_J - \mathbf{L}|^2} \exp \left[-\frac{|\mathbf{R}_I - \mathbf{R}_J - \mathbf{L}|^2}{\sqrt{R_I^{\text{c}\,2} + R_J^{\text{c}\,2}}} \right] \right\}$$
$$\times \sum_s (\mathbf{R}_{I,u} - \mathbf{R}_{J,u} - \mathbf{L}_u)(\mathbf{R}_{I,s} - \mathbf{R}_{J,s} - \mathbf{L}_s)(\mathbf{h}^{\text{t}})_{sv}^{-1} \ . \tag{197}$$

The local part of the pseudopotential $\Delta V_{\text{local}}^I(\mathbf{G})$ and the nonlocal projector functions depend on the cell matrix $\mathbf{h}$ through the volume, the Bessel transform integral and the spherical harmonics function. Their derivatives are lengthy but easy to cal-

culate from their definitions Eqs. (140) and (141)

$$
\frac{\partial \Delta V_{\text{local}}^{I}(\mathbf{G})}{\partial \mathbf{h}_{uv}} = -\Delta V_{\text{local}}^{I}(\mathbf{G})(\mathbf{h}^{\text{t}})_{uv}^{-1}
$$

$$
+\frac{4\pi}{\Omega} \int_{0}^{\infty} dr \, r^2 \, \Delta V_{\text{local}}(r) \left(\frac{\partial j_0(Gr)}{\partial \mathbf{h}_{uv}} \right) Y_{lm}(\tilde{\theta}, \tilde{\phi}) \qquad (198)
$$

$$
\frac{\partial F_{I,i}^{\alpha}}{\partial \mathbf{h}_{uv}} = \frac{4\pi}{\sqrt{\Omega}} \, (-i)^l \sum_{\mathbf{G}} c_i^{\star}(\mathbf{G}) \, S_I(\mathbf{G})
$$

$$
\left[\left(\frac{\partial Y_{lm}(\tilde{\theta}, \tilde{\phi})}{\partial \mathbf{h}_{uv}} - \frac{1}{2} Y_{lm}(\tilde{\theta}, \tilde{\phi})(\mathbf{h}^{\text{t}})_{uv}^{-1} \right) \int_{0}^{\infty} dr \, r^2 \, P_{\alpha}^{I}(r) \, j_l(Gr) \right.
$$

$$
\left. + Y_{lm}(\tilde{\theta}, \tilde{\phi}) \int_{0}^{\infty} dr \, r^2 \, P_{\alpha}^{I}(r) \left(\frac{\partial j_l(Gr)}{\partial \mathbf{h}_{uv}} \right) \right] \quad . \qquad (199)
$$

3.4.5 Non-linear Core Correction

The success of pseudopotentials in density functional calculations relies on two assumptions. The transferability of the core electrons to different environments and the linearization of the exchange and correlation energy. The second assumption is only valid if the frozen core electrons and the valence state do not overlap. However, if there is significant overlap between core and valence densities, the linearization will lead to reduced transferability and systematic errors. The most straightforward remedy is to include "semi–core states" in addition to the valence shell, i.e. one more inner shell (which is from a chemical viewpoint an inert "core level") is treated explicitly. This approach, however, leads to quite hard pseudopotentials which call for large plane wave cutoffs. Alternatively, it was proposed to treat the non–linear parts of the exchange and correlation energy E_{xc} explicitly [374]. This idea does not lead to an increase of the cutoff but ameliorates the above–mentioned problems quite a bit. To achieve this, E_{xc} is calculated not from the valence density $n(\mathbf{R})$ alone, but from a modified density

$$
\tilde{n}(\mathbf{R}) = n(\mathbf{R}) + \tilde{n}_{\text{core}}(\mathbf{R}) \quad , \qquad (200)
$$

where $\tilde{n}_{core}(\mathbf{R})$ denotes a density that is equal to the core density of the atomic reference state in the region of overlap with the valence density

$$
\tilde{n}_{\text{core}}(r) = n_{\text{core}}(r) \quad \text{if } r \rangle r_0 \; ; \qquad (201)
$$

with the vanishing valence density inside r_0. Close to the nuclei a model density is chosen in order to reduce the cutoff for the plane wave expansion. Finally, the two densities and their derivatives are matched at r_0. This procedure leads to a modified total energy in Eq. (176), where E_{xc} is replace by

$$
E_{\text{xc}} = E_{\text{xc}}(n + \tilde{n}_{\text{core}}) \quad , \qquad (202)
$$

and the corresponding potential is

$$
V_{\text{xc}} = V_{\text{xc}}(n + \tilde{n}_{\text{core}}) \quad . \qquad (203)
$$

The sum of all modified core densities

$$\tilde{n}_{core}(\mathbf{G}) = \sum_I \tilde{n}_{core}^I(\mathbf{G})S_I(\mathbf{G}) \tag{204}$$

depends on the nuclear positions, leading to a new contribution to the forces

$$\frac{\partial E_{\mathrm{xc}}}{\partial \mathbf{R}_{I,s}} = -\Omega \sum_{\mathbf{G}} i\mathbf{G}_s V_{\mathrm{xc}}^\star(\mathbf{G})\tilde{n}_{\mathrm{core}}^I(\mathbf{G})S_I(\mathbf{G}) \ , \tag{205}$$

and to the stress tensor

$$\frac{\partial E_{\mathrm{xc}}}{\partial \mathbf{h}_{uv}} = \sum_I \sum_{\mathbf{G}} V_{\mathrm{xc}}^\star(\mathbf{G})\frac{\partial \tilde{n}_{\mathrm{core}}^I(\mathbf{G})}{\partial \mathbf{h}_{uv}}S_I(\mathbf{G}) \ . \tag{206}$$

The derivative of the core charge with respect to the cell matrix can be performed in analogy to the formula given for the local potential. The method of the non-linear core correction dramatically improves results on systems with alkali and transition metal atoms. For practical applications, one should keep in mind that the non-linear core correction should only be applied together with pseudopotentials that were generated using the same energy expression.

3.5 Energy and Force Calculations in Practice

In Sect. 3.4 formulas for the total energy and forces were given in their Fourier space representation. Many terms are in fact calculated most easily in this form, but some terms would require double sums over plane waves. In particular, the calculation of the charge density and the wavefunction gradient originating from the local potential

$$\sum_{\mathbf{G}'} V_{\mathrm{loc}}^\star(\mathbf{G} - \mathbf{G}')c_i(\mathbf{G}') \ . \tag{207}$$

The expression in Eq. (207) is a convolution and can be calculated efficiently by a series of Fourier transforms. The flow charts of this calculations are presented in Fig. 8. Both of these modules contain a Fourier transform of the wavefunctions from $\mathbf{G}$ space to the real space grid. In addition, the calculation of the wavefunction forces requires a back transform of the product of the local potential with the wavefunctions, performed on the real space grid, to Fourier space. This leads to a number of Fourier transforms that is three times the number of states in the system. If enough memory is available on the computer the second transform of the wavefunctions to the grid can be avoided if the wavefunctions are stored in real space during the computation of the density. These modules are further used in the flow chart of the calculation of the local potential in Fig. 9. Additional Fourier transforms are needed in this part of the calculation. However, the number of transforms does not scale with the number of electrons in the system. Additional transforms might be hidden in the module to calculate the exchange and correlation potential (see also Fig. 7) and the Poisson solver in cases when the Hockney method is used (see Fig. 6).

The calculation of the total energy, together with the local potential is shown in Fig. 10. The overlap between the projectors of the nonlocal pseudopotential and
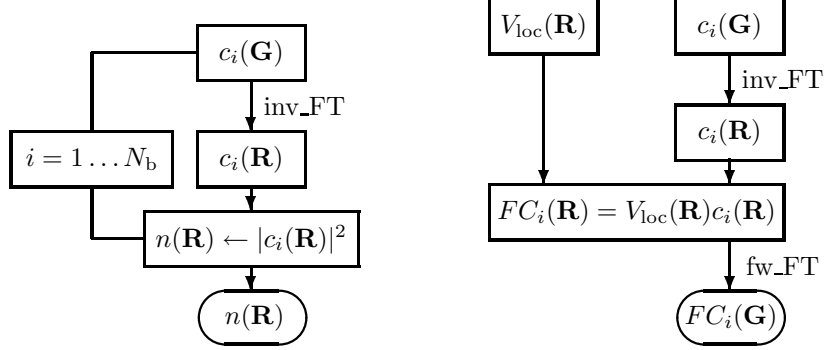
Figure 8. Flow chart for the calculation of the charge density (on the left) and the force on the wavefunction from the local potential (on the right). The charge density calculation requires N_{b} (number of states) three dimensional Fourier transforms. For the application of the local potential two Fourier transforms per state are needed. If enough memory is available the first transform can be avoided if the wavefunction on the real space grid are stored during the density calculation.
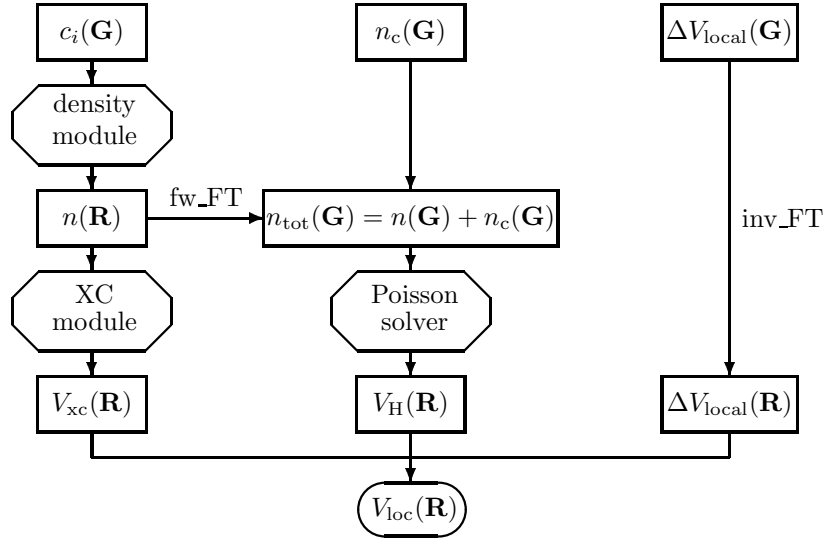

Figure 9. Flow chart for the calculation of the local potential from the Kohn–Sham orbitals. This module calculates also the charge density in real and Fourier space and the exchange and correlation energy, Hartree energy, and local pseudopotential energy.

the wavefunctions calculated in this part will be reused in the calculation of the forces on the wavefunctions. There are three initialization steps marked in Fig. 9. Step one has only to be performed at the beginning of the calculation, as the quantities $\mathbf{g}$ and E_{self} are constants. The quantities calculated in step two depend on the absolute value of the reciprocal space vectors. They have to be recalculated
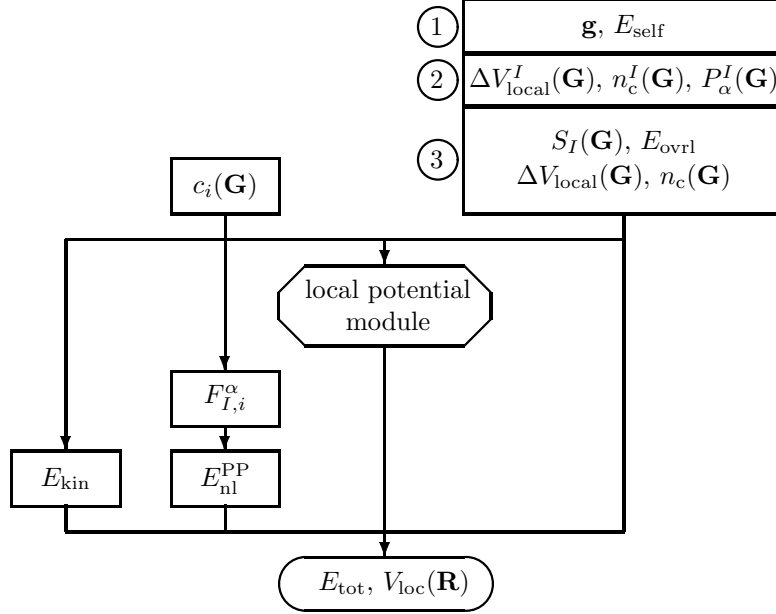
Figure 10. Flow chart for the calculation of the local potential and total energy. Initialization steps are marked with numbers. Step 2 has to be repeated whenever the size of the unit cell changes. Step 3 has to be repeated whenever nuclear positions have changed.

whenever the box matrix $\mathbf{h}$ changes. Finally, the variables in step three depend on the atomic positions and have to be calculated after each change of the nuclear positions. The flow charts of the calculation of the forces for the wavefunctions and the nuclei are shown in Figs. 11 and 12.

3.6 Optimizing the Kohn-Sham Orbitals

Advances in the application of plane wave based electronic structure methods are closely related to improved methods for the solution of the Kohn–Sham equations. There are now two different but equally successful approaches available. Fix–point methods based on the diagonalization of the Kohn–Sham matrix follow the more traditionally ways that go back to the roots of basis set methods in quantum chemistry. Direct nonlinear optimization approaches subject to a constraint were initiated by the success of the Car–Parrinello method. The following sections review some of these methods, focusing on the special problems related to the plane wave basis.
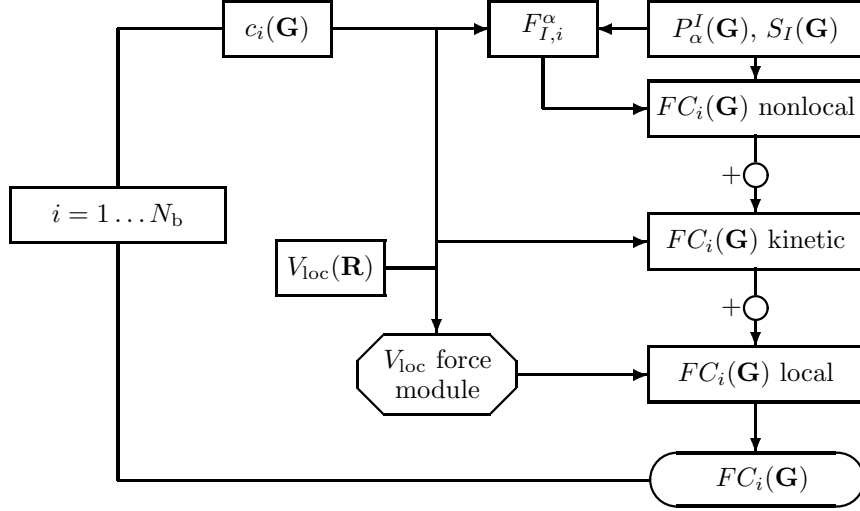
Figure 11. Flow chart for the calculation of the forces on the wavefunctions. Notice that the calculation of the overlap terms $F_{I,i}^\alpha$ is done outside the loop over wavefunctions. Besides the wavefunctions and the local potential, the structure factors and the projectors of the nonlocal pseudopotential are input parameters to this module.
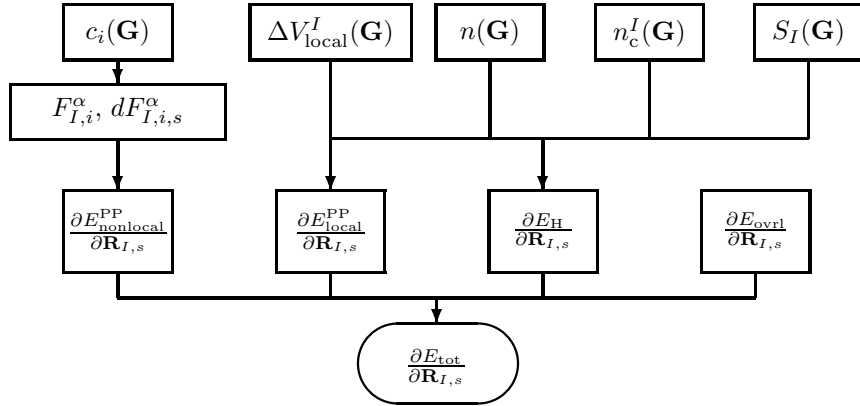

Figure 12. Flow chart for the calculation of the forces on the nuclei.

3.6.1 Initial Guess

The initial guess of the Kohn–Sham orbitals is the first step to a successful calculation. One would like to introduce as much knowledge as possible into the first step of the calculation, but at the same time the procedure should be general and robust. One should also take care not to introduce artifical symmetries that may be preserved during the optimization and lead to false results. The most general

initialization might be, choosing the wavefunction coefficients from a random distribution. It makes sense to weight the random numbers by a function reflecting the relative importance of different basis functions. A good choice is a Gaussian distribution in G^2. This initialization scheme avoids symmetry problems but leads to energies far off the final results and especially highly tuned optimization methods might have problems.

A more educated guess is to use a superposition of atomic densities and then diagonalize the Kohn–Sham matrix in an appropriate basis. This basis can be the full plane wave basis or just a part of it, or any other reasonable choice. The most natural choice of atomic densities and basis sets for a plane wave calculation are the pseudo atomic density and the pseudo atomic wavefunction of the atomic reference state used in the generation of the pseudopotential. In the `CPMD` code this is one possibility, but often the data needed are not available. For this case the default option is to generate a minimal basis out of Slater functions (see Eq. (98) in Sect. 2.8) and combine them with the help of atomic occupation numbers (gathered using the Aufbau principle) to an atomic density. From the superposition of these densities a Kohn–Sham potential is constructed. The Slater orbitals are expanded in plane waves and using the same routines as in the standard code the Kohn–Sham and overlap matrices are calculated in this basis. The general eigenvalue problem is solved and the eigenfunctions can easily be expressed in the plane wave basis that are in turn used as the initial wavefunctions to the optimization routines. Similarly, a given plane wave representation of the total wavefunction can be projected onto an auxiliary set of atom–centered functions. This opens up the possibility to perform population and bond–order analyses (following for instance the schemes of Mulliken or Mayer) in plane wave–pseudopotential calculations [537].

3.6.2 Preconditioning

Optimizations in many dimensions are often hampered by the appearance of different length scales. The introduction of a metric that brings all degrees of freedom onto the same length scale can improve convergence considerably. The application of such a metric is called "preconditioning" and is used in many optimization problems. If the variables in the optimization are decoupled the preconditioning matrix is diagonal and becomes computationally tractable even for very large systems. Fortunately, this is to a large degree the case for a plane wave basis set. For large $\mathbf{G}$ vectors the Kohn–Sham matrix is dominated by the kinetic energy which is diagonal in the plane wave representation. Based on this observation efficient preconditioning schemes have been proposed [616,610,308,344]. The preconditioner implemented in the `CPMD` code is based on the diagonal of the Kohn–Sham matrix $H_{\mathbf{G},\mathbf{G}'}$, which is given by

$$
\begin{aligned}
\mathbf{K}_{\mathbf{G},\mathbf{G}'} &= \mathbf{H}_{\mathbf{G},\mathbf{G}}\, \delta_{\mathbf{G},\mathbf{G}'} && \text{if } |\mathbf{G}| \geq G_c \\
\mathbf{K}_{\mathbf{G},\mathbf{G}'} &= \mathbf{H}_{\mathbf{G}_c,\mathbf{G}_c}\, \delta_{\mathbf{G},\mathbf{G}'} && \text{if } |\mathbf{G}| \leq G_c
\end{aligned}
,
\tag{208}
$$

where G_c is a free parameter that can be adjusted to accelerate convergence. However, it is found that the actual choice is not very critical and for practical purposes it is convenient not to fix G_c, but to use an universal constant of 0.5 Hartree for $H_{\mathbf{G}_c,\mathbf{G}_c}$ that in turn defines G_c for each system.

3.6.3 Direct Methods

The success of the Car–Parrinello approach started the interest in other methods for a direct minimization of the Kohn–Sham energy functional. These methods optimize the total energy using the gradient derived from the Lagrange function

$$\mathcal{L} = E^{\mathrm{KS}}\left(\{\Phi_i\}\right) - \sum_{ij} \lambda_{ij}\left(\langle\Phi_i|\Phi_j\rangle - \delta_{ij}\right) \tag{209}$$

$$\frac{\partial\mathcal{L}}{\partial\Phi_i} = \mathcal{H}_{\mathrm{e}}\Phi_i - \sum_j \langle\Phi_i|\mathcal{H}_{\mathrm{e}}|\Phi_j\rangle\Phi_j \ . \tag{210}$$

Optimization methods differ in the way orbitals are updated. A steepest descent based scheme

$$c_i(\mathbf{G}) \leftarrow c_i(\mathbf{G}) + \alpha\mathbf{K}_{\mathbf{G},\mathbf{G}}^{-1}\psi_i(\mathbf{G}) \tag{211}$$

can be combined with the preconditioner and a line search option to find the optimal step size α. Nearly optimal α's can be found with an interpolation based on a quadratic polynomial. In Eq. (211) $\psi_i(\mathbf{G})$ denote the Fourier components of the wavefunction gradient.

Improved convergence can be achieved by replacing the steepest descent step with a search direction based on conjugate gradients [594,232,616,23,499]

$$c_i(\mathbf{G}) \leftarrow c_i(\mathbf{G}) + \alpha h_i(\mathbf{G}) \ . \tag{212}$$

The conjugate directions are calculated from

$$h_i^{(n)}(\mathbf{G}) = \begin{cases} g_i^{(n)}(\mathbf{G}) & n = 0 \\ g_i^{(n)}(\mathbf{G}) + \gamma^{(n-1)}h_i^{n-1}(\mathbf{G}) & n = 1, 2, 3, \ldots \end{cases} \tag{213}$$

where

$$g_i^{(n)}(\mathbf{G}) = \mathbf{K}_{\mathbf{G},\mathbf{G}}^{-1}\psi_i^{(n)}(\mathbf{G}) \tag{214}$$

$$\gamma^{(n)} = \frac{\sum_i\langle g_i^{(n+1)}(\mathbf{G})|g_i^{(n+1)}(\mathbf{G})\rangle}{\langle g_i^{(n)}(\mathbf{G})|g_i^{(n)}(\mathbf{G})\rangle}. \tag{215}$$

A very efficient implementation of this method [616] is based on a band by band optimization. A detailed description of this method can also be found in Ref. [472].

The direct inversion in the iterative subspace (DIIS) method [495,144,308] is a very successful extrapolation method that can be used in any kind of optimization problems. In quantum chemistry the DIIS scheme has been applied to wavefunction optimizations, geometry optimizations and in post–Hartree–Fock applications. DIIS uses the information of n previous steps. Together with the position vectors $c_i^{(k)}(\mathbf{G})$ an estimate of the error vector $e_i^{(k)}(\mathbf{G})$ for each previous step k is stored. The best approximation to the final solution within the subspace spanned by the n stored vectors is obtained in a least square sense by writing

$$c_i^{(n+1)}(\mathbf{G}) = \sum_{k=1}^n d_k c_i^{(k)}(\mathbf{G}) \ , \tag{216}$$

where the d_k are subject to the restriction

$$\sum_{k=1}^{n} d_k = 1 \qquad (217)$$

and the estimated error becomes

$$e_i^{(n+1)}(\mathbf{G}) = \sum_{k=1}^{n} d_k e_i^{(k)}(\mathbf{G}) \ . \qquad (218)$$

The expansion coefficients d_k are calculated from a system of linear equations

$$\begin{pmatrix} b_{11} & b_{12} & \cdots & b_{1n} & 1 \\ b_{21} & b_{22} & \cdots & b_{2n} & 1 \\ \vdots & \vdots & \ddots & \vdots & \vdots \\ b_{n1} & b_{n2} & \cdots & b_{nn} & 1 \\ 1 & 1 & \cdots & 1 & 0 \end{pmatrix} \begin{pmatrix} d_1 \\ d_2 \\ \vdots \\ d_n \\ -\lambda \end{pmatrix} = \begin{pmatrix} 0 \\ 0 \\ \vdots \\ 0 \\ 1 \end{pmatrix} \qquad (219)$$

where the b_{kl} are given by

$$b_{kl} = \sum_i \langle e_i^k(\mathbf{G}) | e_i^l(\mathbf{G}) \rangle \ . \qquad (220)$$

The error vectors are not known, but can be approximated within a quadratic model

$$e_i^{(k)}(\mathbf{G}) = -\mathbf{K}_{\mathbf{G},\mathbf{G}}^{-1} \psi_i^{(k)}(\mathbf{G}) \ . \qquad (221)$$

In the same approximation, assuming $\mathbf{K}$ to be a constant, the new trial vectors are estimated to be

$$c_i(\mathbf{G}) = c_i^{(n+1)}(\mathbf{G}) + \mathbf{K}_{\mathbf{G},\mathbf{G}}^{-1} \psi_i^{(n+1)}(\mathbf{G}) \ , \qquad (222)$$

where the first derivative of the energy density functional is estimated to be

$$\psi_i^{(n+1)}(\mathbf{G}) = \sum_{k=1}^{n} d_k \psi_i^{(k)}(\mathbf{G}) \ . \qquad (223)$$

The methods described in this section produce new trail vectors that are not orthogonal. Therefore an orthogonalization step has to be added before the new charge density is calculated

$$c_i(\mathbf{G}) \leftarrow \sum_k c_j(\mathbf{G}) \mathbf{X}_{ji} \ . \qquad (224)$$

There are different choices for the rotation matrix $\mathbf{X}$ that lead to orthogonal orbitals. Two of the computationally convenient choices are the Löwdin orthogonalization

$$\mathbf{X}_{ji} = \mathbf{S}_{ji}^{-1/2} \qquad (225)$$

and a matrix form of the Gram–Schmidt procedure

$$\mathbf{X}_{ji} = (\mathbf{G}^T)_{ji}^{-1} \ , \qquad (226)$$

where $\mathbf{S}$ is the overlap matrix and $\mathbf{G}$ is its Cholesky decomposition

$$\mathbf{S} = \mathbf{G}\mathbf{G}^T \ . \tag{227}$$

Recently new methods that avoid the orthogonalization step have been introduced. One of them [483] relies on modified functionals that can be optimized without the orthogonality constraint. These functionals, originally introduced in the context of linear scaling methods [417,452], have the property that their minima coincide with the original Kohn–Sham energy functional. The methods described above can be used to optimize the new functional.

Another approach [309] is to use a variable transformation from the expansion coefficients of the orbitals in plane waves to a set of non–redundant orbital rotation angles. This method was introduced in quantum chemistry [618,149,167] and is used successfully in many optimization problems that involve a set of orthogonal orbitals. A generalization of the orbital rotation scheme allowed the application also for cases where the number of basis functions is orders of magnitudes bigger than the number of occupied orbitals. However, no advantage is gained over the standard methods, as the calculation of the gradient in the transformed variables scales the same as the orthogonalization step. In addition, there is no simple and efficient preconditioner available for the orbital rotation coordinates.

3.6.4 Fix-Point Methods

Originally all methods to find solutions to the Kohn–Sham equations were using matrix diagonalization methods. It became quickly clear that direct schemes can only be used for very small systems. The storage requirements of the Kohn–Sham matrix in the plane wave basis and the scaling proportional to the cube of the basis set size lead to unsurmountable problems. Iterative diagonalization schemes can be adapted to the special needs of a plane wave basis and when combined with a proper preconditioner lead to algorithms that are comparable to the direct methods, both in memory requirements and over all scaling properties. Iterative diagonalization schemes are abundant. Methods based on the Lanczos algorithm [357,151,489] can be used as well as conjugate gradient techniques [616,97]. Very good results have been achieved by the combination of the DIIS method with the minimization of the norm of the residual vector [698,344]. The diagonalization methods have to be combined with an optimization method for the charge density. Methods based on mixing [153,4], quasi-Newton algorithms [92,77,319], and DIIS [495,344,345] are successfully used. Also these methods use a preconditioning scheme. It was shown that the optimal preconditioning for charge density mixing is connected to the charge dielectric matrix [153,4,299,658,48]. For a plane wave basis, the charge dielectric matrix can be approximated by expressions very close to the ones used for the preconditioning in the direct optimization methods.

Fix-point methods have a slightly larger prefactor than most of the direct methods. Their advantage lies in the robustness and capability of treating systems with no or small band gaps.

3.7 Molecular Dynamics

Numerical methods to integrate the equations of motion are an important part of every molecular dynamics program. Therefore an extended literature exists on integration techniques (see Ref. [217] and references in there). All considerations valid for the integration of equations of motion with classical potentials also apply for *ab initio* molecular dynamics if the Born–Oppenheimer dynamics approach is used. These basic techniques will not be discussed here.

A good initial guess for the Kohn–Sham optimization procedure is a crucial ingredient for good performance of the Born–Oppenheimer dynamics approach. An extrapolation scheme was devised [24] that makes use of the optimized wavefunctions from previous time steps. This procedure has a strong connection to the basic idea of the Car–Parrinello method, but is not essential to the method.

The remainder of this section discusses the integration of the Car–Parrinello equations in their simplest form and explains the solution to the constraints equation for general geometric constraints. Finally, a special form of the equations of motion will be used for optimization purposes.

3.7.1 Car–Parrinello Equations

The Car–Parrinello Lagrangian and its derived equations of motions were introduced in Sect. 2.4. Here Eqs. (41), (44), and (45) are specialized to the case of a plane wave basis within Kohn–Sham density functional theory. Specifically the functions ϕ_i are replaced by the expansion coefficients $c_i(\mathbf{G})$ and the orthonormality constraint only depends on the wavefunctions, not the nuclear positions. The equations of motion for the Car–Parrinello method are derived from this specific extended Lagrangian

$$\mathcal{L} = \mu \sum_i \sum_{\mathbf{G}} |\dot{c}_i(\mathbf{G})|^2 + \frac{1}{2} \sum_I M_I \dot{\mathbf{R}}_I^2 - E_{\mathrm{KS}}\left[\{\mathbf{G}\}, \{\mathbf{R_I}\}\right]$$
$$+ \sum_{ij} \Lambda_{ij} \left(\sum_{\mathbf{G}} c_i^\star(\mathbf{G}) c_j(\mathbf{G}) - \delta_{ij} \right) \ , \qquad (228)$$

where μ is the electron mass, and M_I are the masses of the nuclei. Because of the expansion of the Kohn–Sham orbitals in plane waves, the orthonormality constraint does not depend on the nuclear positions. For basis sets that depend on the atomic positions (e.g. atomic orbital basis sets) or methods that introduce an atomic position dependent metric (ultra–soft pseudopotentials [661,351], PAW [143,347], the integration methods have to be adapted (see also Sect. 2.5). Solutions that include these cases can be found in the literature [280,351,143,310]. The Euler–Lagrange equations derived from Eq.(228) are

$$\mu \ddot{c}_i(\mathbf{G}) = -\frac{\partial E}{\partial c_i^\star(\mathbf{G})} + \sum_j \Lambda_{ij} c_j(\mathbf{G}) \qquad (229)$$

$$M_I \ddot{\mathbf{R}}_I = -\frac{\partial E}{\partial \mathbf{R}_I}. \qquad (230)$$

The two sets of equations are coupled through the Kohn–Sham energy functional and special care has to be taken for the integration because of the orthonormality constraint.

The integrator used in the CPMD code is based on the velocity Verlet / RATTLE algorithm [603,638,15]. The velocity Verlet algorithm requires more operations and more storage than the Verlet algorithm [664]. However, it is much easier to incorporate temperature control via velocity scaling into the velocity Verlet algorithm. In addition, velocity Verlet allows to change the time step trivially and is conceptually easier to handle [638,391]. It is defined by the following equations

$$\dot{R}_I(t + \delta t) = \dot{\mathbf{R}}_I(t) + \frac{\delta t}{2M_I}\mathbf{F}_I(t) \tag{231}$$

$$\mathbf{R}_I(t + \delta t) = \mathbf{R}_I(t) + \delta t\, \dot{\tilde{R}}_I(t + \delta t)$$

$$\dot{\tilde{c}}_I(t + \delta t) = \dot{\mathbf{c}}_I(t) + \frac{\delta t}{2\mu}\mathbf{f}_i(t)$$

$$\tilde{\mathbf{c}}_i(t + \delta t) = \mathbf{c}_i(t) + \delta t\, \dot{\tilde{c}}_i(t + \delta t)$$

$$\mathbf{c}_i(t + \delta t) = \tilde{\mathbf{c}}_i(t + \delta t) + \sum_j \mathbf{X}_{ij}\, \mathbf{c}_j(t)$$

$$\text{calculate} \quad \mathbf{F}_I(t + \delta t)$$

$$\text{calculate} \quad \mathbf{f}_i(t + \delta t)$$

$$\dot{\mathbf{R}}_I(t + \delta t) = \dot{\tilde{R}}_I(t + \delta t) + \frac{\delta t}{2M_I}\mathbf{F}_I(t + \delta t)$$

$$\dot{\mathbf{c}}'_i(t + \delta t) = \dot{\tilde{c}}_i(t + \delta t) + \frac{\delta t}{2\mu}\mathbf{f}_i(t + \delta t)$$

$$\dot{\mathbf{c}}_i(t + \delta t) = \dot{\mathbf{c}}'_i(t + \delta t) + \sum_j \mathbf{Y}_{ij}\, \mathbf{c}_j(t + \delta t) \ ,$$

where $\mathbf{R}_I(t)$ and $\mathbf{c}_i(t)$ are the atomic positions of particle I and the Kohn–Sham orbital i at time t respectively. Here, $\mathbf{F}_I$ are the forces on atom I, and $\mathbf{f}_i$ are the forces on Kohn–Sham orbital i. The matrices $\mathbf{X}$ and $\mathbf{Y}$ are directly related to the Lagrange multipliers by

$$\mathbf{X}_{ij} = \frac{\delta t^2}{2\mu}\Lambda^{\mathrm{p}}_{ij} \tag{232}$$

$$\mathbf{Y}_{ij} = \frac{\delta t}{2\mu}\Lambda^{\mathrm{v}}_{ij} \ . \tag{233}$$

Notice that in the RATTLE algorithm the Lagrange multipliers to enforce the orthonormality for the positions Λ^{p} and velocities Λ^{v} are treated as independent variables. Denoting with $\mathbf{C}$ the matrix of wavefunction coefficients $c_i(\mathbf{G})$, the or-

thonormality constraint can be written as

$$\mathbf{C}^{\dagger}(t + \delta t)\mathbf{C}(t + \delta t) - \mathbf{I} = 0 \tag{234}$$

$$\left[\tilde{\mathbf{C}} + \mathbf{XC}\right]^{\dagger}\left[\tilde{\mathbf{C}} + \mathbf{XC}\right] - \mathbf{I} = 0 \tag{235}$$

$$\tilde{\mathbf{C}}^{\dagger}\tilde{\mathbf{C}} + \mathbf{X}\tilde{\mathbf{C}}^{\dagger}\mathbf{C} + \mathbf{C}^{\dagger}\tilde{\mathbf{C}}\mathbf{X}^{\dagger} + \mathbf{XX}^{\dagger} - \mathbf{I} = 0 \tag{236}$$

$$\mathbf{XX}^{\dagger} + \mathbf{XB} + \mathbf{B}^{\dagger}\mathbf{X}^{\dagger} = \mathbf{I} - \mathbf{A} \ , \tag{237}$$

where the new matrices $\mathbf{A}_{ij} = \tilde{\mathbf{c}}_i^{\dagger}(t + \delta t)\tilde{\mathbf{c}}_j(t + \delta t)$ and $\mathbf{B}_{ij} = \mathbf{c}_i^{\dagger}(t)\tilde{\mathbf{c}}_j(t + \delta t)$ have been introduced in Eq. (237). The unit matrix is denoted by the symbol $\mathbf{I}$. By noting that $\mathbf{A} = \mathbf{I} + \mathcal{O}(\delta t^2)$ and $\mathbf{B} = \mathbf{I} + \mathcal{O}(\delta t)$, Eq. (237) can be solved iteratively using

$$\mathbf{X}^{(n+1)} = \frac{1}{2}\left[\mathbf{I} - \mathbf{A} + \mathbf{X}^{(n)}\left(\mathbf{I} - \mathbf{B}\right)\right.$$
$$\left. + \left(\mathbf{I} - \mathbf{B}\right)\mathbf{X}^{(n)} - \left(\mathbf{X}^{(n)}\right)^2\right] \tag{238}$$

and starting from the initial guess

$$\mathbf{X}^{(0)} = \frac{1}{2}(\mathbf{I} - \mathbf{A}) \ . \tag{239}$$

In Eq. (238) it has been made use of the fact that the matrices $\mathbf{X}$ and $\mathbf{B}$ are real and symmetric, which follows directly from their definitions. Eq. (238) can usually be iterated to a tolerance of 10^{-6} within a few iterations.

The rotation matrix $\mathbf{Y}$ is calculated from the orthogonality condition on the orbital velocities

$$\dot{\mathbf{c}}_i^{\dagger}(t + \delta t)\mathbf{c}_j(t + \delta t) + \mathbf{c}_i^{\dagger}(t + \delta t)\dot{\mathbf{c}}_j(t + \delta t) = 0. \tag{240}$$

Applying Eq. (240) to the trial states $\dot{\mathbf{C}}' + \mathbf{YC}$ yields a simple equation for $\mathbf{Y}$

$$\mathbf{Y} = -\frac{1}{2}(\mathbf{Q} + \mathbf{Q}^{\dagger}), \tag{241}$$

where $\mathbf{Q}_{ij} = \mathbf{c}_i^{\dagger}(t+\delta t)\dot{\mathbf{c}'}_i^{\dagger}(t+\delta t)$. The fact that $\mathbf{Y}$ can be obtained without iteration means that the velocity constraint condition Eq. (240) is satisfied exactly at each time step.

3.7.2 Advanced Techniques

One advantage of the velocity Verlet integrator is that it can be easily combined with multiple time scale algorithms [636,639] and still results in reversible dynamics. The most successful implementation of a multiple time scale scheme in connection with the plane wave–pseudopotential method is the harmonic reference system idea [471,639]. The high frequency motion of the plane waves with large kinetic energy is used as a reference system for the integration. The dynamics of this reference system is harmonic and can be integrated analytically. In addition, this can be combined with the basic notion of a preconditioner already introduced in the section on optimizations. The electronic mass used in the Car–Parrinello scheme is a fictitious construct (see Sect. 2.4, Eq. (45)) and it is allowed to generalize the idea by

introducing different masses for different "classical" degrees of freedom [473,610,639]. In agreement with the preconditioner introduced in the optimization section, the new plane wave dependent masses are

$$\mu(\mathbf{G}) = \begin{cases} \mu & \mathbf{H}(\mathbf{G}, \mathbf{G}) \leq \alpha \\ (\mu/\alpha) \left(\frac{1}{2}G^2 + \mathbf{V}(\mathbf{G}, \mathbf{G})\right) & \mathbf{H}(\mathbf{G}, \mathbf{G}) \geq \alpha \end{cases}, \tag{242}$$

where $\mathbf{H}$ and $\mathbf{V}$ are the matrix elements of the Kohn–Sham matrix and the potential respectively. The reference electron mass is μ and the parameter α has been introduced before in Eq. (208) as $\mathbf{H}_{\mathbf{G_c}, \mathbf{G_c}}$. With the preconditioned masses and the harmonic reference system, the equations of motion of the system are

$$\mu(\mathbf{G})\ddot{c}_i(\mathbf{G}) = -\lambda(\mathbf{G})c_i(\mathbf{G}) + \delta\Phi_i(\mathbf{G}) + \sum_j \Lambda_{ij} c_j(\mathbf{G}) . \tag{243}$$

where $\delta\Phi_i(\mathbf{G})$ is the force on orbital i minus $-\lambda(\mathbf{G})$. From Eq. (243) it is easy to see that the frequencies $\omega(\mathbf{G}) = \sqrt{\lambda(\mathbf{G})/\mu(\mathbf{G})}$ are independent of $\mathbf{G}$ and that there is only one harmonic frequency equal to $\sqrt{\alpha/\mu}$. The revised formulas for the integration of the equations of motion for the velocity Verlet algorithm can be found in the literature [639].

The implications of the $\mathbf{G}$ vector dependent masses can be seen by revisiting the formulas for the characteristic frequencies of the electronic system Eqs. (52), (53), and (54). The masses μ are chosen such that all frequencies ω_{ij} are approximately the same, thus optimizing both, adiabaticity and maximal time step. The disadvantage of this method is that the average electron mass seen by the nuclei is drastically enhanced, leading to renormalization corrections [75] on the masses M_I that are significantly higher than in the standard approach and not as simple to estimate by an analytical expression.

3.7.3 Geometrical Constraints

Geometrical constraints are used in classical simulations to freeze fast degrees of freedom in order to allow for larger time steps. Mainly distance constraints are used for instance to fix intramolecular covalent bonds. These type of applications of constraints is of lesser importance in *ab initio* molecular dynamics. However, in the simulation of rare events such as many reactions, constraints play an important role together with the method of thermodynamic integration [217]. The "blue–moon" ensemble method [115,589] enables one to compute the potential of mean force. This potential can be obtained directly from the average force of constraint and a geometric correction term during a molecular dynamics simulation as follows:

$$\mathcal{F}(\xi_2) - \mathcal{F}(\xi_1) = \int_{\xi_1}^{\xi_2} d\xi' \left\langle \frac{\partial \mathcal{H}}{\partial \xi} \right\rangle_{\xi'}^{\text{cond.}} , \tag{244}$$

where $\mathcal{F}$ is the free energy and $\xi(\mathbf{r})$ a one–dimensional reaction coordinate, $\mathcal{H}$ the Hamiltonian of the system and $\langle \cdots \rangle_{\xi'}^{\text{cond.}}$ the conditioned average in the constraint ensemble [589]. By way of the blue moon ensemble, the statistical average is replaced by a time average over a constrained trajectory with the reaction coordinate fixed

at special values, $\xi(\mathbf{R}) = \xi'$, and $\dot{\xi}(\mathbf{R}, \dot{\mathbf{R}}) = 0$. The quantity to evaluate is the mean force

$$\frac{d\mathcal{F}}{d\xi'} = \frac{\left\langle Z^{-1/2} \left[-\lambda + k_B T G\right]\right\rangle_{\xi'}}{\left\langle Z^{-1/2}\right\rangle_{\xi'}} \quad , \tag{245}$$

where λ is the Lagrange multiplier of the constraint,

$$Z = \sum_I \frac{1}{M_I} \left(\frac{\partial \xi}{\partial \mathbf{R}_I}\right)^2 \quad , \tag{246}$$

and

$$G = \frac{1}{Z^2} \sum_{I,J} \frac{1}{M_I M_J} \frac{\partial \xi}{\partial \mathbf{R}_I} \cdot \frac{\partial^2 \xi}{\partial \mathbf{R}_I \partial \mathbf{R}_J} \cdot \frac{\partial \xi}{\partial \mathbf{R}_J} \quad , \tag{247}$$

where $\langle \cdots \rangle_{\xi'}$ is the unconditioned average, as directly obtained from a constrained molecular dynamics run with $\xi(\mathbf{R}) = \xi'$ and

$$\mathcal{F}(\xi_2) - \mathcal{F}(\xi_1) = \int_{\xi_1}^{\xi_2} d\xi' \frac{d\mathcal{F}}{d\xi'} \tag{248}$$

finally defines the free energy difference. For the special case of a simple distance constraint $\xi(\mathbf{R}) = |\mathbf{R}_I - \mathbf{R}_J|$ the parameter Z is a constant and $G = 0$.

The RATTLE algorithm, allows for the calculation of the Lagrange multiplier of arbitrary constraints on geometrical variables within the velocity Verlet integrator. The following algorithm is implemented in the CPMD code. The constraints are defined by

$$\sigma^{(i)}(\{\mathbf{R}_I(t)\}) = 0 \quad , \tag{249}$$

and the velocity Verlet algorithm can be performed with the following steps.

$$\dot{\tilde{R}}_I = \dot{\mathbf{R}}_I(t) + \frac{\delta t}{2M_I} \mathbf{F}_I(t)$$

$$\tilde{\mathbf{R}}_I = \mathbf{R}_I(t) + \delta t\, \dot{\tilde{R}}_I$$

$$\mathbf{R}_I(t + \delta t) = \tilde{\mathbf{R}}_I + \frac{\delta t^2}{2M_I} \mathbf{g}_p(t)$$

$$\text{calculate} \quad \mathbf{F}_I(t + \delta t)$$

$$\dot{\mathbf{R}}'_I = \dot{\tilde{R}}_I + \frac{\delta t}{2M_I} \mathbf{F}_I(t + \delta t)$$

$$\dot{\mathbf{R}}_I(t + \delta t) = \dot{\mathbf{R}}'_I + \frac{\delta t}{2M_I} \mathbf{g}_v(t + \delta t) \quad ,$$

where the constraint forces are defined by

$$\mathbf{g}_p(t) = -\sum_i \lambda_p^i \frac{\partial \sigma^{(i)}(\{\mathbf{R}_I(t)\})}{\partial \mathbf{R}_I} \tag{250}$$

$$\mathbf{g}_v(t) = -\sum_i \lambda_v^i \frac{\partial \sigma^{(i)}(\{\mathbf{R}_I(t)\})}{\partial \mathbf{R}_I} \quad . \tag{251}$$

The Lagrange multiplier have to be determined to ensure that the constraint on the positions and velocities are exactly fulfilled at the end of the time step. For the position, the constraint condition is

$$\sigma^{(i)}(\{\mathbf{R}_I(t+\delta t)\}) = 0 \ .$$ (252)

Eq. (252) is in general a system of nonlinear equations in the Lagrange multipliers λ_{p}^i. These equations can be solved using a generalized Newton algorithm [491] that can be combined with a convergence acceleration scheme based on the direct inversion in the iterative subspace method [495,144]. The error vectors for a given set of Lagrange multipliers λ are calculated from

$$\mathbf{e}_i(\lambda) = -\sum_j \mathbf{J}_{ij}^{-1}(\lambda)\sigma^{(j)}(\lambda) \ .$$ (253)

The Jacobian $\mathbf{J}$ is defined by

$$\mathbf{J}_{ij}(\lambda) = \frac{\partial \sigma^{(i)}(\lambda)}{\partial \lambda^j}$$ (254)

$$= \sum_I \frac{\partial \sigma^{(i)}(\lambda)}{\partial \mathbf{R}_I(\lambda)} \frac{\partial \mathbf{R}_I(\lambda)}{\partial \lambda^j}$$ (255)

$$= -\sum_I \frac{\delta t^2}{2M_I} \mathbf{f}_I^{\mathrm{c}}(\lambda)\mathbf{f}_I^{\mathrm{c}}(0) \ ,$$ (256)

where $\mathbf{f}_I^{\mathrm{c}}(\lambda) = \sum_i \lambda^i \partial\sigma^{(i)}/\partial\mathbf{R}_I$. Typically only a few iterations are needed to converge the Lagrange multipliers to an accuracy of 1×10^{-8}.

The constraint condition for the velocities can be cast into a system of linear equations. Again, as in the case of the orthonormality constraints in the Car–Parrinello method, the Lagrange multiplier for the velocity update can be calculated exactly without making use of an iterative scheme. Defining the derivative matrix

$$\mathbf{A}_{iI} = \frac{\partial \sigma^{(i)}}{\partial \mathbf{R}_I} \ ,$$ (257)

the velocity constraints are

$$\dot{\sigma}^{(i)}(t+\delta t) = 0$$ (258)

$$\sum_I \frac{\partial \sigma^{(i)}}{\partial \mathbf{R}_I}\dot{\mathbf{R}}_I = 0$$ (259)

$$-\sum_j \left(\sum_I \frac{\delta t^2}{2M_I}\mathbf{A}_{iI}\mathbf{A}_{jI}\right)\lambda_j^{\mathrm{v}} = \sum_I \mathbf{A}_{iI}\dot{\mathbf{R}}'_I \ .$$ (260)

The only information needed to implement a new type of constraint are the formulas for the functional value and its derivative with respect to the nuclear coordinates involved in the constraint.

3.7.4 Using Car-Parrinello Dynamics for Optimizations

By adding a friction term, Car–Parrinello molecular dynamics can be turned into a damped second order dynamics scheme (see also Sect. 2.4.6).

The friction can be applied both to the nuclear degrees of freedom and the electronic coordinates. The resulting dynamics equation are a powerful method to simultaneously optimize the atomic structure and the Kohn–Sham orbitals [472,610]. Harmonic reference system integration and plane wave dependent electron masses, introduced above, are especially helpful in this context, as the derived dynamics does not have a direct physical relevance.

Introducing a friction force proportional to the constants γ_n and γ_e the equations of motion can readily be integrated using the velocity Verlet algorithm. The friction terms translate into a simple rescaling of the velocities at the beginning and end of the time step according to

$$\dot{\mathbf{R}}_I(t) = \gamma_\mathrm{n}\dot{\mathbf{R}}_I(t)$$
$$\dot{\mathbf{c}}_i(t) = \gamma_\mathrm{e}\dot{\mathbf{c}}_i(t)$$
$$\mathrm{VELOCITY \quad VERLET \ UPDATE}$$
$$\dot{\mathbf{R}}_I(t+\delta t) = \gamma_\mathrm{n}\dot{\mathbf{R}}_I(t+\delta t)$$
$$\dot{\mathbf{c}}_i(t+\delta t) = \gamma_\mathrm{e}\dot{\mathbf{c}}_i(t+\delta t) \ .$$

It was shown [472,610] that this scheme leads to optimizations that are competitive with other methods described in Sect. 3.6

3.8 Data Structures and Computational Kernels

In the practical implementation of the method, mathematical symbols have to be translated into data structures of the computer language. Then mathematical formulas are set into computer code using the data structures. The layout of the data structures should be such that optimal performance for the algorithms can be achieved. The CPMD code is written in FORTRAN77 and in the following sections the most important data structures and computational kernels will be given in pseudo code form. The following variables are used to denote quantities that measure system size.

N_at	number of atoms
N_p	number of projectors
N_b	number of electronic bands or states
N_PW	number of plane-waves
N_D	number of plane-waves for densities and potentials
N_x, N_y, N_z	number of grid points in x, y, and z direction
$N = N_\mathrm{x}N_\mathrm{y}N_\mathrm{z}$	total number of grid points

In Table 3 the relative size of this variables are given for two systems. The example for a silicon crystal assumes an energy cutoff of 13 Rydberg and s non-locality for the pseudopotential. In the example of a water system the numbers are given per molecule. The cutoff used was 70 Rydberg and the oxygen pseudopotential has a s nonlocal part, the hydrogen pseudopotential is local.

Table 3. Relative size of characteristic variables in a plane wave calculation. See text for details.

	silicon	water
N_{at}	1	3
N_{p}	1	1
N_{b}	2	4
N_{PW}	53	1000
N_{D}	429	8000
N	1728	31250

3.8.1 CPMD *Program: Data Structures*

Important quantities in the pseudopotential plane–wave method depend either not at all, linearly, or quadratically on the system size. Examples for the first kind of data are the unit cell matrix $\mathbf{h}$ and the cutoff E_{cut}. Variables with a size that grows linearly with the system are

$\mathtt{r}(3,N_{at})$	nuclear positions
$\mathtt{v}(3,N_{at})$	nuclear velocities
$\mathtt{f}(3,N_{at})$	nuclear forces
$\mathtt{g}(3,N_{PW})$	plane–wave indices
$\mathtt{ipg}(3,N_{PW})$	mapping of G–vectors (positive part)
$\mathtt{img}(3,N_{PW})$	mapping of G–vectors (negative part)
$\mathtt{rhog}(N_{PW})$	densities (n, n_{c}, n_{tot}) in Fourier–space
$\mathtt{vpot}(N_{PW})$	potentials (V_{loc}, V_{xc}, V_{H}) in Fourier–space
$\mathtt{n}(N_x,N_y,N_z)$	densities (n, n_{c}, n_{tot}) in real–space
$\mathtt{v}(N_x,N_y,N_z)$	potentials (V_{loc}, V_{xc}, V_{H}) in real–space
$\mathtt{vps}(N_D)$	local pseudopotential
$\mathtt{rpc}(N_D)$	core charges
$\mathtt{pro}(N_{PW})$	projectors of non-local pseudopotential.

The pseudopotential related quantities $\mathtt{vps}$, $\mathtt{rpc}$, and $\mathtt{pro}$ are one–dimensional in system size but also depend on the number of different atomic species. In the following it is assumed that this is one. It is easy to generalize the pseudo codes given to more than one atomic species. For real quantities that depend on G–vectors only half of the values have to be stored. The other half can be recomputed when needed by using the symmetry relation

$$A(\mathbf{G}) = A^{\star}(-\mathbf{G}) \ . \tag{261}$$

This saves a factor of two in memory. In addition $\mathbf{G}$ vectors are stored in a linear array, instead of a three-dimensional structure. This allows to store only non–zero variables. Because there is a spherical cutoff, another reduction of a factor of two is achieved for the memory. For the Fourier transforms the variables have to be prepared in a three-dimensional array. The mapping of the linear array to this structure is provided by the information stored in the arrays $\mathtt{ipg}$ and $\mathtt{img}$.
Most of the memory is needed for the storage of quantities that grow quadratically

with system size.

`eigr`(N_D,N_{at})	structure factors
`fnl`(N_p,N_b)	overlap of projectors and bands
`dfnl`(N_p,N_b,3)	derivative of `fnl`
`smat`(N_b,N_b)	overlap matrices between bands
`cr`(N_{PW},N_b)	bands in Fourier space
`cv`(N_{PW},N_b)	velocity of bands in Fourier space
`cf`(N_{PW},N_b)	forces of bands in Fourier space

In order to save memory it is possible to store the structure factors only for the **G** vectors of the wave function basis or even not to store them at all. However, this requires that the missing structure factors are recomputed whenever needed. The structure factors `eigr` and the wavefunction related quantities `cr, cv, cf` are complex numbers. Other quantities, like the local pseudopotential `vps`, the core charges `rpc`, and the projectors `pro` can be stored as real numbers if the factor $(-i)^l$ is excluded.

3.8.2 CPMD *Program: Computational Kernels*

Most of the calculations in a plane wave code are done in only a few kernel routines. These routines are given in this section using a pseudo code language. Where possible an implementation using basic linear algebra (BLAS) routines is given. The first kernel is the calculation of the structure factors. The exponential function of the structure factor separates in three parts along the directions s_x, s_y, s_z.

```
MODULE StructureFactor
FOR i=1:N_at
   s(1:3) = 2 * PI * MATMUL[htm1(1:3,1:3),r(1:3,i)]
   dp(1:3) = CMPLX[COS[s(1:3)],SIN[s(1:3)]]
   dm(1:3) = CONJG[dp(1:3)]
   e(0,1:3,i) = 1
   FOR k=1:g_max
      e(k,1:3,i) = e(k-1,1:3,i) * dp
      e(-k,1:3,i) = e(-k+1,1:3,i) * dm
   END
   FOR j=0:N_D
      eigr(j,i) = e(g(1,j),1,i) * e(g(2,j),2,i) * e(g(3,j),3,i)
   END
END
```

In the module above `htm1` is the matrix $(\mathbf{h}^t)^{-1}$. One of the most important calculation is the inner product of two vectors in Fourier space. This kernel appears for example in the calculation of energies

$$e = \sum_{\mathbf{G}} A^{\star}(\mathbf{G})B(\mathbf{G}) \ . \tag{262}$$

Making use of the fact that both functions are real the sum can be restricted to half

of the **G** vectors, and only real operations have to be performed. Approximately a factor of three in operations can be save this way. Special care has to be taken for the zero **G** vector. It is assumed that this plane wave component is stored in the first position of the arrays.

```
MODULE DotProduct
e = A(1) * B(1)
FOR i=2:N_D
   ar = REAL(A(i))
   ai = IMAG(A(i))
   br = REAL(B(i))
   bi = IMAG(B(i))
   e = e + 2 * (ar * br + ai * bi)
END
```

This loop structure is available in the BLAS library, optimized on most computer architectures. To use the BLAS routines for real variables, complex numbers have to be stored as two real numbers in contiguous memory locations.

```
e = A(1) * B(1) + 2 * sdot(2 * N_D - 2,A(2),1,B(2),1)
```

The calculation of overlap matrices between sets of vectors in real space is a important task in the orthogonalization step

$$S_{ij} = \sum_{\mathbf{G}} A_i^\star(\mathbf{G}) B_j(\mathbf{G}) \ . \tag{263}$$

It can be executed by using matrix multiply routines from the BLAS library. The special case of the zero **G** vector is handled by a routine that performs a rank 1 update of the final matrix.

```
MODULE Overlap
CALL SGEMM('T','N',N_b,N_b,2*N_PW,2,&
          & ca(1,1),2*N_PW,cb(1,1),2*N_PW,0,smat,N_b)
CALL SDER(N_b,N_b,-1,ca(1,1),2*N_PW,cb(1,1),2*N_PW,smat,N_b)
```

For a symmetric overlap additional time can be saved by using the symmetric matrix multiply routine. The overlap routines scale like $N_b^2 N_{PW}$. It is therefore very important to have an implementation of these parts that performs close to peek performance.

```
MODULE SymmetricOverlap
CALL SSYRK('U','T',N_b,2*N_PW,2,ca(1,1),2*N_PW,0,smat,N_b)
CALL SDER(N_b,N_b,-1,ca(1,1),2*N_PW,cb(1,1),2*N_PW,smat,N_b)
```

Another operation that scales as the overlap matrix calculations is the rotation of

a set of wavefunctions in Fourier space

$$B_i(\mathbf{G}) = \sum_j A_j(\mathbf{G}) S_{ji} \quad .$$

(264)

Again this kernel can be executed by using the optimized BLAS matrix multiply routines.

```
MODULE Rotation
CALL SGEMM('N','N',2*N_PW,N_b,N_b,1,ca(1,1),2*N_PW,&
           & smat,N_b,0,cb(1,1),2*N_PW)
```

The overlap calculation of the projectors of the nonlinear pseudopotential with the wavefunctions in Fourier space scales as $N_p N_b N_{PW}$. As the projectors are stored as real quantities, the imaginary prefactor and the structure factor have to be applied before the inner product can be calculated. The following pseudo code calculates M projectors at a time, making use of the special structure of the prefactor. This allows again to do all calculations with real quantities. The code assumes that the total number of projectors is a multiple of M. A generalization of the code to other cases is straightforward. By using batches of projectors the overlap can be calculated using matrix multiplies. The variable `lp(i)` holds the angular momentum of projector i.

```
MODULE FNL
FOR i=1:N_p,M
   IF (MOD(lp(i),2) == 0) THEN
      FOR j=0:M-1
         pf = -1**(lp(i+j)/2)
         FOR k=1:N_PW
            t = pro(k) * pf
            er = REAL[eigr(k,iat(i+j))]
            ei = IMAG[eigr(k,iat(i+j))]
            scr(k,j) = CMPLX[t * er,t * ei]
         END
      END
   ELSE
      FOR j=0:M-1
         pf = -1**(lp(i+j)/2+1)
         FOR k=1:N_PW
            t = pro(k) * pf
            er = REAL[eigr(k,iat(i+j))]
            ei = IMAG[eigr(k,iat(i+j))]
            scr(k,j) = CMPLX[-t * ei,t * er]
         END
      END
   END IF
   scr(1,0:M-1) = scr(1,0:M-1)/2
```

```
        CALL SGEMM('T','N',M,$N_\mathrm{b}$,2*$N_\mathrm{PW}$,2,&
                  & scr(1,0),2*$N_\mathrm{PW}$,cr(1,1),2*$N_\mathrm{PW}$,0,fnl(i,1),$N_\mathrm{p}$)
END
```

Fourier transform routines are assumed to work on complex data and return also arrays with complex numbers. The transform of data with the density cutoff is shown in the next two pseudo code sections. It is assumed that a three dimensional fast Fourier transform routine exists. This is in fact the case on most computers where optimized scientific libraries are available. The next two pseudo code segments show the transform of the charge density from Fourier space to real space and back.

```
MODULE INVFFT
scr(1:$N_\mathrm{x}$,1:$N_\mathrm{y}$,1:$N_\mathrm{z}$) = 0
FOR i=1:$N_\mathrm{D}$
   scr(ipg(1,i),ipg(2,i),ipg(3,i)) = rhog(i)
   scr(img(1,i),img(2,i),img(3,i)) = CONJG[rhog(i)]
END
CALL FFT3D("INV",scr)
n(1:$N_\mathrm{x}$,1:$N_\mathrm{y}$,1:$N_\mathrm{z}$) = REAL[scr(1:$N_\mathrm{x}$,1:$N_\mathrm{y}$,1:$N_\mathrm{z}$)]

MODULE FWFFT
scr(1:$N_\mathrm{x}$,1:$N_\mathrm{y}$,1:$N_\mathrm{z}$) = n(1:$N_\mathrm{x}$,1:$N_\mathrm{y}$,1:$N_\mathrm{z}$)
CALL FFT3D("FW",scr)
FOR i=1:$N_\mathrm{D}$
   rhog(i) = scr(ipg(1,i),ipg(2,i),ipg(3,i))
END
```

Special kernels are presented for the calculation of the density and the application of the local potential. These are the implementation of the flow charts shown in Fig. 8. The operation count of these routines is $N_\mathrm{b}N\log[N]$. In most applications these routines take most of the computer time. Only for the biggest applications possible on todays computers the cubic scaling of the orthogonalization and the nonlocal pseudopotential become dominant. A small prefactor and the optimized implementation of the overlap are the reasons for this.

In the Fourier transforms of the wavefunction two properties are used to speed up the calculation. First, because the wavefunctions are real two transforms can be done at the same time, and second, the smaller cutoff of the wavefunctions can be used to avoid some parts of the transforms. The use of the sparsity in the Fourier transforms is not shown in the following modules. In an actual implementation a mask will be generated and only transforms allowed by this mask will be executed. Under optimal circumstances a gain of almost a factor of two can be achieved.

```
MODULE Density
rho(1:$N_x$,1:$N_y$,1:$N_z$) = 0
FOR i=1:$N_b$,2
   scr(1:$N_x$,1:$N_y$,1:$N_z$) = 0
   FOR j=1:$N_{PW}$
      scr(ipg(1,i),ipg(2,i),ipg(3,i)) = c(j,i) + I * c(j,i+1)
      scr(img(1,i),img(2,i),img(3,i)) = CONJG[c(j,i) + I * c(j,i+1)]
   END
   CALL FFT3D("INV",scr)
   rho(1:$N_x$,1:$N_y$,1:$N_z$) = rho(1:$N_x$,1:$N_y$,1:$N_z$) + &
      & REAL[scr(1:$N_x$,1:$N_y$,1:$N_z$)]**2 + IMAG[scr(1:$N_x$,1:$N_y$,1:$N_z$)]**2
END

MODULE VPSI
FOR i=1:$N_b$,2
   scr(1:$N_x$,1:$N_y$,1:$N_z$) = 0
   FOR j=1:$N_{PW}$
      scr(ipg(1,i),ipg(2,i),ipg(3,i)) = c(j,i) + I * c(j,i+1)
      scr(img(1,i),img(2,i),img(3,i)) = CONJG[c(j,i) + I * c(j,i+1)]
   END
   CALL FFT3D("INV",scr)
   scr(1:$N_x$,1:$N_y$,1:$N_z$) = scr(1:$N_x$,1:$N_y$,1:$N_z$) * &
      & vpot(1:$N_x$,1:$N_y$,1:$N_z$)
   CALL FFT3D("FW",scr)
   FOR j=1:$N_{PW}$
      FP = scr(ipg(1,i),ipg(2,i),ipg(3,i)) &
            & + scr(img(1,i),img(2,i),img(3,i))
      FM = scr(ipg(1,i),ipg(2,i),ipg(3,i)) &
            & - scr(img(1,i),img(2,i),img(3,i))
      fc(j,i) = f(i) * CMPLX[REAL[FP],IMAG[FM]]
      fc(j,i+1) = f(i+1) * CMPLX[IMAG[FP],-REAL[FM]]
   END
END
```

3.9   Parallel Computing

3.9.1   Introduction

Ab initio molecular dynamics calculation need large computer resources. Memory and CPU time requirement make it necessary to run projects on the biggest computers available. It is exclusively parallel computers that provide these resources today. There are many different types of parallel computers available. Computers differ in their memory access system and their communication system. Widely different performances are seen for bandwidth and latency. In addition, different programming paradigms are supported. In order to have a portable code that can be used on most of the current computer architectures, CPMD was programmed us-

ing standard communication libraries and making no assumption on the topology of the processor network and memory access system.

Minimizing the communication was the major goal in the implementation of the parallel plane wave code in CPMD. Therefore, the algorithms had to be adapted to the distributed data model chosen. The most important decisions concern the data distribution of the largest arrays in the calculation. These arrays are the ones holding information on the wavefunctions. Three distribution strategies can be envisaged and were used before [90,137,687,688,117].

First, the data are distributed over the bands [687]. Each processor holds all expansion coefficients of an electronic band locally. Several problems arise with this choice. The number of bands is usually of the same magnitude as the number of processors. This leads to a severe load-balancing problem that can only be avoided for certain magic numbers, namely if the number of bands is a multiple of the number of CPU's. Furthermore this approach requires to perform three-dimensional Fourier transforms locally. The memory requirements for the Fourier transform only increase linearly with system size, but their prefactor is very big and a distribution of these arrays is desirable. In addition, all parts of the program that do not contain loops over the number of bands have to be parallelized using another scheme, leading to additional communication and synchronization overhead.

Second, the data is distributed over the Fourier space components and the real space grid is also distributed [90,137,117]. This scheme allows for a straight forward parallelization of all parts of the program that involve loops over the Fourier components or the real space grid. Only a few routines are not covered by this scheme. The disadvantage is that all three-dimensional Fourier transforms require communication.

Third, it is possible to use a combination of the above two schemes [688]. This leads to the most complicated scheme, as only a careful arrangement of algorithms avoids the disadvantages of the other schemes while still keeping their advantages.

Additionally, it is possible to distribute the loop over $\mathbf{k}$–points. As most calculation only use a limited number of $\mathbf{k}$–points or even only the Γ–point, this method is of limited use. However, combining the distribution of the k-points with one of the other method mentioned above might result in a very efficient approach.

The CPMD program is parallelized using the distribution in Fourier and real space. The data distribution is held fixed during a calculation, i.e. static load balancing is used. In all parts of the program where the distribution of the plane waves does not apply, an additional parallelization over the number of atoms or bands is used. However, the data structures involved are replicated on all processors.

A special situation exists for the case of path integral calculations (see Sect. 4.4), where an inherent parallelization over the Trotter slices is present. The problem is "embarrassingly parallel" in this variable and perfect parallelism can be observed on all types of computers, even on clusters of workstations or supercomputers ("meta–computing"). In practice the parallelization over the Trotter slices will be combined with one of the schemes mentioned above, allowing for good results even on massively parallel machines with several hundred processors.

In addition to the variables used in the serial version, local copies have to be defined. These local variables will be indexed by a superscript indicating the processor number. The total number of processors is P. Each processor has a certain number of plane waves, atoms, electronic bands and real space grid points assigned.

N_{at}^p	number of atoms on processor p
N_{p}^p	number of projectors on processor p
N_{b}^p	number of electronic bands or states on processor p
N_{PW}^p	number of plane-waves on processor p
N_{D}^p	number of plane-waves for densities and potentials on processor p
N_{x}^p, N_{y}, N_{z}	number of grid points in x, y, and z direction on processor p
$N^p = N_{\text{x}}^p N_{\text{y}} N_{\text{z}}$	total number of grid points on processor p

The real space grid is only distributed over the x coordinates. This decision is related to the performance of the Fourier transform that will be discussed in more detail in the following sections. The distribution algorithm for atoms, projectors and bands just divides the total number of these quantities in equal junks based on their arbitrary numbering. The algorithms that use these parallelization schemes do not play a major role in the overall performance of the program (at least for the systems accessible with the computers available today) and small imperfections in load balancing can be ignored.

Data structures that are replicated on all processors:

`r(3,`N_{at}`)`	nuclear positions
`v(3,`N_{at}`)`	nuclear velocities
`f(3,`N_{at}`)`	nuclear forces
`fnl(`N_p`,`N_b`)`	overlap of projectors and bands
`smat(`N_b`,`N_b`)`	overlap matrices between bands.

Data structures that are distributed over all processors:

`g(3,`N_{PW}^p`)`	plane–wave indices
`ipg(3,`N_{PW}^p`)`	mapping of G–vectors (positive part)
`img(3,`N_{PW}^p`)`	mapping of G–vectors (negative part)
`rhog(`N_{PW}^p`)`	densities (n, n_{c}, n_{tot}) in Fourier–space
`vpot(`N_{PW}^p`)`	potentials (V_{loc}, V_{xc}, V_{H}) in Fourier–space
`n(`N_x^p`,`N_y`,`N_z`)`	densities (n, n_{c}, n_{tot}) in real–space
`v(`N_x^p`,`N_y`,`N_z`)`	potentials (V_{loc}, V_{xc}, V_{H}) in real–space
`vps(`N_D^p`)`	local pseudopotential
`rpc(`N_D^p`)`	core charges
`pro(`N_{PW}^p`)`	projectors of non-local pseudopotential
`eigr(`N_D^p`,`N_{at}`)`	structure factors
`dfnl(`N_p`,`N_b^p`,3)`	derivative of `fnl`
`cr(`N_{PW}^p`,`N_b`)`	bands in Fourier space
`cv(`N_{PW}^p`,`N_b`)`	velocity of bands in Fourier space
`cf(`N_{PW}^p`,`N_b`)`	forces of bands in Fourier space.

Several different goals should be achieved in the distribution of the plane waves

over processors. All processors should hold approximately the same number of plane waves. If a plane wave for the wavefunction cutoff is on a certain processor, the same plane wave should be on the same processor for the density cutoff. The distribution of the plane waves should be such that at the beginning or end of a three dimensional Fourier transform no additional communication is needed. To achieve all of these goals the following heuristic algorithm [137] is used. The plane waves are ordered into "pencils". Each pencil holds all plane waves with the same g_y and g_z components. The pencils are numbered according to the total number of plane waves that are part of it. Pencils are distributed over processors in a "round robin" fashion switching directions after each round. This is first done for the wavefunction cutoff. For the density cutoff the distribution is carried over, and all new pencils are distributed according to the same algorithm. Experience shows that this algorithm leads to good results for the load balancing on both levels, the total number of plane waves and the total number of pencils. The number of pencils on a processor is proportional to the work for the first step in the three-dimensional Fourier transform.

Special care has to be taken for the processor that holds the $\mathbf{G} = \mathbf{0}$ component. This component has to be treated individually in the calculation of the overlaps. The processor that holds this component will be called $p0$.

3.9.3 CPMD *Program: Computational Kernels*

There are three communication routines mostly used in the parallelization of the CPMD code. All of them are collective communication routines, meaning that all processors are involved. This also implies that synchronization steps are performed during the execution of these routines. Occasionally other communication routines have to be used (e.g. in the output routines for the collection of data) but they do not appear in the basic computational kernels. The three routines are the Broadcast, GlobalSum, and MatrixTranspose. In the Broadcast routine data is send from one processor (px) to all other processors

$$x^p \leftarrow x^{\mathrm{px}} \ . \tag{265}$$

In the GlobalSum routine a data item is replaced on each processor by the sum over this quantity on all processors

$$x^p \leftarrow \sum_p x^p \ . \tag{266}$$

The MatrixTranspose changes the distribution pattern of a matrix, e.g. from row distribution to column distribution

$$x(p,:) \leftarrow x(:,p) \ . \tag{267}$$

On a parallel computer with P processors, a typical latency time t_L (time for the first data to arrive) and a bandwidth of B, the time spend in the communication routines is

Broadcast	$\log_2[P]\{t_L + N/B\}$
GlobalSum	$\log_2[P]\{t_L + N/B\}$
MatrixTranspose	$Pt_L + N/(PB)$

Table 4. Distribution of plane waves and "pencils" in parallel runs on different numbers of processors. Example for a cubic box with a volume of 6479.0979 bohr^3 and a 70 Rydberg cutoff for the wavefunctions. This is the simulation box needed for 32 water molecules at normal pressure.

	wavefunction cutoff			
PE	plane waves		pencils	
	max	min	max	min
1	32043	32043	1933	1933
2	16030	16013	967	966
4	8016	8006	484	482
8	4011	4000	242	240
16	2013	1996	122	119
32	1009	994	62	59
64	507	495	32	29
128	256	245	16	14
	density cutoff			
PE	plane waves		pencils	
	max	min	max	min
1	256034	256034	7721	7721
2	128043	127991	3859	3862
4	64022	63972	1932	1929
8	32013	31976	966	964
16	16011	15971	484	482
32	8011	7966	242	240
64	4011	3992	122	119
128	2006	1996	62	59

where it is assumed that the amount of data N is constant. The time needed in `Broadcast` and `GlobalSum` will increase with the logarithm of the number of processors involved. The time for the matrix transposition scales for one part linearly with the number of processors. Once this part is small, then the latency part will be dominant and increase linearly. Besides load balancing problems, the communication routines will limit the maximum speedup that can be achieved on a parallel computer for a given problem size. Examples will be shown in the last part of this section.

With the distribution of the data structures given, the parallelization of the computational kernels is in most cases easy. In the `StructureFactor` and `Rotation` routines the loop over the plane waves N_D has to be replaced by N_D^p. The routines performing inner products have to be adapted for the $\mathbf{G} = \mathbf{0}$ term and the global summation of the final result.

```
MODULE DotProduct
IF (p == P0) THEN
   ab = A(1) * B(1) + 2 * sdot(2 * (N_D^p - 1),A(2),1,B(2),1)
ELSE
```

```
    ab = 2 * sdot(2 * N_D^p,A(1),1,B(1),1)
END IF
CALL GlobalSum[ab]

MODULE Overlap
CALL SGEMM('T','N',N_b,N_b,2*N_PW^p,2,&
           & ca(1,1),2*N_PW^p,cb(1,1),2*N_PW^p,0,smat,N_b)
IF (p == P0) CALL SDER(N_b,N_b,-1,ca(1,1),2*N_PW^p,&
           & cb(1,1),2*N_PW^p,smat,N_b)
CALL GlobalSum[smat]
```

Similarly, the overlap part of the `FNL` routine has to be changed and the loops restricted to the local number of plane waves.

```
MODULE FNL
FOR i=1:N_p,M
   IF (MOD(lp(i),2) == 0) THEN
      FOR j=0:M-1
         pf = -1**(lp(i+j)/2)
         FOR k=1:N_PW^p
            t = pro(k) * pf
            er = REAL[eigr(k,iat(i+j))]
            ei = IMAG[eigr(k,iat(i+j))]
            scr(k,j) = CMPLX[t * er,t * ei]
         END
      END
   ELSE
      FOR j=0:M-1
         pf = -1**(lp(i+j)/2+1)
         FOR k=1:N_PW^p
            t = pro(k) * pf
            er = REAL[eigr(k,iat(i+j))]
            ei = IMAG[eigr(k,iat(i+j))]
            scr(k,j) = CMPLX[-t * ei,t * er]
         END
      END
   END IF
   IF (p == P0) scr(1,0:M-1) = scr(1,0:M-1)/2
   CALL SGEMM('T','N',M,N_b,2*N_PW^p,2,&
              & scr(1,0),2*N_PW^p,cr(1,1),2*N_PW^p,0,fnl(i,1),N_p)
END
CALL GlobalSum[fnl]
```

The routines that need the most changes are the once that include Fourier transforms. Due to the complicated break up of the plane waves a new mapping has to be introduced. The map `mapxy` ensures that all pencils occupy contiguous memory

locations on each processor.

```
MODULE INVFFT
scr1(1:$N_\mathrm{x}$,1:$N_\mathrm{pencil}^\mathrm{D}$) = 0
FOR i=1:$N_\mathrm{D}^p$
   scr1(ipg(1,i),mapxy(ipg(2,i),ipg(3,i))) = rhog(i)
   scr1(img(1,i),mapxy(img(2,i),img(3,i))) = CONJG[rhog(i)]
END
CALL ParallelFFT3D("INV",scr1,scr2)
n(1:$N_\mathrm{x}^p$,1:$N_\mathrm{y}$,1:$N_\mathrm{z}$) = REAL[scr2(1:$N_\mathrm{x}^p$,1:$N_\mathrm{y}$,1:$N_\mathrm{z}$)]

MODULE FWFFT
scr2(1:$N_\mathrm{x}^p$,1:$N_\mathrm{y}$,1:$N_\mathrm{z}$) = n(1:$N_\mathrm{x}^p$,1:$N_\mathrm{y}$,1:$N_\mathrm{z}$)
CALL ParallelFFT3D("FW",scr1,scr2)
FOR i=1:$N_\mathrm{D}^p$
   rhog(i) = scr1(ipg(1,i),mapxy(ipg(2,i),ipg(3,i)))
END
```

Due to the mapping of the y and z direction in Fourier space onto a single dimension, input and output array of the parallel Fourier transform do have different shapes.

```
MODULE Density
rho(1:$N_\mathrm{x}^p$,1:$N_\mathrm{y}$,1:$N_\mathrm{z}$) = 0
FOR i=1:$N_\mathrm{b}$,2
   scr1(1:$N_\mathrm{x}$,1:$N_\mathrm{pencil}^\mathrm{PW}$) = 0
   FOR j=1:$N_\mathrm{PW}^p$
      scr1(ipg(1,i),mapxy(ipg(2,i),ipg(3,i))) = &
           & c(j,i) + I * c(j,i+1)
      scr1(img(1,i),mapxy(img(2,i),img(3,i))) = &
           & CONJG[c(j,i) + I * c(j,i+1)]
   END
   CALL ParallelFFT3D("INV",scr1,scr2)
   rho(1:$N_\mathrm{x}^p$,1:$N_\mathrm{y}$,1:$N_\mathrm{z}$) = rho(1:$N_\mathrm{x}^p$,1:$N_\mathrm{y}$,1:$N_\mathrm{z}$) + &
      & REAL[scr2(1:$N_\mathrm{x}^p$,1:$N_\mathrm{y}$,1:$N_\mathrm{z}$)]**2 + &
      & IMAG[scr2(1:$N_\mathrm{x}^p$,1:$N_\mathrm{y}$,1:$N_\mathrm{z}$)]**2
END

MODULE VPSI
FOR i=1:$N_\mathrm{b}$,2
   scr1(1:$N_\mathrm{x}$,1:$N_\mathrm{pencil}^\mathrm{PW}$) = 0
   FOR j=1:$N_\mathrm{PW}^p$
      scr1(ipg(1,i),mapxy(ipg(2,i),ipg(3,i))) = &
           & c(j,i) + I * c(j,i+1)
      scr1(img(1,i),mapxy(img(2,i),img(3,i))) = &
           & CONJG[c(j,i) + I * c(j,i+1)]
```

88

```
      END
   CALL ParallelFFT3D("INV",scr1,scr2)
   scr2(1:$N_x^p$,1:$N_y$,1:$N_z$) = scr2(1:$N_x^p$,1:$N_y$,1:$N_z$) * &
      & vpot(1:$N_x^p$,1:$N_y$,1:$N_z$)
   CALL ParallelFFT3D("FW",scr1,scr2)
   FOR j=1:$N_{PW}^p$
      FP = scr1(ipg(1,i),mapxy(ipg(2,i),ipg(3,i))) &
            & + scr1(img(1,i),mapxy(img(2,i),img(3,i)))
      FM = scr1(ipg(1,i),mapxy(ipg(2,i),ipg(3,i))) &
            & - scr1(img(1,i),mapxy(img(2,i),img(3,i)))
      fc(j,i) = f(i) * CMPLX[REAL[FP],IMAG[FM]]
      fc(j,i+1) = f(i+1) * CMPLX[IMAG[FP],-REAL[FM]]
   END
END
```

The parallel Fourier transform routine can be built from a multiple one-dimensional Fourier transform and a parallel matrix transpose. As mentioned above, only one dimension of the real space grid is distributed in the CPMD code. This allows to combine the transforms in y and z direction to a series of two-dimensional transforms. The handling of the plane waves in Fourier space breaks the symmetry and two different transpose routines are needed, depending on the direction. All the communication is done in the routine ParallelTranspose. This routine consists of a part where the coefficients are gathered into matrix form, the parallel matrix transpose, and a final part where the coefficients are put back according to the mapping used.

```
MODULE ParallelFFT3D(tag,a,b)
IF (tag == "INV") THEN
   CALL MLTFFT1D(a)
   CALL ParallelTranspose("INV",b,a)
   CALL MLTFFT2D(b)
ELSE
   CALL MLTFFT2D(b)
   CALL ParallelTranspose("FW",b,a)
   CALL MLTFFT1D(a)
END IF
```

All other parts of the program use the same patterns for the parallelization as the ones shown in this section.

3.9.4 Limitations

Two types of limitations can be encountered when trying to run a parallel code on a computer. Increasing the number of processors working on a problem will no longer lead to a faster calculation or the memory available is not sufficient to perform a calculation, independently on the number of processors available. The first type of
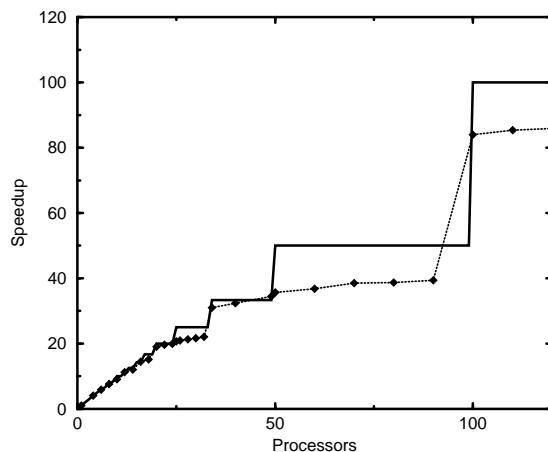
Figure 13. Maximal theoretical speedup for a calculation with a real space grid of dimension 100 (solid line). Effective speedup for a 32 water molecule system with an energy cutoff of 70 Rydberg and a real space grid of dimension 100 (dotted line with diamonds)

limitation is related to bad load-balancing or the computation becomes dominated by the non-scaling part of the communication routines. Load–balancing problems in the CPMD code are almost exclusively due to the distribution of the real space arrays. Only the x coordinate is distributed. There are typically of the order of 100 grid points in each direction. Figure 13 shows the maximal theoretical speedup for a calculation with a real space grid of dimension 100. The steps are due to the load–balancing problems initiated by the granularity of the problem (the dimension is an integer value). No further speedup can be achieved once 100 processors are reached. The second curve in Fig. 13 shows actual calculations of the full CPMD code. It is clearly shown that the load balancing problem in the Fourier transforms affects the performance of this special example. Where this steps appear and how severe the performance losses are depends of course on the system under consideration.

To overcome this limitation a method based on processor groups has been implemented into the code. For the two most important routines where the real space grid load–balancing problem appears, the calculation of the charge density and the application of the local potential, a second level of parallelism is introduced. The processors are arranged into a two-dimensional grid and groups are build according to the row and column indices. Each processor is a member of its column group (colgrp) and its row group (rowgrp). In a first step a data exchange in the column group assures that all the data needed to perform Fourier transforms within the row groups are available. Then each row group performs the Fourier transforms independently and in the end another data exchange in the column groups rebuilds the original data distribution. This scheme (shown in the pseudo code for the density calculation) needs roughly double the amount of communication. Advantages

are the improved load–balancing for the Fourier transforms and the bigger data packages in the matrix transposes. The number of plane waves in the row groups (N_{PW}^{pr}) is calculated as the sum over all local plane waves in the corresponding column groups.

```
MODULE Density
rho(1:N_x^{pr},1:N_y,1:N_z) = 0
FOR i=1:N_b,2*Pc
   CALL ParallelTranspose(c(:,i),colgrp)
   scr1(1:N_x,1:N_{pencil,r}^{PW}) = 0
   FOR j=1:N_PW^{pr}
      scr1(ipg(1,i),mapxy(ipg(2,i),ipg(3,i))) = &
            & c(j,i) + I * c(j,i+1)
      scr1(img(1,i),mapxy(img(2,i),img(3,i))) = &
            & CONJG[c(j,i) + I * c(j,i+1)]
   END
   CALL ParallelFFT3D("INV",scr1,scr2,rowgrp)
   rho(1:N_x^{pr},1:N_y,1:N_z) = rho(1:N_x^{pr},1:N_y,1:N_z) + &
      & REAL[scr2(1:N_x^p,1:N_y,1:N_z)]**2 + &
      & IMAG[scr2(1:N_x^p,1:N_y,1:N_z)]**2
END
CALL GlobalSum(rho,colgrp)
```

The use of two task groups in the example shown in Fig. 13 leads to an increase of speedup for 256 processors from 120 to 184 on a Cray T3E/600 computer.

The effect of the non-scalability of the global communication used in CPMD is shown in Fig. 14. This example shows the percentage of time used in the global communication routines (global sums and broadcasts) and the time spend in the parallel Fourier transforms for a system of 64 silicon atoms with a energy cutoff of 12 Rydberg. It can clearly be seen that the global sums and broadcasts do not scale and therefore become more important the more processors are used. The Fourier transforms on the other hand scale nicely for this range of processors. Where the communication becomes dominant depends on the size of the system and the performance ratio of communication to cpu.

Finally, the memory available on each processor may become a bottleneck for large computations. The replicated data approach for some arrays adapted in the implementation of the code poses limits on the system size that can be processed on a given type of computer. In the outline given in this chapter there are two types of arrays that scale quadratically in system size that a replicated. The overlap matrix of the projectors with the wavefunctions (fnl) and the overlap matrices of the wavefunctions themselves (smat). The fnl matrix is involved in two types of calculations where the parallel loop goes either over the bands or the projectors. To avoid communication, two copies of the array are kept on each processor. Each copy holds the data needed in one of the distribution patterns. This scheme needs only a small adaptation of the code described above.

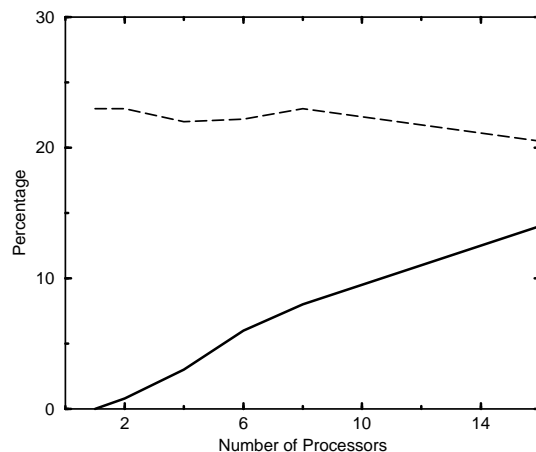The distribution of the overlap matrices (smat) causes some more problems. In

Figure 14. Percentage of total CPU time spend in global communication routines (solid line) and in Fourier transform routines (dashed line) for a system of 64 silicon atoms on a Cray T3E/600 computer.

addition to the adaptation of the overlap routine, also the matrix multiply routines needed for the orthogonalization step have to be done in parallel. Although there are libraries for these tasks available the complexity of the code is considerably increased.

3.9.5 Summary

Efficient parallel algorithms for the plane wave–pseudopotential density functional theory method exist. Implementations of these algorithms are available and were used in most of the large scale applications presented at the end of this paper (Sect. 5). Depending on the size of the problem, excellent speedups can be achieved even on computers with several hundreds of processors. The limitations presented in the last paragraph are of importance for high–end applications. Together with the extensions presented, existing plane wave codes are well suited also for the next generation of supercomputers.

4 Advanced Techniques: Beyond ...

4.1 Introduction

The discussion up to this point revolved essentially around the "basic" *ab initio* molecular dynamics methodologies. This means in particular that *classical* nuclei evolve in the electronic *ground state* in the *microcanonical* ensemble. This combination allows already a multitude of applications, but many circumstances exist where the underlying approximations are unsatisfactory. Among these cases are

situations where

- it is necessary to keep temperature and /or pressure constant (such as during journeys in phase diagrams or in the investigation of solid–state phase transitions),

- there is a sufficient population of excited electronic states (such as in materials with a small or vanishing electronic gap) or dynamical motion occurs in a single excited states (such as after photoexcitation events),

- light nuclei are involved in crucial steps of a process (such as in studies of proton transfer or muonium impurities).

In the following subsections techniques are introduced which transcede these limitations. Thus, the realm of *ab initio* molecular dynamics is considerably increased beyond the basic setup as discussed in general terms in Sect. 2 and concerning its implementation in Sect. 3. The presented "advanced techniques" are selected because they are available in the current version of the CPMD package [142], but their implementation is not discussed in detail here.

4.2 Beyond Microcanonics

4.2.1 Introduction

In the framework of statistical mechanics all ensembles can be formally obtained from the microcanonical or NVE ensemble – where particle number, volume and energy are the external thermodynamic control variables – by suitable Laplace transforms of its partition function; note that V is used for volume when it comes to labeling the various ensembles in Sect. 4 and its subsections. Thermodynamically this corresponds to Legendre transforms of the associated thermodynamic potentials where intensive and extensive conjugate variables are interchanged. In thermodynamics, this task is achieved by a "sufficiently weak" coupling of the original system to an appropriate infinitely large bath or reservoir via a link that establishes thermodynamic equilibrium. The same basic idea is instrumental in generating distribution functions of such ensembles by computer simulation [98,250]. Here, two important special cases are discussed: thermostats and barostats, which are used to impose temperature instead of energy and / or pressure instead of volume as external control parameters [12,445,270,585,217].

4.2.2 Imposing Temperature: Thermostats

In the limit of ergodic sampling the ensemble created by standard molecular dynamics is the microcanonical or NVE ensemble where in addition the total momentum is conserved [12,270,217]. Thus, the temperature is not a control variable in the Newtonian approach to molecular dynamics and whence it cannot be preselected and fixed. But it is evident that also within molecular dynamics the possibility to control the average temperature (as obtained from the average kinetic energy of the nuclei and the energy equipartition theorem) is welcome for physical reasons. A *deterministic* algorithm of achieving temperature control in the spirit of extended

system dynamics [14] by a sort of dynamical friction mechanism was devised by Nosé and Hoover [442,443,444,307], see e.g. Refs. [12,445,270,585,217] for reviews of this well–established technique. Thereby, the canonical or NVT ensemble is generated in the case of ergodic dynamics.

As discussed in depth in Sect. 2.4, the Car–Parrinello approach to *ab initio* molecular dynamics works due to a dynamical separation between the physical and fictitious temperatures of the nuclear and electronic subsystems, respectively. This separability and thus the associated metastability condition breaks down if the electronic excitation gap becomes comparable to the thermal energy or smaller, that is in particular for metallic systems. In order to satisfy nevertheless adiabaticity in the sense of Car and Parrinello it was proposed to couple separate thermostats [583] to the classical fields that stem from the electronic degrees of freedom [74,204]. Finally, the (long–term) stability of the molecular dynamics propagation can be increased due to the same mechanism, which enables one to increase the time step that still allows for adiabatic time evolution [638]. Note that these technical reasons to include additional thermostats are by construction absent from any Born–Oppenheimer molecular dynamics scheme.

It is well–known that the standard Nosé–Hoover thermostat method suffers from non–ergodicity problems for certain classes of Hamiltonians, such as the harmonic oscillator [307]. A closely related technique, the so–called Nosé–Hoover–chain thermostat [388], cures that problem and assures ergodic sampling of phase space even for the pathological harmonic oscillator. This is achieved by thermostatting the original thermostat by another thermostat, which in turn is thermostatted and so on. In addition to restoring ergodicity even with only a few thermostats in the chain, this technique is found to be much more efficient in imposing the desired temperature.

Nosé–Hoover–chain thermostatted Car–Parrinello molecular dynamics was introduced in Ref. [638]. The underlying equations of motion read

$$M_I \ddot{\mathbf{R}}_I = -\nabla_I E^{\mathrm{KS}} - M_I \dot{\xi}_1 \dot{\mathbf{R}}_I \tag{268}$$

$$Q_1^{\mathrm{n}} \ddot{\xi}_1 = \left[\sum_I M_I \dot{\mathbf{R}}_I^2 - g k_{\mathrm{B}} T \right] - Q_1^{\mathrm{n}} \dot{\xi}_1 \dot{\xi}_2$$

$$Q_k^{\mathrm{n}} \ddot{\xi}_k = \left[Q_{k-1}^{\mathrm{n}} \dot{\xi}_{k-1}^2 - k_{\mathrm{B}} T \right] - Q_k^{\mathrm{n}} \dot{\xi}_k \dot{\xi}_{k+1} \left(1 - \delta_{kK} \right) \quad \text{where } k = 2, \dots, K$$

for the nuclear part and

$$\mu \ddot{\phi}_i = -H_{\mathrm{e}}^{\mathrm{KS}} \phi_i + \sum_{ij} \Lambda_{ij} \phi_j - \mu \dot{\eta}_1 \dot{\phi}_i \tag{269}$$

$$Q_1^{\mathrm{e}} \ddot{\eta}_1 = 2 \left[\sum_i^{\mathrm{occ}} \mu \langle \dot{\phi}_i | \dot{\phi}_i \rangle - T_{\mathrm{e}}^0 \right] - Q_1^{\mathrm{e}} \dot{\eta}_1 \dot{\eta}_2$$

$$Q_l^{\mathrm{e}} \ddot{\eta}_l = \left[Q_{l-1}^{\mathrm{e}} \dot{\eta}_{l-1}^2 - \frac{1}{\beta_{\mathrm{e}}} \right] - Q_l^{\mathrm{e}} \dot{\eta}_l \dot{\eta}_{l+1} \left(1 - \delta_{lL} \right) \quad \text{where } l = 2, \dots, L$$

for the electronic contribution. These equations are written down in density functional language (see Eq. (75) and Eq. (81) for the definitions of E^{KS} and $H_{\mathrm{e}}^{\mathrm{KS}}$,

respectively), but completely analogues expressions are operational if other electronic structure approaches are used instead. Using separate thermostatting baths $\{\xi_k\}$ and $\{\eta_l\}$, chains composed of K and L coupled thermostats are attached to the nuclear and electronic equations of motion, respectively.

By inspection of Eq. (268) it becomes intuitively clear how the thermostat works: $\dot{\xi}_1$ can be considered as a *dynamical* friction coefficient. The resulting "dissipative dynamics" leads to non–Hamiltonian flow, but the friction term can aquire positive or negative sign according to its equation of motion. This leads to damping or acceleration of the nuclei and thus to cooling or heating if the instantaneous kinetic energy of the nuclei is higher or lower than $k_B T$ which is preset. As a result, this extended system dynamics can be shown to produce a canonical ensemble in the subspace of the nuclear coordinates and momenta. In spite of being non–Hamiltonian, Nosé–Hoover (–chain) dynamics is also distinguished by conserving an energy quantity of the extended system, see Eq. (272).

The desired average physical temperature is given by T and g denotes the number of dynamical degrees of freedom to which the nuclear thermostat chain is coupled (i.e. constraints imposed on the nuclei have to be subtracted). Similarly, T_e^0 is the desired fictitious kinetic energy of the electrons and $1/\beta_e$ is the associated temperature. In principle, β_e should be chosen such that $1/\beta_e = 2T_e^0/N_e$ where N_e is the number of dynamical degrees of freedom needed to parameterize the wavefunction minus the number of constraint conditions. It is found that this choice requires a very accurate integration of the resulting equations of motion (for instance by using a high–order Suzuki–Yoshida integrator, see Sect. VI.A in Ref. [638]). However, relevant quantities are rather insensitive to the particular value so that N_e can be replaced heuristically by N_e' which is the number of orbitals ϕ_i used to expand the wavefunction [638].

The choice of the "mass parameters" assigned to the thermostat degrees of freedom should be made such that the overlap of their power spectra and the ones the thermostatted subsystems is maximal [74,638]. The relations

$$Q_1^n = \frac{g k_B T}{\omega_n^2} \quad , \qquad Q_k^n = \frac{k_B T}{\omega_n^2} \qquad (270)$$

$$Q_1^e = \frac{2 T_e^0}{\omega_e^2} \quad , \qquad Q_l^e = \frac{1}{\beta_e \omega_e^2} \qquad (271)$$

assures this if ω_n is a typical phonon or vibrational frequency of the nuclear subsystem (say of the order of 2000 to 4000 cm^{-1}) and ω_e is sufficiently large compared to the maximum frequency ω_n^{max} of the nuclear power spectrum (say 10 000 cm^{-1} or larger). The integration of these equations of motion is discussed in detail in Ref. [638] using the velocity Verlet / RATTLE algorithm.

In some instances, for example during equilibration runs, it is advantageous to go one step further and to actually couple one chain of Nosé–Hoover thermostats to every individual nuclear degree of freedom akin to what is done in path integral molecular dynamics simulations [637,644,646], see also Sect. 4.4. This so–called "massive thermostatting approach" is found to accelerate considerably the expensive equilibration periods within *ab initio* molecular dynamics, which is useful for both Car–Parrinello and Born–Oppenheimer dynamics.

In classical molecular dynamics two quantities are conserved during a simulation, the total energy and the total momentum. The same constants of motion apply to (exact) microcanonical Born–Oppenheimer molecular dynamics because the only *dynamical* variables are the nuclear positions and momenta as in classical molecular dynamics. In microcanonical Car–Parrinello molecular dynamics the total energy of the *extended* dynamical system composed of nuclear and electronic positions and momenta, that is E_{cons} as defined in Eq. (48), is also conserved, see e.g. Fig. 3 in Sect. 2.4. There is also a conserved energy quantity in the case of thermostatted molecular dynamics according to Eq. (268)–(269). Instead of Eq. (48) this constant of motion reads

$$
\begin{aligned}
E_{\text{cons}}^{\text{NVT}} = {} & \sum_i^{\text{occ}} \mu \left\langle \dot{\phi}_i \middle| \dot{\phi}_i \right\rangle + \sum_I \frac{1}{2} M_I \dot{\mathbf{R}}_I^2 + E^{\text{KS}} \left[\{\phi_i\}, \{\mathbf{R}_I\} \right] \\
& + \sum_{l=1}^{L} \frac{1}{2} Q_l^{\text{e}} \dot{\eta}_l^2 + \sum_{l=2}^{L} \frac{\eta_l}{\beta_{\text{e}}} + 2 T_{\text{e}}^0 \eta_1 \\
& + \sum_{k=1}^{K} \frac{1}{2} Q_k^{\text{n}} \dot{\xi}_k^2 + \sum_{k=2}^{K} k_{\text{B}} T \xi_k + g k_{\text{B}} T \xi_1
\end{aligned}
\tag{272}
$$

for Nosé–Hoover–chain thermostatted canonical Car–Parrinello molecular dynamics [638].

In microcanonical Car–Parrinello molecular dynamics the total nuclear momentum $\mathbf{P}_{\text{n}}$ is no more a constant of motion as a result of the fictitious dynamics of the wavefunction; this quantity as well as other symmetries and associated invariants are discussed in Ref. [467]. However, a generalized linear momentum which embraces the electronic degrees of freedom

$$
\mathbf{P}_{\text{CP}} = \mathbf{P}_{\text{n}} + \mathbf{P}_{\text{e}} = \sum_I \mathbf{P}_I + \sum_i^{\text{occ}} \mu \left\langle \dot{\phi}_i \middle| -\nabla_{\mathbf{r}} \middle| \phi_i \right\rangle + \text{c.c.}
\tag{273}
$$

can be defined [467,436]; $\mathbf{P}_I = M_I \dot{\mathbf{R}}_I$. This quantity is a constant of motion in unthermostatted Car–Parrinello molecular dynamics due to an exact cancellation of the nuclear and electronic contributions [467,436]. As a result, the nuclear momentum $\mathbf{P}_{\text{n}}$ fluctuates during such a run, but in practice $\mathbf{P}_{\text{n}}$ is conserved *on the average* as shown in Fig. 1 of Ref. [436]. This is analogues to the behavior of the physical total energy E_{phys} Eq. (49), which fluctuates slightly due to the presence of the fictitious kinetic energy of the electrons T_{e} Eq. (51).

As recently outlined in detail it is clear that the coupling of more than one thermostat to a dynamical system, such as done in Eq. (268)–(269), destroys the conservation of momentum [436], i.e. $\mathbf{P}_{\text{CP}}$ is no more an invariant. In unfavorable cases, in particular in small–gap or metallic regimes where there is a substantial coupling of the nuclear and electronic subsystems, momentum can be transferred to the nuclear subsystem such that $\mathbf{P}_{\text{n}}$ grows in the course of a simulation. This problem can be cured by controlling the nuclear momentum (using e.g. scaling or constraint methods) so that the total nuclear momentum $\mathbf{P}_{\text{n}}$ remains small [436].

4.2.3 Imposing Pressure: Barostats

Keeping the pressure constant is a desirable feature for many applications of molecular dynamics. The concept of barostats and thus constant–pressure molecular dynamics was introduced in the framework of extended system dynamics by Hans Andersen [14], see e.g. Refs. [12,270,585,217] for introductions. This method was devised to allow for isotropic fluctuations in the volume of the supercell. A powerful extension consists in also allowing for changes of the *shape* of the supercell to occur as a result of applying external pressure [459,460,461,678], including the possibility of non–isotropic *external* stress [460]; the additional fictitious degrees of freedom in the Parrinello–Rahman approach [459,460,461] are the lattice vectors of the supercell, whereas the strain tensor is the dynamical variable in the Wentzcovitch approach [678]. These variable–cell approaches make it possible to study dynamically structural phase transitions in solids at finite temperatures. With the birth of *ab initio* molecular dynamics both approaches were combined starting out with isotropic volume fluctuations [94] *à la* Andersen [14] and followed by Born–Oppenheimer [681,682] and Car–Parrinello [201,202,55,56] variable–cell techniques.

The basic idea to allow for changes in the cell shape consists in constructing an extended Lagrangian where the primitive Bravais lattice vectors $\mathbf{a}_1$, $\mathbf{a}_2$ and $\mathbf{a}_3$ of the simulation cell are additional dynamical variables similar to the thermostat degree of freedom ξ, see Eq. (268). Using the 3×3 matrix $\mathbf{h} = [\mathbf{a}_1, \mathbf{a}_2, \mathbf{a}_3]$ (which fully defines the cell with volume Ω) the real–space position $\mathbf{R}_I$ of a particle in this original cell can be expressed as

$$\mathbf{R}_I = \mathbf{h}\mathbf{S}_I \tag{274}$$

where $\mathbf{S}_I$ is a scaled coordinate with components $\mathbf{S}_{I,u} \in [0,1]$ that defines the position of the Ith particle in a unit cube (i.e. $\Omega_{\text{unit}} = 1$) which is the scaled cell [459,460], see Sect. 3.1 for some definitions. The resulting metric tensor $\mathcal{G} = \mathbf{h}^{\text{t}}\mathbf{h}$ converts distances measured in scaled coordinates to distances as given by the original coordinates according to Eq. (106) and periodic boundary conditions are applied using Eq. (107).

In the case of *ab initio* molecular dynamics the orbitals have to be expressed suitably in the scaled coordinates $\mathbf{s} = \mathbf{h}^{-1}\mathbf{r}$. The normalized original orbitals $\phi_i(\mathbf{r})$ as defined in the unscaled cell $\mathbf{h}$ are transformed according to

$$\phi_i(\mathbf{r}) = \frac{1}{\sqrt{\Omega}}\,\phi_i\left(\mathbf{s}\right) \tag{275}$$

satisfying

$$\int_\Omega d\mathbf{r}\,\phi_i^\star(\mathbf{r})\phi_i(\mathbf{r}) = \int_{\Omega_{\text{unit}}} d\mathbf{s}\,\phi_i^\star(\mathbf{s})\phi_i(\mathbf{s}) \tag{276}$$

so that the resulting charge density is given by

$$n(\mathbf{r}) = \frac{1}{\Omega}\,n\left(\mathbf{s}\right)\;. \tag{277}$$

in the scaled cell, i.e. the unit cube. Importantly, the scaled fields $\phi_i(\mathbf{s})$ and thus their charge density $n(\mathbf{s})$ do *not* depend on the dynamical variables associated to the cell degrees of freedom and thus can be varied independently from the cell; the

original unscaled fields $\phi_i(\mathbf{r})$ do depend on the cell variables $\mathbf{h}$ via the normalization by the cell volume $\Omega = \det \mathbf{h}$ as evidenced by Eq. (275).

After these preliminaries a variable–cell extended Lagrangian for *ab initio* molecular dynamics can be postulated [202,201,55]

$$\mathcal{L} = \sum_i \mu \left\langle \dot{\phi}_i(\mathbf{s}) \,\middle|\, \dot{\phi}_i(\mathbf{s}) \right\rangle - E^{\mathrm{KS}} \left[\{\phi_i\}, \{\mathbf{h}\mathbf{S}_I\} \right]$$

$$+ \sum_{ij} \Lambda_{ij} \left(\langle \phi_i(\mathbf{s}) \,|\, \phi_j(\mathbf{s}) \rangle - \delta_{ij} \right)$$

$$+ \sum_I \frac{1}{2} M_I \left(\dot{\mathbf{S}}_I^{\mathrm{t}} \mathcal{G} \dot{\mathbf{S}}_I \right) + \frac{1}{2} W \, \mathrm{Tr} \, \dot{\mathbf{h}}^{\mathrm{t}} \dot{\mathbf{h}} - p \, \Omega \ , \tag{278}$$

with additional nine dynamical degrees of freedom that are associated to the lattice vectors of the supercell $\mathbf{h}$. This constant–pressure Lagrangian reduces to the constant–volume Car–Parrinello Lagrangian, see e.g. Eq. (41) or Eq. (58), in the limit $\dot{\mathbf{h}} \to 0$ of a rigid cell (apart from a constant term $p\,\Omega$). Here, p defines the externally applied hydrostatic pressure, W defines the fictitious mass or inertia parameter that controls the time–scale of the motion of the cell $\mathbf{h}$ and the interaction energy E^{KS} is of the form that is defined in Eq. (75). In particular, this Lagrangian allows for symmetry–breaking fluctuations – which might be necessary to drive a solid–state phase transformation – to take place spontaneously. The resulting equations of motion read

$$M_I \ddot{\mathbf{S}}_{I,u} = -\sum_{v=1}^{3} \frac{\partial E^{\mathrm{KS}}}{\partial \mathbf{R}_{I,v}} \left(\mathbf{h}^{\mathrm{t}} \right)^{-1}_{vu} - M_I \sum_{v=1}^{3} \sum_{s=1}^{3} \mathcal{G}_{uv}^{-1} \dot{\mathcal{G}}_{vs} \dot{S}_{I,s} \tag{279}$$

$$\mu \ddot{\phi}_i(\mathbf{s}) = -\frac{\delta E^{\mathrm{KS}}}{\delta \phi_i^{\star}(\mathbf{s})} + \sum_j \Lambda_{ij} \phi_j(\mathbf{s}) \tag{280}$$

$$W \ddot{\mathbf{h}}_{uv} = \Omega \sum_{s=1}^{3} \left(\mathbf{\Pi}^{\mathrm{tot}}_{us} - p \, \delta_{us} \right) \left(\mathbf{h}^{\mathrm{t}} \right)^{-1}_{sv} \ , \tag{281}$$

where the total internal stress tensor

$$\mathbf{\Pi}^{\mathrm{tot}}_{us} = \frac{1}{\Omega} \sum_I M_I \left(\dot{\mathbf{S}}_I^{\mathrm{t}} \mathcal{G} \dot{\mathbf{S}}_I \right)_{us} + \Pi_{us} \tag{282}$$

is the sum of the thermal contribution due to nuclear motion at finite temperature and the electronic stress tensor [440,441] Π which is defined in Eq. (189) and the following equations, see Sect. 3.4.

Similar to the thermostat case discussed in the previous section one can recognize a sort of frictional feedback mechanism. The average internal pressure $\langle (1/3) \, \mathrm{Tr} \, \mathbf{\Pi}^{\mathrm{tot}} \rangle$ equals the externally applied pressure p as a result of maintaining dynamically a balance between $p \, \delta$ and the instantaneous internal stress $\mathbf{\Pi}^{\mathrm{tot}}$ by virtue of the friction coefficient $\propto \dot{\mathcal{G}}$ in Eq. (279). Ergodic trajectories obtained from solving the associated *ab initio* equations of motion Eq. (279)–(281) lead to a sampling according to the isobaric–isoenthalpic or NpH ensemble. However, the generated dynamics is fictitious similar to the constant–temperature case discussed

in the previous section. The isobaric–isothermal or NpT ensemble is obtained by combining barostats and thermostats, see Ref. [389] for a general formulation and Ref. [391] for reversible integration schemes.

An important practical issue in isobaric *ab initio* molecular dynamics simulations is related to problems caused by using a finite basis set, i.e. "incomplete–basis–set" or Pulay–type contributions to the stress, see also Sect. 2.5. Using a finite plane wave basis (together with a finite number of **k**–points) in the presence of a fluctuating cell [245,211] one can either fix the number of plane waves or fix the energy cutoff; see Eq. (122) for their relation according to a rule–of–thumb. A constant number of plane waves implies no Pulay stress but a decreasing precision of the calculation as the volume of the supercell increases, whence leading to a systematically biased (but smooth) equation of state. The constant cutoff procedure has better convergence properties towards the infinite–basis–set limit [245]. However, it produces in general unphysical discontinuities in the total energy and thus in the equation of state at volumes where the number of plane waves changes abruptly, see e.g. Fig. 5 in Ref. [211].

Computationally, the number of plane waves has to be fixed in the framework of Car–Parrinello variable–cell molecular dynamics [94,202,201,55], whereas the energy cutoff can easily be kept constant in Born–Oppenheimer approaches to variable–cell molecular dynamics [681,682]. Sticking to the Car–Parrinello technique a practical remedy [202,55] to this problem consists in modifying the electronic kinetic energy term Eq. (173) in a plane wave expansion Eq. (172) of the Kohn–Sham functional E^{KS} Eq. (75)

$$E_{\mathrm{kin}} = \sum_i f_i \sum_{\mathbf{q}} \frac{1}{2} |\mathbf{G}|^2 \, |c_i(\mathbf{q})|^2 \ , \tag{283}$$

where the unscaled $\mathbf{G}$ and scaled $\mathbf{q} = 2\pi\mathbf{g}$ reciprocal lattice vectors are interrelated via the cell $\mathbf{h}$ according to Eq. (111) (thus $\mathbf{Gr} = \mathbf{qs}$) and the cutoff Eq. (121) is defined as $(1/2)\,|\mathbf{G}|^2 \leq E_{\mathrm{cut}}$ for a fixed number of $\mathbf{q}$–vectors, see Sect. 3.1. The modified kinetic energy at the Γ–point of the Brillouin zone associated to the supercell reads

$$\tilde{E}_{\mathrm{kin}} = \sum_i f_i \sum_{\mathbf{q}} \frac{1}{2} \left| \tilde{\mathbf{G}} \left(A, \sigma, E_{\mathrm{cut}}^{\mathrm{eff}} \right) \right|^2 |c_i(\mathbf{q})|^2 \tag{284}$$

$$\left| \tilde{\mathbf{G}} \left(A, \sigma, E_{\mathrm{cut}}^{\mathrm{eff}} \right) \right|^2 = |\mathbf{G}|^2 + A \left\{ 1 + \mathrm{erf} \left[\frac{\frac{1}{2}|\mathbf{G}|^2 - E_{\mathrm{cut}}^{\mathrm{eff}}}{\sigma} \right] \right\} \tag{285}$$

where A, σ and $E_{\mathrm{cut}}^{\mathrm{eff}}$ are positive definite constants and the number of scaled vectors $\mathbf{q}$, that is the number of plane waves, is strictly kept fixed.

In the limit of a vanishing smoothing ($A \to 0; \sigma \to \infty$) the constant number of plane wave result is recovered. In limit of a sharp step function ($A \to \infty; \sigma \to 0$) all plane waves with $(1/2)\,|\mathbf{G}|^2 \gg E_{\mathrm{cut}}^{\mathrm{eff}}$ have a negligible weight in $\tilde{E}_{\mathrm{kin}}$ and are thus effectively suppressed. This situation mimics a constant cutoff calculation at an "effective cutoff" of $\approx E_{\mathrm{cut}}^{\mathrm{eff}}$ within a constant number of plane wave scheme. For this trick to work note that $E_{\mathrm{cut}} \gg E_{\mathrm{cut}}^{\mathrm{eff}}$ has to be satisfied. In the case $A\rangle 0$ the electronic stress tensor Π given by Eq. (189) features an additional term (due to

changes in the "effective basis set" as a result of variations of the supercell), which is related to the Pulay stress [219,660].

Finally, the strength of the smoothing A⟩0 should be kept as modest as possible since the modification Eq. (284) of the kinetic energy leads to an increase of the highest frequency in the electronic power spectrum $\propto A$. This implies a decrease of the permissible molecular dynamics time step $\Delta t^{\max}$ according to Eq. (55). It is found that a suitably tuned set of the additional parameters $(A, \sigma, E_{\mathrm{cut}}^{\mathrm{eff}})$ leads to an efficiently converging constant–pressure scheme in conjunction with a fairly small number of plane waves [202,55]. Note that the cutoff was kept strictly constant in applications of the Born–Oppenheimer implementation [679] of variable–cell molecular dynamics [681,682], but the smoothing scheme presented here could be implemented in this case as well. An efficient method to correct for the discontinuities of *static* total energy calculations performed at constant cutoff was proposed in Ref. [211]. Evidently, the best way to deal with the incomplete–basis–set problem is to increase the cutoff such that the resulting artifacts become negligible on the physically relevant energy scale.

4.3   Beyond Ground States

4.3.1   Introduction

Extending *ab initio* molecular dynamics to a single non–interacting excited state is straightforward in the framework of wavefunction–based methods such as Hartree–Fock [365,254,191,379,281,284,316,293], generalized valence bond (GVB) [282,283,228,229,230], complete active space SCF (CASSCF) [566,567], or full configuration interaction (FCI) [372] approaches, see Sect. 2.7. However, these methods are computationally quite demanding – given present–day algorithms and hardware. Promising steps in the direction of including several excited states and non–adiabatic couplings are also made [385,386,387,71].

Density functional theory offers an alternative route to approximately solving electronic structure problems and recent approaches to excited–state properties within this framework look promising. In the following, two limiting and thus certainly idealistic situations will be considered, which are characterized by either

- many closely–spaced excited electronic states with a *broad thermal* distribution of fractional occupation numbers, or by

- a single electronic state that is *completely decoupled* from all other states.

The first situation is encountered for metallic systems with collective excitations or for materials at high temperatures compared to the Fermi temperature. It is noted in passing that associating fractional occupation numbers to one–particle orbitals is also one route to go beyond a single–determinant ansatz for constructing the charge density [458,168]. The second case applies for instance to large–gap molecular systems which complete a chemical reaction in a single excited state as a result of e.g. a vertical HOMO / LUMO or instantaneous one–particle / one–hole photoexcitation.

4.3.2 Many Excited States: Free Energy Functional

The free energy functional approach to excited–state molecular dynamics [5,7] is a mean–field approach similar in spirit to Ehrenfest molecular dynamics, see Sect. 2.2. The total wavefunction is first factorized into a nuclear and an electronic wavefunction Eq. (3) followed by taking the classical limit for the nuclear subsystem. Thus, classical nuclei move in the *average* field as obtained from averaging over all electronic states Eq. (25). A difference is that according to Ehrenfest molecular dynamics the electrons are propagated in real time and can perform non–adiabatic transitions by virtue of direct coupling terms $\propto \mathbf{d}^{kl}$ between all states Ψ_k subject to energy conservation, see Sect. 2.2 and in particular Eqs. (27)–(29). The average force or Ehrenfest force is obtained by weighting the different states k according to their diagonal density matrix elements (that is $\propto |c_k(t)|^2$ in Eq. (27)) whereas the coherent transitions are driven by the off–diagonal contributions (which are $\propto c_k^\star c_l$, see Eq. (27)).

In the free energy approach [5,7], the excited states are populated according to the Fermi–Dirac (finite–temperature equilibrium) distribution which is based on the assumption that the electrons "equilibrate" more rapidly than the timescale of the nuclear motion. This means that the set of electronic states evolves at a given temperature "isothermally" (rather than adiabatically) under the inclusion of *incoherent* electronic transitions at the nuclei move. Thus, instead of computing the force acting on the nuclei from the electronic ground–state energy it is obtained from the electronic *free* energy as defined in the canonical ensemble. By allowing such electronic transitions to occur the free energy approach transcends the usual Born–Oppenheimer approximation. However, the approximation of an instantaneous equilibration of the electronic subsystem implies that the electronic structure at a given nuclear configuration $\{\mathbf{R}_I\}$ is completely independent from previous configurations along a molecular dynamics trajectory. Due to this assumption the notion "free energy Born–Oppenheimer approximation" was coined in Ref. [101] in a similar context. Certain non–equilibrium situations can also be modeled within the free energy approach by starting off with an initial orbital occupation pattern that does not correspond to any temperature in its thermodynamic meaning, see e.g. Refs. [570,572,574] for such applications.

The free energy functional as defined in Ref. [5] is introduced most elegantly [7,9] by starting the discussion for the special case of *non*–interacting Fermions

$$H_{\mathrm{s}} = -\frac{1}{2}\nabla^2 - \sum_I \frac{Z_I}{|\mathbf{R}_I - \mathbf{r}|} \tag{286}$$

in a *fixed* external potential due to a collection of nuclei at positions $\{\mathbf{R}_I\}$. The associated grand partition function and its thermodynamic potential ("grand free energy") are given by

$$\Xi_{\mathrm{s}}(\mu V T) = \det{}^2 \left(1 + \exp\left[-\beta\left(H_{\mathrm{s}} - \mu\right)\right]\right) \tag{287}$$

$$\Omega_{\mathrm{s}}(\mu V T) = -k_{\mathrm{B}} T \ln \Xi_{\mathrm{s}}(\mu V T) \ , \tag{288}$$

where μ is the chemical potential acting on the electrons and the square of the

determinant stems from considering the spin–unpolarized special case only. This reduces to the well–known grand potential expression

$$\Omega_{\mathrm{s}}(\mu VT) = -2k_{\mathrm{B}}T \ln \det \left(1 + \exp\left[-\beta\left(H_{\mathrm{s}} - \mu\right)\right]\right)$$
$$= -2k_{\mathrm{B}}T \sum_i \ln\left(1 + \exp\left[-\beta\left(\epsilon_{\mathrm{s}}^{(i)} - \mu\right)\right]\right) \tag{289}$$

for non–interacting spin–1/2 Fermions where $\{\epsilon_{\mathrm{s}}^{(i)}\}$ are the eigenvalues of a one–particle Hamiltonian such as Eq. (286); here the standard identity $\ln \det \mathbf{M} = \mathrm{Tr}\ln \mathbf{M}$ was invoked for positive definite $\mathbf{M}$.

According to thermodynamics the Helmholtz free energy $\mathcal{F}(NVT)$ associated to Eq. (288) can be obtained from an appropriate Legendre transformation of the grand free energy $\Omega(\mu VT)$

$$\mathcal{F}_{\mathrm{s}}(NVT) = \Omega_{\mathrm{s}}(\mu VT) + \mu N + \sum_{I \langle J} \frac{Z_I Z_J}{|\mathbf{R}_I - \mathbf{R}_J|} \tag{290}$$

by fixing the average number of electrons N and determining μ from the conventional thermodynamic condition

$$N = -\left(\frac{\partial\Omega}{\partial\mu}\right)_{VT} . \tag{291}$$

In addition, the internuclear Coulomb interactions between the classical nuclei were included at this stage in Eq. (290). Thus, derivatives of the free energy Eq. (290) with respect to ionic positions $-\nabla_I \mathcal{F}_{\mathrm{s}}$ define forces on the nuclei that could be used in a (hypothetical) molecular dynamics scheme using non–interacting electrons.

The interactions between the electrons can be "switched on" by resorting to Kohn–Sham density functional theory and the concept of a non–interacting reference system. Thus, instead of using the simple one–particle Hamiltonian Eq. (286) the effective Kohn–Sham Hamiltonian Eq. (83) has to be utilized. As a result, the grand free energy Eq. (287) can be written as

$$\Omega^{\mathrm{KS}}(\mu VT) = -2k_{\mathrm{B}}T \ln\left[\det\left(1 + \exp\left[-\beta\left(H^{\mathrm{KS}} - \mu\right)\right]\right)\right] \tag{292}$$

$$H^{\mathrm{KS}} = -\frac{1}{2}\nabla^2 - \sum_I \frac{Z_I}{|\mathbf{R}_I - \mathbf{r}|} + V_{\mathrm{H}}(\mathbf{r}) + \frac{\delta\Omega_{\mathrm{xc}}[n]}{\delta n(\mathbf{r})} \tag{293}$$

$$H^{\mathrm{KS}}\phi_i = \epsilon_i \phi_i \tag{294}$$

where Ω_{xc} is the exchange–correlation functional at finite temperature. By virtue of Eq. (289) one can immediately see that Ω^{KS} is nothing else than the "Fermi–Dirac weighted sum" of the bare Kohn–Sham eigenvalues $\{\epsilon_i\}$. Whence, this term is the extension to finite temperatures of the "band–structure energy" (or of the "sum of orbital energies" in the analogues Hartree–Fock case [604,418]) contribution to the total electronic energy, see Eq. (86).

In order to obtain the correct total electronic free energy of the interacting electrons as defined in Eq. (86) the corresponding extra terms (properly generalized to finite temperatures) have to be included in Ω^{KS}. This finally allows one to write

down the generalization of the Helmholtz free energy of the interacting many–electron case

$$\mathcal{F}^{\mathrm{KS}}(NVT) = \Omega^{\mathrm{KS}}(\mu VT) + \mu \int d\mathbf{r} \ n(\mathbf{r}) + \sum_{I \langle J} \frac{Z_I Z_J}{|\mathbf{R}_I - \mathbf{R}_J|}$$

$$- \frac{1}{2} \int d\mathbf{r} \ V_{\mathrm{H}}(\mathbf{r}) \ n(\mathbf{r}) + \Omega_{\mathrm{xc}} - \int d\mathbf{r} \ \frac{\delta \Omega_{\mathrm{xc}}[n]}{\delta n(\mathbf{r})} \ n(\mathbf{r}) \qquad (295)$$

in the framework of a Kohn–Sham–like formulation. The corresponding one–particle density at the Γ–point is given by

$$n(\mathbf{r}) = \sum_i f_i(\beta) \ |\phi_i(\mathbf{r})|^2 \qquad (296)$$

$$f_i(\beta) = (1 + \exp[\beta(\epsilon_i - \mu)])^{-1} \ , \qquad (297)$$

where the fractional occupation numbers $\{f_i\}$ are obtained from the Fermi–Dirac distribution at temperature T in terms of the Kohn–Sham eigenvalues $\{\epsilon_i\}$. Finally, *ab initio* forces can be obtained as usual from the nuclear gradient of $\mathcal{F}^{\mathrm{KS}}$, which makes molecular dynamics possible.

By construction, the total free energy Eq. (295) reduces to that of the non–interacting toy model Eq. (290) once the electron–electron interaction is switched off. Another useful limit is the ground–state limit $\beta \to \infty$ where the free energy $\mathcal{F}^{\mathrm{KS}}(NVT)$ yields the standard Kohn–Sham total energy expression E^{KS} as defined in Eq. (86) after invoking the appropriate limit $\Omega_{\mathrm{xc}} \to E_{\mathrm{xc}}$ as $T \to 0$. Most importantly, stability analysis [5,7] of Eq. (295) shows that this functional shares the same stationary point as the exact finite–temperature functional due to Mermin [424], see e.g. the textbooks [458,168] for introductions to density functional formalisms at finite temperatures. This implies that the self–consistent density, which defines the stationary point of $\mathcal{F}^{\mathrm{KS}}$, is identical to the exact one. This analysis reveals furthermore that, unfortunately, this stationary point is not an extremum but a saddle point so that no variational principle and, numerically speaking, no direct minimization algorithms can be applied. For the same reason a Car–Parrinello fictitious dynamics approach to molecular dynamics is not a straightforward option, whereas Born–Oppenheimer dynamics based on diagonalization can be used directly.

The band–structure energy term is evaluated in the CPMD package [142] by diagonalizing the Kohn–Sham Hamiltonian after a suitable "preconditioning" [5], see Sect. 3.6.2. Specifically, a second–order Trotter approximation is used

$$\mathrm{Tr} \ \exp\left[-\beta H^{\mathrm{KS}}\right] = \sum_i \exp[-\beta \epsilon_i] = \sum_i \rho_{ii}(\beta) \qquad (298)$$

$$= \mathrm{Tr} \left(\left\{ \exp\left[-\frac{\Delta\tau}{2}\left(-\frac{1}{2}\nabla^2\right)\right] \exp\left[-\Delta\tau V^{\mathrm{KS}}[n]\right] \right. \right.$$

$$\left. \left. \exp\left[-\frac{\Delta\tau}{2}\left(-\frac{1}{2}\nabla^2\right)\right] \right\} + \mathcal{O}\left(\Delta\tau^3\right) \right)^P \qquad (299)$$

$$\approx \sum_i \left\{\rho_{ii}(\Delta\tau)\right\}^P = \sum_i \left\{\exp[-\Delta\tau \epsilon_i]\right\}^P \qquad (300)$$

in order to compute first the diagonal elements $\rho_{ii}(\Delta\tau)$ of the "high–temperature" Boltzmann operator $\rho(\Delta\tau)$; here $\Delta\tau = \beta/P$ and P is the Trotter "time slice" as introduced in Sect. 4.4.2. To this end, the kinetic and potential energies can be conveniently evaluated in reciprocal and real space, respectively, by using the split–operator / FFT technique [183]. The Kohn–Sham eigenvalues ϵ_i are finally obtained from the density matrix via $\epsilon_i = -(1/\Delta\tau)\ln\rho_{ii}(\Delta\tau)$. They are used in order to compute the occupation numbers $\{f_i\}$, the density $n(\mathbf{r})$, the band–structure energy Ω^{KS}, and thus the free energy Eq. (295).

In practice a diagonalization / density–mixing scheme is employed in order to compute the self–consistent density $n(\mathbf{r})$. Grossly speaking a suitably constructed trial input density n_{in} (see e.g. the Appendix of Ref. [571] for such a method) is used in order to compute the potential $V^{KS}[n_{in}]$. Then the lowest–order approximant to the Boltzmann operator Eq. (300) is diagonalized using an iterative Lanczos–type method. This yields an output density n_{out} and the corresponding free energy $\mathcal{F}^{KS}[n_{out}]$. Finally, the densities are mixed and the former steps are iterated until a stationary solution n_{scf} of $\mathcal{F}^{KS}[n_{scf}]$ is achieved, see Sect. 3.6.4 for some details on such methods. Of course the most time–consuming part of the calculation is in the iterative diagonalization. In principle this is not required, and it should be possible to compute the output density directly from the Fermi–Dirac density matrix even in a linear scaling scheme [243], thus circumventing the explicit calculation of the Kohn–Sham eigenstates. However, to date efforts in this direction have failed, or given methods which are too slow to be useful [9].

As a method, molecular dynamics with the free energy functional is most appropriate to use when the excitation gap is either small, or in cases where the gap might close during a chemical transformation. In the latter case no instabilities are encountered with this approach, which is not true for ground–state *ab initio* molecular dynamics methods. The price to pay is the quite demanding iterative computation of well–converged forces. Besides allowing such applications with physically relevant excitations this method can also be straightforwardly combined with $\mathbf{k}$–point sampling and applied to metals at "zero" temperature. In this case, the electronic "temperature" is only used as a smearing parameter of the Fermi edge by introducing fractional occupation numbers, which is known to improve greatly the convergence of these ground–state electronic structure calculations [220,232,185,676,680,343,260,344,414,243].

Finite–temperature expressions for the exchange–correlation functional Ω_{xc} are available in the literature. However, for most temperatures of interest the corrections to the ground–state expression are small and it seems justified to use one of the various well–established parameterizations of the exchange–correlation energy E_{xc} at zero temperature, see Sect. 2.7.

4.3.3 A Single Excited State: S_1–Dynamics

For large–gap systems with well separated electronic states it might be desirable to single out a particular state in order to allow the nuclei to move on the associated excited state potential energy surface. Approaches that rely on fractional occupation numbers such as ensemble density functional theories – including the

free energy functional discussed in the previous section – are difficult to adapt for cases where the symmetry and / or spin of the electronic state should be fixed [168]. An early approach in order to select a particular excited state was based on introducing a "quadratic restoring potential" which vanishes only at the eigenvalue of the particular state [417,111].

A method that combines Roothaan's symmetry–adapted wavefunctions with Kohn–Sham density functional theory was proposed in Ref. [214] and used to simulate a photoisomerization via molecular dynamics. Viewed from Kohn–Sham theory this approach consists in building up the spin density of an open–shell system based on a symmetry–adapted wavefunction that is constructed from spin–restricted determinants (the "microstates"). Viewed from the restricted open–shell Hartree–Fock theory *à la* Roothaan it amounts essentially to replacing Hartree–Fock exchange by an approximate exchange–correlation density functional. This procedure leads to an orbital–dependent density functional which was formulated explicitly for the first–excited singlet state S_1 in Ref. [214]. The relation of this approach to previous theories is discussed in some detail in Ref. [214]. In particular, the success of the closely–related Ziegler–Rauk–Baerends "sum methods" [704,150,600] was an important stimulus. More recently several papers [252,439,193,195,196] appeared that are similar in spirit to the method of Ref. [214]. The approach of Refs. [193,195,196] can be viewed as a generalization of the special case (S_1 state) worked out in Ref. [214] to arbitrary spin states. In addition, the generalized method [193,195,196] was derived within the framework of density functional theory, whereas the wavefunction perspective was the starting point in Ref. [214].

In the following, the method is outlined with the focus to perform molecular dynamics in the S_1 state. Promoting one electron from the HOMO to the LUMO in a closed–shell system with $2n$ electrons assigned to n doubly occupied orbitals (that is spin–restricted orbitals that have the same spatial part for both spin up α and spin down β electrons) leads to four different excited wavefunctions or determinants, see Fig. 15 for a sketch. Two states $|t_1\rangle$ and $|t_2\rangle$ are energetically degenerate triplets t whereas the two states $|m_1\rangle$ and $|m_2\rangle$ are not eigenfunctions of the total spin operator and thus degenerate mixed states m ("spin contamination"). Note in particular that the m states do not correspond – as is well known – to singlet states despite the suggestive occupation pattern in Fig. 15.

However, suitable Clebsch–Gordon projections of the mixed states $|m_1\rangle$ and $|m_2\rangle$ yield another triplet state $|t_3\rangle$ and the desired first excited singlet or S_1 state $|s_1\rangle$. Here, the ansatz [214] for the total energy of the S_1 state is given by

$$E_{S_1}[\{\phi_i\}] = 2E_m^{\mathrm{KS}}[\{\phi_i\}] - E_t^{\mathrm{KS}}[\{\phi_i\}] \tag{301}$$

where the energies of the mixed and triplet determinants

$$E_m^{\mathrm{KS}}[\{\phi_i\}] = T_{\mathrm{s}}[n] + \int d\mathbf{r} \; V_{\mathrm{ext}}(\mathbf{r})n(\mathbf{r}) + \frac{1}{2}\int d\mathbf{r} \; V_{\mathrm{H}}(\mathbf{r})n(\mathbf{r}) + E_{\mathrm{xc}}[n_m^\alpha, n_m^\beta] \tag{302}$$

$$E_t^{\mathrm{KS}}[\{\phi_i\}] = T_{\mathrm{s}}[n] + \int d\mathbf{r} \; V_{\mathrm{ext}}(\mathbf{r})n(\mathbf{r}) + \frac{1}{2}\int d\mathbf{r} \; V_{\mathrm{H}}(\mathbf{r})n(\mathbf{r}) + E_{\mathrm{xc}}[n_t^\alpha, n_t^\beta] \tag{303}$$

are expressed in terms of (restricted) Kohn–Sham spin–density functionals constructed from the set $\{\phi_i\}$, cf. Eq. (75). The associated S_1 wavefunction is given
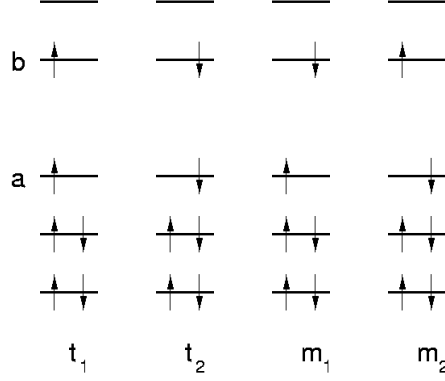
Figure 15. Four possible determinants $|t_1\rangle$, $|t_2\rangle$, $|m_1\rangle$ and $|m_2\rangle$ as a result of the promotion of a single electron from the HOMO to the LUMO of a closed shell system, see text for further details. Taken from Ref. [214].

by

$$| s_1 [\{\phi_i\}] \rangle = \sqrt{2} \, | m [\{\phi_i\}] \rangle - | t [\{\phi_i\}] \rangle \qquad (304)$$

where the "microstates" m and t are both constructed from the same set $\{\phi_i\}$ of $n+1$ spin–*restricted* orbitals. Using this particular set of orbitals the total density

$$n(\mathbf{r}) = n_m^\alpha(\mathbf{r}) + n_m^\beta(\mathbf{r}) = n_t^\alpha(\mathbf{r}) + n_t^\beta(\mathbf{r}) \qquad (305)$$

is of course identical for both the m and t determinants whereas their spin densities clearly differ, see Fig. 16. Thus, the decisive difference between the m and t functionals Eq. (302) and Eq. (303), respectively, comes exclusively from the exchange–correlation functional E_{xc}, whereas kinetic, external and Hartree energy are identical by construction. Note that this basic philosophy can be generalized to other spin–states by adapting suitably the microstates and the corresponding coefficients in Eq. (301) and Eq. (304).

Having defined a density functional for the first excited singlet state the corresponding Kohn–Sham equations are obtained by varying Eq. (301) using Eq. (302) and Eq. (303) subject to the orthonormality constraint $\sum_{i,j=1}^{n+1} \Lambda_{ij}(\langle \phi_i | \phi_j \rangle - \delta_{ij})$. Following this procedure the equation for the doubly occupied orbitals $i = 1, \ldots, n-1$ reads

$$
\begin{aligned}
\Big\{ &-\frac{1}{2}\nabla^2 + V_{\text{H}}(\mathbf{r}) + V_{\text{ext}}(\mathbf{r}) \\
&+ V_{\text{xc}}^\alpha[n_m^\alpha(\mathbf{r}), n_m^\beta(\mathbf{r})] + V_{\text{xc}}^\beta[n_m^\alpha(\mathbf{r}), n_m^\beta(\mathbf{r})] \\
&- \frac{1}{2}V_{\text{xc}}^\alpha[n_t^\alpha(\mathbf{r}), n_t^\beta(\mathbf{r})] - \frac{1}{2}V_{\text{xc}}^\beta[n_t^\alpha(\mathbf{r}), n_t^\beta(\mathbf{r})] \Big\} \phi_i(\mathbf{r}) = \sum_{j=1}^{n+1} \Lambda_{ij}\phi_j(\mathbf{r}) \qquad (306)
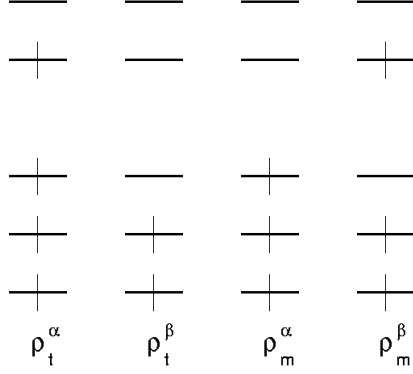\end{aligned}
$$

Figure 16. Four patterns of spin densities n_t^α, n_t^β, n_m^α, and n_m^β corresponding to the two spin–restricted determinants $|t\rangle$ and $|m\rangle$ sketched in Fig. 15, see text for further details. Taken from Ref. [214].

whereas

$$\left\{ \frac{1}{2}\left[-\frac{1}{2}\nabla^2 + V_H(\mathbf{r}) + V_{ext}(\mathbf{r}) \right] \right.$$
$$\left. + V_{xc}^\alpha[n_m^\alpha(\mathbf{r}), n_m^\beta(\mathbf{r})] - \frac{1}{2}V_{xc}^\alpha[n_t^\alpha(\mathbf{r}), n_t^\beta(\mathbf{r})] \right\}\phi_a(\mathbf{r}) = \sum_{j=1}^{n+1}\Lambda_{aj}\phi_j(\mathbf{r}) , \quad (307)$$

and

$$\left\{ \frac{1}{2}\left[-\frac{1}{2}\nabla^2 + V_H(\mathbf{r}) + V_{ext}(\mathbf{r}) \right] \right.$$
$$\left. + V_{xc}^\beta[n_m^\alpha(\mathbf{r}), n_m^\beta(\mathbf{r})] - \frac{1}{2}V_{xc}^\alpha[n_t^\alpha(\mathbf{r}), n_t^\beta(\mathbf{r})] \right\}\phi_b(\mathbf{r}) = \sum_{j=1}^{n+1}\Lambda_{bj}\phi_j(\mathbf{r}) . \quad (308)$$

are two *different* equations for the two singly–occupied open–shell orbitals a and b, respectively, see Fig. 15. Note that these Kohn–Sham–like equations feature an orbital–dependent exchange–correlation potential where $V_{xc}^\alpha[n_m^\alpha, n_m^\beta] = \delta E_{xc}[n_m^\alpha, n_m^\beta]/\delta n_m^\alpha$ and analogues definitions hold for the β and t cases.

The set of equations Eq. (306)–(308) could be solved by diagonalization of the corresponding "restricted open–shell Kohn–Sham Hamiltonian" or alternatively by direct minimization of the associated total energy functional. The algorithm proposed in Ref. [240], which allows to properly and efficiently minimize such orbital–dependent functionals including the orthonormality constraints, was implemented in the CPMD package [142]. Based on this minimization technique Born–Oppenheimer molecular dynamics simulations can be performed in the first excited singlet state.

107

The alternative Car–Parrinello formulation seems inconvenient because the singly and doubly occupied orbitals would have to be constrained not to mix.

4.4 Beyond Classical Nuclei

4.4.1 Introduction

Up to this point the nuclei were approximated as classical point particles as customarily done in standard molecular dynamics. There are, however, many situations where quantum dispersion broadening and tunneling effects play an important role and cannot be neglected if the simulation aims at being realistic – which is the generic goal of *ab initio* simulations. The *ab initio* path integral technique [395] and its extension to quasiclassical time evolution [411] is able to cope with such situations at finite temperatures. It is also implemented in the CPMD package [142]. The central idea is to quantize the nuclei using Feynman's path integrals and at the same time to include the electronic degrees of freedom akin to *ab initio* molecular dynamics – that is "on–the–fly". The main ingredients and approximations underlying the *ab initio* path integral approach [395,399,644,404] are

- the adiabatic separation of electrons and nuclei where the electrons are kept in their ground state without any coupling to electronically excited states (Born–Oppenheimer or "clamped–nuclei" approximation),

- using a particular approximate electronic structure theory in order to calculate the interactions,

- approximating the continuous path integral for the nuclei by a finite discretization (Trotter factorization) and neglecting the indistinguishability of identical nuclei (Boltzmann statistics), and

- using finite supercells with periodic boundary conditions and finite sampling times (finite–size and finite–time effects) as usual.

Thus, quantum effects such as zero–point motion and tunneling as well as thermal fluctuations are included at some preset temperature without further simplifications consisting e.g. in quasiclassical or quasiharmonic approximations, restricting the Hilbert space, or in artificially reducing the dimensionality of the problem.

4.4.2 Ab Initio Path Integrals: Statics

For the purpose of introducing *ab initio* path integrals [395] it is convenient to start directly with Feynman's formulation of quantum–statistical mechanics in terms of path integrals as opposed to Schrödinger's formulation in terms of wavefunctions which was used in Sect. 2.1 in order to derive *ab initio* molecular dynamics. For a general introduction to path integrals the reader is referred to standard textbooks [187,188,334], whereas their use in numerical simulations is discussed for instance in Refs. [233,126,542,120,124,646,407].

The derivation of the expressions for *ab initio* path integrals is based on assuming the non–relativistic standard Hamiltonian, see Eq. (2). The corresponding canonical partition function of a collection of interacting nuclei with positions $\mathbf{R} = \{\mathbf{R}_I\}$

and electrons $\mathbf{r} = \{\mathbf{r}_i\}$ can be written as a path integral

$$\mathcal{Z} = \oint' \mathcal{D}\mathbf{R} \oint' \mathcal{D}\mathbf{r} \exp\left[-\frac{1}{\hbar} \int_0^{\hbar\beta} d\tau \, \mathcal{L}_{\mathrm{E}} \left(\{\dot{\mathbf{R}}_I(\tau)\}, \{\mathbf{R}_I(\tau)\}; \{\dot{\mathbf{r}}_i(\tau)\}, \{\mathbf{r}_i(\tau)\}\right)\right] \quad (309)$$

where

$$\begin{aligned}
\mathcal{L}_{\mathrm{E}} &= T(\dot{\mathbf{R}}) + V(\mathbf{R}) + T(\dot{\mathbf{r}}) + V(\mathbf{r}) + V(\mathbf{R}, \mathbf{r}) \\
&= \sum_I \frac{1}{2} M_I \left(\frac{d\mathbf{R}_I}{d\tau}\right)^2 + \sum_{I\langle J} \frac{\mathrm{e}^2 Z_I Z_J}{|\mathbf{R}_I - \mathbf{R}_J|} \\
&\quad + \sum_i \frac{1}{2} m_{\mathrm{e}} \left(\frac{d\mathbf{r}_i}{d\tau}\right)^2 + \sum_{i\langle j} \frac{\mathrm{e}^2}{|\mathbf{r}_i - \mathbf{r}_j|} - \sum_{I,i} \frac{\mathrm{e}^2 Z_I}{|\mathbf{R}_I - \mathbf{r}_i|} \quad , \quad (310)
\end{aligned}$$

denotes the *Euclidean* Lagrangian. The primes in Eq. (309) indicate that the proper sums over all permutations corresponding to Bose–Einstein and/or Fermi–Dirac statistics have to be included. It is important to note that in Eq. (309) and (310) the positions $\{\mathbf{R}_I\}$ and $\{\mathbf{r}_i\}$ are not operators but simply *functions* of the imaginary time $\tau \in [0, \hbar\beta]$ which parameterizes fluctuations around the classical path. This implies that the dots denote here derivatives with respect to imaginary time τ as defined in Eq. (310). According to Eq. (309) exact quantum mechanics at finite temperature $T = 1/k_{\mathrm{B}}\beta$ is recovered if all closed paths $[\{\mathbf{R}_I\}; \{\mathbf{r}_i\}]$ of "length" $\hbar\beta$ are summed up and weighted with the exponential of the Euclidean action measured in units of $\hbar$; atomic units will be used again from here on. The partial trace over the electronic subsystem can formally be written down exactly

$$\mathcal{Z} = \oint' \mathcal{D}\mathbf{R} \exp\left[-\int_0^\beta d\tau \left(T(\dot{\mathbf{R}}) + V(\mathbf{R})\right)\right] \mathcal{Z}[\mathbf{R}] \quad , \quad (311)$$

with the aid of the influence functional [187,334]

$$\mathcal{Z}[\mathbf{R}] = \oint' \mathcal{D}\mathbf{r} \exp\left[-\int_0^\beta d\tau \left(T(\dot{\mathbf{r}}) + V(\mathbf{r}) + V(\mathbf{R}, \mathbf{r})\right)\right] \quad . \quad (312)$$

Note that $\mathcal{Z}[\mathbf{R}]$ is a complicated and unknown functional for a given nuclear path configuration $[\{\mathbf{R}_I\}]$. As a consequence the interactions between the nuclei become highly nonlocal in imaginary time due to memory effects.

In the standard Born–Oppenheimer or "clamped nuclei" approximation, see Ref. [340] for instance, the nuclei are frozen in some configuration and the complete electronic problem is solved for this single static configuration. In addition to the nondiagonal correction terms that are already neglected in the adiabatic approximation, the diagonal terms are now neglected as well. Thus the potential for the nuclear motion is simply defined as the bare electronic eigenvalues obtained from a series of fixed nuclear configurations.

In the statistical mechanics formulation of the problem Eq. (311)–(312) the Born–Oppenheimer approximation amounts to a "quenched average": at imaginary time τ the nuclei are frozen at a particular configuration $\mathbf{R}(\tau)$ and the electrons explore their configuration space subject only to that single configuration. This

implies that the electronic degrees of freedom at different imaginary times τ and τ' become completely decoupled. Thus, the influence functional $\mathcal{Z}[\mathbf{R}]$ has to be local in τ and becomes particularly simple; a discussion of adiabatic corrections in the path integral formulation can be found in Ref. [101]. For each τ the influence functional $\mathcal{Z}[\mathbf{R}]$ is given by the partition function of the electronic subsystem evaluated for the respective nuclear configuration $\mathbf{R}(\tau)$. Assuming that the temperature is small compared to the gap in the electronic spectrum only the electronic ground state with energy $E_0(\mathbf{R}(\tau))$ (obtained from solving Eq. (20) without the internuclear Coulomb repulsion term) is populated. This electronic ground state dominance leads to the following simple expression

$$\mathcal{Z}[\mathbf{R}]_{\mathrm{BO}} = \exp\left[-\int_0^\beta d\tau\, E_0(\mathbf{R}(\tau))\right] \;\;, \tag{313}$$

which yields the final result

$$\mathcal{Z}_{\mathrm{BO}} = \oint \mathcal{D}\mathbf{R}\,\exp\left[-\int_0^\beta d\tau\left(T(\dot{\mathbf{R}}) + V(\mathbf{R}) + E_0(\mathbf{R})\right)\right]\;\;. \tag{314}$$

Here nuclear exchange is neglected by assuming that the nuclei are distinguishable so that they can be treated within Boltzmann statistics, which corresponds to the Hartree approximation for the *nuclear* density matrix. The presentation given here follows Ref. [399] and alternative derivations were given in Sect. 2.3 of Refs. [124] and in the appendix of Ref. [427]. There, a wavefunction basis instead of the position basis as in Eq. (312) was formally used in order to evaluate the influence functional due to the electrons.

The partition function Eq. (314) together with the Coulomb Hamiltonian Eq. (2) leads after applying the lowest–order Trotter factorization [334] to the following discretized expression

$$\mathcal{Z}_{\mathrm{BO}} = \lim_{P\to\infty} \prod_{s=1}^{P}\prod_{I=1}^{N}\left[\left(\frac{M_I P}{2\pi\beta}\right)^{3/2}\int d\mathbf{R}_I^{(s)}\right]$$

$$\times \exp\left[-\beta\sum_{s=1}^{P}\left\{\sum_{I=1}^{N}\frac{1}{2}M_I\omega_P^2\left(\mathbf{R}_I^{(s)} - \mathbf{R}_I^{(s+1)}\right)^2 + \frac{1}{P}E_0\left(\{\mathbf{R}_I\}^{(s)}\right)\right\}\right] \tag{315}$$

for the path integral with $\omega_P^2 = P/\beta^2$ Thus, the continuous parameter $\tau \in [0,\beta]$ is discretized using P so–called Trotter slices or "time slices" $s = 1,\dots,P$ of "duration" $\Delta\tau = \beta/P$. The paths

$$\left\{\{\mathbf{R}_I\}^{(s)}\right\} = \left(\{\mathbf{R}_I\}^{(1)};\dots;\{\mathbf{R}_I\}^{(P)}\right)$$

$$= \left(\mathbf{R}_1^{(1)},\dots,\mathbf{R}_N^{(1)};\dots;\mathbf{R}_1^{(P)},\dots,\mathbf{R}_N^{(P)}\right) \tag{316}$$

have to be closed due to the trace condition, i.e. they are periodic in imaginary time τ which implies $\mathbf{R}_I(0) \equiv \mathbf{R}_I(\beta)$ and thus $\mathbf{R}_I^{(P+1)} = \mathbf{R}_I^{(1)}$; the internuclear Coulomb repulsion $V(\mathbf{R})$ is now included in the definition of the total electronic energy E_0. Note that Eq. (315) is an *exact* reformulation of Eq. (314) in the limit of an infinitely fine discretization $P \to \infty$ of the paths.

The effective classical partition function Eq. (315) with a fixed discretization P is isomorphic to that for N polymers each comprised by P monomers [233,126,120]. Each quantum degree of freedom is found to be represented by a ring polymer or necklace. The intrapolymeric interactions stem from the kinetic energy $T(\dot{\mathbf{R}})$ and consist of harmonic nearest–neighbor couplings $\propto \omega_P$ along the closed chain. The interpolymeric interaction is given by the scaled potential $E_0^{(s)}/P$ which is only evaluated for configurations $\{\mathbf{R}_I\}^{(s)}$ at the *same* imaginary time slice s.

In order to evaluate operators based on an expression like Eq. (315) most numerical path integral schemes utilize Metropolis Monte Carlo sampling with the effective potential

$$V_{\text{eff}} = \sum_{s=1}^{P} \left\{ \sum_{I=1}^{N} \frac{1}{2} M_I \omega_P^2 \left(\mathbf{R}_I^{(s)} - \mathbf{R}_I^{(s+1)} \right)^2 + \frac{1}{P} E_0 \left(\{\mathbf{R}_I\}^{(s)} \right) \right\} \tag{317}$$

of the isomorphic classical system [233,126,542,120,124,646,407]. Molecular dynamics techniques were also proposed in order to sample configuration space, see Refs. [99,490,462,501,273] for pioneering work and Ref. [646] for an authoritative review. Formally a Lagrangian can be obtained from the expression Eq. (317) by extending it

$$\mathcal{L}_{\text{PIMD}} = \sum_{s=1}^{P} \left\{ \sum_{I=1}^{N} \left(\frac{1}{2M_I'} \mathbf{P}_I^{(s)} - \frac{1}{2} M_I \omega_P^2 \left(\mathbf{R}_I^{(s)} - \mathbf{R}_I^{(s+1)} \right)^2 \right) - \frac{1}{P} E_0 \left(\{\mathbf{R}_I\}^{(s)} \right) \right\} \tag{318}$$

with $N \times P$ fictitious momenta $\mathbf{P}_I^{(s)}$ and corresponding (unphysical) fictitious masses M_I'. At this stage the time dependence of positions and momenta and thus the time evolution in *phase space* as generated by Eq. (318) has no physical meaning. The sole use of "time" is to parameterize the deterministic dynamical exploration of *configuration space*. The trajectories of the positions in configuration space, can, however, be analyzed similar to the ones obtained from the stochastic dynamics that underlies the Monte Carlo method.

The crucial ingredient in *ab initio* [395,399,644,404] as opposed to standard [233,126,542,120,124,646,407] path integral simulations consists in computing the interactions E_0 "on–the–fly" like in *ab initio* molecular dynamics. In analogy to this case both the Car–Parrinello and Born–Oppenheimer approaches from Sects. 2.4 and 2.3, respectively, can be combined with any electronic structure method. The first implementation [395] was based on the Car–Parrinello / density functional combination from Sect. 2.4 which leads to the following extended Lagrangian

$$
\begin{aligned}
\mathcal{L}_{\text{AIPI}} = \frac{1}{P} \sum_{s=1}^{P} &\left\{ \sum_i \mu \left\langle \dot{\phi}_i^{(s)} \middle| \dot{\phi}_i^{(s)} \right\rangle - E^{\text{KS}} \left[\{\phi_i\}^{(s)}, \{\mathbf{R}_I\}^{(s)} \right] \right. \\
&\left. + \sum_{ij} \Lambda_{ij}^{(s)} \left(\left\langle \phi_i^{(s)} \middle| \phi_j^{(s)} \right\rangle - \delta_{ij} \right) \right\} \\
&+ \sum_{s=1}^{P} \left\{ \sum_I \frac{1}{2} M_I' \left(\dot{\mathbf{R}}_I^{(s)} \right)^2 - \sum_{I=1}^{N} \frac{1}{2} M_I \omega_P^2 \left(\mathbf{R}_I^{(s)} - \mathbf{R}_I^{(s+1)} \right)^2 \right\} \, , \quad (319)
\end{aligned}
$$

where the interaction energy $E^{\text{KS}}[\{\phi_i\}^{(s)}, \{\mathbf{R}_I\}^{(s)}]$ at time slice s is defined in Eq. (75); note that here and in the following the dots denote derivatives with respect to propagation time t and that $E_0^{\text{KS}} = \min E^{\text{KS}}$. The standard Car–Parrinello Lagrangian, see e.g. Eq. (41) or Eq. (58), is recovered in the limit $P = 1$ which corresponds to classical nuclei. Mixed classical / quantum systems can easily be treated by representing an arbitrary subset of the nuclei in Eq. (319) with only one time slice.

This simplest formulation of *ab initio* path integrals, however, is insufficient for the following reason: ergodicity of the trajectories and adiabaticity in the sense of Car–Parrinello simulations are not guaranteed. It is known since the very first molecular dynamics computer experiments that quasiharmonic systems (such as coupled stiff harmonic oscillators subject to weak anharmonicities, i.e. the famous Fermi–Pasta–Ulam chains) can easily lead to nonergodic behavior in the sampling of phase space [210]. Similarly "microcanonical" path integral molecular dynamics simulations might lead to an insufficient exploration of configuration space depending on the parameters [273]. The severity of this nonergodicity problem is governed by the stiffness of the harmonic intrachain coupling $\propto \omega_P$ and the anharmonicity of the overall potential surface $\propto E^{\text{KS}}/P$ which establishes the coupling of the modes. For a better and better discretization P the harmonic energy term dominates according to $\sim P$ whereas the mode–mixing coupling decreases like $\sim 1/P$. This problem can be cured by attaching Nosé–Hoover chain thermostats [388], see also Sect. 4.2, to all path integral degrees of freedom [637,644].

The second issue is related to the separation of the power spectra associated to nuclear and electronic subsystems during Car–Parrinello *ab initio* molecular dynamics which is instrumental for maintaining adiabaticity, see Sect. 2.4. In *ab initio* molecular dynamics with classical nuclei the highest phonon or vibrational frequency $\omega_{\text{n}}^{\text{max}}$ is dictated by the physics of the system, see e.g. Fig. 2. This means in particular that an upper limit is given by stiff intramolecular vibrations which do not exceed $\omega_{\text{n}}^{\text{max}} \leq 5000$ cm^{-1} or 150 THz. In *ab initio* path integral simulations, on the contrary, $\omega_{\text{n}}^{\text{max}}$ is given by ω_P which actually diverges with increasing discretization as $\sim \sqrt{P}$. The simplest counteraction would be to compensate this artifact by decreasing the fictitious electron mass μ until the power spectra are again separated for a fixed value of P and thus ω_P. This, however, would lead to a prohibitively small time step because $\Delta t^{\text{max}} \propto \sqrt{\mu}$. This dilemma can be solved by thermostatting the electronic degrees of freedom as well [395,399,644], see Sect. 4.2 for a related discussion in the context of metals.

Finally, it is known that diagonalizing the harmonic spring interaction in Eq. (319) leads to more efficient propagators [637,644]. One of these transformation and the resulting Nosé–Hoover chain thermostatted equations of motion will be outlined in the following section, see in particular Eqs. (331)–(337). In addition to keeping the average temperature fixed it is also possible to generate path trajectories in the isobaric–isothermal NpT ensemble [646,392]. Instead of using Car–Parrinello fictitious dynamics in order to evaluate the interaction energy in Eq. (318), which is implemented in the `CPMD` package [142], it is evident that also the Born–Oppenheimer approach from Sect. 2.3 or the free energy functional from Sect. 4.3 can be used. This route eliminates the adiabaticity problem and was taken

up e.g. in Refs. [132,37,596,597,428,429,333].

A final observation concerning parallel supercomputers might be useful, see also Sect. 3.9. It is evident from the Lagrangian Eq. (319) and the resulting equations of motion (e.g. Eqs. (331)–(337)) that most of the numerical workload comes from calculating the *ab initio* forces on the nuclei. Given a fixed path configuration Eq. (316) the P underlying electronic structure problems are independent from each other and can be solved without communication on P nodes of a distributed memory machine. Communication is only necessary to send the final result, essentially the forces, to a special node that computes the quantum kinetic contribution to the energy and integrates finally the equations of motions. It is even conceivable to distribute this task on different supercomputers, i.e. "meta–computing" is within reach for such calculations. Thus, the algorithm is "embarrassingly parallel" provided that the memory per node is sufficient to solve the complete Kohn–Sham problem at a given time slice. If this is not the case the electronic structure calculation itself has to be parallelized on another hierarchical level as outlined in Sect. 3.9.

4.4.3 Ab Initio Path Centroids: Dynamics

Initially the molecular dynamics approach to path integral simulations was invented merely as a trick in order to sample configuration space similar to the Monte Carlo method. This perception changed recently with the introduction of the so–called "centroid molecular dynamics" technique [102], see Refs. [103,104,105,665,505,506,507] for background information. In a nutshell it is found that the time evolution of the centers of mass or centroids

$$\mathbf{R}_I^c(t) = \frac{1}{P} \sum_{s'=1}^{P} \mathbf{R}_I^{(s')}(t) \tag{320}$$

of the closed Feynman paths that represent the quantum nuclei contains quasiclassical information about the true quantum dynamics. The centroid molecular dynamics approach can be shown to be exact for harmonic potentials and to have the correct classical limit. The path centroids move in an effective potential which is generated by all the other modes of the paths at the given temperature. This effective potential thus includes the effects of quantum fluctuations on the (quasiclassical) time evolution of the centroid degrees of freedom. Roughly speaking the trajectory of the path centroids can be regarded as a classical trajectory of the system, which is approximately "renormalized" due to quantum effects.

The original centroid molecular dynamics technique [102,103,104,105,665] relies on the use of model potentials as the standard time–independent path integral simulations. This limitation was overcome independently in Refs. [469,411] by combining *ab initio* path integrals with centroid molecular dynamics. The resulting technique, *ab initio* centroid molecular dynamics can be considered as a quasiclassical generalization of standard *ab initio* molecular dynamics. At the same time, it preserves the virtues of the *ab initio* path integral technique [395,399,644,404] to generate exact time–independent quantum equilibrium averages.

Here, the so–called adiabatic formulation [105,390,106] of *ab initio* centroid molecular dynamics [411] is discussed. In close analogy to *ab initio* molecular dynamics with classical nuclei also the effective centroid potential is generated "on–the–fly" as the centroids are propagated. This is achieved by singling out the centroid coordinates in terms of a normal mode transformation [138] and accelerating the dynamics of all non–centroid modes artificially by assigning appropriate fictitious masses. At the same time, the fictitious electron dynamics *à la* Car–Parrinello is kept in order to calculate efficiently the *ab initio* forces on *all* modes from the electronic structure. This makes it necessary to maintain two levels of adiabaticity in the course of simulations, see Sect. 2.1 of Ref. [411] for a theoretical analysis of that issue.

The partition function Eq. (315), formulated in the so-called "primitive" path variables $\{\mathbf{R}_I\}^{(s)}$, is first transformed [644,646] to a representation in terms of the normal modes $\{\mathbf{u}_I\}^{(s)}$, which diagonalize the harmonic nearest–neighbor harmonic coupling [138]. The transformation follows from the Fourier expansion of a cyclic path

$$\mathbf{R}_I^{(s)} = \sum_{s'=1}^{P} \mathbf{a}_I^{(s')} \exp\left[2\pi i(s-1)(s'-1)/P\right] \ , \tag{321}$$

where the coefficients $\{\mathbf{a}_I\}^{(s)}$ are complex. The normal mode variables $\{\mathbf{u}_I\}^{(s)}$ are then given in terms of the expansion coefficients according to

$$\mathbf{u}_I^{(1)} = \mathbf{a}_I^{(1)}$$
$$\mathbf{u}_I^{(P)} = \mathbf{a}_I^{((P+2)/2)}$$
$$\mathbf{u}_I^{(2s-2)} = \text{Re } (\mathbf{a}_I^{(s)})$$
$$\mathbf{u}_I^{(2s-1)} = \text{Im } (\mathbf{a}_I^{(s)}) \ . \tag{322}$$

Associated with the normal mode transformation is a set of normal mode frequencies $\{\lambda\}^{(s)}$ given by

$$\lambda^{(2s-1)} = \lambda^{(2s-2)} = 2P \left[1 - \cos\left(\frac{2\pi(s-1)}{P}\right)\right] \tag{323}$$

with $\lambda^{(1)} = 0$ and $\lambda^{(P)} = 4P$. Equation (321) is equivalent to direct diagonalization of the matrix

$$\mathbf{A}_{ss'} = 2\delta_{ss'} - \delta_{s,s'-1} - \delta_{s,s'+1} \tag{324}$$

with the path periodicity condition $\mathbf{A}_{s0} = \mathbf{A}_{sP}$ and $\mathbf{A}_{s,P+1} = \mathbf{A}_{s1}$ and subsequent use of the unitary transformation matrix $\mathbf{U}$ to transform from the "primitive" variables $\{\mathbf{R}_I\}^{(s)}$ to the normal mode variables $\{\mathbf{u}_I\}^{(s)}$

$$\mathbf{R}_I^{(s)} = \sqrt{P} \sum_{s'=1}^{P} \mathbf{U}_{ss'}^{\dagger} \mathbf{u}_I^{(s')}$$

$$\mathbf{u}_I^{(s)} = \frac{1}{\sqrt{P}} \sum_{s'=1}^{P} \mathbf{U}_{ss'} \mathbf{R}_I^{(s')} \ . \tag{325}$$

The eigenvalues of $\mathbf{A}$ when multiplied by P are precisely the normal mode frequencies $\{\lambda\}^{(s)}$. Since the transformation is unitary, its Jacobian is unity. Finally, it is convenient to define a set of normal mode masses

$$M_I^{(s)} = \lambda^{(s)} M_I \tag{326}$$

that vary along the imaginary time axis $s = 1, \ldots, P$, where $\lambda^{(1)} = 0$ for the centroid mode $\mathbf{u}_I^{(1)}$.

Based on these transformations the Lagrangian corresponding to the *ab initio* path integral expressed in normal modes is obtained [644]

$$
\begin{aligned}
\mathcal{L}_{\text{AIPI}} = \frac{1}{P} \sum_{s=1}^{P} &\left\{ \sum_i \mu \left\langle \dot{\phi}_i^{(s)} \middle| \dot{\phi}_i^{(s)} \right\rangle - E \left[\{\phi_i\}^{(s)}, \left\{ \mathbf{R}_I \left(\mathbf{u}_I^{(1)}, \ldots, \mathbf{u}_I^{(P)} \right) \right\}^{(s)} \right] \right. \\
&\left. + \sum_{ij} \Lambda_{ij}^{(s)} \left(\left\langle \phi_i^{(s)} \middle| \phi_j^{(s)} \right\rangle - \delta_{ij} \right) \right\} \\
&+ \sum_{s=1}^{P} \left\{ \sum_{I=1}^{N} \frac{1}{2} M_I'^{(s)} \left(\dot{\mathbf{u}}_I^{(s)} \right)^2 - \sum_{I=1}^{N} \frac{1}{2} M_I^{(s)} \omega_P^2 \left(\mathbf{u}_I^{(s)} \right)^2 \right\} \ ,
\end{aligned}
\tag{327}
$$

where the masses $M_I'^{(s)}$ will be defined later, see Eq. (338). As indicated, the electronic energy $E^{(s)}$ is always evaluated in practice in terms of the "primitive" path variables $\{\mathbf{R}_I\}^{(s)}$ in Cartesian space. The necessary transformation to switch forth and back between "primitive" and normal mode variables is easily performed as given by the relations Eq. (325).

The chief advantage of the normal mode representation Eq. (325) for the present purpose is that the lowest–order normal mode $\mathbf{u}_I^{(1)}$

$$\mathbf{u}_I^{(1)} = \mathbf{R}_I^{\text{c}} = \frac{1}{P} \sum_{s'=1}^{P} \mathbf{R}_I^{(s')} \tag{328}$$

turns out to be identical to the centroid $\mathbf{R}_I^{\text{c}}$ of the path that represents the Ith nucleus. The centroid force can also be obtained from the matrix $\mathbf{U}$ according to [644]

$$\frac{\partial E}{\partial \mathbf{u}_I^{(1)}} = \frac{1}{P} \sum_{s'=1}^{P} \frac{\partial E^{(s')}}{\partial \mathbf{R}_I^{(s')}} \tag{329}$$

since $\mathbf{U}_{1s} = \mathbf{U}_{s1}^{\dagger} = 1/\sqrt{P}$ and the remaining normal mode forces are given by

$$\frac{\partial E}{\partial \mathbf{u}_I^{(s)}} = \frac{1}{\sqrt{P}} \sum_{s'=1}^{P} \mathbf{U}_{ss'} \frac{\partial E^{(s')}}{\partial \mathbf{R}_I^{(s')}} \quad \text{for } s = 2, \ldots, P \tag{330}$$

in terms of the "primitive" forces $-\partial E^{(s)}/\partial \mathbf{R}_I^{(s)}$. Here, E on the left–hand–side with no superscript (s) refers to the average electronic energy $E = (1/P) \sum_{s=1}^{P} E^{(s)}$ from which the forces have to be derived. Thus, the force Eq. (329) acting on each *centroid* variable $\mathbf{u}_I^{(1)}$, $I = 1, \ldots N$, is exactly the force averaged over imaginary time $s = 1, \ldots, P$, i.e. the *centroid force* on the Ith nucleus as already given in

Eq. (2.21) of Ref. [644]. This is the desired relation which allows in centroid molecular dynamics the centroid forces to be simply obtained as the average force which acts on the lowest–order normal mode Eq. (328). The non–centroid normal modes $\mathbf{u}_I^{(s)}$, $s = 2, 3, \ldots, P$ of the paths establish the effective potential in which the centroid moves.

At this stage the equations of motion for adiabatic *ab initio* centroid molecular dynamics [411] can be obtained from the Euler–Lagrange equations. These equations of motion read

$$M_I'^{(1)} \ddot{\mathbf{u}}_I^{(1)} = -\frac{1}{P} \sum_{s=1}^{P} \frac{\partial E\left[\{\phi_i\}^{(s)}, \{\mathbf{R}_I\}^{(s)}\right]}{\partial \mathbf{R}_I^{(s)}} \tag{331}$$

$$M_I'^{(s)} \ddot{u}_{I,\alpha}^{(s)} = -\frac{\partial}{\partial u_{I,\alpha}^{(s)}} \frac{1}{P} \sum_{s'=1}^{P} E\left[\{\phi_i\}^{(s')}, \left\{\mathbf{R}_I\left(\mathbf{u}_I^{(1)}, \ldots, \mathbf{u}_I^{(P)}\right)\right\}^{(s')}\right]$$
$$-M_I'^{(s)} \omega_P^2 u_{I,\alpha}^{(s)} - M_I'^{(s)} \dot{\xi}_{I,\alpha,1}^{(s)} \dot{u}_{I,\alpha}^{(s)} \quad , s = 2, \ldots, P \tag{332}$$

$$\mu \ddot{\phi}_i^{(s)} = -\frac{\delta E\left[\{\phi_i\}^{(s)}, \{\mathbf{R}_I\}^{(s)}\right]}{\delta \phi_i^{\star(s)}} + \sum_j \Lambda_{ij}^{(s)} \phi_j^{(s)} - \mu \dot{\eta}_1^{(s)} \dot{\phi}_i^{(s)} \quad , s = 1, \ldots, P \tag{333}$$

where $u_{I,\alpha}^{(s)}$ denotes the Cartesian components of a given normal mode vector $\mathbf{u}_I^{(s)} = (u_{I,1}^{(s)}, u_{I,2}^{(s)}, u_{I,3}^{(s)})$. In the present scheme, independent Nosé–Hoover chain thermostats [388] of length K are coupled to all non–centroid mode degrees of freedom $s = 2, \ldots, P$

$$Q^n \ddot{\xi}_{I,\alpha,1}^{(s)} = \left[M_I'^{(s)} \left(\dot{u}_{I,\alpha}^{(s)}\right)^2 - k_B T\right] - Q^n \dot{\xi}_{I,\alpha,1}^{(s)} \dot{\xi}_{I,\alpha,2}^{(s)} \tag{334}$$

$$Q^n \ddot{\xi}_{I,\alpha,k}^{(s)} = \left[Q^n \left(\dot{\xi}_{I,\alpha,k-1}^{(s)}\right)^2 - k_B T\right] - Q^n \dot{\xi}_{I,\alpha,k}^{(s)} \dot{\xi}_{I,\alpha,k+1}^{(s)} (1 - \delta_{kK}), k = 2, ..., K \tag{335}$$

and all orbitals at a given imaginary time slice s are thermostatted by one such thermostat chain of length L

$$Q_1^e \ddot{\eta}_1^{(s)} = 2\left[\sum_i \mu \left\langle \phi_i^{(s)} \middle| \phi_i^{(s)} \right\rangle - T_e^0\right] - Q_1^e \dot{\eta}_1^{(s)} \dot{\eta}_2^{(s)} \tag{336}$$

$$Q_l^e \ddot{\eta}_l^{(s)} = \left[Q_{l-1}^e \left(\dot{\eta}_{l-1}^{(s)}\right)^2 - \frac{1}{\beta_e}\right] - Q_l^e \dot{\eta}_l^{(s)} \dot{\eta}_{l+1}^{(s)} (1 - \delta_{lL}) \quad , l = 2, \ldots, L \; ; \tag{337}$$

note that for standard *ab initio* path integral runs as discussed in the previous section the centroid mode should be thermostatted as well. The desired fictitious kinetic energy of the electronic subsystem T_e^0 can be determined based on a short equivalent classical Car–Parrinello run with $P = 1$ and using again the relation $1/\beta_e = 2T_e^0/6N_e'$ where N_e' is the number of orbitals. The mass parameters $\{Q_l^e\}$ associated to the orbital thermostats are the same as those defined in Eq. (271), whereas the single mass parameter Q^n for the nuclei is determined by the harmonic interaction and is given by $Q^n = k_B T/\omega_P^2 = \beta/P$. The characteristic thermostat

frequency of the electronic degrees of freedom $\omega_{\rm e}$ should again lie above the frequency spectrum associated to the fictitious nuclear dynamics. These is the method that is implemented in the `CPMD` package [142].

An important issue for adiabatic *ab initio* centroid molecular dynamics [411] is how to establish the time–scale separation of the non–centroid modes compared to the centroid modes. This is guaranteed if the *fictitious* normal mode masses $M_I'^{(s)}$ are taken to be

$$
\begin{aligned}
M_I'^{(1)} &= M_I \\
M_I'^{(s)} &= \gamma\, M_I^{(s)} \quad , s = 2, \ldots, P \ ,
\end{aligned}
\tag{338}
$$

where M_I is the *physical* nuclear mass, $M_I^{(s)}$ are the normal mode masses Eq. (326), and γ is the "centroid adiabaticity parameter"; note that this corrects a misprint of the definition of $M_I'^{(s)}$ for $s \geq 2$ in Ref. [411]. By choosing $0\langle\gamma \ll 1$, the required time–scale separation between the centroid and non–centroid modes can be controlled so that the motion of the non–centroid modes is artificially accelerated, see Sect. 3 in Ref. [411] for a systematic study of the γ–dependence. Thus, the centroids with associated physical masses move quasiclassically in real–time in the centroid effective potential, whereas the fast dynamics of all other nuclear modes $s\rangle1$ is fictitious and serves only to generate the centroid effective potential "on–the–fly". In this sense γ (or rather γM_I) is similar to μ, the electronic adiabaticity parameter in Car–Parrinello molecular dynamics.

4.4.4   Other Approaches

It is evident from the outset that the Born–Oppenheimer approach to generate the *ab initio* forces can be used as well as Car–Parrinello molecular dynamics in order to generate the *ab initio* forces on the quantum nuclei. This variation was utilized in a variety of investigations ranging from clusters to molecular solids [132,37,596,597,428,429,333]. Closely related to the *ab initio* path integral approach as discussed here is a method that is based on Monte Carlo sampling of the path integral [672]. It is similar in spirit and in its implementation to Born–Oppenheimer molecular dynamics sampling as long as only time–averaged static observables are calculated. A semiempirical ("CNDO" and "INDO") version of Born–Oppenheimer *ab initio* path integral simulations was also devised [656] and applied to study muonated organic molecules [656,657].

A non–self–consistent approach to *ab initio* path integral calculations was advocated and used in a series of publications devoted to study the interplay of nuclear quantum effects and electronic structure in unsaturated hydrocarbons like benzene [544,503,81,543,504]. According to this philosophy, an ensemble of nuclear path configurations Eq. (316) is first generated at finite temperature with the aid of a parameterized model potential (or using a tight–binding Hamiltonian [504]). In a second, independent step electronic structure calculations (using Pariser–Parr–Pople, Hubbard, or Hartree–Fock Hamiltonians) are performed for this fixed ensemble of discretized quantum paths. The crucial difference compared to the self–consistent approaches presented above is that the creation of the thermal ensemble and the

subsequent analysis of its electronic properties is performed using different Hamiltonians.

Several attempts to treat also the electrons in the path integral formulation – instead of using wavefunctions as in the *ab initio* path integral family – were published [606,119,488,449,450]. These approaches are exact in principle, i.e. non–adiabaticity and full electron–phonon coupling is included at finite temperatures. However, they suffer from severe stability problems [121] in the limit of degenerate electrons, i.e. at very low temperatures compared to the Fermi temperature, which is the temperature range of interest for typical problems in chemistry and materials science. Recent progress on computing electronic forces from path integral Monte Carlo simulations was also achieved [708].

More traditional approaches use a wavefunction representation for both the electrons in the ground state and for nuclear density matrix instead of path integrals. The advantage is that real–time evolution is obtained more naturally compared to path integral simulations. A review of such methods with the emphasis of computing the interactions "on–the–fly" is provided in Ref. [158]. An approximate wavefunction–based quantum dynamics method which includes several excited states and their couplings was also devised and used [385,386,387,45]. An alternative approach to approximate quantum dynamics consists in performing instanton or semiclassical *ab initio* dynamics [325,47]. Also the approximate vibrational self–consistent field approach to nuclear quantum dynamics was combined with "on–the–fly" MP2 electronic structure calculations [122].

5 Applications: From Materials Science to Biochemistry

5.1 Introduction

Ab initio molecular dynamics was called a "virtual matter laboratory" [234], a notion that is fully justified in view of its relationship to experiments performed in the real laboratory. Ideally, a system is prepared in some initial state and than evolves according to the basic laws of physics – without the need of experimental input. It is clear to every practitioner that this viewpoint is highly idealistic for more than one reason, but still this philosophy allows one to compute observables with predictive power and also implies a broad range of applicability.

It is evident from the number of papers dealing with *ab initio* molecular dynamics, see for instance Fig. 1, that a truly comprehensive survey of applications cannot be given. Instead, the strategy chosen is to provide the reader with a wealth of references that try cover the full scope of this approach – instead of discussing in depth the physics or chemistry of only a few specific applications. To this end the selection is based on a general literature search in order to suppress personal preferences as much as possible. In addition the emphasis lies on recent applications that could not be covered in earlier reviews. This implies that several older key reference papers on similar topics are in general missing.

The first application of Car–Parrinello molecular dynamics [108] dealt with silicon, one of the basic materials in semiconductor industry. Classic solid–state application of this technique focus on the properties of crystals, such as those of CuCl where anharmonicity and off–center displacements of the Cu along the (111) directions were found to be important to describe the crystal structure as a function of temperature and pressure [64]. Various properties of solid nitromethane [647], crystalline nitric acid trihydrate [602], solid benzene [420], stage–1 alkali–graphite intercalation compounds [286,287], and of the one-dimensional intercalation compound 2HgS•SnBr$_2$ [530] were determined based on first principles. The molecular solid HBr undergoes various phase transitions upon compression. The dynamical behavior of one of these phases, disordered HBr–I, could be clarified using *ab initio* molecular dynamics [313]. Structure, phase transitions and short–time dynamics of magnesium silicate perovskites were analyzed in terms of *ab initio* trajectories [670]. The A7 to simple cubic transformation in As was investigated using *ab initio* molecular dynamics at constant–pressure[568]. By applying external pressure the hydrogen sublattice was found to undergo amorphization in Mg(OH)$_2$ and Ca(OH)$_2$ a phenomenon that was interpreted in terms of frustration [511]. Properties of solid cubane C$_8$H$_8$ were obtained in constant pressure simulations and compared to experiment [514]. *Ab initio* simulations of the graphitization of flat and stepped diamond (111) surfaces uncovered that the transition temperature depends sensibly on the type of the surface [327].

Sliding of grain boundaries in aluminum as a typical ductile metal was generated and analyzed in terms of atomistic rearrangements [432]. Microfracture in a sample of amorphous silicon carbide was induced by uniaxial strain and found to induce Si segregation at the surface [226]. The early stages of nitride growth on cubic silicon carbide including wetting were modeled by depositing nitrogen atoms on the Si–terminated SiC(001) surface [225].

Classical proton diffusion in crystalline silicon at high temperatures was an early application to the dynamics of atoms in solids [93]. Using the *ab initio* path integral technique [395,399,644,404], see Sect. 4.4 the preferred sites of hydrogen and muonium impurities in crystalline silicon [428,429], or the proton positions in HCl • nH$_2$O crystalline hydrates [516] could be located. The radiation–induced formation of H$_2^\star$ defects in c–Si via vacancies and self–interstitials was simulated by *ab initio* molecular dynamics [178]. The classical diffusion of hydrogen in crystalline GaAs was followed in terms of diffusion paths [668] and photoassisted reactivation of H–passivated Si donors in GaAs was simulated based on first principles [430]. Oxygen diffusion in p–doped silicon can be enhanced by adding hydrogen to the material, an effect that could be rationalized by simulations [107]. *Ab initio* dynamics helped in quantifying the barrier for the diffusion of atomic oxygen in a model silica host [279]. The microscopic mechanism of the proton diffusion in protonic conductors, in particular Sc–doped SrTiO$_3$ and Y–doped SrCeO$_3$, is studied via *ab initio* molecular dynamics, where is it found that covalent OH–bonds are formed during the process [561]. Ionic diffusion in a ternary superionic conductor was obtained by *ab initio* dynamics [677]. Proton motion and isomerization pathways of a complex photochromic molecular

crystal composed of 2–(2,4–dinitrobenzyl)pyridine dyes was generated by *ab initio* methods [216].

Also materials properties of polymers are investigated in quite some detail. Early applications of semiempirical ZDO molecular dynamics [666] were devoted to defects in conducting polymers, in particular to solitons, polarons and alkali doping in polyacetylene [666,667] as well as to muonium implanted in *trans* and *cis* polyacetylene [200]. More recent are calculations of Young's modulus for crystalline polyethylene [271], soliton dynamics in positively charged polyacetylene chains [125], charge localization in doped polypyrroles [140], chain rupture of polyethylene chains under tensile load [533], the influence of a knot on the strength of a polymer strand [534], or ion diffusion in polyethylene oxide [456].

5.3 *Surfaces, Interfaces, and Adsorbates*

A host of studies focusing on atoms and in particular on molecules interacting with surfaces appeared over the years. Recent studies focussed for instance on C_2H_2, C_2H_4, and trimethylgallium adsorbates on the GaAs(001)–(2×4) surface [248], thiophene on the catalytically active MoS_2(010) [512] or RuS_2 [580] surfaces, small molecules on a nitric acid monohydrate crystal surface [624], CO on Si(001) [314], small molecules on TiO_2 [554,41], sulfur on Si(100) at various coverages [707], and sulfuric acid adsorbed on ZrO_2(101) and ZrO_2(001) [269].

Specific to *ab initio* molecular dynamics is its capability to describe also chemisorption as well as dynamical processes on (and of) surfaces including surface reactions [500]. The *ab initio* calculations of surface phonons in semiconductor surfaces can be based on the frozen–phonon, linear–response or nowadays molecular dynamics approaches, see Ref. [218] for a discussion and comparison. A review on the structure and energetics of oxide surfaces including molecular processes occurring on such surfaces is provided in Ref. [235], whereas Ref. [256] concentrates on the interaction of hydrogen with clean and adsorbate covered metal and semiconductor surfaces.

Recent applications in surface science include the transition from surface vibrations to liquid–like diffusional dynamics of the Ge(111) surface [607], the diffusion of Si adatoms on a double–layer stepped Si(001) surface [330], the structure of chemisorbed acetylene on the Si(001)–(2×1) surface [423], chemisorption of quinizarin on α–Al_2O_3 [212,213], the diffusion of a single Ga adatom on the GaAs(100)–c(4×4) surface [367], homoepitaxial crystal growth on Si(001) and the low–temperature dynamics of Si(111)–(7×7) [595,611], dissociation of an H_2O molecule on MgO [358,359], dissociation of Cl_2 on GaAs(110) [380], chlorine adsorption and reactions on Si(100) [691], molecular motion of NH_3 on MgO [358], dynamics and reactions of hydrated α–alumina surfaces [289], molecular vs. dissociative adsorption of water layers on MgO(100) as a function of coverage [448], oxidation of CO on Pt(111) [8,705], the reaction HCl + HOCl → H_2O + Cl_2 as it occurs on an ice surface [373], or desorption of D_2 from Si(100) [255]. Thermal contraction, the formation of adatom-vacancy pairs, and finally premelting was observed in *ab initio* simulations of the Al(110) surface at temperatures up to 900 K [415] Early stages of the oxidation of a Mg(0001) surface by direct attack of molecular O_2 was dynamically simulated [96] including

the penetration of the oxidation layer into the bulk. Similarly, the growth of an oxide layer was generated on an Si(100) surface [653].

The water–Pd(100), water–O/Pd(100) and water–Si(111) interfaces were simulated based on *ab initio* molecular dynamics [336,655]. Water covering the surface of a microscopic model of muscovite mica is found to form a two–dimensional network of hydrogen bonds, called two–dimensional ice, on that surface [447]. The metal–organic junction of monolayers of Pd–porphyrin and perylene on Au(111) was analyzed using an *ab initio* approach [355]. An interesting possibility is to compute the tip–surface interactions in atomic force microscopy as e.g. done for a neutral silicon tip interacting with an InP(110) surface [619] or Si(111) [481,482].

5.4 Liquids and Solutions

Molecular liquids certainly belong to the classic realm of molecular dynamics simulations. Water was and still is a challenge [581] for both experiment and simulations due to the directional nature and the weakness of the hydrogen bonds which leads to delicate association phenomena. Pioneering *ab initio* simulations of pure water at ambient [352] and supercritical conditions [205] were reported only a few years ago. More recently, these gradient–corrected density functional theory–based simulations were extended into several directions [587,573,575,576,579,118]. In the mean time (minimal–basis) Hartree–Fock *ab initio* molecular dynamics [291] as well as more approximate schemes [455] were also applied to liquid water. Since chemical reactions often occur in aqueous media the solvation properties of water are of utmost importance so that the hydration of ions [403,620,621,377,502] and small molecules [353,354,433] was investigated. Similarly to water liquid HF is a strongly associated liquid which features short–lived hydrogen–bonded zig–zag chains [521]. Another associated liquid, methanol, was simulated at 300 K using an adaptive finite–element method [634] in conjunction with Born–Oppenheimer molecular dynamics [635]. In agreement with experimental evidence, the majority of the molecules is found to be engaged in short linear hydrogen–bonded chains with some branching points [635]. Partial reviews on the subject of *ab initio* simulations as applied to hydrogen–bonded liquids can be found in the literature [586,406,247].

The *ab initio* simulated solvation behavior of "unbound electrons" in liquid ammonia at 260 K was found to be consistent with the physical picture extracted from experiment [155,156]. Similarly, *ab initio* molecular dynamics of dilute [553,203] and concentrated [569] molten $K_x \cdot (KCl)_{1-x}$ mixtures were performed at 1300 K entering the metallic regime. The structure of liquid ammonia at 273 K was investigated with a variety of techniques so that limitations of using classical nuclei, simple point charge models, small systems, and various density functionals could be assessed [164].

Ab initio molecular dynamics is also an ideal tool to study other complex fluids with partial covalency, metallic fluids, and their transformations as a function of temperature, pressure, or concentration. The properties of water–free KF ● nHF melts depend crucially on polyfluoride anions $H_m F_{m+1}^-$ and solvated K^+ cations. *Ab initio* simulations allow for a direct comparison of these complexes in the liquid, gaseous and crystalline phase [515]. The changes of the measured structure factor of liquid sulfur as a function of temperature can be rationalized on the atomistic

level by various chain and ring structures that can be statistically analyzed in *ab initio* molecular dynamics simulations [631]. Liquid $GeSe_2$ is characterized by strong chemical bonds that impose a structure beyond the usual very short distances due to network formation [416]. Zintl–alloys such as liquid NaSn [552] or KPb [556] have very interesting bonding properties that manifest themselves in strong temperature– and concentration dependences of their structure factors (including the appearance of the so–called first sharp diffraction peak [555]) or electric conductivities.

Metals are ideal systems to investigate the metal–insulator transition upon expansion of the liquid [346,63] or melting [689]. Liquid copper was simulated at 1500 K: structural and dynamical data were found to be in excellent agreement with experimental [464]. Transport coefficients of liquid metals (including in particular extreme conditions) can also be obtained from first principles molecular dynamics using the Green–Kubo formalism [571,592]. The microscopic mechanism of the semiconductor–metal transition in liquid As_2Se_3 could be rationalized in terms of a structural change as found in *ab initio* simulations performed as a function of temperature and pressure [563]. The III–V semiconductors, such as GaAs, assume metallic behavior when melted, whereas the II–VI semiconductor CdTe does not. The different conductivities could be traced back to pronounced structural dissimilarities of the two systems in the melt [236].

5.5 *Glasses and Amorphous Systems*

Related to the simulation of dynamically disordered fluid systems are investigations of amorphous or glassy materials. In view of the severe limitations on system size and time scale (and thus on correlation lengths and times) *ab initio* molecular dynamics can only provide fairly local information in this sense. Within these inherent constraints the microscopic structure of amorphous selenium [304] and tetrahedral amorphous carbon [384], the amorphization of silica [684], boron doping in amorphous Si:H [181] or in tetrahedral amorphous carbon [227], as well as the Raman spectrum [465] and dynamic structure factor [466] of quartz glass and their relation to short–range order could be studied.

The properties of supercooled CdTe were compared to the behavior in the liquid state in terms of its local structure [237]. Defects in amorphous $Si_{1-x}Ge_x$ alloys generated by *ab initio* annealing were found to explain ESR spectra of this system [329]. The infrared spectrum of a sample of amorphous silicon was obtained and found to be in quantitative agreement with experimental data [152]. The CO_2 insertion into a model of argon–bombarded porous SiO_2 was studied [508]. In particular the electronic properties of amorphous GaN were investigated using *ab initio* methods [601].

Larger systems and longer annealing times are accessible after introducing more approximations into the first principle treatment of the electronic structure that underlies *ab initio* molecular dynamics. Using such methods [551], a host of different amorphous carbon nitride samples with various stoichiometries and densities could be generated and characterized in terms of trends [675]. Similarly, the pressure–induced glass–to–crystal transition in condensed sodium was investigated [22] and two structural models of amorphous GaN obtained at different densities were examined

in terms of their electronic structure [601].

5.6 Matter at Extreme Conditions

A strong advantage of *ab initio* simulations is their predictive power also at extreme conditions, an area where molecular dynamics relying on fitted potential models might encounter severe difficulties. Thus, high pressures and / or high temperatures such as those in the earth's core, on other planets, or on stars can be easily achieved in the virtual laboratory. This opens up the possibility to study phase transformations and chemical reactions at such conditions [56]. Furthermore, conditions of geophysical and astrophysical interest can nowadays be produced in the real laboratory, using techniques based on diamond anvil cells, shock waves, or lasers. The limitations of these experimental approaches are, however, not so much related to generating the extreme conditions as one might expect, but rather to measuring observables.

In the virtual laboratory this information is accessible and the melting of diamond at high pressure [222], the phase transformation from the antiferromagnetic insulating δ–O_2 phase to a nonmagnetic metallic molecular ζ–O_2 phase [557], the phase diagram of carbon at high pressures and temperatures [261] as well as transformations of methane [13], carbon monoxide [54], molecular CO_2 [267,558], water ice [363,364,58,50,51,52], solid [305,337,65,66,333] and hot fluid [5] hydrogen, solid $Ar(H_2)_2$ [53] under pressure could be probed. Along similar lines properties of a liquid Fe–S mixture under earth's core conditions [11], the viscosity of liquid iron [690,592], the sound velocity of dense hydrogen at conditions on jupiter [6], the phase diagram of water and ammonia up to 7000 K and 300 GPa [118], the laser heating of silicon [570,572] and graphite [574] etc. were investigated at extreme state points. A review on *ab initio* simulations relevant to minerals at conditions found in the earth's mantle is provided in Ref. [683].

5.7 Clusters, Fullerenes, and Nanotubes

Investigations of clusters by *ab initio* molecular dynamics were among the first applications of this technique. Here, the feasibility to conduct finite–temperature simulations and in particular the possibility to search globally for minima turned out to be instrumental [302,31,303,550,517,519], see e.g. Refs. [16,321,32] for reviews. Such investigations focus more and more on clusters with varying composition [518,293,199,348,349,161]. Cluster melting is also accessible on an *ab initio* footing [84,531,525,526] and molecular clusters, complexes or cluster aggregates are actively investigated [612,645,613,70,596,597,133,701,524].

III–V semiconductor clusters embedded in sodalite show quantum confinement and size effects that can be rationalized by *ab initio* simulations [625,95]. Supported clusters such as Cu_n on an MgO(100) surface are found to diffuse by "rolling" and "twisting" motions with very small barriers [438]. The diffusion of protonated helium clusters in various sodalite cages was generated using *ab initio* dynamics [198]. Photo–induced structural changes in Se chains and rings were generated by a vertical HOMO → LUMO excitation and monitored by *ab initio* dynamics [306]. With the discovery and production of finite carbon assemblies *ab initio* investigations of the

properties of fullerenes [19,17,451], the growth process of nanotubes [127,62,72], or the electrical conductivity of nanowires [38,272] became of great interest.

5.8 Complex and Floppy Molecules

The determination of the structure of a RNA duplex including its hydration water [311], investigations of geometry and electronic structure of porphyrins and porphyrazines [356], and the simulation of a bacteriochlorophyll crystal [381] are some applications to large molecules. Similarly, the "carboplatin" complex [623]– a drug with large ligands – as well as the organometallic complex Alq(3) [148] – an electroluminescent material used in organic light–emitting diodes – were investigated with respect to structural, dynamical and electronic properties.

The organometallic compound $C_2H_2Li_2$ has an unexpected ground–state structure that was found by careful *ab initio* simulated annealing [521]. In addition, this complex shows at high temperatures intramolecular hydrogen migration that is mediated via a lithium hydride unit [521]. Ground–state fluxionality of protonated methane CH_5^+ [397,408] including some isotopomers [409] and of protonated acetylene $C_2H_3^+$ [400] was shown to be driven by quantum effects. The related dynamical exchange of atoms in these molecules can also be excited by thermal fluctuations [630,85,401]. In addition it was shown that CH_5^+ is three–center two–electron bonded and that this bonding topology does not qualitatively change in the presence of strong quantum motion [402]. The fluxional behavior of the protonated ethane molecular ion $C_2H_7^+$ was investigated by *ab initio* molecular dynamics as well [172].

The neutral and ionized SiH_5 and Si_2H_3 species display a rich dynamical behavior which was seen during *ab initio* molecular dynamics simulations [246]. The lithium pentamer Li_5 was found to perform pseudorotational motion on a time scale of picoseconds or faster at temperatures as low as 77 K [231]. Using *ab initio* instanton dynamics the inversion splitting of the NH_3, ND_3, and PH_3 molecules due to the umbrella mode was estimated [325]. Similarly, a semiclassical *ab initio* dynamics approach as used to compute the tunneling rate for intramolecular proton transfer in malonaldehyde [47]. *Ab initio* simulated annealing can be used to explore the potential energy landscape and to locate various minima, such as for instance done for protonated water clusters [673]. Molecular dynamics simulations of the trimethylaluminum $Al(CH_3)_3$ have been carried out in order to investigate the properties of the gas–phase dimer [29]. The structures and vibrational frequencies of tetrathiafulvalene in different oxidation states was probed by *ab initio* molecular dynamics [324]. Implanted muons in organic molecules (benzene, 3–quinolyl nitronyl nitroxide, para–pyridyl nitronyl nitroxide, phenyl nitronyl nitroxide and para–nitrophenyl nitronyl nitroxide) were investigated using approximate *ab initio* path integral simulations that include the strong quantum broadening of the muonium [656,657].

5.9 Chemical Reactions and Transformations

Early applications of *ab initio* molecular dynamics were devoted to reactive scattering in the gas phase such as $CH_2 + H_2 \rightarrow CH_4$ [669] or $H^- + CH_4 \rightarrow CH_4 + H^-$ [365]. The "on–the–fly" approach can be compared to classical trajectory cal-

culations on very accurate global potential energy surfaces. This was for instance done for the well–studied exothermic exchange reaction F + H$_2$ → HF + H in Ref. [565]. Other gas phase reactions studied were Li(2p) + H$_2$ → LiH($^1\Sigma$) + H(^{1}S) in Ref. [387], F + C$_2$H$_4$ → C$_2$H$_3$F + H in Ref. [83], 2O$_3$ → 3O$_2$ in Ref. [170], F$^-$ + CH$_3$Cl → CH$_3$F + Cl$^-$ in Ref. [605], hydroxyl radical with nitrogen dioxide radical [165], formaldehyde radical anion with CH$_3$Cl in Ref. [700], the reduction of OH$^\bullet$ with 3-hexanone [215] or the hydrolysis (or solvolysis, S$_N$2 nucleophilic substitution) of methyl chloride with water [2,3]. Photoreactions of molecules slowly become accessible to *ab initio* dynamics, such as for instance the *cis–trans* photoisomerization in ethylene [46], excited–state dynamics in conjugated polymers [71], bond breaking in the S$_8$ ring [562], transformations of diradicales [195,196], or the S$_0$ → S$_1$ photo isomerization of formaldimine [214].

In addition to allowing to study complex gas phase chemistry, *ab initio* molecular dynamics opened the way to simulate reactions in solution at finite temperatures. This allows liquid state chemistry to take place in the virtual laboratory where thermal fluctuations and solvation effects are included. Some applications out of this emerging field are the cationic polymerization of 1,2,5–trioxane [146,147], the initial steps of the dissociation of HCl in water [353,354], the formation of sulfuric acid by letting SO$_3$ react in liquid water [421] or the acid–catalyzed addition of water to formaldehyde [422].

Proton transfer is a process of broad interest and implications in many fields. Intramolecular proton transfer was studied recently in malonaldehyde [695,47], a Mannich base [182], and formic acid dimers [427]. Pioneering *ab initio* molecular dynamics simulations of proton and hydroxyl diffusion in liquid water were reported in the mid nineties [640,641,642]. Related to this problem is the auto–dissociation of pure water at ambient conditions [628,629]. Since recently it became possible to study proton motion including nuclear quantum effects [645,410,412] by using the *ab initio* path integral technique [395,399,644,404], see Sect. 4.4.

Ab initio molecular dynamics also allows chemical reactions to take place in solid phases, in particular if a constant pressure methodology is used [56], see Sect. 4.2. For instance solid state reactions such as pressure–induced transformations of methane [13] and carbon monoxide [54] or the polymerization [57] and amorphization [56] of acetylene were investigated.

5.10   Catalysis and Zeolites

The polymerization of olefines is an important class of chemical reactions that is operated on the industrial scale. In the light of such applications the detailed understanding of these reactions might lead to the design of novel catalysts. Driven by such stimulations several catalysts were investigated in detail such as metal alkyles [609], platinum–phospine complexes [141], or Grubbs' ruthenium–phosphine complexes [1], metallocenes [696]. In addition, elementary steps of various chemical processes were the focus of *ab initio* molecular dynamics simulations. Among those are chain branching and termination steps in polymerizations [696], ethylene metathesis [1], "living polymerization" of isoprene with ethyl lithium [522], Ziegler–Natta heterogenous polymerization of ethylene [79,80], Reppe carbonylation of Ni–

CH=CH$_2$ using Cl(CO)$_2$ [20], or Sakakura–Tanaka functionalization [382]. As in the real laboratory, side reactions can occur also in the virtual laboratory, such as e.g. the β–hydrogen elimination as an unpredicted reaction path [383]. A digression on using finite–temperature *ab initio* dynamics in homogeneous catalysis research can be found in Ref. [697].

Zeolites often serve as catalysists as well and are at the same time ideal candidates for finite–temperature *ab initio* simulations in view of their chemical complexity. A host of different studies [559,100,268,614,545,206,560,598,207,315,208,209,546] contributed greatly to the understanding of these materials and the processes occurring therein such as the initial stages of the methanol to gasoline conversion [599]. Heterogenous catalysts are often poisoned, which was for instance studied in the case of hydrogen dissociation on the Pd(100) surface in the presence adsorbed sulfur layers [257].

5.11 Biophysics and Biochemistry

Applications of *ab initio* molecular dynamics to molecules and processes of interest in life sciences begin to emerge [18,113]. Investigations related to these interests are investigations of the crystal structure of a hydrated RNA duplex (sodium guanylyl–3'–5'–cytidine nona–hydrate) [311], structure models for the cytochrom P450 enzyme family [547,548,549], nanotubular polypeptides [112], a synthetic biomimetic model of galactose oxidase [523], aspects of the process of vision in form of the 11–*cis* to *all*–*trans* isomerization in rhodopsin [67,68,474], interconversion pathways of the protonated β–ionone Schiff base [615], or of the binding properties of small molecules of physiological relevance such as O$_2$, CO or NO to iron–porphyrines and its complexes [527,528,529].

Proton transport throught water wires is an important biophysical process in the chemiosmotic theory for biochemical ATP production. Using the *ab initio* path integral technique [395,399,644,404] the properties of linear water wires with an excess proton were studied at room temperature [419]. Amino acids are important ingredients as they are the building blocks of polypeptides, which in turn form channels and pores for ion exchange. Motivated by their ubiquity, glycine and alanine as well as some of their oligopeptides and helical (periodic) polypeptides were studied in great detail [323].

5.12 Outlook

Ab initio molecular dynamics is by now not only a standard tool in academic research but also becomes increasingly attractive to industrial researchers. Analysis of data bases, see caption of Fig. 1 for details, uncovers that quite a few companies seem to be interested in this methodology. Researchers affiliated to Bayer, Corning, DSM, Dupont, Exxon, Ford, Hitachi, Hoechst, Kodak, NEC, Philips, Pirelli, Shell, Toyota, Xerox and others cite the Car–Parrinello paper Ref. [108] or use *ab initio* molecular dynamics in their work. This trend will certainly be enhanced by the availability of efficient and general *ab initio* molecular dynamics packages which are commercially available.

Acknowledgments

References

1. O. M. Aagaard, R. J. Meier, and F. Buda, J. Am. Chem. Soc. **120**, 7174 (1998).
2. M. Aida, H. Yamataka, and M. Dupuis, Chem. Phys. Lett. **292**, 474 (1998).
3. M. Aida, H. Yamataka, and M. Dupuis, Theor. Chem. Acc. **102**, 262 (1999).
4. H. Akai and P.H. Dederichs, J. Phys. C **18**, 2455 (1985).
5. A. Alavi, J. Kohanoff, M. Parrinello, and D. Frenkel, Phys. Rev. Lett. **73**, 2599 (1994).
6. A. Alavi, M. Parrinello, and D. Frenkel, Science **269**, 1252 (1995).
7. A. Alavi, in *Monte Carlo and Molecular Dynamics of Condensed Matter Systems*, Chapt. 25, p. 648, eds. K. Binder and G. Ciccotti (Italien Physical Society SIF, Bologna, 1996).
8. A. Alavi, P. Hu, T. Deutsch, P. L. Silvestrelli, and J. Hutter, Phys. Rev. Lett. **80**, 3650 (1998).
9. A. Alavi, private communication.
10. M. Albrecht, A. Shukla, M. Dolg, P. Fulde, and H. Stoll, Chem. Phys. Lett. **285**, 174 (1998).
11. D. Alfe and M. J. Gillan, Phys. Rev. B **58**, 8248 (1998).
12. M. P. Allen and D. J. Tildesley, *Computer Simulation of Liquids* (Clarendon Press, Oxford, 1987; reprinted 1990).
13. F. Ancilotto, G. L. Chiarotti, S. Scandolo, and E. Tosatti, Science **275**, 1288 (1997).
14. H. C. Andersen, J. Chem. Phys. **72**, 2384 (1980).
15. H. C. Andersen, J. Comput. Phys. **52**, 24 (1983).
16. W. Andreoni, Z. Phys. D **19**, 31 (1991).
17. W. Andreoni, Annu. Rev. Phys. Chem. **49**, 405 (1998).
18. W. Andreoni, Perspect. Drug Discovery Des. **9–11**, 161 (1998).
19. W. Andreoni and A. Curioni, Appl. Phys. A **A66**, 299 (1998).
20. F. De Angelis, N. Re, A. Sgamellotti, A. Selloni, J. Weber, and C. Floriani, Chem. Phys. Lett. **291**, 57 (1998).
21. J. F. Annett, Comput. Mat. Sci **4**, 23 (1995).
22. M. I. Aoki and K. Tsumuraya, Phys. Rev. B **56**, 2962 (1997).
23. T. A. Arias, M. C. Payne, and J. D. Joannopoulos, Phys. Rev. Lett. **69**, 1077 (1992).
24. T. A. Arias, M. C. Payne, and J. D. Joannopoulos, Phys. Rev. B **45**, 1538 (1992).

25. T. A. Arias, Rev. Mod. Phys. **71**, 267 (1999).
26. E. Artacho, D. Sánchez–Portal, P. Ordejón, A. Garcia, and J. M. Soler, phys. stat. sol. (b) **215**, 809 (1999).
27. N. W. Ashcroft and N. D. Mermin, *Solid State Physics* (Saunders College Publishing, Philadelphia, 1976).
28. G. B. Bachelet, D. R. Hamann, and M. Schlüter, Phys. Rev. B **26**, 4199 (1982).
29. S. Balasubramanian, C. J. Mundy, and M. L. Klein, J. Phys. Chem. B **102**, 10 136 (1998).
30. A. Baldereschi, Phys. Rev. B **7**, 5212 (1973).
31. P. Ballone, W. Andreoni, R. Car, and M. Parrinello, Phys. Rev. Lett. **60**, 271 (1988).
32. P. Ballone and W. Andreoni, in *Metal Clusters*, ed. W. Ekardt (Wiley, New York, 1999).
33. P. Bandyopadhyay, S. Ten–no, and S. Iwata, J. Phys. Chem. A **103**, 6442 (1999).
34. R. N. Barnett, U. Landman, and A. Nitzan, J. Chem. Phys. **89**, 2242 (1988).
35. R. N. Barnett, U. Landman, A. Nitzan, and G. Rajagopal, J. Chem. Phys. **94**, 608 (1991).
36. R. N. Barnett and U. Landman, Phys. Rev. B **48**, 2081 (1993).
37. R. N. Barnett, H.–P. Cheng, H. Hakkinen, and U. Landman, J. Phys. Chem. **99**, 7731 (1995).
38. R. N. Barnett and U. Landman, Nature (London) **387**, 788 (1997).
39. S. Baroni and P. Giannozzi, Europhys. Lett. **17**, 547 (1992).
40. U. von Barth and L. Hedin, J. Phys. C **5**, 1629 (1972).
41. S. P. Bates, M. J. Gillan, and G. Kresse, J. Phys. Chem. B **102**, 2017 (1998).
42. A. D. Becke, Phys. Rev. A **38**, 3098 (1988).
43. A. D. Becke, J. Chem. Phys. **98**, 1372 (1993).
44. A. D. Becke, J. Chem. Phys. **98**, 5648 (1993).
45. M. Ben–Nun and T. J. Martinez, J. Chem. Phys. **108**, 7244 (1998).
46. M. Ben–Nun and T. J. Martinez, Chem. Phys. Lett. **298**, 57 (1998).
47. M. Ben–Nun and T. J. Martinez, J. Phys. Chem. A **103**, 6055 (1999).
48. P. Bendt and A. Zunger, Phys. Rev. B **26**, 3114 (1982).
49. P. Bendt and A. Zunger, Phys. Rev. Lett. **50**, 1684 (1983).
50. M. Benoit, D. Marx, and M. Parrinello, Nature (London) **392**, 258 (1998); see also J. Teixeira, Nature (London) **392**, 232 (1998).
51. M. Benoit, D. Marx, and M. Parrinello, Comp. Mat. Sci. **10**, 88 (1998).
52. M. Benoit, D. Marx, and M. Parrinello, Solid State Ionics **125**, 23 (1999).
53. S. Bernard, P. Loubeyre, and G. Zerah, Europhys. Lett. **37**, 477 (1997).
54. S. Bernard, G. L. Chiarotti, S. Scandolo, and E. Tosatti, Phys. Rev. Lett. **81**, 2092 (1998).
55. M. Bernasconi, G. L. Chiarotti, P. Focher, S. Scandolo, E. Tosatti, and M. Parrinello, J. Phys. Chem. Solids **56**, 501 (1995).
56. M. Bernasconi, M. Benoit, M. Parrinello, G. L. Chiarotti, P. Focher, and E. Tosatti, Phys. Scr. **T66**, 98 (1996).
57. M. Bernasconi, G. L. Chiarotti, P. Focher, M. Parrinello, and E. Tosatti, Phys.

Rev. Lett. **78**, 2008 (1997).

58. M. Bernasconi, P. L. Silvestrelli, and M. Parrinello, Phys. Rev. Lett. **81**, 1235 (1998).
59. B. J. Berne, G. Ciccotti, and D. F. Coker (Eds.), *Classical and Quantum Dynamics in Condensed Phase Simulations* (World Scientific, Singapore, 1998).
60. J. Bernholc, N. O. Lipari, and S. T. Pantelides, Phys. Rev. B **21**, 3545 (1980).
61. J. Bernholc, J.–Y. Yi, and D. J. Sullivan, Faraday Discuss. Chem. Soc. **92**, 217 (1991).
62. J. Bernholc, C. Brabec, M. B. Nardelli, A. Maiti, C. Roland, and B. I. Yakobson, Appl. Phys. A **67**, 39 (1998).
63. S. R. Bickham, O. Pfaffenzeller, L. A. Collins, J. D. Kress, and D. Hohl, Phys. Rev. B **58**, R11 813 (1998).
64. S. R. Bickham, J. D. Kress, L. A. Collins, and R. Stumpf, Phys. Rev. Lett. **83**, 568 (1999).
65. S. Biermann, D. Hohl, and D. Marx, J. Low Temp. Phys. **110**, 97 (1998).
66. S. Biermann, D. Hohl, and D. Marx, Solid State Commun. **108**, 337 (1998).
67. A. Bifone, H. J. M. de Groot, and F. Buda, J. Phys. Chem. B **101**, 2954 (1997).
68. A. Bifone, H. J. M. de Groot, and F. Buda, Pure Appl. Chem. **69**, 2105 (1997).
69. K. Binder and G. Ciccotti (Eds.), *Monte Carlo and Molecular Dynamics of Condensed Matter Systems* (Italien Physical Society SIF, Bologna 1996).
70. G. Bischof, A. Silbernagel, K. Hermansson, and M. Probst, Int. J. Quantum Chem. **65**, 803 (1997).
71. E. R. Bittner and D. S. Kosov, J. Chem. Phys. **110**, 6645 (1999).
72. X. Blase, A. De Vita, J.–C. Charlier, and R. Car, Phys. Rev. Lett. **80**, 1666 (1998).
73. P. E. Blöchl, Phys. Rev. B **41**, 5414 (1990).
74. P. E. Blöchl and M. Parrinello, Phys. Rev. B **45**, 9413 (1992).
75. P. E. Blöchl, Phys. Rev. B **50**, 17 953 (1994).
76. P. E. Blöchl, J. Chem. Phys. **103**, 7422 (1995).
77. S. Blügel, Ph.D. Thesis (Rheinisch–Westfälische Technische Hochschule Aachen, Aachen, 1988).
78. M. Bockstedte, A. Kley, J. Neugebauer, and M. Scheffler, Comput. Phys. Comm. **107**, 187 (1997).
79. M. Boero, M. Parrinello, and K. Terakura, J. Am. Chem. Soc. **120**, 2746 (1998).
80. M. Boero, M. Parrinello, and K. Terakura, Surf. Sci. **438**, 1 (1999).
81. M. C. Böhm, R. Ramírez, and J. Schulte, Chem. Phys. **227**, 271 (1998).
82. K. Bolton, W. L. Hase, and G. H. Peslherbe, in *Modern Methods for Multidimensional Dynamics Computations in Chemistry*, ed. D. L. Thompson (World Scientific, Singapore, 1998).
83. K. Bolton, B. H. Schlegel, W. L. Hase, and K. Song, Phys. Chem. Chem. Phys. **1**, 999 (1999).
84. V. Bonačić-Koutecký, J. Jellinek, M. Wiechert, and P. Fantucci, J. Chem. Phys. **107**, 6321 (1997).

85. D. W. Boo, Z. F. Liu, A. G. Suits, J. S. Tse, and Y. T. Lee, Science **269**, 57 (1995).

86. F. A. Bornemann and C. Schütte, Numer. Math. **78**, 359 (1998).

87. F. A. Bornemann and C. Schütte, Numer. Math. **83**, 179 (1999).

88. S. F. Boys and F. Bernardi, Mol. Phys. **19**, 553 (1970).

89. E. L. Briggs, D. J. Sullivan, and J. Bernholc, Phys. Rev. B **52**, R5471 (1995).

90. K. D. Brommer, B. E. Larson, M. Needels, and J. D. Joannopoulos, Computers in Physics **7**, 350 (1993).

91. J. Broughton and F. Kahn, Phys. Rev. B **40**, 12 098 (1989).

92. C. G. Broyden, Math. Comput. **19**, 577 (1965).

93. F. Buda, G. L. Chiarotti, R. Car, and M. Parrinello, Phys. Rev. Lett. **63**, 294 (1989).

94. F. Buda, R. Car, and M. Parrinello, Phys. Rev. B **41**, 1680 (1990).

95. F. Buda and A. Fasolino, Phys. Rev. B **60**, 6131 (1999).

96. C. Bungaro, C. Noguera, P. Ballone, and W. Kress, Phys. Rev. Lett. **79**, 4433 (1997).

97. D.M. Bylander, L. Kleinman, and S. Lee, Phys. Rev. B **42**, 1394 (1990).

98. T. Cagin and J. R. Ray, Phys. Rev. A **37**, 247 (1988).

99. D. J. E. Callaway and A. Rahman, Phys. Rev. Lett. **49**, 613 (1982).

100. L. Campana, A. Selloni, J. Weber, and A. Goursot, J. Phys. Chem. B **101**, 9932 (1997).

101. J. Cao and B. J. Berne, J. Chem. Phys. **99**, 2902 (1993).

102. J. Cao and G. A. Voth, J. Chem. Phys. **99**, 10 070 (1993).

103. J. Cao and G. A. Voth, J. Chem. Phys. **100**, 5106 (1994).

104. J. Cao and G. A. Voth, J. Chem. Phys. **101**, 6157 (1994).

105. J. Cao and G. A. Voth, J. Chem. Phys. **101**, 6168 (1994).

106. J. Cao and G. J. Martyna, J. Chem. Phys. **104**, 2028 (1996).

107. R. B. Capaz, L. V. C. Assali, L. C. Kimerling, K. Cho, and J. D. Joannopoulos, Phys. Rev. B **59**, 4898 (1999).

108. R. Car and M. Parrinello, Phys. Rev. Lett. **55**, 2471 (1985).

109. R. Car and M. Parrinello, Solid State Commun. **62**, 403 (1987).

110. R. Car, M. Parrinello, and M. Payne, J. Phys.: Condens. Matter **3**, 9539 (1991).

111. R. Car, in *Monte Carlo and Molecular Dynamics of Condensed Matter Systems*, Chapt. 23, p. 601, eds. K. Binder and G. Ciccotti (Italien Physical Society SIF, Bologna, 1996).

112. P. Carloni, W. Andreoni, and M. Parrinello Phys. Rev. Lett. **79**, 761 (1997).

113. P. Carloni and F. Alber, Perspect. Drug Discovery Des. **9–11**, 169 (1998).

114. A. Caro, S. Ramos de Debiaggi, and M. Victoria, Phys. Rev. B **41**, 913 (1990).

115. E. A. Carter, G. Ciccotti, J. T. Hynes, and R. Kapral, Chem. Phys. Lett. **156**, 472 (1989).

116. CASTEP: Molecular Simulations Inc.; see Ref. [472].

117. C. Cavazzoni, Ph.D. Thesis: *Large Scale First–Principles Simulations of Water and Ammonia at High Pressure and Temperature* (Scuola Internazionale Superiore di Studi Avanzati (SISSA), Trieste, 1998).

118. C. Cavazzoni, G. L. Chiarotti, S. Scandolo, E. Tosatti, M. Bernasconi, and M.

Parrinello, Science **283**, 44 (1999).

119. D. M. Ceperley, Phys. Rev. Lett. **69**, 331 (1992).

120. D. M. Ceperley, Rev. Mod. Phys. **67**, 279 (1995); for errata and updates see `http://www.ncsa.uiuc.edu/Apps/CMP/papers/cep95a/cep95a.html`.

121. D. M. Ceperley in *Monte Carlo and Molecular Dynamics of Condensed Matter Systems*, Chapt. 16, p. 443, eds. K. Binder and G. Ciccotti (Italien Physical Society SIF, Bologna, 1996).

122. G. M. Chaban, J. O. Jung, and R. B. Gerber, J. Chem. Phys. **111**, 1823 (1999) and preprint.

123. D. J. Chadi and M. L. Cohen, Phys. Rev. B **8**, 5747 (1973).

124. Ch. Chakravarty, Int. Rev. Phys. Chem. **16**, 421 (1997).

125. B. Champagne, E. Deumens, Y. Öhrn, J. Chem. Phys. **107**, 5433 (1997).

126. D. Chandler in *Liquids, Freezing, and Glass Transition*, eds. J. P. Hansen, D. Levesque, and J. Zinn–Justin, (Elsevier, Amsterdam, 1991).

127. J.–C. Charlier, A. de Vita, X. Blase, and R. Car, Science **275**, 646 (1997).

128. S. Chawla and G. A. Voth, J. Chem. Phys. **108**, 4697 (1998).

129. J. R. Chelikowsky and S. G. Louie, Phys. Rev. B **29**, 3470 (1984).

130. J. R. Chelikowsky, N. Troullier, and Y. Saad, Phys. Rev. Lett. **72**, 1240 (1994).

131. J. R. Chelikowsky, N. Troullier, K. Wu, and Y. Saad, Phys. Rev. B **50**, 11 355 (1994).

132. H.–P. Cheng, R. N. Barnett, and U. Landman, Chem. Phys. Lett. **237**, 161 (1995).

133. H.–P. Cheng, J. Phys. Chem. A **102**, 6201 (1998).

134. K. Cho, T. A. Arias, J. D. Joannopoulos, and P. K. Lam, Phys. Rev. Lett. **71**, 1808 (1993).

135. G. Ciccotti, D. Frenkel, and I. R. McDonald, *Simulation of Liquids and Solids* (North–Holland, Amsterdam 1987).

136. G. Ciccotti and J. P. Ryckaert, Comput. Phys. Rep. **4**, 345 (1987).

137. L. J. Clarke, I. Štich, and M. C. Payne, Comput. Phys. Commun. **72**, 14 (1993).

138. R. D. Coalson, J. Chem. Phys. **85**, 926 (1986).

139. M. H. Cohen and V. Heine, Phys. Rev. **122**, 1821 (1961).

140. R. Colle and A. Curioni, J. Am. Chem. Soc. **120**, 4832 (1998).

141. B. B. Coussens, F. Buda, H. Oevering, and R. J. Meier, Organometallics **17**, 795 (1998).

142. CPMD Version 3.3: developed by J. Hutter, A. Alavi, T. Deutsch, M. Bernasconi, St. Goedecker, D. Marx, M. Tuckerman, and M. Parrinello, Max–Planck–Institut für Festkörperforschung and IBM Zurich Research Laboratory (1995–1999).

143. CP-PAW: P. E. Blöchl, IBM Zurich Research Laboratory; see Ref. [75].

144. C. Császár and P. Pulay, J. Mol. Struc. **114**, 31 (1984).

145. T. R. Cundari, M. T. Benson, M. L. Lutz, and S. O. Sommerer, in *Reviews in Computational Chemistry Vol. 8*, p. 145, eds. K. B. Lipkowitz and D. B. Boyd (VCH, New York, 1996).

146. A. Curioni, W. Andreoni, J. Hutter, H. Schiffer, and M. Parrinello, J. Am.

Chem. Soc. **116**, 11 251 (1994).

147. A. Curioni, M. Sprik, W. Andreoni, H. Schiffer, J. Hutter, and M. Parrinello, J. Am. Chem. Soc. **119**, 7218 (1997).

148. A. Curioni, M. Boero, and W. Andreoni, Chem. Phys. Lett. **294**, 263 (1998).

149. E. Dalgaard and P. Jorgensen, J. Chem. Phys. **69**, 3833 (1978).

150. C. Daul, Int. J. Quantum Chem. **52**, 867 (1994).

151. E. R. Davidson, J. Comput. Phys. **17**, 87 (1975).

152. A. Debernardi, M. Bernasconi, M. Cardona, and M. Parrinello, Appl. Phys. Lett. **71**, 2692 (1997).

153. P. H. Dederichs and R. Zeller, Phys. Rev. B **28**, 5462 (1983).

154. J. B. Delos, W. R. Thorson, and S. K. Knudson, Phys. Rev. A **6**, 709 (1972); see also following two papers.

155. Z. Deng, G. J. Martyna, and M. L. Klein, Phys. Rev. Lett. **68**, 2496 (1992).

156. Z. Deng, G. J. Martyna, and M. L. Klein, Phys. Rev. Lett. **71**, 267 (1993).

157. P. J. H. Denteneer and W. van Haeringen, J. Phys. C: Solid State Phys. **18**, 4127 (1985).

158. E. Deumens, A. Diz, R. Longo, and Y. Öhrn, Rev. Mod. Phys. **66**, 917 (1994).

159. A. Devenyi, K. Cho, T. A. Arias, and J. D. Joannopoulos, Phys. Rev. B **49**, 13 373 (1994).

160. B. K. Dey, A. Askar, and H. Rabitz, J. Chem. Phys. **109**, 8770 (1998).

161. A. Dhavale, D. G. Kanhere, C. Majumder, and G. P. Das, Eur. Phys. J. D **6**, 495 (1999).

162. P. A. M. Dirac, Proc. Cambridge Phil. Soc. **26**, 376 (1930).

163. P. A. M. Dirac, *The Principles of Quantum Mechanics* (Oxford University Press, Oxford, 1947; third edition); see in particular Chapt. V-§31–32.

164. M. Diraison, G. J. Martyna, and M. E. Tuckerman, J. Chem. Phys. **111**, 1096 (1999).

165. K. Doclo and U. Röthlisberger, Chem. Phys. Lett. **297**, 205 (1998).

166. M. Dolg and H. Stoll, in *Handbook on the Physics and Chemistry of Rare Earths Vol. 22*, p. 607, eds. K. A. Gschneidner Jr. and L. Eyring (Elsevier, Amsterdam, 1996).

167. J. Douady, Y. Ellinger, R. Subra, and B. Levy, J. Chem. Phys. **72**, 1452 (1980).

168. R. M. Dreizler and E. K. U. Gross, *Density–Functional Theory* (Springer, Berlin, 1990); see also the upcoming revised edition.

169. B. I. Dunlap, J. W. D. Connolly, and J. R. Sabin, J. Chem. Phys. **71**, 3396 (1979).

170. B. I. Dunlap, Int. J. Quantum Chem. **69**, 317 (1998).

171. B. I. Dunlap and R. W. Warren, Adv. Quantum Chem. **33**, 167 (1998).

172. A. L. L. East, Z. F. Liu, C. McCague, K. Cheng, and J. S. Tse, J. Phys. Chem. A **102**, 10 903 (1998).

173. J. W. Eastwood and D. R. K. Brownrigg, J. Comp. Phys. **32**, 24 (1979).

174. P. Ehrenfest, Z. Phys. **45**, 455 (1927).

175. E. Ermakova, J. Solca, H. Huber, and D. Marx, Chem. Phys. Lett. **246**, 204 (1995).

176. M. Ernzerhof and G. E. Scuseria, J. Chem. Phys. **110**, 5029 (1999).

177. R. Esser, P. Grassberger, J. Grotendorst, and M. Lewerenz (Eds.), *Molecular Dynamics on Parallel Computers* (World Scientific, Singapore, 2000).

178. S. K. Estreicher, J. L. Hastings, and P. A. Fedders, Phys. Rev. Lett. **82**, 815 (1999).

179. R. A. Evarestov and V. P. Smirnov, Phys. Stat. Sol. (b) **119**, 9 (1983).

180. M. Fähnle, C. Elsässer, and H. Krimmel, phys. stat. sol. (b) **191**, 9 (1995).

181. P. A. Fedders and D. A. Drabold, Phys. Rev. B **56**, 1864 (1997).

182. A. Fedorowicz, J. Mavri, P. Bala, and A. Koll, Chem. Phys. Lett. **289**, 457 (1998).

183. M. D. Feit, J. A. Fleck, Jr., and A. Steiger, J. Comput. Phys. **47**, 412 (1982).

184. P. Fernandez, A. Dal Corso, A. Baldereschi, and F. Mauri, Phys. Rev. B **55**, R1909 (1997).

185. G. W. Fernando, G.–X. Qian, M. Weinert, and J. W. Davenport, Phys. Rev. B **40**, 7985 (1989).

186. R. P. Feynman, Phys. Rev. **56**, 340 (1939); see in particular equation (2).

187. R. P. Feynman and A. R. Hibbs, *Quantum Mechanics and Path Integrals* (McGraw–Hill, New York, 1965).

188. R. P. Feynman, *Statistical Mechanics* (Addison–Wesley, Redwood City, 1972).

189. `fhi98md:` see Ref. [78].

190. M. J. Field, Chem. Phys. Lett. **172**, 83 (1990).

191. M. J. Field, J. Phys. Chem. **95**, 5104 (1991).

192. M. Filatov and W. Thiel, Mol. Phys. **91**, 847 (1997).

193. M. Filatov and S. Shaik, Chem. Phys. Lett. **288**, 689 (1998).

194. M. Filatov and W. Thiel, Phys. Rev. A **57**, 189 (1998).

195. M. Filatov and S. Shaik, J. Chem. Phys. **110**, 116 (1999).

196. M. Filatov and S. Shaik, Chem. Phys. Lett. **304**, 429 (1999).

197. A. Filippetti, D. Vanderbilt, W. Zhong, Y. Cai, and G.B. Bachelet, Phys. Rev. B **52**, 11793 (1995).

198. F. Filippone and F. A. Gianturco, J. Chem. Phys. **111**, 2761 (1999).

199. F. Finocchi and C. Noguera, Phys. Rev. B **57**, 14 646 (1998).

200. A. J. Fisher, W. Hayes, and F. L. Pratt, J. Phys.: Condens. Matter **3**, L9823 (1991).

201. P. Focher, G. L. Chiarotti, M. Bernasconi, E. Tosatti, and M. Parrinello, Europhys. Lett. **26**, 345 (1994).

202. P. Focher, Ph.D. Thesis: *First–principle studies of structural phase transformations* (Scuola Internazionale Superiore di Studi Avanzati (SISSA), Trieste, 1994).

203. E. S. Fois, A. Selloni, M. Parrinello, and R. Car, J. Phys. Chem. **92**, 3268 (1988).

204. E. S. Fois, J. I. Penman, and P. A. Madden, J. Chem. Phys. **98**, 6361 (1993).

205. E. S. Fois, M. Sprik, and M. Parrinello, Chem. Phys. Lett. **223**, 411 (1994).

206. E. Fois and A. Gamba, J. Phys. Chem. B **101**, 4487 (1997).

207. E. Fois, A. Gamba, and G. Tabacchi, J. Phys. Chem. B **102**, 3974 (1998).

208. E. Fois and A. Gamba, J. Phys. Chem. B **103**, 1794 (1999).

209. E. Fois, A. Gamba, and G. Tabacchi, Phys. Chem. Chem. Phys. **1**, 531 (1999).

210. J. Ford, Phys. Rep. **213**, 271 (1992).
211. G. P. Francis and M. C. Payne, J. Phys.: Condens. Matter **2**, 4395 (1990).
212. I. Frank, D. Marx, and M. Parrinello, J. Amer. Chem. Soc. **117**, 8037 (1995).
213. I. Frank, D. Marx, and M. Parrinello, J. Chem. Phys. **104**, 8143 (1996).
214. I. Frank, J. Hutter, D. Marx, and M. Parrinello, J. Chem. Phys. **108**, 4060 (1998).
215. I. Frank, M. Parrinello, and A. Klamt, J. Phys. Chem. A **102**, 3614 (1998).
216. I. Frank, D. Marx, and M. Parrinello, J. Phys. Chem. A **103**, 7341 (1999).
217. D. Frenkel and B. Smit, *Understanding Molecular Simulation – From Algorithms to Applications* (Academic Press, San Diego, 1996).
218. J. Fritsch and U. Schröder, Phys. Rep. **309**, 209 (1999).
219. S. Froyen and M. L. Cohen, J. Phys. C **19**, 2623 (1986).
220. C.–L. Fu and K.–M. Ho, Phys. Rev. B **28**, 5480 (1983).
221. M. Fuchs and M. Scheffler, Comput. Phys. Commun. **119**, 67 (1999).
222. G. Galli, R. M. Martin, R. Car, and M. Parrinello, Science **250**, 1547 (1990).
223. G. Galli and M. Parrinello, in *Computer Simulations in Materials Science*, p. 282, eds. M. Meyer and V. Pontikis (Kluwer, Dordrecht, 1991).
224. G. Galli and A. Pasquarello, in *Computer Simulation in Chemical Physics*, eds. M. P. Allen and D. J. Tildesley (Kluwer, Dordrecht, 1993).
225. G. Galli, A. Catellani, and F. Gygi, Phys. Rev. Lett. **83**, 2006 (1999).
226. G. Galli and F. Gygi, Phys. Rev. Lett. **82**, 3476 (1999).
227. A. Gambirasio and M. Bernasconi, Phys. Rev. B **60**, 12 007 (1999).
228. D. A. Gibson and E. A. Carter, J. Phys. Chem. **97**, 13 429 (1993).
229. D. A. Gibson, I. V. Ionova, and E. A. Carter, Chem. Phys. Lett. **240**, 261 (1995).
230. D. A. Gibson and E. A. Carter, Mol. Phys. **89**, 1265 (1996).
231. D. A. Gibson and E. A. Carter, Chem. Phys. Lett. **271**, 266 (1997).
232. M. J. Gillan, J. Phys.: Condens. Matter **1**, 689 (1989).
233. M. J. Gillan in *Computer Modelling of Fluids, Polymers, and Solids*, eds. C. R. A. Catlow, S. C. Parker, and M. P. Allen (Kluwer, Dordrecht, 1990).
234. M. J. Gillan, Contemp. Phys. **38**, 115 (1997).
235. M. J. Gillan, P. J. D. Lindan, L. N. Kantorovich, and S. P. Bates, Mineral. Mag. **62**, 669 (1998).
236. V. V. Godlevsky, J. J. Derby, and J. R. Chelikowsky, Phys. Rev. Lett. **81**, 4959 (1998).
237. V. V. Godlevsky, M. Jain, J. J. Derby, and J. R. Chelikowsky, Phys. Rev. B **60**, 8640 (1999).
238. S. Goedecker and K. Maschke, Phys. Rev. A **45**, 88 (1992).
239. S. Goedecker, M. Teter, and J. Hutter, Phys. Rev. B **54**, 1703 (1996).
240. S. Goedecker and C. J. Umrigar, Phys. Rev. A **55**, 1765 (1997).
241. S. Goedecker and O. V. Ivanov, Solid State Commun. **105**, 665 (1998).
242. S. Goedecker and O. V. Ivanov, Computers in Physics **12**, 548 (1998).
243. S. Goedecker, Rev. Mod. Phys. **71**, 1085 (1999).
244. H. Goldstein, *Klassische Mechanik* (Aula–Verlag, Wiesbaden, 1987).
245. P. Gomes Dacosta, O. H. Nielsen, and K. Kunc, J. Phys. C **19**, 3163 (1986).
246. X. G. Gong, D. Guenzburger, and E. B. Saitovitch, Chem. Phys. Lett. **275**,

392 (1997).

247. L. Gorb and J. Leszczynski, Comput. Chem. **3**, 179 (1999).

248. C. M. Goringe, L. J. Clark, M. H. Lee, M. C. Payne, I. Štich, J. A. White, M. J. Gillan, and A. P. Sutton, J. Phys. Chem. B **101**, 1498 (1997).

249. A. Görling, Phys. Rev. B **53**, 7024 (1996).

250. H. W. Graben and J. R. Ray, Mol. Phys. **80**, 1183 (1993).

251. T. Grabo, E. K. U. Gross, and M. Lüders, *Orbital Functionals in Density Functional Theory: The Optimized Effective Potential Method*; see `http://psi-k.dl.ac.uk/psi-k/highlights.html` and `ftp://ftp.dl.ac.uk/psik-network/Highlight_16.ps`.

252. J. Gräfenstein, E. Kraka, and D. Cremer, Chem. Phys. Lett. **288**, 593 (1998).

253. C. G. Gray and K. E. Gubbins, *Theory of Molecular Fluids Vol. 1* (Oxford, Clarendon, 1984).

254. J. C. Greer, R. Ahlrichs, and I. V. Hertel, Z. Phys. D **18**, 413 (1991); see in particular Sect. 3.

255. A. Gross, M. Bockstedte, and M. Scheffler, Phys. Rev. Lett. **79**, 701 (1997).

256. A. Gross, Surf. Sci. Rep. **32**, 291 (1998).

257. A. Gross, C.–M. Wei, and M. Scheffler, Surf. Sci. **416**, L1095 (1998).

258. E. K. U. Gross and W. Kohn, Adv. Quant. Chem. **21**, 255 (1990).

259. F. Grossmann, Comments At. Mol. Phys. **34**, 141 (1999).

260. M. P. Grumbach, D. Hohl, R. M. Martin, and R. Car, J. Phys.: Condens. Matter **6**, 1999 (1994).

261. M. P. Grumbach and R. M. Martin, Phys. Rev. B **54**, 15 730 (1996).

262. F. Gygi and A. Baldereschi, Phys. Rev. B **34**, 4405 (1986).

263. F. Gygi, Europhys. Lett. **19**, 617 (1992).

264. F. Gygi, Phys. Rev. B **48**, 11 692 (1993).

265. F. Gygi, Phys. Rev. B **51**, 11 190 (1995).

266. F. Gygi and G. Galli, Phys. Rev. B **52**, R2229 (1995).

267. F. Gygi, Comput. Mater. Sci. **10**, 63 (1998).

268. F. Haase, J. Sauer, and J. Hutter, Chem. Phys. Lett. **266**, 397 (1997).

269. F. Haase and J. Sauer, J. Am. Chem. Soc. **120**, 13 503 (1998).

270. R. Haberlandt, S. Fritzsche, G. Peinel, and K. Heinzinger, *Molekulardynamik – Grundlagen und Anwendungen* (Vieweg Verlag, Braunschweig, 1995).

271. J. C. L. Hageman, R. J. Meier, M. Heinemann, and R. A. de Groot, Macromolecules **30**, 5953 (1997).

272. H. Hakkinen, R. N. Barnett, and U. Landman, J. Phys. Chem. B **103**, 8814 (1999).

273. R. W. Hall and B. J. Berne, J. Chem. Phys. **81**, 3641 (1984).

274. D. R. Hamann, M. Schlüter, and C. Ciang, Phys. Rev. Lett. **43**, 1494 (1979).

275. D. R. Hamann, Phys. Rev. B **51**, 7337 (1995).

276. D. R. Hamann, Phys. Rev. B **51**, 9508 (1995).

277. D. R. Hamann, Phys. Rev. B **54**, 1568 (1996).

278. D. R. Hamann, Phys. Rev. B **56**, 14 979 (1997).

279. D. R. Hamann, Phys. Rev. Lett. **81**, 3447 (1998).

280. S. Hammes–Schiffer and H. C. Andersen, J. Chem. Phys. **99**, 523 (1993).

281. B. Hartke and E. A. Carter, Chem. Phys. Lett. **189**, 358 (1992).

282. B. Hartke and E. A. Carter, J. Chem. Phys. **97**, 6569 (1992).

283. B. Hartke and E. A. Carter, Chem. Phys. Lett. **216**, 324 (1993).

284. B. Hartke, D. A. Gibson, and E. A. Carter, Int. J. Quantum Chem. **45**, 59 (1993).

285. B. Hartke, private communication.

286. C. Hartwigsen, W. Witschel, and E. Spohr, Ber. Bunsenges. Phys. Chem. **101**, 859 (1997).

287. C. Hartwigsen, W. Witschel, and E. Spohr, Phys. Rev. B **55**, 4953 (1997).

288. C. Hartwigsen, S. Goedecker, and J. Hutter, Phys. Rev. B **58**, 3661 (1998).

289. K. C. Hass, W. F. Schneider, A. Curioni, and W. Andreoni, Science **282**, 265 (1998).

290. M. Head–Gordon and J. A. Pople, J. Phys. Chem. **92**, 3063 (1988).

291. F. Hedman and A. Laaksonen, Mol. Simul. **20**, 265 (1998).

292. W. J. Hehre, L. Radom, P. v. R. Schleyer, and J. A. Pople, *Ab Initio Molecular Orbital Theory* (John Wiley & Sons, New York, 1986).

293. A. Heidenreich and J. Sauer, Z. Phys. D **35**, 279 (1995).

294. V. Heine and D. Weaire, Solid St. Phys. **24**, 249 (1970).

295. H. Hellmann, Z. Phys. **85**, 180 (1933), see equation (3b); note that Hellmann already connects the "Hellmann–Feynman theorem" to first–order perturbation theory for cases where it does not hold rigorously, for instance when the wavefunction used to evaluate the expectation value is not the exact one.

296. H. Hellmann, J. Chem. Phys. **3**, 61 (1935).

297. H. Hellmann and W. Kassatotschkin, J. Chem. Phys. **4**, 324 (1936).

298. C. Herring, Phys. Rev. **57**, 1169 (1940).

299. K.–M. Ho, J. Ihm, and J. D. Joannopoulos, Phys. Rev. B **25**, 4260 (1982).

300. R. W. Hockney, Methods Comput. Phys. **9**, 136 (1970).

301. P. Hohenberg and W. Kohn, Phys. Rev. **136**, B864 (1964).

302. D. Hohl, R. O. Jones, R. Car, and M. Parrinello, Chem. Phys. Lett. **139**, 540 (1987).

303. D. Hohl, R. O. Jones, R. Car, and M. Parrinello, J. Chem. Phys. **89**, 6823 (1988).

304. D. Hohl and R. O. Jones, Phys. Rev. B **43**, 3856 (1991).

305. D. Hohl, V. Natoli, D. M. Ceperley, and R. M. Martin, Phys. Rev. Lett. **71**, 541 (1993).

306. K. Hoshino, F. Shimojo, and T. Nishida, J. Phys. Soc. Jap. **68**, 1907 (1999).

307. W. G. Hoover, Phys. Rev. A **31**, 1695 (1985).

308. J. Hutter, H. P. Lüthi, and M. Parrinello, Comput. Mat. Sci. **2**, 244 (1994).

309. J. Hutter, M. Parrinello, and S. Vogel, J. Chem. Phys. **101**, 3862 (1994).

310. J. Hutter, M. E. Tuckerman, and M. Parrinello, J. Chem. Phys. **102**, 859 (1995).

311. J. Hutter, P. Carloni, and M. Parrinello, J. Am. Chem. Soc. **118**, 8710 (1996).

312. J. Ihm, A. Zunger, and M. L. Cohen, J. Phys. C **12**, 4409 (1979).

313. T. Ikeda, M. Sprik, K. Terakura, and M. Parrinello, Phys. Rev. Lett. **81**, 4416 (1998).

314. Y. Imamura, N. Matsui, Y. Morikawa, M. Hada, T. Kubo, M. Nishijima, and H. Nakatsuji, Chem. Phys. Lett. **287** 131 (1998).

315. Y. Jeanvoine, J. G. Ángyán, G. Kresse, and J. Hafner, J. Phys. Chem. B **102**, 7307 (1998).
316. J. Jellinek, V. Bonačić–Koutecký, P. Fantucci, and M. Wiechert, J. Chem. Phys. **101**, 10 092 (1994).
317. J. Jellinek, S. Srinivas, and P. Fantucci, Chem. Phys. Lett. **288**, 705 (1998).
318. B. G. Johnson, P. M. W. Gill, and J. A. Pople, J. Chem. Phys. **98**, 5612 (1993).
319. D. D. Johnson, Phys. Rev. B **38**, 12087 (1988).
320. R. O. Jones and O. Gunnarsson, Rev. Mod. Phys. **61**, 689 (1989).
321. R. O. Jones, Angew. Chem. Int. Ed. Engl. **30**, 630 (1991).
322. Y.–M. Juan and E. Kaxiras, Phys. Rev. B **48**, 14 944 (1993).
323. R. Kaschner and D. Hohl, J. Phys. Chem. A **102**, 5111 (1998).
324. C. Katan, J. Phys. Chem. A **103**, 1407 (1999).
325. M. I. Katsnelson, M. van Schilfgaarde, V. P. Antropov, and B. N. Harmon, Phys. Rev. A **54**, 4802 (1996).
326. G. P. Kerker, J. Phys. C **13**, L189 (1980).
327. G. Kern and J. Hafner, Phys. Rev. B **58**, 13 167 (1998).
328. V. Keshari and Y. Ishikawa, Chem. Phys. Lett. **218**, 406 (1994).
329. E. Kim, Y. H. Lee, J. J. Lee, and Y. G. Hwang, Europhys. Lett. **40**, 147 (1997).
330. E. Kim, C. W. Oh, Y. H. Lee, Phys. Rev. Lett. **79**, 4621 (1997).
331. F. Kirchhoff, G. Kresse, and M. J. Gillan, Phys. Rev. B **57**, 10 482 (1998).
332. S. Kirkpatrick, C. D. Gelatt, Jr., and M. P. Vecchi, Science **220**, 671 (1983).
333. H. Kitamura, S. Tsuneyuki, T. Ogitsu, and T. Miyake, *Quantum distribution of protons in solid molecular hydrogen under megabar pressure*, preprint.
334. H. Kleinert, *Path Integrals in Quantum Mechanics, Statistics and Polymer Physics* (World Scientific, Singapore, 1990).
335. L. Kleinman and D. M. Bylander, Phys. Rev. Lett. **48**, 1425 (1982).
336. A. Klesing, D. Labrenz, R. A. van Santen, J. Chem. Soc., Faraday Trans. **94**, 3229 (1998).
337. J. Kohanoff, S. Scandolo, G. L. Chiarotti, and E. Tosatti, Phys. Rev. Lett. **78**, 2783 (1997).
338. W. Kohn and L. J. Sham, Phys. Rev. **140**, A1133 (1965).
339. W. Kohn, Chem. Phys. Lett. **208**, 167 (1993).
340. W. Kołos, Adv. Quant. Chem. **5**, 99 (1970).
341. R. Kosloff, J. Phys. Chem. **92**, 2087 (1988).
342. R. Kosloff, Annu. Rev. Phys. Chem. **45**, 145 (1994).
343. G. Kresse and J. Hafner, Phys. Rev. B **47**, 558 (1993).
344. G. Kresse and J. Furthmüller, Phys. Rev. B **54**, 11 169 (1996).
345. G. Kresse and J. Furthmüller, Comput. Mat. Sci **6**, 15 (1996).
346. G. Kresse and J. Hafner, Phys. Rev. B **55**, 7539 (1997).
347. G. Kresse and D. Joubert, Phys. Rev. B **59**, 1758 (1999).
348. V. Kumar and V. Sundararajan, Phys. Rev. B **57**, 4939 (1998).
349. V. Kumar, Phys. Rev.B **60**, 2916 (1999).
350. W. Kutzelnigg, Mol. Phys. **90**, 909 (1997).
351. K. Laasonen, A. Pasquarello, R. Car, C. Lee, and D. Vanderbilt, Phys. Rev.

B **47**, 10 142 (1993).

352. K. Laasonen, M. Sprik, M. Parrinello, and R. Car, J. Chem. Phys. **99**, 9080 (1993).
353. K. Laasonen and M. L. Klein, J. Amer. Chem. Soc. **116**, 11 620 (1994).
354. K. Laasonen and M. L. Klein, J. Phys. Chem. **98**, 10 079 (1994).
355. D. Lamoen, P. Ballone, and M. Parrinello, Phys. Rev. B **54**, 5097 (1996).
356. D. Lamoen and M. Parrinello, Chem. Phys. Lett. **248**, 309 (1996).
357. C. Lanczos, J. Res. Nat. Bur. Stand. **45**, 255 (1950).
358. W. Langel and M. Parrinello, Phys. Rev. Lett. **73**, 504 (1994).
359. W. Langel and M. Parrinello, J. Chem. Phys. **103**, 3240 (1995).
360. W. Langel, Chem. Phys. Lett. **259**, 7 (1996).
361. G. Lauritsch and P.–G. Reinhard, Int. J. Mod. Phys. C **5**, 65 (1994).
362. C. Lee, W. Yang, and R. G. Parr, Phys. Rev. B **37**, 785 (1988).
363. C. Lee, D. Vanderbilt, K. Laasonen, R. Car, and M. Parrinello, Phys. Rev. Lett. **69**, 462 (1992).
364. C. Lee, D. Vanderbilt, K. Laasonen, R. Car, and M. Parrinello, Phys. Rev. B **47**, 4863 (1993).
365. C. Leforestier, J. Chem. Phys. **68**, 4406 (1978).
366. C. Leforestier, R. H. Bisseling, C. Cerjan, M. D. Feit, R. Friesner, A. Guldberg, A. Hammerich, G. Jolicard, W. Karrlein, H.–D. Meyer, N. Lipkin, O. Roncero, and R. Kosloff, J. Comp. Phys. **94**, 59 (1991).
367. J. G. LePage, M. Alouani, D. L. Dorsey, J. W. Wilkins, and P. E. Blöchl, Phys. Rev. B **58**, 1499 (1998).
368. I. N. Levine, *Quantum Chemistry* (Allyn and Bacon, Boston, 1983).
369. J.S. Lin, A. Qteish, M.C. Payne, and V. Heine, Phys. Rev. B **47**, 4174 (1993).
370. G. Lippert, J. Hutter, and M. Parrinello, Molec. Phys. **92**, 477 (1997).
371. G. Lippert, J. Hutter, and M. Parrinello, Theor. Chem. Acc. **103**, 124 (1999).
372. Z. Liu, L. E. Carter, and E. A. Carter, J. Phys. Chem. **99**, 4355 (1995).
373. Z. F. Liu, C. K. Siu, and J. S. Tse, Chem. Phys. Lett. **309**, 335 (1999).
374. S. G. Louie, S. Froyen, and M. L. Cohen, Phys. Rev. B **26**, 1738 (1982).
375. H. Löwen, P. A. Madden, and J.–P. Hansen, Phys. Rev. Lett. **68**, 1081 (1992); see also Ref. [376].
376. H. Löwen and I. D'amico, J. Phys.: Condens. Matter **9**, 8879 (1997).
377. M. Lubin and J. H. Weare, Mineral. Mag. **62A**, 915 (1998).
378. G. Makov and M. C. Payne, Phys. Rev. B **51**, 4014 (1995).
379. S. A. Maluendes and M. Dupuis, Int. J. Quantum Chem. **42**, 1327 (1992).
380. A. Marcellini, C. A. Pignedoli, M. Ferrario, and C. M. Bertoni, Surf. Sci. **402**–**404**, 47 (1998).
381. M. Marchi, J. Hutter, and M. Parrinello, J. Am. Chem. Soc. **118**, 7847 (1996).
382. P. Margl, T. Ziegler, and P. E. Blöchl, J. Am. Chem. Soc. **117**, 12 625 (1995).
383. P. M. Margl, T. K. Woo, P. E. Blöchl, and T. Ziegler, J. Am. Chem. Soc. **120**, 2174 (1998).
384. N. A. Marks, D. R. McKenzie, B. A. Pailthorpe, M. Barnasconi, and M. Parrinello, Phys. Rev. Lett. **76**, 768 (1996).
385. T. J. Martinez, M. Ben–Nun, and G. Ashkenazi, J. Chem. Phys. **104**, 2847 (1996).

386. T. J. Martinez, M. Ben–Nun, and R. D. Levine, J. Phys. Chem. **100**, 7884 (1996).

387. T. J. Martinez, Chem. Phys. Lett. **272**, 139 (1997).

388. G. J. Martyna, M. L. Klein, and M. Tuckerman, J. Chem. Phys. **97**, 2635 (1992).

389. G. J. Martyna, D. J. Tobias, and M. L. Klein, J. Chem. Phys. **101**, 4177 (1994).

390. G. J. Martyna, J. Chem. Phys. **104**, 2018 (1996).

391. G. J. Martyna, M. E. Tuckerman, D. J. Tobias, and M. L. Klein, Mol. Phys. **87**, 1117 (1996).

392. G. J. Martyna, A. Hughes, and M. E. Tuckerman, J. Chem. Phys. **110**, 3275 (1999).

393. G. J. Martyna and M. E. Tuckerman, J. Chem. Phys. **110**, 2810 (1999).

394. G. J. Martyna, K. Pihakari, and M. E. Tuckerman, to be published.

395. D. Marx and M. Parrinello, Z. Phys. B (Rapid Note) **95**, 143 (1994); a misprinted sign in the Lagrangian is correctly given in Eq. (319) of the present review.

396. D. Marx, J. Hutter, and M. Parrinello, Chem. Phys. Lett. **241**, 457 (1995).

397. D. Marx and M. Parrinello, Nature (London) **375**, 216 (1995).

398. D. Marx, E. Fois, and M. Parrinello, Int. J. Quantum Chem. **57**, 655 (1996).

399. D. Marx and M. Parrinello, J. Chem. Phys. **104**, 4077 (1996).

400. D. Marx and M. Parrinello, Science **271**, 179 (1996).

401. D. Marx and M. Parrinello, Z. Phys. D **41**, 253 (1997).

402. D. Marx and A. Savin, Angew. Chem. Int. Ed. Engl. **36**, 2077 (1997); Angew. Chem. **109**, 2168 (1997).

403. D. Marx, M. Sprik, and M. Parrinello, Chem. Phys. Lett. **272**, 360 (1997); see also Refs. [396,398].

404. D. Marx, in *Classical and Quantum Dynamics in Condensed Phase Simulations* Chapt. 15, eds. B. J. Berne, G. Ciccotti, und D. F. Coker (World Scientific, Singapore, 1998).

405. D. Marx, Nachr. Chem. Tech. Lab. **47**, 186 (1999).

406. D. Marx, in *New Approaches to Problems in Liquid State Theory* p. 439, eds. C. Caccamo, J.–P. Hansen, and G. Stell (Kluwer, Dordrecht, 1999).

407. D. Marx and M. H. Müser, J. Phys.: Condens. Matter **11**, R117 (1999).

408. D. Marx and M. Parrinello, Science **284**, 59 (1999); see also Ref. [408].

409. D. Marx and M. Parrinello, Science **286**, 1051 (1999); see
http://www.sciencemag.org/cgi/content/full/286/5442/1051a.

410. D. Marx, M. E. Tuckerman, J. Hutter, and M. Parrinello, Nature (London) **397**, 601 (1999); see also J. T. Hynes, Nature (London) **397**, 565 (1999).

411. D. Marx, M. E. Tuckerman, and G. J. Martyna, Comput. Phys. Commun. **118**, 166 (1999); the misprinted definition of the fictitious normal mode masses given in Eq. (2.51) is corrected in Eq. (338) of the present review. However, the correct definition was implemented in the CPMD package [142] so that all data reported in the paper are unaffected.

412. D. Marx, M. E. Tuckerman, and M. Parrinello, *Solvated excess protons in water: Quantum effects on the hydration structure*, J. Phys.: Condens. Matter

(in press).

413. N. Marzari and D. Vanderbilt, Phys. Rev. B **56**, 12 847 (1997).

414. N. Marzari, D. Vanderbilt, and M. C. Payne, Phys. Rev. Lett. **79**, 1337 (1997).

415. N. Marzari, D. Vanderbilt, A. De Vita and M. C. Payne, Phys. Rev. Lett. **82**, 3296 (1999).

416. C. Massobrio, A. Pasquarello, and R. Car, Phys. Rev. Lett. **80**, 2342 (1998).

417. F. Mauri, G. Galli, and R. Car, Phys. Rev. B **47**, 9973 (1993).

418. R. McWeeny, *Methods of Molecular Quantum Mechanics* (Academic Press, London, 1992).

419. H. S. Mei, M. E. Tuckerman, D. E. Sagnella, and M. L. Klein, J. Phys. Chem. B **102**, 10 446 (1998).

420. E. J. Meijer and M. Sprik, J. Chem. Phys. **105**, 8684 (1996).

421. E. J. Meijer and M. Sprik, J. Phys. Chem. A **102**, 2893 (1998).

422. E. J. Meijer and M. Sprik, J. Am. Chem. Soc. **120**, 6345 (1998).

423. B. Meng, D. Maroudas, and W. H. Weinberg, Chem. Phys. Lett. **278**, 97 (1997).

424. N. D. Mermin, Phys. Rev. **137**, A1441 (1965).

425. A. Messiah, *Quantum Mechanics* (North–Holland Publishing Company, Amsterdam, 1964); see in particular Chapter VI.I.4 in Volume I.

426. H.–D. Meyer and W. H. Miller, J. Chem. Phys. **70**, 3214 (1979).

427. S. Miura, M. E. Tuckerman, and M. L. Klein, J. Chem. Phys. **109**, 5290 (1998).

428. T. Miyake, T. Ogitsu, and S. Tsuneyuki, Phys. Rev. Lett. **81**, 1873 (1998).

429. T. Miyake, T. Ogitsu, and S. Tsuneyuki, *First–principles study of the quantum states of muonium and hydrogen in crystalline silicon*, Phys. Rev. B (in press).

430. Y. Miyamoto, O. Sugino, and Y. Mochizuki, Appl. Phys. Lett. **75**, 2915 (1999).

431. N. A. Modine, G. Zumbach, and E. Kaxiras, Phys. Rev. B **55**, 10 289 (1997).

432. C. Molteni, N. Marzari, M. C. Payne, and V. Heine, Phys. Rev. Lett. **79**, 869 (1997).

433. C. Molteni and M. Parrinello, J. Am. Chem. Soc. **120**, 2168 (1998); see also Ref. [434].

434. C. Molteni and M. Parrinello, Chem. Phys. Lett. **275**, 409 (1998).

435. H. J. Monkhorst and J. D. Pack, Phys. Rev. B **13**, 5189 (1976).

436. T. Morishita and S. Nosé, Phys. Rev. B **59**, 15126 (1999).

437. J. J. Mortensen and M. Parrinello, to be published.

438. V. Musolino, A. Selloni, and R. Car, Phys. Rev. Lett. **83**, 3242 (1999).

439. Á. Nagy, Phys. Rev. A **57**, 1672 (1998).

440. O. H. Nielsen and R. M. Martin, Phys. Rev. Lett. **50**, 697 (1983).

441. O. H. Nielsen and R. M. Martin, Phys. Rev. B **32**, 3780 (1985); **32**, 3792 (1985).

442. S. Nosé and M. L. Klein, Mol. Phys. **50**, 1055 (1983).

443. S. Nosé, Mol. Phys. **52**, 255 (1984).

444. S. Nosé, J. Chem. Phys. **81**, 511 (1984).

445. S. Nosé, Prog. Theor. Phys. Suppl. **103**, 1 (1991).

446. `NWChem:` developed and distributed by Pacific Northwest National Laboratory, USA.

447. M. Odelius, M. Bernasconi, and M. Parrinello, Phys. Rev. Lett. **78**, 2855 (1997).

448. M. Odelius, Phys. Rev. Lett. **82**, 3919 (1999).

449. K.–d. Oh and P. A. Deymier, Phys. Rev. Lett. **81**, 3104 (1998).

450. K.–d. Oh and P. A. Deymier, Phys. Rev. B **58**, 7577 (1998).

451. T. Ohtsuki, K. Ohno, K. Shiga, Y. Kawazoe, Y. Maruyama, and K. Masumoto, Phys. Rev. Lett. **81**, 967 (1998).

452. P. Ordejon, D. Drabold, M Grumbach, and R.M. Martin, Phys. Rev. B **48**, 14646 (1993).

453. P. Ordejón, Comp. Mater. Sci. **12**, 157 (1998).

454. J. Ortega, J. P. Lewis, and O. F. Sankey, Phys. Rev. B **50**, 10 516 (1994).

455. J. Ortega, J. P. Lewis, and O. F. Sankey, J. Chem. Phys. **106**, 3696 (1997).

456. A. Palma, A. Pasquarello, G. Ciccotti, and R. Car, J. Chem. Phys. **108**, 9933 (1998).

457. M. Palummo, L. Reining, and P. Ballone, J. Phys. IV (Paris) **3:(C7)**, 1955 (1993).

458. R. G. Parr and W. Yang, *Density–Functional Theory of Atoms and Molecules* (Oxford University Press, Oxford, 1989).

459. M. Parrinello and A. Rahman, Phys. Rev. Lett. **45**, 1196 (1980).

460. M. Parrinello and A. Rahman, J. Appl. Phys. **52**, 7182 (1981).

461. M. Parrinello and A. Rahman, J. Chem. Phys. **76**, 2662 (1982).

462. M. Parrinello and A. Rahman, J. Chem. Phys. **80**, 860 (1984).

463. M. Parrinello, Solid State Commun. **102**, 107 (1997).

464. A. Pasquarello, K. Laasonen, R. Car, Ch. Lee, and D. Vanderbilt, Phys. Rev. Lett. **69**, 1982 (1992).

465. A. Pasquarello and R. Car, Phys. Rev. Lett. **80**, 5145 (1998).

466. A. Pasquarello, J. Sarnthein, and R. Car, Phys. Rev. B: **57**, 14 133 (1998).

467. G. Pastore, E. Smargiassi, and F. Buda, Phys. Rev. A **44**, 6334 (1991).

468. G. Pastore, in *Monte Carlo and Molecular Dynamics of Condensed Matter Systems*, Chapt. 24, p. 635, eds. K. Binder and G. Ciccotti (Italien Physical Society SIF, Bologna, 1996).

469. M. Pavese, D. R. Berard, and G. A. Voth, Chem. Phys. Lett. **300**, 93 (1999).

470. M. C. Payne, J. Phys.: Condens. Matter **1**, 2199 (1989).

471. M. C. Payne, J. D. Joannopoulos, D. C. Allan, M. P. Teter, and D. Vanderbilt, Phys. Rev. Lett. **56**, 2656 (1986).

472. M. C. Payne, M. P. Teter, D. C. Allan, T. A. Arias, and J. D. Joannopoulos, Rev. Mod. Phys. **64**, 1045 (1992).

473. M. Pearson, E. Smargiassi, and P. Madden, J. Phys. Condens. Matter **5**, 3221 (1993).

474. G. La Penna, F. Buda, A. Bifone, and H. J. M. de Groot, Chem. Phys. Lett. **294**, 447 (1998).

475. J. P. Perdew and A. Zunger, Phys. Rev. B **23**, 5048 (1981).

476. J. P. Perdew, Phys. Rev. B **33**, 8822 (1986); Erratum: Phys. Rev. B **34**, 7406 (1986).

477. J. P. Perdew, J. A. Chevary, S. H. Vosko, K. A. Jackson, M. R. Pederson, D. J. Singh, and C. Fiolhais, Phys. Rev. B **46**, 6671 (1992); Erratum: Phys. Rev. B **48**, 4978 (1993).

478. J. P. Perdew and Y. Wang, Phys. Rev. B **45**, 13 244 (1992).

479. J. P. Perdew, K. Burke, M. Ernzerhof, Phys. Rev. Lett. **77**, 3865 (1996); Erratum: Phys. Rev. Lett. **78**, 1396 (1997); see Refs. [480,706] for revised versions of the "PBE" functional.

480. J. P. Perdew, K. Burke, M. Ernzerhof, Phys. Rev. Lett. **80**, 891 (1998).

481. R. Perez, M. C. Payne, I. Štich, and K. Terakura, Appl. Surf. Sci. **123/124**, 249 (1998).

482. R. Perez, I. Štich I, M. C. Payne MC, and K. Terakura, Appl. Surf. Sci. **140**, 320 (1999).

483. B. G. Pfrommer, J. Demmel, and H. Simon, J. Comput. Phys. **150**, 287 (1999).

484. J. C. Phillips, Phys. Rev. **112**, 685 (1958).

485. J. C. Phillips and L. Kleinman, Phys. Rev. **116**, 287 (1959).

486. Physics and Astronomy Classification Scheme (PACS); see `http://publish.aps.org/PACS`.

487. W. E. Pickett, Comput. Phys. Rep. **9**, 115 (1989).

488. C. Pierleoni, D. M. Ceperley, B. Bernu, and W. R. Magro, Phys. Rev. Lett. **73**, 2145 (1994).

489. W.T. Pollard and R.A. Friesner, J. Chem. Phys. **99**, 6742 (1993).

490. J. Polonyi and H. W. Wild, Phys. Rev. Lett. **51**, 2257 (1983).

491. W. H. Press, S. A. Teukolsky, W. T. Vetterling, and B. P. Flannery, *Numerical Recipes – The Art of Scientific Computing*, Chapt. 9.6, (Cambridge University Press, Cambridge, 1992).

492. W. H. Press, S. A. Teukolsky, W. T. Vetterling, and B. P. Flannery, *Numerical Recipes – The Art of Scientific Computing*, Chapt. 12.1, (Cambridge University Press, Cambridge, 1992).

493. E. I. Proynov, S. Sirois, and D. R. Salahub, Int. J. Quantum Chem. **64**, 427 (1997).

494. P. Pulay, Molec. Phys. **17**, 197 (1969).

495. P. Pulay, Chem. Phys. Lett. **73**, 393 (1980).

496. P. Pulay, Adv. Chem. Phys. **69**, 241 (1987).

497. A. Putrino and G. B. Bachelet, in *Advances in Computational Materials Science II*, eds. V. Fiorentini and F. Meloni (SIF, Bologna, 1998).

498. M. Qiu, X.–Y. Zhou, M. Jiang, P.–L. Cao, and Z. Zeng, Phys. Lett. A **245**, 430 (1998).

499. A. Qteish, Phys. Rev. B **52**, 14497 (1995).

500. M. R. Radeke and E. A. Carter, Annu. Rev. Phys. Chem. **48**, 243 (1997).

501. B. De Raedt, M. Sprik, and M. L. Klein, J. Chem. Phys. **80**, 5719 (1984).

502. L. M. Ramaniah, M. Bernasconi, and M. Parrinello, J. Chem. Phys. **111**, 1587 (1999).

503. R. Ramírez, J. Schulte, and M. C. Böhm, Chem. Phys. Lett. **275**, 377 (1997).

504. R. Ramírez, E. Hernandez, J. Schulte, and M. C. Böhm, Chem. Phys. Lett. **291**, 44 (1998).

505. R. Ramírez, T. López–Ciudad, and J. C. Noya, Phys. Rev. Lett. **81**, 3303 (1998).

506. R. Ramírez and T. López–Ciudad, J. Chem. Phys. **111**, 3339 (1999).

507. R. Ramírez and T. López–Ciudad, Phys. Rev. Lett. **83**, 4456 (1999).

508. G. Ranghino, A. Anselmino, L. Meda, C. Tonini, and G. F. Cerofolini, J. Phys. Chem. B **101**, 7723 (1997).

509. A. M. Rappe, K. M. Rabe, E. Kaxiras, and J. D. Joannopoulos, Phys. Rev. B **41**, 1227 (1990).

510. A. M. Rappe, J. D. Joannopoulos, and P. A. Bash, J. Am. Chem. Soc. **114**, 6466 (1992).

511. S. Raugei, P. L. Silvestrelli, and M. Parrinello, Phys. Rev. Lett. **83**, 2222 (1999).

512. P. Raybaud, J. Hafner, G. Kresse, and H. Toulhoat, Phys. Rev. Lett. **80**, 1481 (1998).

513. D. K. Remler and P. A. Madden, Molec. Phys. **70**, 921 (1990).

514. S. L. Richardson and J. L. Martins, Phys. Rev. B **58**, 15 307 (1998).

515. T. von Rosenvinge, M. Parrinello, and M. L. Klein, J. Chem. Phys. **107**, 8012 (1997).

516. T. von Rosenvinge, M. E. Tuckerman, and M. L. Klein, Faraday Discuss. **106**, 273 (1997).

517. U. Röthlisberger and W. Andreoni, J. Chem. Phys. **94**, 8129 (1991).

518. U. Röthlisberger and W. Andreoni, Chem. Phys. Lett. **198**, 478 (1992).

519. U. Röthlisberger, W. Andreoni, and M. Parrinello, Phys. Rev. Lett. **72**, 665 (1994).

520. U. Röthlisberger and M. L. Klein, J. Am. Chem. Soc. **117**, 42 (1995).

521. U. Röthlisberger and M. Parrinello, J. Chem. Phys. **106**, 4658 (1997).

522. U. Röthlisberger, M. Sprik, and M. L. Klein, J. Chem. Soc., Faraday Trans. **94**, 501 (1998).

523. U. Röthlisberger and P. Carloni, Int. J. Quantum Chem. **73**, 209 (1999).

524. R. Rousseau, G. Dietrich, S. Krückeberg, K. Lützenkirchen, D. Marx, L. Schweikhard, and C. Walther, Chem. Phys. Lett. **295**, 41 (1998).

525. R. Rousseau and D. Marx, Phys. Rev. Lett. **80**, 2574 (1998).

526. R. Rousseau and D. Marx, J. Chem. Phys. **111**, 5091 (1999).

527. C. Rovira and M. Parrinello, Int. J. Quantum Chem. **70**, 387 (1998).

528. C. Rovira, K. Kunc, J. Hutter, P. Ballone, and M. Parrinello, Int. J. Quantum Chem. **69**, 31 (1998).

529. C. Rovira and M. Parrinello, Chem. Eur. J. **5**, 250 (1999).

530. E. Ruiz and M. C. Payne, Chem. Eur. J. **4**, 2485 (1998).

531. A. Rytkonen, H. Hakkinen, and M. Manninen, Phys. Rev. Lett. **80**, 3940 (1998).

532. U. Saalmann and R. Schmidt, Z. Phys. D **38**, 153 (1996).

533. A. M. Saitta and M. L. Klein, J. Chem. Phys. **111**, 9434 (1999).

534. A. M. Saitta, P. D. Soper, E. Wasserman, and M. L. Klein, Nature (London) **399**, 46 (1999).

535. J. J. Sakurai, *Modern Quantum Mechanics* (Addison–Wesley Publishing Company, Redwood City, 1985); see in particular Chapter 2.4.

536. H. Sambe and R. H. Felton, J. Chem. Phys. **62**, 1122 (1975).

537. D. Sánchez–Portal, E. Artacho, and J. M. Soler, J. Phys.: Condens. Matter **8**, 3859 (1996).

538. E. Sandré and A. Pasturel, Mol. Simul. **20**, 63 (1997).

539. G. C. Schatz, Rev. Mod. Phys. **61**, 669 (1989).

540. F. Scheck, *Mechanik* (Springer Verlag, Berlin, 1988); see in particular Chapter 2.35.

541. R. Schinke, *Photodissociation Dynamics* (Cambridge University Press, Cambridge, 1995).

542. K. E. Schmidt and D. M. Ceperley, in *The Monte Carlo Method in Condensed Matter Physics*, p. 205, ed. K. Binder (Springer Verlag, Berlin, 1992).

543. J. Schulte, M. C. Böhm, and R. Ramírez, Mol. Phys. **93**, 801 (1998).

544. J. Schütt, M. C. Böhm, and R. Ramírez, Chem. Phys. Lett. **248**, 379 (1996).

545. K. Schwarz, E. Nusterer, P. Margl, and P. E. Blöchl, Int. J. Quantum Chem. **61**, 369 (1997).

546. K. Schwarz, E. Nusterer, and P. E. Blöchl, Catal. Today **50**, 501 (1999).

547. M. D. Segall, M. C. Payne, S. W. Ellis, G. T. Tucker, and R. N. Boyes, Eur. J. Drug Metab. Pharmacokinet. **22**, 283 (1997).

548. M. D. Segall, M. C. Payne, S. W. Ellis, G. T. Tucker, and R. N. Boyes, Phys. Rev. E **57**, 4618 (1998).

549. M. D. Segall, M. C. Payne, S. W. Ellis, G. T. Tucker, and P. J. Eddershaw, Xenobiotica **29**, 561 (1999).

550. G. Seifert and R. O. Jones, Z. Phys. D **20**, 77 (1991).

551. G. Seifert, D. Porezag, and Th. Frauenheim, Int. J. Quantum Chem. **58**, 185 (1996).

552. G. Seifert, R. Kaschner, M. Schöne, and G. Pastore, J. Phys.: Condens. Matter **10**, 1175 (1998).

553. A. Selloni, P. Carnevali, R. Car, and M. Parrinello, Phys. Rev. Lett. **59**, 823 (1987).

554. A. Selloni, A. Vittadini, M. Grätzel, Surf. Sci. **402–404**, 219 (1998).

555. Y. Senda, F. Shimojo, and K. Hoshino, J. Phys.: Condens. Matter **11**, 2199 (1999).

556. Y. Senda, F. Shimojo, and K. Hoshino, J. Phys.: Condens. Matter **11**, 5387 (1999).

557. S. Serra, G. Chiarotti, S. Scandolo, and E. Tosatti, Phys. Rev. Lett. **80**, 5160 (1998).

558. S. Serra, C. Cavazzoni, G. L. Chiarotti, S. Scandolo, and E. Tosatti, Science **284**, 788 (1999).

559. R. Shah, M. C. Payne, M.-H. Lee, and J. D. Gale, Science **271**, 1395 (1996).

560. R. Shah, M. C. Payne, and J. D. Gale, Int. J. Quantum Chem. **61**, 393 (1997).

561. F. Shimojo, K. Hoshino, and H. Okazaki, Solid State Ionics **113**, 319 (1998).

562. F. Shimojo, K. Hoshino, and Y. Zempo, J. Phys.: Condens. Matter **10**, L177 (1998).

563. F. Shimojo, S. Munejiri, K. Hoshino, and Y. Zempo, J. Phys.: Condens. Matter **11**, L153 (1999).

564. E. L. Shirley, D. C. Allan, R. M. Martin, and J. D. Joannopoulos, Phys. Rev.

B **40**, 3652 (1989).

565. A. J. R. da Silva, H.–Y. Cheng, D. A. Gibson, K. L. Sorge, Z. Liu, and E. A. Carter, Spectrochim. Acta A **53**, 1285 (1997).

566. A. J. R. da Silva, M. R. Radeke, and E. A. Carter, Surf. Sci. Lett. **381**, L628 (1997).

567. A. J. R. da Silva, J. W. Pang, E. A. Carter, and D. Neuhauser, J. Phys. Chem. A **102**, 881 (1998).

568. C. R. S. da Silva and R. W. Wentzcovitch, Comp. Mat. Sci. **8**, 219 (1997).

569. P. L. Silvestrelli, A. Alavi, M. Parrinello, and D. Frenkel, Europhys. Lett. **33**, 551 (1996).

570. P. L. Silvestrelli, A. Alavi, M. Parrinello, and D. Frenkel, Phys. Rev. Lett. **77**, 3149 (1996).

571. P. L. Silvestrelli, A. Alavi, and M. Parrinello, Phys. Rev. B **55**, 15 515 (1997).

572. P. L. Silvestrelli, A. Alavi, M. Parrinello, and D. Frenkel, Phys. Rev. B **56**, 3806 (1997).

573. P. L. Silvestrelli, M. Bernasconi, and M. Parrinello, Chem. Phys. Lett. **277**, 478 (1997).

574. P. L. Silvestrelli and M. Parrinello, J. Appl. Phys. **83**, 2478 (1998).

575. P. L. Silvestrelli and M. Parrinello, Phys. Rev. Lett. **82**, 3308 (1999); Erratum: Phys. Rev. Lett. **82**, 5415 (1999).

576. P. L. Silvestrelli and M. Parrinello, J. Chem. Phys. **111**, 3572 (1999).

577. F. Sim, A. St.–Amant, I. Papai, and D. R. Salahub, J. Am. Chem. Soc. **114**, 4391 (1992).

578. D. J. Singh, *Planewaves, Pseudopotentials and the* LAPW *Method* (Kluwer, Dordrecht, 1994).

579. L. D. Site, A. Alavi, and R. M. Lynden–Bell, Mol. Phys. **96**, 1683 (1999).

580. V. Smelyansky, J. Hafner, and G. Kresse, Phys. Rev. B **58**, R1782 (1998).

581. A. K. Soper, J. Phys.: Condens. Matter **9**, 2717 (1997).

582. M. Sprik and M. L. Klein, J. Chem. Phys. **89**, 1592 (1988); Erratum: J. Chem. Phys. **90**, 7614 (1989).

583. M. Sprik, J. Phys. Chem. **95**, 2283 (1991).

584. M. Sprik, in *Computer Simulation in Chemical Physics*, eds. M. P. Allen and D. J. Tildesley (Kluwer, Dordrecht, 1993).

585. M. Sprik, in *Monte Carlo and Molecular Dynamics of Condensed Matter Systems*, Chapt. 2, p. 43, eds. K. Binder and G. Ciccotti (Italien Physical Society SIF, Bologna, 1996).

586. M. Sprik, J. Phys.: Condens. Matter **8**, 9405 (1996).

587. M. Sprik, J. Hutter, and M. Parrinello, J. Chem. Phys. **105**, 1142 (1996).

588. M. Sprik, in *Classical and Quantum Dynamics in Condensed Phase Simulations*, Chapt. 13, eds. B. J. Berne, G. Ciccotti, and D. F. Coker (World Scientific, Singapore, 1998).

589. M. Sprik and G. Ciccotti, J. Chem. Phys. **109**, 7737 (1998).

590. M. Springborg (Ed.), *Density–Functional Methods in Chemistry and Materials Science*, (John Wiley & Sons, New York, 1997).

591. G. P. Srivastava and D. Weaire, Adv. Phys. **36**, 463 (1987).

592. R. Stadler, A. Alfe, G. Kresse, G. A. de Wijs, and M. J. Gillan, J. Non–Cryst.

Solids **250–252**, 82 (1999).

593. T. Starkloff and J.D. Joannopoulos, Phys. Rev. B **16**, 5212 (1977).
594. I. Štich, R. Car, M. Parrinello, and S. Baroni, Phys. Rev. B **39**, 4997 (1989).
595. I. Štich, Surf. Sci. **368**, 152 (1996).
596. I. Štich, D. Marx, M. Parrinello, and K. Terakura, Phys. Rev. Lett. **78**, 3669 (1997).
597. I. Štich, D. Marx, M. Parrinello, and K. Terakura, J. Chem. Phys. **107**, 9482 (1997).
598. I. Štich, J. D. Gale, K. Terakura, and M. C. Payne, Chem. Phys. Lett. **283**, 402 (1998).
599. I. Štich, J. D. Gale, K. Terakura, and M. C. Payne, J. Am. Chem. Soc. **121**, 3292 (1999).
600. A. C. Stückl, C. A. Daul, and H. U. Güdel, Int. J. Quantum Chem. **61**, 579 (1997).
601. P. Stumm and D. A. Drabold, Phys. Rev. Lett. **79**, 677 (1997).
602. D. M. Sullivan, K. Bagchi, M. E. Tuckerman, and M. L. Klein, J. Phys. Chem. A **103**, 8678 (1999).
603. W. C. Swope, H. C. Andersen, P. H. Berens, and K. R. Wilson, J. Chem. Phys. **76**, 637 (1982).
604. A. Szabo and N. S. Ostlund, *Modern Quantum Chemistry – Introduction to Advanced Electronic Structure Theory* (McGraw–Hill Publishing Company, New York, 1989).
605. H. Tachikawa and M. Igarashi, Chem. Phys. Lett. **303**, 81 (1999).
606. M. Takahashi and M. Imada, J. Phys. Soc. Japan **53**, 963 (1984); **53**, 3765 (1984); **53**, 3770 (1984).
607. N. Takeuchi, A. Selloni, and E. Tosatti, Phys. Rev. B **55**, 15 405 (1997).
608. S. Tanaka, J. Chem. Phys. **100**, 7416 (1994).
609. A. Tarazona, E. Koglin, F. Buda, B. B. Coussens, J. Renkema, S. van Heel, and R. J. Maier, J. Phys. Chem. B **101**, 4370 (1997).
610. F. Tassone, F. Mauri, and R. Car, Phys. Rev. B **50**, 10 561 (1994).
611. K. Terakura, T. Yamasaki, T. Uda, and I. Štich, Surf. Sci. **386**, 207 (1997).
612. V. Termath and J. Sauer, Chem. Phys. Lett. **255**, 187 (1996).
613. V. Termath and J. Sauer, Mol. Phys. **91**, 963 (1997).
614. V. Termath, F. Haase, J. Sauer, J. Hutter, and M. Parrinello, J. Am. Chem. Soc. **120**, 8512 (1998).
615. F. Terstegen, E. A. Carter, and V. Buss, Int. J. Quantum Chem. **75**, 141 (1999).
616. M. P. Teter, M. C. Payne, and D. C. Allen, Phys. Rev. B **40**, 12 255 (1989).
617. J. Theilhaber, Phys. Rev. B **46**, 12 990 (1992)
618. D. Thouless, J. Nucl. Phys. **21**, 225 (1960).
619. J. Tobik, I. Štich, R. Perez, and K. Terakura, Phys. Rev. B **60**, 11 639 (1999).
620. A. Tongraar, K. R. Liedl, and B. M. Rode, J. Phys. Chem. A **101**, 6299 (1997).
621. A. Tongraar, K. R. Liedl, and B. M. Rode, J. Phys. Chem. A **102**, 10 340 (1998).
622. W.C. Topp and J.J. Hopfield, Phys. Rev. B **7**, 1295 (1974).

623. E. Tornaghi, W. Andreoni, P. Carloni, J. Hutter, and M. Parrinello, Chem. Phys. Lett. **246**, 469 (1995).

624. G. Toth, J. Phys. Chem. A **101**, 8871 (1997).

625. A. Trave, F. Buda, and A. Fasolino, Phys. Rev. Lett. **77**, 5405 (1996).

626. N. Trouiller and J. L. Martins, Phys. Rev. B **43**, 1993 (1991).

627. N. Trouiller and J. L. Martins, Phys. Rev. B **43**, 8861 (1991).

628. B. L. Trout and M. Parrinello, Chem. Phys. Lett. **288**, 343 (1998).

629. B. L. Trout and M. Parrinello, J. Phys. Chem. B **103**, 7340 (1999).

630. J. S. Tse, D. D. Klug, and K. Laasonen, Phys. Rev. Lett. **74**, 876 (1995).

631. J. S. Tse and D. D. Klug, Phys. Rev. B **59**, 34 (1999).

632. E. Tsuchida and M. Tsukada, Solid State Commun. **94**, 5 (1995).

633. E. Tsuchida and M. Tsukada, Phys. Rev. B **52**, 5573 (1995).

634. E. Tsuchida and M. Tsukada, J. Phys. Soc. Japan **67**, 3844 (1998).

635. E. Tsuchida, Y. Kanada, and M. Tsukada, Chem. Phys. Lett. **311**, 236 (1999).

636. M. Tuckerman, B. J. Berne, and G. J. Martyna, J. Chem. Phys. **97**, 1990 (1992).

637. M. E. Tuckerman, B. J. Berne, G. J. Martyna, and M. L. Klein, J. Chem. Phys. **99**, 2796 (1993).

638. M. E. Tuckerman and M. Parrinello, J. Chem. Phys. **101**, 1302 (1994); see also Ref. [310].

639. M. E. Tuckerman and M. Parrinello, J. Chem. Phys. **101**, 1316 (1994).

640. M. Tuckerman, K. Laasonen, M. Sprik, and M. Parrinello, J. Phys.: Condens. Matter **6**, A93 (1994).

641. M. Tuckerman, K. Laasonen, M. Sprik, and M. Parrinello, J. Phys. Chem. **99**, 5749 (1995).

642. M. Tuckerman, K. Laasonen, M. Sprik, and M. Parrinello, J. Chem. Phys. **103**, 150 (1995).

643. M. E. Tuckerman, P. J. Ungar, T. von Rosenvinge, and M. L. Klein, J. Phys. Chem. **100**, 12 878 (1996).

644. M. E. Tuckerman, D. Marx, M. L. Klein, and M. Parrinello, J. Chem. Phys. **104**, 5579 (1996).

645. M. E. Tuckerman, D. Marx, M. L. Klein, and M. Parrinello, Science **275**, 817 (1997).

646. M. E. Tuckerman and A. Hughes, in *Classical and Quantum Dynamics in Condensed Phase Simulations*, Chapt. 14, p. 311, eds. B. J. Berne, G. Ciccotti, and D. F. Coker (World Scientific, Singapore, 1998).

647. M. E. Tuckerman and M. L. Klein, Chem. Phys. Lett. **283**, 147 (1998).

648. M. E. Tuckerman, private communication.

649. J. C. Tully, in *Modern Theoretical Chemistry: Dynamics of Molecular Collisions*, Part B, p. 217, ed. W. H. Miller (Plenum Press, New York, 1976).

650. J. C. Tully, in *Modern Methods for Multidimensional Dynamics Computations in Chemistry*, ed. D. L. Thompson (World Scientific, Singapore, 1998).

651. J. C. Tully, in *Classical and Quantum Dynamics in Condensed Phase Simulations*, Chapt. 21, p. 489, eds. B. J. Berne, G. Ciccotti, and D. F. Coker (World Scientific, Singapore, 1998).

652. C. J. Tymczak and X.–Q. Wang, Phys. Rev. Lett. **78**, 3654 (1997).

653. T. Uchiyama, T. Uda, and K. Terakura, Surf. Sci. **433–435**, 896 (1999).

654. K. Uehara, M. Ishitobi, T. Oda, and Y. Hiwatari, Mol. Simul. **18**, 385 (1997); Mol. Simul. **19**, 75 (1997).

655. C. P. Ursenbach, A. Calhoun, and G. A. Voth, J. Chem. Phys. **106**, 2811 (1997).

656. R. M. Valladares, A. J. Fisher, and W. Hayes, Chem. Phys. Lett. **242**, 1 (1995).

657. R. M. Valladares, A. J. Fisher, S. J. Blundell, and W. Hayes, J. Phys.: Condens. Matter **10**, 10 701 (1998).

658. D. Vanderbilt and S. G. Louie, Phys. Rev. B **30**, 6118 (1984).

659. D. Vanderbilt, Phys. Rev. B **32**, 8412 (1985).

660. D. Vanderbilt, Phys. Rev. Lett. **59**, 1456 (1987).

661. D. Vanderbilt, Phys. Rev. B **41**, 7892 (1990).

662. T. Van Voorhis and G. Scuseria, J. Chem. Phys. **109**, 400 (1998).

663. `VASP`: see Ref. [344].

664. L. Verlet, Phys. Rev. **159**, 98 (1967).

665. G. A. Voth, Adv. Chem. Phys. **93**, 135 (1996).

666. D. S. Wallace, A. M. Stoneham, W. Hayes, A. J. Fisher, and A. H. Harker, J. Phys.: Condens. Matter **3**, 3879 (1991).

667. D. S. Wallace, A. M. Stoneham, W. Hayes, A. J. Fisher, and A. Testa, J. Phys.: Condens. Matter **3**, 3905 (1991).

668. C. Wang and Q.–M. Zhang, Phys. Rev. B **59**, 4864 (1999).

669. I. S. Y. Wang and M. Karplus, J. Amer. Chem. Soc. **95**, 8160 (1973).

670. M. C. Warren, G. J. Ackland, B. B. Karki, and S. J. Clark, Mineral. Mag. **62**, 585 (1998).

671. A. Warshel and M. Karplus, Chem. Phys. Lett. **32**, 11 (1975).

672. R. O. Weht, J. Kohanoff, D. A. Estrin, and C. Chakravarty, J. Chem. Phys. **108**, 8848 (1998).

673. D. Wei and D. R. Salahub, J. Chem. Phys. **106**, 6086 (1997).

674. S. Wei and M. Y. Chou, Phys. Rev. Lett. **76**, 2650 (1996).

675. F. Weich, J. Widany, and Th. Frauenheim, Carbon **37**, 545 (1999).

676. M. Weinert and J. W. Davenport, Phys. Rev. B **45**, 13 709 (1992).

677. S. Wengert, R. Nesper, W. Andreoni, and M. Parrinello, Phys. Rev. Lett. **77**, 5083 (1996).

678. R. M. Wentzcovitch, Phys. Rev. B **44**, 2358 (1991).

679. R. M. Wentzcovitch and J. L. Martins, Solid State Commun. **78**, 831 (1991).

680. R. M. Wentzcovitch, J. L. Martins, and P. B. Allen, Phys. Rev. B **45**, 11 372 (1992).

681. R. M. Wentzcovitch, J. L. Martins, and G. D. Price, Phys. Rev. Lett. **70**, 3947 (1993).

682. R. M. Wentzcovitch, Phys. Rev. B **50**, 10 358 (1994).

683. R. M. Wentzcovitch and G. D. Price, Top. Mol. Organ. Eng. **15**, 39 (1997).

684. R. M. Wentzcovitch, C. da Silva, J. R. Chelikowsky, and N. Binggeli, Phys. Rev. Lett. **80**, 2149 (1998).

685. J. A. White and D. M. Bird, Phys. Rev. B **50**, 4954 (1994).

686. S. R. White, J. W. Wilkins, and M. P. Teter, Phys. Rev. B **39**, 5819 (1989).

687. J. Wiggs and H. Jónsson, Comput. Phys. Commun. **81**, 1 (1994).

688. J. Wiggs and H. Jónsson, Comput. Phys. Commun. **87**, 319 (1995).

689. G. A. de Wijs, G. Kresse, and M. J. Gillan, Phys. Rev. B **57**, 8223 (1998).

690. G. A. de Wijs, G. Kresse, L. Vocadlo, K. Dobson, D. Alfe, M. J. Gillan, and G. D. Price, Nature (London) **392**, 805 (1998).

691. G. A. de Wijs, A. De Vita, and A. Selloni, Phys. Rev. B **57**, 10 021 (1998).

692. A. Willetts and N. C. Handy, Chem. Phys. Lett. **227**, 194 (1994).

693. M. Wilson and P. M. Madden, J. Phys.: Condens. Matter **5**, 2687 (1993).

694. E. Wimmer, Science **269**, 1397 (1995).

695. K. Wolf, W. Mikenda, E. Nusterer, K. Schwarz, and C. Ulbricht, Chem. Eur. J. **4**, 1418 (1998).

696. T. K. Woo, P. M. Margl, T. Ziegler, and P. E. Blöchl, Organometallics **16**, 3454 (1997).

697. T. K. Woo, P. M. Margl, L. Deng, L. Cavallo, and T. Ziegler, Catal. Today **50**, 479 (1999).

698. D. M. Wood and A. Zunger, Phys. Rev. A **18**, 1343 (1985).

699. K. Yamaguchi and T. Mukoyama, J. Phys. B **29**, 4059 (1996).

700. H. Yamataka, M. Aida, and M. Dupuis, Chem. Phys. Lett. **300**, 583 (1999).

701. L. Ye and H.-P. Cheng, J. Chem. Phys. **108**, 2015 (1998).

702. J.–Y. Yi, D. J. Oh, J. Bernholc, and R. Car, Chem. Phys. Lett. **174**, 461 (1990).

703. M.T. Yin and M.L. Cohen, Phys. Rev. B **26**, 3259 (1982).

704. T. Ziegler, A. Rauk, and E. J. Baerends, Theor. Chim. Acta **43**, 261 (1977).

705. C. J. Zhang, P. J. Hu, and A. Alavi, J. Am. Chem. Soc. **121**, 7931 (1999).

706. Y. Zhang and W. Yang, Phys. Rev. Lett. **80**, 890 (1998).

707. Y.–J. Zhao, J. Ming, G. Lai, and P.–L. Cao, Phys. Lett. A **255**, 361 (1999).

708. F. Zong and D. M. Ceperley, Phys. Rev. E **58**, 5123 (1998).